ACTIVITY OF *CAMELLIA SINENSIS* (GREEN TEA) AGAINST TROPHOZOITE AND CYSTIC FORMS OF *ACANTHAMOEBA CASTELLANII* IN VITRO

LENU BARINEME FAKAE, DVM

Thesis submitted to the University of Nottingham for the degree of Doctor of Philosophy

September 2022

ABSTRACT

Acanthamoeba castellanii is a free-living unicellular protozoan, which causes acanthamoebiasis clinically seen as granulomatous amoebic encephalitis (GAE) of the brain and *Acanthamoeba* keratitis (AK) of the eyes. The conclusive effective treatment for these diseases is yet to be determined. This work focused on investigating the amoebicidal and cysticidal effect of *Camellia sinensis* by subjecting *A. castellanii* forms to serial concentrations of *C. sinensis* brews, solvent extract and their bioactive components. From the brew studies, serial concentrations of 25% - 100%(v/v) of *C. sinensis* brews exhibited a dose-dependent inhibition of trophozoite replication. A similar dose-dependent activity was observed with the exposure of *A. castellanii* to serial concentrations of 156.25µg/mL - 5000 µg/mL of *C. sinensis* solvent extract. Ultrastructural alterations in *C. sinensis*-treated *A. castellanii* was investigated with electron microscopy studies which revealed loss of cellular membrane integrity of trophozoites and destruction of cysts. These results were corroborated with light microscopy evaluations. Cytotoxicity analysis of *C. sinensis* against mammalian host cells revealed that *C. sinensis* exhibited low cytotoxic effects on primary corneal stromal cells and immortalized human corneal epithelial cells (iHCE-2s), with high toxicity to Madin-Darby Canine Kidney cells (MDCKs). Evaluation of the *C. sinensis* chemical components revealed that epigallocatechin gallate (EGCG) and caffeine exhibited dose-dependent anti-acanthamoebic activity by inhibiting trophozoite replication within the concentrations of 3.125µM - 200µM, and also inhibited encystation alongside theobromine. Proteomic analysis of *C. sinensis* treated trophozoites showed inhibition of 14-3-3 protein sigma and Keratin type I cytoskeletal 10, while TPI, TrxRases and alpha-enolase inhibited trophozoites replication by inhibition protein and cellulose synthesis. These inhibitions were confirmed by the lack of amide I and II band peaks expression in the treated trophozoites by Fourier-transform infrared spectroscopy (FTIR) analysis. Taken together, these results demonstrated that *C. sinensis* possess anti-acanthamoebic capability making it a potential novel compound which can be further investigated for anti-acanthamoebic drug production.

ACKNOWLEDGEMENTS

This work was funded from personal and family resources.

At the risk of resembling an Oscar speech, there are quite a number of people whom I owe much gratitude, without them, my studies would not have either commenced, or have been completed.

Firstly, I would like to thank my supervisors Carl Stevenson and Hany Elsheikha for their outstanding advice, patience, support and encouragement. I appreciate your belief in me, for pushing me and ensuring I kept my eye on the ball. Thank you for not giving up when I was met with winds of change just a few weeks to my first-year review, and also for understanding the peculiarities that came with my funding challenges. Again, I specially thank Hany (Sensei as I call him) for initiating the project and staying with it throughout the duration of my study. I appreciate his support prior to the commencement of my studies, and also outside the walls of the lab where his words of encouragements served as necessary winds under my sail. Your words to kept me afloat when I thought I was sinking. I do appreciate your humour and hope that I have been a good student and a respectable representation of your lab, I hope we can get to practice some *Katas* together soon. I also thank my internal assessor, Kevin Gough for his critical assessment and feedback of my work.

My thanks to those I worked with within the labs, the techs and admins who ensured things ran smoothly, Scott, Catherine, Lucy, Ceri, James, Chris, Leigh, Ally, Sheila, Lorraine and many others. A special thank-you to the SLIM team, especially Denise McLean for her immeasurable help and support; you made working in QMC and the NMRC an awesome and homely experience. Thanks to Subba who for all his “madness” was the closest thing I had to a brother, you always had “out of the box” ideas that made me almost love industrial chemistry. A special thanks to the RHN family led by Pastor Sam, and especially my first friend in The UK Tolani, who though was troublesome became more than just a friend; a sister, confidant and daughter. Also, I specially thank my bestie Agatha and Feggie for being a family; your

care and support cannot be measured. I cannot forget the love shown me by my Nottingham family; The Oppals, led by the crazy Fozia, amiable Naseem and gentle Imran. And to my friends who rendered so much support and advice; Abdullah, Aisha, Tosin, Mayowa, Doreen, Sharon, Kunle, Deborah, Ofunne, Lebia, Vivian, Esosa, Jude, Iwai, Uche, Maureen to name but a few. I am fortunate to count you as my friends and I would love to say a huge thank you. Also, a heartfelt gratitude to Andrew who went above and beyond within TETFund to secure additional support for me, and TETFund for their initial support. To all my housemates, I thank you for dealing with my mercurial personality, you all deserve awards for not dropping hot water on my annoying head.

Finally, I would like to say a huge thank you to my family, for their unending love and support. My Twin Lebia, you have been most awesome and your support, advice and humour in the face of "*eevvunn doers"*, made this journey worthwhile. To Nia, Suanu, TM, Super K, Sam, and all your families; your humours kept me smiling and I always have to keep a straight face in the lab, so I don't LOL and look like an ass in the lab when I remember your quips. To my Dad, you have been a great and visionary source of knowledge, encouragement and inspiration with your never-ending advice and feedbacks. It is noteworthy to say that you cut out and paved the path which I am walking today, making it easy for me to blaze ahead without much of a "pathfinding", I owe you more than I can ever repay you. Mum, you have supported me in more ways than one as your prayers have kept me protected and directed towards my goal; God bless you immensely.

I reserved the most special thanks to my Dearest Ruth for being the most awesome partner I could ever have asked for. You held down the fort in my absence and kept our three "Js" together (Jesse, Joanna & Jada). At the end of it all, God made all things most beautiful with you in the centre of it all. I love you always.

This PhD journey was an arduous one, I am honoured to have travelled it with you all. Above all, I thank God for His mercies.

TABLE OF CONTENTS

LIST OF FIGURES

LIST OF TABLES

LIST OF ABBREVIATIONS

A	Alpha
β	Beta
%	Percent
~	Approximately
^{0}	Degrees
+ve Ctrl	Positive control
µl	Microliter
µm	Micrometre
1H NMR	Hydrogen-1 nuclei Nuclear magnetic resonance
2DE PAGE	Two-dimensional polyacrylamide gel electrophoresis
3CLpro	3 chymotrypsin-like protease
AbAm	Antibiotic-Antimycotic
Abs	Absorbance
AcLAP	Leucine aminopeptidase of *A. castellanii*
AIDS	Acquired immunodeficiency syndrome
AK	*Acanthamoeba* keratitis
ANOVA	Analysis of variance
AO	Acridine orange
APCs	Alkylphosphocholines
APES	3-Aminopropyltriethoxysilane

APP	Amyloid precursor protein
ATPases	Adenosine triphosphatase
BBB	Blood brain barrier
Bp	Base pair
C	Centigrade
Ca^{2+}	Calcium ion
CaF_2	Calcium fluoride
cAMP	Cyclic adenosine monophosphate
CC_{50}	Cytotoxic concentration
CCS	Cold *C. sinensis*
cDNA	Complementary DNA
CHX	Chlorhexidine
cm^2	Square centimetres
CNS	Central nervous system
Conc.	Concentration
CO2	Carbon dioxide
CSCs	Corneal stromal cells
CSP21	Cyst-specific protein of 21 kDa
CT	Computerized tomography
DAPI	4′,6′-diamidino-2-phenylindole
D.F.	Dilution factor

DHFR	Dihydrofolate reductase
DIA-MS	Data-independent acquisition mass spectrometry
DMEM	Dulbecco’s Modified Eagle Medium
DMP	Dimethylaminomethyl phenol
DMSO	Dimethyl sulfoxide
DNA	Deoxyribonucleic acid
dsDNA	Double stranded DNA
DTH	Delayed-type hypersensitivity
EC	Epicatechin
EC50	Half maximal effective concentration
ECG	(−)-epicatechin-3-gallate
EDTA	Ethylenediaminetetraacetic acid
EGC	(−)-epigallocatechin
EGCG	(−)-epigallocatechin-3-gallate
EM	Electron microscopy
EPGM	Epilife growth medium
EVs	Extracellular vehicles
FAdV-4	Fowl adenovirus type 4
FBS	Foetal bovine serum
FC	Final concentration
FDA	Food and Drug Administration

FDR	False discovery rate
FLA	Free-living amoeba
FTIR	Fourier-transform infrared spectroscopy
GAE	Granulomatous Amoebic Encephalitis
gm	Gram
GTPs	Polyphenolic flavanols
h	Hour
H&E	Haematoxylin and eosin
HBMECs	Human Brain Microvascular Endothelial Cells
HCS	Hot *C. sinensis*
HIF-1	Hypoxia-inducible factor-1
HIV	Human immunodeficiency virus
HKGS	Human Keratinocyte Growth Supplement
HPLC	High performance liquid chromatography
HSPs	Heat shock proteins
IC_{50}	Half-maximal inhibitory concentration
IDA	Information Dependent Acquisition
IgA	Immunoglobulin A
IgG	Immunoglobulin G
iHCEC	Immortalised human corneal epithelial cell
IMS	Industrial methylated spirit

IR	Infra-Red
IVCM	*in vivo* confocal microscopy
kb	Kilobases
kDa	Kilodalton
LAP	Leucine aminopeptidase
LBP	Laminin-binding protein
LC-MS	Liquid chromatography–mass spectrometry
LDH	Lactate dehydrogenase
L-Glut	L-Glutamine
M	Molar
MBP	Mannose-binding protein
MDCK	Madin-Darby Canine Kidney cells
min	Minutes
mL	Millilitre
mM	Micromolar
MRI	Magnetic resonance imaging
mRNA	Messenger Ribosomal ribonucleic acid
Na_2EDTA	Ethylenediaminetetraacetic Acid, Disodium Salt
NaOH	Sodium hydroxide
nm	Nanometre
nM	Nanomolar

NN	Non-nutritional
OD	Optical Density
OLE	Olive Leaf Extracts
PARP	Poly (ADP-ribose) polymerase
PBS	Phosphate-buffered saline
PC	Principal component
PCA	Principal component analysis
PCR	Polymerase chain reaction
PFA	Paraformaldehyde
PGY	Proteose-peptone-Glucose-Yeast
pH	Potential of hydrogen
PHMB	Polyhexamethylene biguanide
PI-3k	Phosphatidylinositol 3-kinase
PMSF	Phenylmethylsulfonyl fluoride
RFU	Relative fluorescent unit
RM ANOVA	Repeated measures Analysis of variance
RNA	Ribosomal ribonucleic acid
ROS	Reactive Oxygen Species
rRNA	Ribosomal ribonucleic acid
RT-PCR	Real-time polymerase chain reaction
SDS	Sodium dodecyl sulfate

SDS-PAGE	SDS-polyacrylamide gel electrophoresis
SEM	Scanning electron microscopy
SI	Selectivity index
SIgA	Secretory Immunoglobulin A
siRNA	Small interfering Ribosomal ribonucleic acid
SRB	Sulforhodamine B
ssDNA	Single stranded DNA
TCA	Trichloroacetic Acid
TEM	Transmission electron microscopy
TFPI-2	Tissue factor pathway inhibitor-2
TLR-4	Toll-like receptor-4
TPI	Triosephosphate isomerase
TrxRases	Thioredoxin reductases
UHPLC-QTOF-MS	Ultra-high performance liquid chromatography-quadrupole time-of-flight mass spectrometry
UVA	Ultraviolet light A
v/v	Volume by volume
-ve Ctrl	Negative control
w/v	Weight by volume
xg	Times gravity
ZnS	Zinc sulfide

SCHORLARLY OUTPUTS DURING STUDY

Fakae, L.B.; Stevenson, C.W.; Zhu, X.Q.; Elsheikha, H.M. In vitro activity of *Camellia sinensis* (green tea) against trophozoites and cysts of *Acanthamoeba castellanii*. Int J Parasitol Drugs Drug Resist 2020, 13, 59-72, doi:10.1016/j.ijpddr.2020.05.001.

Dickson, A., Cooper, E., **Fakae, L.B**., Wang, B., Chan, K.L.A. and Elsheikha, H.M., In Vitro Growth-and Encystation-Inhibitory Efficacies of Matcha Green Tea and Epigallocatechin Gallate Against *Acanthamoeba Castellanii*. Pathogens, 2020, 9(9), p.763, DOI: 10.3390/pathogens9090763

Fakae, L.B., Ting, D.S., Dua, H.S., Stevenson, C.W., Zhu, X.Q., Elsheikha, H.M. The trophocidal and cysticidal properties of solvent extracts from *Camellia sinensis* (Green tea) against *Acanthamoeba castellanii.* ***(Draft submitted and awaiting publication)*.**

Fakae, L.B., Zhong, J., Chan, K.A., Cave, G.W., Stevenson, C.W., Elsheikha, H.M. Characterization of *Camellia sinensis* solvent extract effects on trophozoites and cysts of *Acanthamoeba castellanii.* ***(Draft completed and awaiting publication)*.**

1 INTRODUCTION

1.1 OVERVIEW

Acanthamoeba castellanii (*A. castellanii)* is a free-living unicellular protozoan with two distinct morphologies: the infective trophozoite and dormant cyst form found in every natural eco-system. Virulent forms of *A. castellanii* causes granulomatous amoebic encephalitis (GAE), leading to serious brain and spinal cord infections, and *Acanthamoeba* keratitis (AK), which, if not diagnosed early and treated, leads to blindness in humans (Siddiqui and Khan, 2012; Lorenzo-Morales et al., 2015). These diseases occur mostly in immunocompromised individuals, with complications of cutaneous keratitis, nasal, pulmonary, kidney infections and give rise to other opportunistic pathogenic infections (Trabelsi et al., 2012; Lorenzo-Morales et al., 2013b). They can also occur in immunocompetent individuals in cases where the organism gains entrance through pulmonary inhalation or skin lesions followed by its spread through haematogenous means (Khan, 2007; Lackner et al., 2010). The primary step in the ensuing infection is by the adhesion of *A. castellanii* to host organs and tissues, such as the cornea and human brain microvascular endothelial cells (Alsam et al., 2003), using tiny spiny structures of actin-based fibres known as acanthopodia. Adherence triggers mechanisms that allow the organism to invade the target tissue and initiate infection. Outside its normal habitat of oxygenated layers of soil and in the presence of adverse conditions of increased osmolarity, temperature and chemotherapeutic challenges, the trophozoites adapt to their environment rapidly by encystation, which is the production of double walled cysts as protection for the organism, excysting only when the conditions improve (Lloyd, 2014). Adhesion and encystation are the most fundamental mechanisms by which the organism establishes infection and survives harsh environmental conditions. The dynamism exhibited by these processes makes it necessary to understand the molecular interactions that underpin both processes with the aim of providing information that makes it possible to have a definitive therapeutic protocol against *A. castellanii* infections.

1.2 BACKGROUND OF STUDY

1.2.1 Historical account on Acanthamoeba

Acanthamoeba species are ubiquitous unicellular protozoa found in every aspect of the natural environment such as soil, water, air, vegetables, fruits, sewage and on practically every surface including objects, medical equipment, air conditioning systems, contact lenses and their storage fluid and cases, sporting facilities like swimming pools and also human systems such as the nostrils and the mouth (Mergeryan, 1991; Zaman et al., 1999; Shoff et al., 2008; Chomicz et al., 2010; Trabelsi et al., 2010; Lemgruber et al., 2010; Trabelsi et al., 2012). Though considered a rare source of infection, an epidemiological study of outbreaks in the UK between 2010-2011 and 2012-2014 identified hygiene as the major factor responsible for outbreaks, with 95% of the cases being diagnosed in contact lens users(Carnt et al., 2018). *Acanthamoeba* has been classified as a free-living amoeba (FLA) alongside *Balamuthia mandrillaris*, *Naegleria fowleri* and *Sappinia diploidea*, and as being an aerobic, mitochondriate which causes opportunistic and non-opportunistic infections globally in humans and animals (Visvesvara et al., 2007). *Acanthamoeba spp*. in their virulent forms can cause GAE and AK in humans, leading to a serious brain and spinal cord infection for GAE and total blindness for AK. These diseases occur mostly in immunocompromised individuals with complications of cutaneous keratitis, nasal, pulmonary and kidney infections (Trabelsi et al., 2012; Lorenzo-Morales et al., 2013a) and can give rise to other pathogenic infections even in immunocompetent individuals (Ly and Muller, 1990; Swanson and Hammer, 2000; Thom et al., 1992). In 1930, Castellani isolated an *Amoeba* which was found as a contaminant in a yeast culture, *Cryptococcus pararoseus,* and later named it *Acanthamoeba castellanii* following the generic morphological designation created by Volkonsky in 1931 (Visvesvara et al., 2007; Khan, 2006b).

1.2.2 Phylogenetic classification and genotypes of *Acanthamoeba*

Based on its morphology, the pathogen is classified under the Super Group *Amoebozoa*: *Acanthamoebidae* (Adl et al., 2005). Being under the genus *Amoebae*, *Acanthamoeba spp*. Is among the earliest organisms to be studied following the advent of the microscope (Siddiqui and Khan, 2012). There are more than 24 species of *Acanthamoeba* based on their morphology and cyst size. The organism is categorized into three groups. Group I are large *Amoebae* with cysts of 16-30µm, group II *amoebae* possess cysts of 18µm and smaller, while group III also has *amoebae* with a cyst size of 18µm and smaller but have slight morphological differences (Visvesvara et al., 2007). These groups can be further designated by using hexokinase, esterase and acid phosphatase profiles. The ability of different species of *Acanthamoeba* such as *A. castellanii*, *A. culbertsoni*, A. hatchetti, *A. healyi*, *A. polyphaga*, *A. rhysodes*, *A. astronyxis*, and *A. divionensis* to survive outside their natural hosts is notable. They are also able to house some viable bacteria for up to 60 days (Sanchez‐Hidalgo et al., 2017) and house other bacteria such as *Mycobacterium leprae* for up to 8 months within their amoebic cysts (Wheat et al., 2014). While within a natural environment like water, the cyst form can persist for to 24 years (Mazur et al., 1995), and alternatively also survive within natural hosts classifying them as amphizoic *amoebae* (Visvesvara et al., 2007). Using ribosomal rRNA gene sequences, 15 different genotypes (T1-T15) of *Acanthamoeba* have been established. The differences in *Acanthamoeba* DNA genotypes are about ~5% but they can also be classified based on their virulence and the infections that they elicit (Stothard et al., 1998; Siddiqui and Khan, 2012). The T4 genotype of *A. castellanii* is one of the most virulent and easily transmissible genotypes of importance in human infections and is largely responsible for causing AK and GAE; 90% of AK's occurrence is associated to the T4 genotype (Siddiqui and Khan, 2012). Apart from having large numbers of mitochondria, the genotype T4 has mitochondrial DNA with a genome size of 41,591 bp (Burger et al., 1995). In the analysis of its gene makeup with 200 different genes, *A. castellanii* has an average of 3 exons per gene which is higher than 1.3 for *Entamoeba histolytica* and 2.3 for *Dictyostelium*

discoideum (Anderson et al., 2005). Exons are the segments of DNA molecule which contains information coding for a protein or peptide. These exons through transcription can be transformed into mature messenger RNA (mRNA); they encode proteins and translate them to amino acids.

1.2.3 Morphological features of *A. castellanii* life cycle forms

The designation “acanth” is of Greek origin meaning “spikes”, which for *Acanthamoeba spp*. is currently known as “acanthopodia” (Siddiqui and Khan, 2012), and *amoeba* which is an organism that can alter its shape. *A. castellanii* has a plasma membrane within which lies large numbers of mitochondria. The organism possesses a large single nucleus which is about one sixth the size of the organism. It also has different types of vacuoles among which includes digestive vacuoles, lysosomes, glycogen-containing vacuoles, and contractile vacuoles which contain alkaline phosphate, aiding active transport and osmotic regulation (Bowers and Korn, 1973; Siddiqui and Khan, 2012). Possessing an actin-based cytoskeleton and driven by chemotaxis, the parasite moves by means of hyaline pseudopodium formation both on solid and liquid surfaces by adhering to the surfaces (Pollard et al., 1970; Siddiqui and Khan, 2012).

Studies show that the plasma membrane of *A. castellanii* consists of 33% proteins, 25% phospholipids, 13% sterols (ergosterol and 7-dehydrostigmasterol), and 29% lipophosphonoglycan (Siddiqui and Khan, 2012). The organism contains fatty acids of 40-50% oleic acids, 20-30% polyunsaturated fatty acids, and glycolipids of 60% glucose (Ulsamer et al., 1971). Cytoplasmic protrusions and tension resistivity of the organism are enabled by actin filaments consolidated underneath the plasma membrane (Siddiqui and Khan, 2012). The organism *A. castellanii* has two different life forms; the trophozoite and the cyst form. The trophozoite form is an infective, vegetative and feeding stage which reproduces by binary fission, while the cyst form is a dormant resistant stage which occurs as a morphological differentiation of trophozoites to cysts in a defence reaction to protect the organism from adverse conditions (Khan, 2006b; Visvesvara et al., 2007; Fouque et al., 2012).

1.2.3.1 Trophozoites

The trophozoite stage of *A. castellanii* is a flat and irregular shape recognised by a single nucleus with a large centrally located karyosome. The organism measures between 20-40µm in diameter (Martinez and Visvesvara, 1997; Khan, 2006b) and is bounded externally by a rough surface with multiple acanthopodia which serve a vital role in the adhesion of the organism to biological and inert surfaces (Niederkorn et al., 1999; Khan, 2006b; Visvesvara and Martinez, 2010). The acanthopodia protoplasmic motion ensures the organism's motility as well as enhances the capture of bacteria and other smaller organisms for food via pinocytosis and phagocytosis (Clarke and Niederkorn, 2006b; Khan, 2006a; Trabelsi et al., 2012). The dynamism of the organism is seen even within its different phases where they seemingly respond in a defensive way. In some studies, the presence of another organism, like bacteria in a culture medium, may lead to an increase in size of the trophozoites, which supposedly happens after the trophozoites may have ingested some of these organisms (Lloyd, 2014). The trophozoite possesses fundamental organelles which include the nucleus, Golgi apparatus (for processing proteins), digestive vacuoles, endoplasmic reticulum (for protein synthesis and transport), mitochondria (for energy generation, metabolism and cellular respiration) and contractile vacuole (for osmoregulation), all within a plasma membrane (Bowers and Korn, 1969; Khan, 2006b).

Trophozoites which are secondary decomposers vary in size based on isolates of species and genotypes and also feed on primary decomposers like bacteria, yeast, algae, and small organic particles. While excreting their by-products they promote plant growth by mineralizing the soil with phosphorus, carbon and nitrogen, while regulating the bacterial population and nutrient cycle, which leads to varied strata of fertile soil (Ronn et al., 2002; Clarholm, 2002; Bonkowski, 2004; Rosenberg et al., 2009). *A. castellanii* trophozoites reproduce asexually by binary fission and subsist only in ambient conditions of plentiful food, temperature, pH and osmolarity (Khan, 2006b). Physiological changes in the form of lack of food or nutrients, extreme temperature, osmolarity, pH and dehydration trigger morphological differentiation of

the trophozoites in a process known as encystation into a resistant phase, which is a dormant, metabolically inactive double walled cyst. This cyst phase reverses back to trophozoite in an excystation process when favourable conditions arise (Trabelsi et al., 2012).

1.2.3.2 Cysts

The cyst phase of *A. castellanii* is made up of a double walled structure consisting of an ectocyst with a fibrous matrix and an endocyst consisting of granular matrix formed by fine fibrils within which lies a uni-nucleated organism with a dense nucleus (Lemgruber et al., 2010; Anwar et al., 2018). Lemgruber et al. (2010) reported that the ectocyst-endocyst layers are separated by a space except in the presentation of opercula by the ostioles which are small pores that provide a means of exit during excystation, where the organism dislodges the operculum and excysts to revert to its trophozoite phase. *A. castellanii* cysts measure approximately 5-20µm in diameter, varying in size based on isolates of species and genotypes (Visvesvara et al., 2007). The endocyst of the T4 genotype of *A. castellanii* is made up of polysaccharides of mainly cellulose while the ectocyst is made up of 33% proteins, 4-6% lipids, 35% carbohydrates, 8% Ash and 20% of an unknown substance, with cellulose as a major component (Neff and Neff, 1969; Weisman, 1976; Hirukawa et al., 1998). A study by Anwar (et. al., 2018), showed that galactose and not glucose is the major constituent of the cyst wall, with 48% galactose and 44% glucose (Anwar et al., 2018). The endocyst can appear in different shapes: stellate, polygonal, oval or spherical (Visvesvara et al., 2007). On the other hand, the ectocyst appears crumpled with a combination of acid-insoluble proteins, cellulose and other polysaccharides in an unknown composition (Neff and Neff, 1969; Fouque et al., 2012).

A. castellanii cysts are resistant to chlorination and can survive at low temperatures of 0-2^{0}C. Empirical therapies against them using a combination of different antibiotics and antimicrobial agents have not given a desired therapeutic response (Khan, 2006b). With favourable conditions (plentiful food, temperature, pH and osmolarity), the cysts undergo excystation, releasing the trophozoite within to initiate *Acanthamoeba* infections. Being made up of

cellulose, there are suggestions that enzymes which act like serine protease and cysteine proteases are involved in the synthesis of cellulose, and are involved in the encystment and excystment process (Anderson et al., 2005; Fouque et al., 2012). Studies have also shown absence of CSP21 (cyst-specific protein of 21 kDa), which is a hydrophilic cyst-specific protein in the trophozoite phase of *A. castellanii* (Hirukawa et al., 1998; Siddiqui et al., 2012).

Each *A. castellanii* cyst is an independent organism but they have been observed to exhibit an interesting phenomenon in which when introduced to adverse environments, like encystation buffers and hyperosmotic solutions during encystation experiments, where the cysts form clumps or bunches of about 4 to 500 cells (Ahearn and Gabriel, 1997; Fakae et al., 2020). This phenomenon, which might be enabled by chemotaxis, might be a defensive response. It is noteworthy that *A. castellanii* cysts can survive for more than 20 years in their natural environments and excyst without losing their virulence; the more tropical the environment, the more viable the excysted organism (Mazur et al., 1995).

1.3 LIFE CYCLE OF *A. CASTELLANII*

As mentioned above, *A. castellanii* has two distinctive cellular stages in its life cycle (Figure 1:1), the active trophozoite phase and cyst phase (the encystment phase and the excystment phase). The infective phase of trophozoite feeds and reproduces mitotically within 30 minutes via binary fission. The reproduction is enabled by continuous synthesis of the cellular materials thereby increasing the cell mass, building up to its division by mitosis and cytokinesis (Siddiqui et al., 2012). After cellular division, there is rapid growth of the trophozoites, which is followed by decreased growth before the stationary phase of no growth preceding the trophozoite division again (Siddiqui et al., 2012). Active trophozoites are produced during the phase of rapid growth, while the cyst phase occurs during the stationary phase except in situations where the organisms form cysts in response to adverse conditions (Neff and Neff, 1969; Band and Mohrlok, 1973; Siddiqui et al., 2012). Upon exposure to harsh and adverse conditions, cellular differentiation occurs, triggering the encystment phase. This results in the formation of

a double walled cyst (Siddiqui and Khan, 2012), which can subsist for many months only to excyst during favourable conditions.

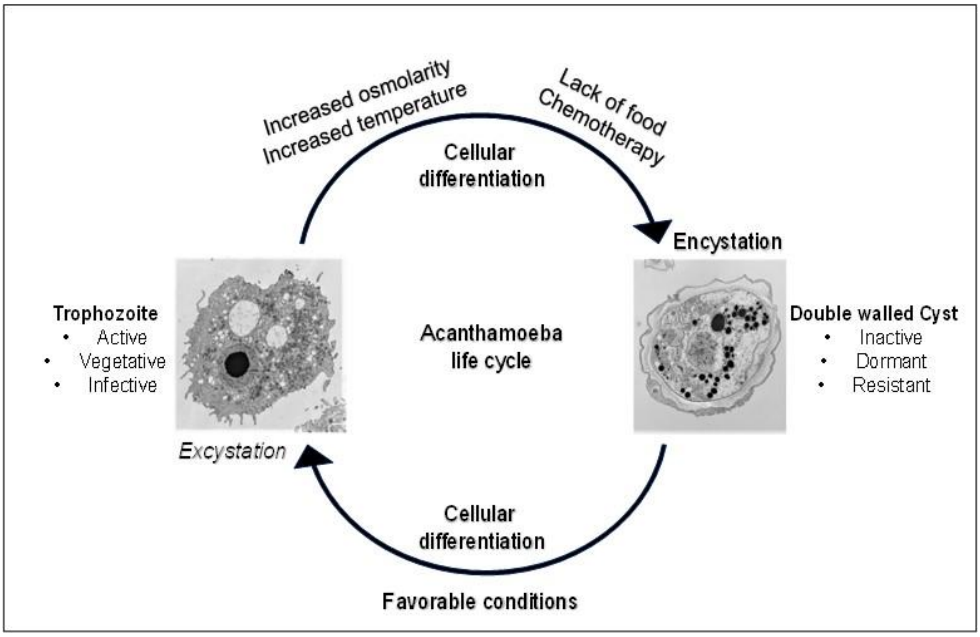

Figure 1:1: Life cycle of *A. castellanii*

The excystation process of *A. castellanii* is morphologically enabled by their pores (ostioles) which assess the conditions and designate them “favourable”, thereby triggering the excystment process (Khan, 2006b), and serves as an egress route for the excysting trophozoites (Siddiqui and Khan, 2012). During the encystment phase, the trophozoites are metabolically inactive with a reduced volume of cellular contents. There is a decrease of its cytoplasmic mass by the expulsion of surplus food and water, leading to the condensation of the organism which forms a double-walled cyst as a protection from the surrounding adverse environment.

1.4 A. CASTELLANII ADAPTATION MECHANISMS

The mechanisms of action which direct the “Jekyll and Hyde” reversible morphological and functional characteristics of *A. castellanii* trophozoites and cysts is noteworthy. The ability of the parasite to adhere to host tissue, to encyst when challenged and also excyst when the environment promotes its viability demonstrates the sustainability of the organism’s pathogenicity, especially in the presence of chemotherapy.

1.4.1 Adherence of *A. castellanii*

The primary step in the organism’s pathogenesis is the adhesion of *A. castellanii* to host organs and tissues (Alsam et al., 2003) using acanthopodia. The adherence is enabled by a 130 kDa mannose-binding protein (MBP) (Siddiqui and Khan, 2012), a 28.2kDa and 55kDa laminin-binding protein (LBP), and a 207kDa adhesion protein (Siddiqui and Khan, 2012; Hong et al., 2004). The process of adherence (Figure 1:2) leads to the secretion of toxins, serine proteases and also phagocytosis resulting in an *A. castellanii*-mediated host cell death via a phosphatidylinositol 3-kinase (PI-3k)-dependent mechanism; programmed cell death (Sissons et al., 2005). The *A. castellanii* MBP gene is comprised of 6 exons and 5 introns that span 3.6 kb of the amoeba genome. The MBP cDNA codes for a precursor protein of 833 amino acids with a signal sequence with 1-21 residues, an extracellular domain (residues 22-733) displaying five targets of N- glycosylation and three O-glycosylation sites, a 22-amino acid long transmembrane domain (residues 734-755), and a short 78-amino acid C-terminal domain (Garate et al., 2004).

Although host response comes into play via typical antigen-antibody response mechanisms, it is thought that immunoglobulin A (IgA) secretion is repressed, allowing the *A. castellanii* MBP to bind with the mannose glycoproteins at a docking site enabled by the host Toll-like receptor-4 (TLR4). While understanding of the mechanism of adhesion and its resulting permeability of the blood brain barrier (BBB) is still vague, there is interactive parasite-host exchange. While the parasite expresses adhesins, proteases, and phospholipids, the host

responds by releasing interleukin-beta, interleukin-alpha, tumour necrosis factor- alpha and interferon-gamma (Siddiqui and Khan, 2012).

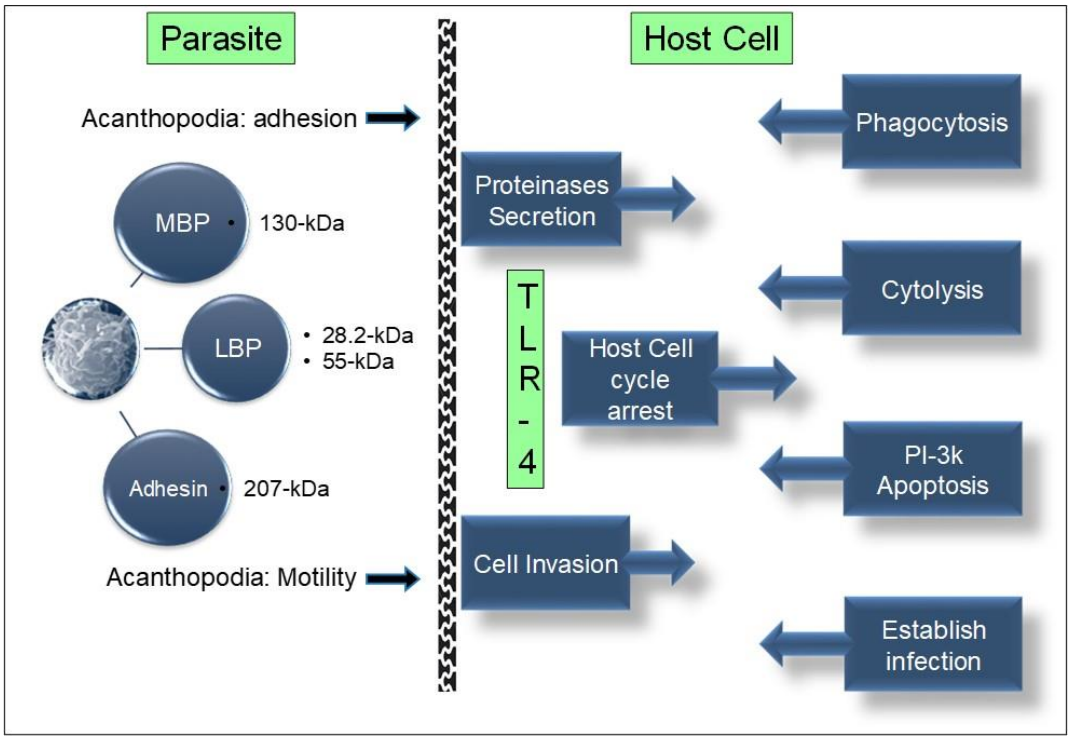

Figure 1:2: Schematic showing adhesion and host immune system invasive process of *A. castellanii.* (MBP: mannose-binding protein, LBP: laminin-binding protein, TLR-4: Toll-like receptor-4)

Various compounds have been screened to determine which possess molecules that inhibit adherence, but no definitive set of molecules has given the desired results of inhibiting adhesion and also maintaining cellular integrity. Therefore, there is a need to carry out more studies with the aid of modified surfaces, and to also expose trophozoites to compounds with the aim of assessing their rate of adhesion. More studies might lead to the possibility of recognizing some unidentified molecules that play crucial roles in parasite-host cell adherence.

1.4.2 Encystation of *A. castellanii*

Outside their normal habitat of oxygenated layers of soil and sediments, *A. castellanii* trophozoites adapt to their environment rapidly by differentiating into cysts (Lloyd, 2014). Above, it is noted that the cyst wall is made up of polysaccharides and proteins. Galactose and glucose of 48% and 44%, respectively, make up the 35% carbohydrate component of the cyst wall (Neff and Neff, 1969; Weisman, 1976; Hirukawa et al., 1998; Anwar et al., 2018), making them probably the most important components of the cyst wall alongside proteins. The full picture of the encystation process is yet to be discovered with 20% of an unknown compound. However, the known aspects (Figure 1:3) suggest that within 6-8 hours of being exposed to adverse conditions, cellulose synthesis with β1,4 glucans homopolysaccharide end point, 1,3-Galactose polymer synthesis with 1,3-galactopyranose endpoint, and protein synthesis with fibrous cyst wall specific protein endpoint occur to form the cyst wall (Anwar et al., 2018).

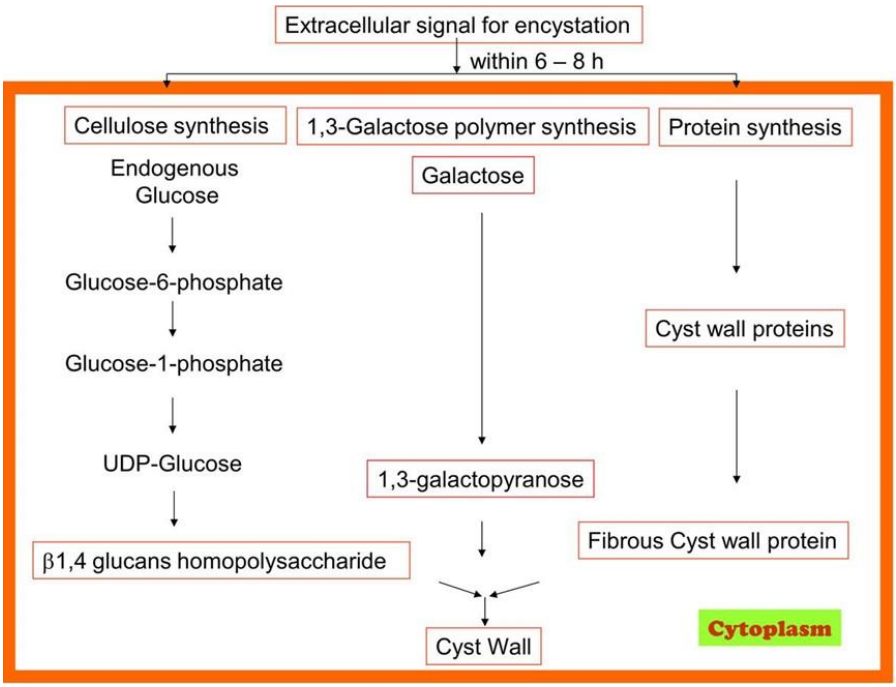

Figure 1:3: Synthesis of cellulose, galactose and protein in the encystation process of *A. castellanii* (adapted from Anwar et al., 2018)

The secretion of various proteinases such as neuraminidases, superoxide dismutase, *Acanthamoeba*-induced plasminogen activation, elastases, cytotoxic and cytolytic proteases, phospholipases, and glycosidase (Lorenzo-Morales et al., 2015) are also instrumental in regulating the pathogenicity and differentiation of *A. castellanii*. Although the specific roles of proteases in the encystation and excystation processes have not been established, introducing phenylmethylsulfonyl fluoride (PMSF) (a serine protease inhibitor) inhibited both processes (Dudley et al., 2008). Metalloprotease was also inhibited by 1,10-phenanthroline (Alsam et al., 2005). Serine proteases are known to cause host cell membrane permeability (Alsam et al., 2005), cytolysis, and probably play a role in parasite pathogenicity, since only the T4 genotype secretes serine proteases (Khan et al., 2000b). In the process of understanding the role of metalloprotease in encystation, a study showed that leucine aminopeptidase (LAP) of *A. castellanii* is functionally involved in the encystation process. This was revealed by inducing a decrease of LAP with small interfering RNA (siRNA) which resulted in the knockdown of LAP (Lee et al., 2015).

Researchers have carried out several studies to tackle the complexities of *A. castellanii* encystation. These studies have made use of chemical and natural compounds which have proffered solutions when used *in vivo*, but there have also been undesirable outcomes, making it impossible for some of the studies to be adopted for empirical therapy. The impediment with most chemical compounds is that despite their ability to inhibit encystation and also destroy already formed cysts, they are traumatic to host cells when tested *in vitro*. Therefore, there is still a need for the discovery of compounds that will not only inhibit encystation and excystation, but will also maintain host cellular health and integrity.

1.5 TRANSMISSION

As mentioned above, *Acanthamoeba* species are quite ubiquitous and are found in every aspect of the natural environment. Based on two clinical forms; AK and GAE, the modes of

transmission can be either through corneal epithelial adhesion, which leads to corneal stromal invasion by inflammatory cells as a defensive response for *Acanthamoeba* keratitis (Niederkorn et al., 1999), especially for contact lens users. Transmission through pulmonary inhalation and skin lesions also occurs. This leads to vascular circulation and subsequently invasion of the central nervous system by *A. castellanii* trophozoites after breaching the blood brain barrier, resulting in granulomatous amoebic encephalitis (Siddiqui and Khan, 2012).

1.6 CLINICAL DISEASES CAUSED BY *A. CASTELLANII*

The ability of human disease being caused by *A. castellanii* was first suggested during a polio vaccine safety trial in 1958, where animals inoculated with tissue culture fluids died from encephalitis, leading to subsequent reports that the identified *A. castellanii* was a cause of human disease (Marciano-Cabral and Cabral, 2003). Virulent strains of *Acanthamoeba spp*. have been known to cause GAE and AK in humans, leading to a serious brain and spinal cord infection for GAE and summarily blindness for AK (Figure 1:4). The organism does not discriminate between immunocompromised individuals and immunocompetent individuals (Marciano-Cabral and Cabral, 2003) as seen in cases of GAE for immunocompetent individuals with skin lesions (Lackner et al., 2010). An epidemiological study demonstrated the clinical importance of *Acanthamoeba*-mediated disease which was represented in 50-100% of the population who carry antibodies (SIgA) against *A. castellanii* antigens (Cerva, 1989). This is representative of how ubiquitous the organism is.

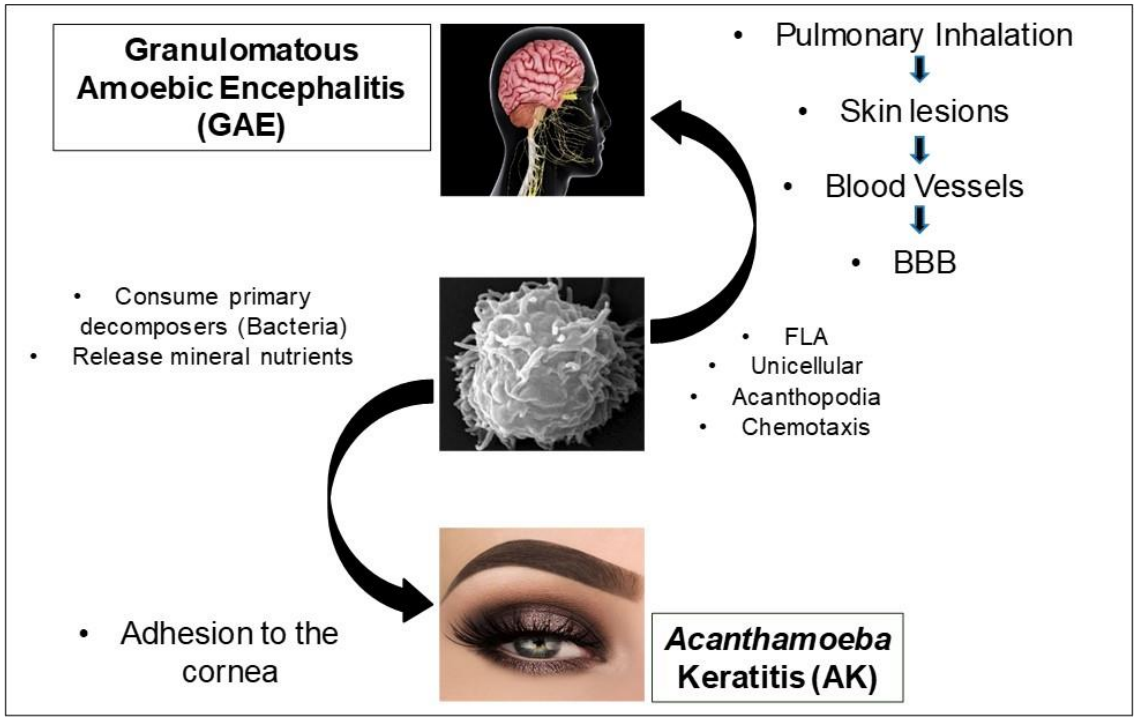

Figure 1:4: *A. castellanii* clinical forms and primary modes of transmission. (FLA: Free-living amoebae, BBB: blood–brain barrier)

1.6.1 *Acanthamoeba* keratitis

AK is an acute clinical form of a virulent *A. castellanii* strain infection of the cornea (Figure 1:5), which, if not treated promptly, might result in permanent visual impairment. Even when detected early and prompt treatment is conducted, the outcome may be unfavourable such as irreversible damage of the cornea (Patel and McGhee, 2009; Lloyd, 2014). AK was first diagnosed in 1973. With its discovery, reports indicated that the highest incidence occurs with the use of contact lens, especially in cases where AK was not diagnosed early, resulting in irreparable damage of the cornea and total visual impairment (Patel and McGhee, 2009). AK is characterised by blurred vision, photophobia, unilateral red eye, unbearable pain arising from radial neuritis, stromal infiltration, and stromal opacity. These signs can be accompanied by anterior uveitis, sclera inflammation (Khan, 2006b; Lorenzo-Morales et al., 2015; Behera and Satpathy, 2016) and epithelia changes such as dendritiform epitheliopathy, sub-epithelial infiltration, ring infiltration, stromal neovascularization, hypopyon, and reduced corneal

sensation (Illingworth and Cook, 1998; Patel and McGhee, 2009). The increase in the popularity of soft contact lenses also paved the way for the increase in disease incidence in the 1990s (Bacon et al., 1993), with a high incidence of 1.2 per million adults in the United States and to 2 per 10,000 soft contact lens wearers in the United Kingdom each year (Stehrgreen et al., 1989; Seal et al., 1999; Parmar et al., 2006).

At the onset of infection, the physical signs may not be seen and when they do occur, they might appear in the form of epithelial micro-erosions with some anomalies as well as corneal opacity and microcystic oedema (Illingworth and Cook, 1998). When the infection progresses, the signs and epithelia changes previously listed occur and most importantly radial keratoneuritis, which was initially considered prominently pathognomonic for AK (Moore et al., 1986), has been contested (Roels et al., 2017).

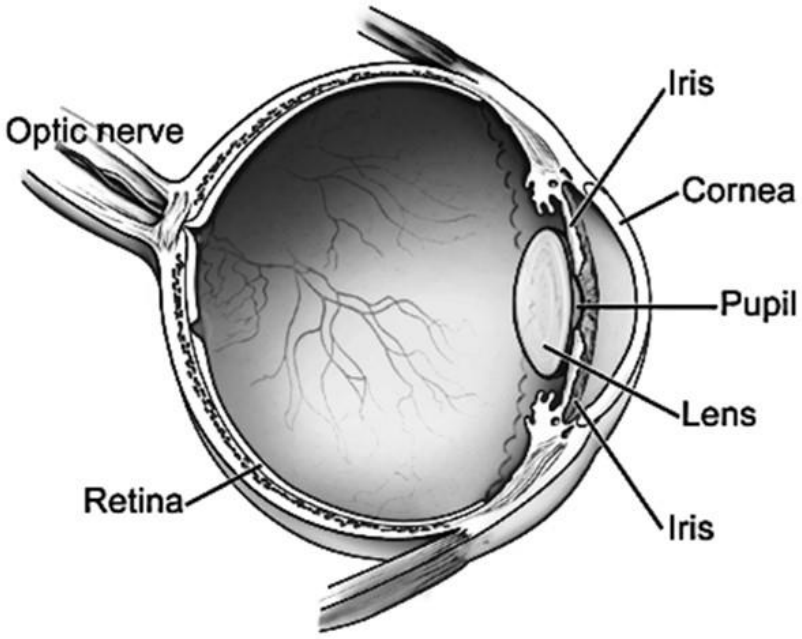

Figure 1:5: Diagram of the human eye. The cornea is the point of adhesion for *A. castellanii* trophozoites during infection. (Author/Copyright holder: National Eye Institute. Copyright terms and licence: Public Domain).

The pathogenesis of AK consists of corneal epithelial adhesion, extensive corneal desquamation, stromal invasion and neuritis, which begins with the secretion of 130kDa MBP on the trophozoite membrane. Though the mechanism of host cell adhesion is not yet fully understood, this adhesion heralds some interaction that leads to host cell cycle arrest by interrupting and inhibiting their signalling pathways (Lorenzo-Morales et al., 2015). The interaction between the organism and host cell triggers the release of various proteinases: neuraminidases, superoxide dismutases, Acanthamoeba-induced plasminogen activation, elastases, cytotoxic proteases, phospholipases and glycosidases (Lorenzo-Morales et al., 2015). The secreted enzymes instigate the desquamation of epithelial cells through cytolysis, phagocytosis and apoptosis, during which the instigation of PI-3k mediated cellular death occurs (Sissons et al., 2005). In an *in vitro* study where *A. castellanii* was inoculated into tissue culture the result was suggestive of a cytopathic effect of the proteinases triggered during parasite-host cell interaction (Visvesvara et al., 2007).

The factors that affect pathogenesis of AK can either be physical or environmental. These factors can happen directly or indirectly. Direct factors include the presence of MBP, cellular phagocytosis, expression of ecto-ATPases which have cytotoxic capabilities and regulate contact-dependent and -independent mechanisms, and neuraminidase activities, which can initiate corneal damage suggestive of the colonization of the organism (Siddiqui and Khan, 2012). Other direct factors include, superoxide dismutase with anti-oxidative properties, elastase which degrades connective tissues, proteases which exhibit cellular degrading properties, phospholipase which breaks up phospholipids leading to cell invasion and lysis, and glycoside which encourages cellulose degradation in cells (Lorenzo-Morales et al., 2015; Siddiqui and Khan, 2012). The indirect factors include cellular differentiation into cyst or trophozoite forms which is reversible based on favourable or unfavourable physical conditions as earlier described (physiologic tolerance, chemotherapeutic resistance, and host response to organism, osmolarity, ambient temperature, food, pH, and chemotherapeutic compounds) (Lorenzo-Morales et al., 2015). Though the mechanism of adaptation for strains of *A.*

castellanii in extreme conditions is not yet understood, it is thought that their virulence involves their ability to withstand the range of factors mentioned (Khan, 2006b; Siddiqui and Khan, 2012). The ability of *A. castellanii* to encyst outside and inside the host environment indicates that infection can be sustained by the cyst form when the already infiltrated trophozoite form undergoes encystation. The persisting cyst can cause re-infection after excystation occurs (Lorenzo-Morales et al., 2015).

Although there is geographical variation in the incidence of AK (Baig et al., 2013b), it can be related to the wearing of contact lenses, especially by individuals who are oblivious to the inherent risks of use in conditions of poor hygienic practices that support the virulent *A. castellanii* organism. The use of non-sterile disinfecting solution has also been reported as a major source of infection (Bryant et al., 2007; Verani et al., 2009). With the introduction of cosmetic contact lenses, the population of people wearing contact lenses has increased, thereby increasing the number of individuals predisposed to AK. For non-contact lens users hygiene is the key factor, the infection only arises after an individual is exposed to contaminated soil, stored or flowing water (Clarke and Niederkorn, 2006b). AK has also been reported to arise following ocular surgical traumas (Dart et al., 2009).

1.6.2 Granulomatous amoebic encephalitis

GAE is a rare chronic disease of the brain and spinal cord which some scientists consider to be an opportunistic infection. It is fatal, especially for individuals with a compromised immune system, making it a noteworthy disease for immunocompromised individuals with a need for organ transplant. Individuals with bone marrow suppression due to chemotherapy or immunosuppressive treatments and use of excess steroids, excess use of antibiotics, diabetes, blood disorders, liver and kidney disease, systemic lupus erythematosus and AIDS patients all stand the risk of being infected (Martinez and Visvesvara, 1997; Khan and Siddiqui, 2009; Siddiqui and Khan, 2012; Thamtam et al., 2016). GAE does not exhibit visual pathognomonic signs through which it can be identified, but has clinical manifestations of fever and headaches as well as various neurological manifestations, which can include

hemiparesis, seizures, aphasia, ataxia, behavioural changes, nausea, intracranial pressure, severe meningeal irritation, encephalitis and coma (Martinez, 1991; Martinez and Visvesvara, 1997; Khan, 2010). Pathological representation of the infection seen during brain autopsies includes severe oedema and haemorrhagic necrosis, and severe angitis and fibrinoid necrosis of the vascular wall with perivascular cuffing by lymphocytes and plasma cells with microscopic signs of *A. castellanii* cyst in Virchow–Robin spaces of the basal ganglia and midbrain (Lu et al., 1999; Siddiqui and Khan, 2012; Matsui et al., 2018).

Like AK, the pathogenesis of GAE ensues after the organism has gained entrance into the host (Figure 1:6). It progresses by adhering to target cells using its acanthopodia enabled by the secretion of MBP, which coats the organism's surface (Garate et al., 2004). Entry into the host is presumably through pulmonary inhalation or skin lesions and has also been found in nasal airways of asymptomatic individuals, followed by its dissemination through haematogenous means (Khan, 2007; Lackner et al., 2010). The risk factor for the skin lesion mode of transmission is predicated on the presence of trauma in the form of surgical sites, and bite marks from man and animals (Walia et al., 2007). It has not been possible to determine the source of the infection in established cases due to the length of the incubation period (might be up to months) between infection and clinical manifestation (Martinez and Janitschke, 1985). Once the organism is in the blood, its entry into the CNS is via the BBB (Siddiqui and Khan, 2012).

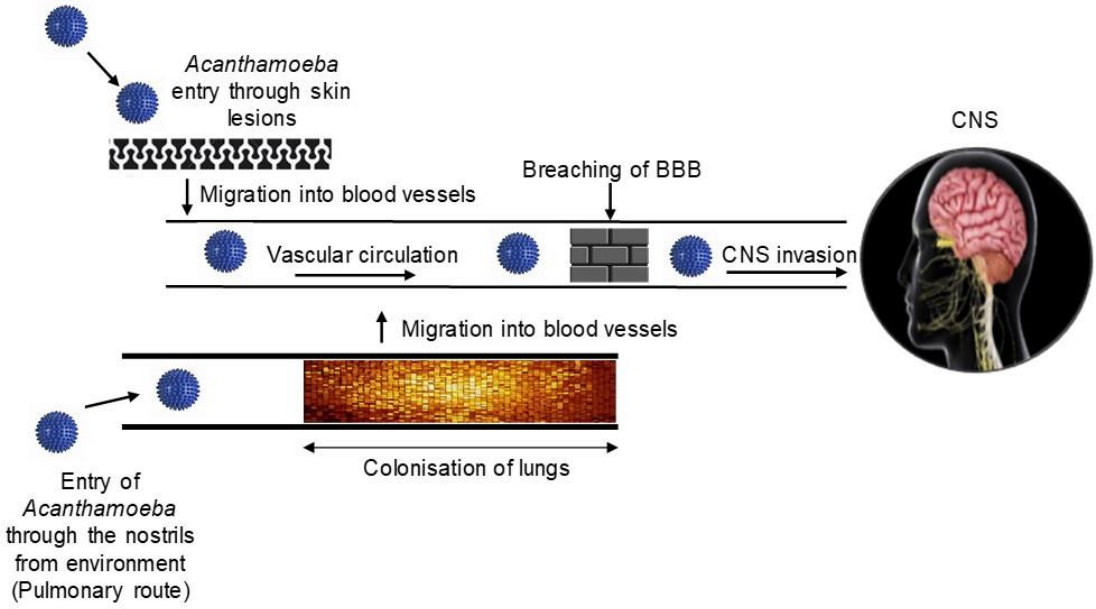

Figure 1:6: Schematic of systemic *Acanthamoeba* invasion leading to granulomatous amoebic encephalitis (BBB: blood-brain barrier, CNS: central nervous system)

Although the interaction of *A. castellanii* trophozoites with the BBB is not yet fully understood, an *in vitro* study with human brain microvascular endothelial cells (HBMECs) used to simulate the BBB showed that the parasite can cross the HBMECs after altering its integrity by degrading the occludin and zonula occludens-1 tight junction proteins, which increases their penetrability to the parasite (Khan, 2007; Khan and Siddiqui, 2009). Another study suggests that the penetration of the BBB by *A. castellanii* occurs via the degrading of types I and IV collagen, elastin, fibronectin, fibrinogen, IgG, IgA, albumin, and haemoglobin by serine proteinase (Kong et al., 2000). When in contact with HBMECs, the characteristic instigation of PI-3k-mediated cellular death occurs. Expression of ecto-ATPases for caspase-3 activation, undisrupted parasite colonization enabled by neuraminidase activities, hydrolytic enzymes (elastases, phospholipases, glycosidases) and a mix of both essential and non-essential amino acids like serine and cysteine are involved in the pathogenesis of GAE (Siddiqui and Khan, 2012). Epidemiological studies of GAE using immunosuppression and incidence of

HIV/AIDS suggest that although the disease is rare, the mortality rate for recorded cases is more than 95% (Martinez and Visvesvara, 1997).

1.7 DIAGNOSIS OF *A. CASTELLANII* INFECTION

The nature of both GAE and AK makes for a challenging diagnosis. This requires an insightful decision for doctors to zero in on *A. castellanii* infections while an infected individual is still alive, especially for GAE. Since different clinical signs are presented for each form of infection, the technique for arriving at a tentative diagnosis will differ. Although magnetic resonance imaging (MRI) and computerized tomography (CT) scans are normally used when clinical signs associated with the central nervous system (CNS) are presented, these techniques do not provide any definitive evidence of GAE (Siddiqui and Khan, 2012). As such, there are no specific clinical, laboratory or radiology protocols to diagnose GAE infection. Microscopic examination of stained biopsies of the brain tissue, skin, or cornea by haematoxylin and eosin (H&E) staining and by immunofluorescence testing (Walia et al., 2007) is the most common mode of diagnosis. Definitive diagnosis is arrived at when the microscopic examination reveals trophozoites and cysts, and can be confirmed using molecular techniques (e.g., PCR) of the brain tissue (Coven et al., 2017); this is always done post mortem in cases of brain tissue infections. The inability of early detection of the diseases caused by *A. castellanii* may also be caused by the failure of the parasite to induce either delayed-type hypersensitivity (DTH) or serum IgG antibody against parasite antigens (Van Klink et al., 1997). In attempting to measure the immune responses of *A. castellanii* infection using AK, serological analysis of the serum IgG and tear IgA levels of healthy contact lens users showed that between 50-100% of them possess antibodies against *Acanthamoeba* antigens, with these levels being much lower for infected patients (Niederkorn, 2002; Clarke and Niederkorn, 2006a). It has also been shown that more than 80% of a diverse population of the world possess natural IgG antibodies against *Acanthamoeba* species (Brindley et al., 2009).

With the exception of severe cases of AK infection, which presents a high density of *A. castellanii* parasite that enables clinicians to detect trophozoites and cysts by direct or phase contrast microscopy of tissue samples (Lorenzo-Morales et al., 2015), arriving at a tentative diagnosis requires employing the use of *in vivo* confocal microscopy (IVCM) (Dart et al., 2009; Zhivov et al., 2010). IVCM is a non-invasive imaging technique for acquiring high-resolution images of corneal samples. Though the trophozoites may be hard to spot, the double walled cysts can be clearly seen using IVCM (Labbe et al., 2009; Zhivov et al., 2010). Other methods with high specificity include immunofluorescence assays, real-time polymerase chain reaction (RT-PCR) assays (Qvarnstrom et al., 2006; Riviere et al., 2006; Walia et al., 2007; Ikeda et al., 2012), 1H NMR spectroscopy (Siddiqui and Khan, 2012), polymerase chain reaction (PCR), and culture of corneal scrapes (Goh et al., 2018). Despite the use of IVCM and molecular techniques (e.g. PCR) as alternative diagnostic techniques (Mathers et al., 2000), definitive diagnosis still relies on tissue culture, which is a time consuming method. Researchers are working to improve the sensitivity of existing molecular techniques and as such it is known that the efficiency of the PCR assay for rapid detection of *Acanthamoeba* spp. using genus-specific probes can be achieved by combining alumina nanoparticles with optimal concentrations of graphene oxide and copper oxide as a nanoPCR assay (Gabriel et al., 2018).

1.8 PREVENTION AND CONTROL OF *A. CASTELLANII*

A. castellanii is an opportunistic organism with the ability to enhance the survival and virulence of other microorganisms. Studies using them as hosts for specific bacteria have shown the organism amplifying the virulence of the bacteria as seen with *Legionella pneumophila* which causes a fatal form of pneumonia (Legionnaires disease) (Swart et al., 2018), *Mycobacterium avium*, which is one of the most common causes of systemic bacterial infections in AIDS patients (Cirillo et al., 1997; Cirillo et al., 1999), and the fungus *Cryptococcus neoformans*, which causes meningitis in immunocompromised individuals (Steenbergen et al., 2001). The studies stated above show that the importance of the organism does not only lie with the

virulence of the organism but also the role of hosts as suggested in similar studies (Thewes et al., 2019). Their ability to host other microorganisms controls their incidence, especially for virulent species like the T4 genotype. Studies also suggest that *A. castellanii* is the host of Medusa virus enabled by the same phylogenies of many key genes as well as DNA polymerase, with their genome homologs including the same major capsid protein, and also their ability to permit lateral gene transfers (Yoshikawa et al., 2019). With respect to the known clinical forms of *A. castellanii* infection, control can be directed to proper management of possible modes of transmission as mentioned above.

1.9 TREATMENT OF *A. CASTELLANII* INFECTIONS

GAE and AK are rare infections, and this notion may be responsible for the limited interest in developing new anti-acanthamoebic drugs, and therefore delaying the discovery of more effective therapeutic protocols for *A. castellanii* infections. Though the infections caused by *A. castellanii* may be rare, the ≥90% mortality caused by cases of GAE makes it of high medical importance and also because of the limited known therapy (Marciano-Cabral and Cabral, 2003; Siddiqui et al., 2016a). So far, the treatment of *A. castellanii* infections has employed the use of biguanides and the combination of antibiotics. To improve therapeutic outcome, suggestions have been made to improve existing drugs, repurpose existing anti-microbial drugs, use natural compounds, and use siRNA therapeutics (Yousuf et al., 2016).

1.9.1 Biguanides

The most common treatment for *A. castellanii* infections involves the use of chlorhexidine gluconate (0.02% to 0.2%). This compound is a biguanide which is an antiseptic/antibacterial agent commonly used in dental and surgical practices. Chlorhexidine (CHX) is positively charged and thereby reacts with the negatively charged plasma membrane of the parasite, leading to the compromise of its structural integrity and imminent leakage of cytoplasmic contents, resulting in cell death (Jones, 1997). Although it is supposedly an effective anti-acanthamoebic drug, the concentration which will totally destroy infective parasites will also

impair the physiology of host cells (Jones, 1997; Siddiqui et al., 2016a), hence its limitation. Treatment with chlorhexidine has involved its combination with diamidines and neomycin, but their withdrawal leads to a relapse of infection (Siddiqui et al., 2016a). For the treatment of AK with chlorhexidine and any other topical drugs, there is always the need to regulate the concentration of topical agents used due to their adverse action on host cells. When this is done, the compounds lack the desired potency to inhibit parasite growth and halt infection, and also express a wide-spectrum of non-specific activity (Lim et al., 2008), making them less amenable for inclusion in empirical tests for mainstream production of anti-acanthamoebic drugs. Other biguanide compounds such as polyhexamethylene (0.02% to 0.06%) and alexidine have been tested in treating *A. castellanii* infections. Polyhexamethylene biguanide (polyhexadine or polyaminopropyl biguanide) (PHMB) mimics the action of chlorhexidine. It is known to interact with phospholipids of parasite cell membranes, also compromising their integrity and allowing for leakage of ionic composition and subsequently cell death (Siddiqui et al., 2016a).

1.9.2 Diamidines

Although biguanides are one primary class of compounds of choice for *A. castellanii* therapy, the use of diamidines in a combination therapy has been proposed with the possibility of producing a more desirable outcome. Diamidines act by modifying the structural integrity of the cell membrane, leading to its permeability; this is followed by the denaturing of cytoplasmic proteins and inactivation of cellular enzymes (Dart et al., 2009). The diamidines (pentamidine isethionate, propamidine isethionate and diminazene aceturate) are effective against trophozoites and cysts. Pentamidine acts synergistically with chlorhexidine, and propamidine shows an additive effect to the biguanide (Hay et al., 1994). Despite the promising effect of diamidines, the clinically resistant *A. castellanii* isolates cultured from human samples after their administration makes them contraindicative for monotherapy (Dart et al., 2009).

1.9.3 Antimicrobial combinations

To further improve efficacy during therapy, empirical treatment regimens combining antibiotics such as trimethoprim/sulfamethoxazole (Aichelburg et al., 2008), ketoconazole (Singhal et al., 2001), dicloxacillin, ciprofloxacin, voriconazole, amphotericin B (Walia et al., 2007), fluconazole, rifampin, pentamidine and macrolide have been carried out (Visvesvara et al., 2007; Maritschnegg et al., 2011). These drugs have not given the desired therapeutic effects. An investigational drug miltefosine, which is an alkylphosphocholine, has also been reported to cure a case of GAE, but rehabilitation in a specialized neurological institution for rehabilitation did not improve the ataxic condition or hearing impairment of the patient (Aichelburg et al., 2008). Other compounds like heterocyclic alkylphosphocholines (APCs) (Garajova et al., 2014) demonstrate strong efficacy *in vitro* against *A. castellanii* trophozoites. Despite reported success in some cases (Walia et al., 2007), the use of current antimicrobials is still a lengthy and rigorous process with a possibility of infection relapse.

1.9.4 Repurposed therapeutics

In the quest for exhausting the potential of existing medications, researchers have tried repurposing existing medications for their promising anti-acanthamoebic activity. In a study (Anwar et al., 2019c), three clinically available antidiabetic drugs Glimepiride, Vildagliptin and Repaginate were evaluated for their possible anti-acanthamoebic activity. In the study, these drugs were conjugated with silver nanoparticles (AgNPs) to enhance their anti-acanthamoebic effects, the drugs showed trophocidal and cysticidal effects against *A. castellanii* and significantly blocked the encystation. In another study, Ethylenediaminetetraacetic acid (EDTA) and pirenoxine eye drops which are recognised Ca^{2+} chelating agents, were used in depleting Ca^{2+} of clinically obtained *A. castellanii* trophozoites. This resulted in the inhibition of growth and viability of trophozoites (Baig et al., 2019). Amlodipine, loperamide, and prochlorperazine which are FDA-approved drugs (Baig et al., 2013a), procyclidine, used as anti-Parkinsonian agent (Elsheikha et al., 2020), have shown some potency against *Acanthamoeba*. An *in vitro* study with gentamicin and gatifloxacin also showed anti-

amoebicidal activity of these drugs (Thongseesuksai et al., 2019). With recurring keratitis after taking single prescription medications, drug combinations become necessary which as earlier stated still do not do the work of eradicating the *A. castellanii*, making repurposing of existing drugs still necessary. Another of such drugs is corifungin, which is a water-soluble polyene macrolide reported to show disruption of cytoplasmic and plasma membranes and alterations in mitochondria of *N. fowleri* trophozoites. Corifungin caused definitive lysis of the *Amoebae* and also induced encystation of *A. castellanii* trophozoites which ended in the lysis of the encysted *Amoebae* (Debnath et al., 2012; Debnath et al., 2014). Haloperidol and loperamide combination which target important cellular receptors and biochemical pathways of parasites have also been seen to be highly effective against *A. castellanii*, digoxin and amlodipine combinations have also been seen to be effective (Kulsoom et al., 2014).

1.9.5 Alternative therapeutics

To increase the prospect of managing *A. castellanii* infections in light of suboptimal medication, some alternative therapeutics are being investigated. Photodynamic chemotherapy which employs the use of light-sensitive medication and a light source to destroy cells (Ferro et al., 2006), pathogen reduction therapy by the combination of ultraviolet light A (UVA) and riboflavin (B2) (Khan et al., 2011), and silencing or knocking down specific mRNA using synthesized siRNA (Lorenzo-Morales et al., 2010) are some of the alternative therapeutics proposed for *A. castellanii* infections. Due to the inability of existing drugs to cross the BBB and reach the CNS without damaging the host cells in cases of GAE, some other alternative therapeutics have involved the conjugation of metal nanoparticles and anti-*A. castellanii* drugs for increased drug delivery to targeted sites during infections (Anwar et al., 2018). Experimental triggering of anti-acanthamoebic potential of titanium oxide by ultraviolet radiation *in vitro* (Gomart et al., 2018), improved photochemotherapy with zinc doped titanium oxide nanoparticles (Imran et al., 2016), improving of commercial lens disinfection solution with gold and silver nanoparticles (Niyyati et al., 2018). The use of cobalt nanoparticles as anti-acanthamoebic compounds (Anwar et al., 2019a) and other experimental studies have

also shown anti-acanthamoebic activity of unconjugated metal nanoparticles against *A. castellanii*. Another study employed the use of synthetic dihydropyridines which exhibited amoebicidal and cysticidal activity with low cytotoxicity against human cells (Anwar et al., 2019b).

1.9.6 Nutraceuticals

Studies are delving into the use of natural sources for experimental *in vitro* studies with the hope of identifying molecules locked within these sources that might be the answer to combating *A. castellanii* infection. The assessment of Olive Leaf Extracts (OLE) against A. castellanii trophozoites showed dose dependent parasite inhibition (Sifaoui et al., 2013). This was followed up to identify the molecules involved such as apigenine, which was present in the plant. With PI-3k mediated *Acanthamoeba* death seen in the study above, apigenine was revealed as a prospective inclusion in anti-acanthamoebic therapy (Sifaoui et al., 2017). Another study employing aqueous extract of *Trigonella foenum graecum* showed *in vitro* activity against trophozoites and cysts with no cytotoxicity against corneal cells (Dodangeh et al., 2018). *Trigonella foenum graecum* seeds against *A. castellanii* forms exhibited amoebicidal and cysticidal activity (Dodangeh et al., 2018). The methanolic extract of fenugreek (*Trigonella foenum-graecum*) was tested against *Acanthamoeba* cysts, which displayed amoebicidal activity (Kaya et al., 2019). *Ornithogalum sigmoideum* leaves, flowers and stem also exhibited amoebicidal and cysticidal activity(Kaynak et al., 2018). Chloroformic fraction of *Ziziphus vulgaris* exhibited amoebicidal activity to both forms of the parasite (Dodangeh et al., 2017). *In vitro* studies and *in vivo* testing of tea tree oil in treatment of *Acanthamoeba* infection solid medium containing non-nutritional agar (NN) covered with *Aerobacter aerogenes* bacteria exhibited amoebicidal (Hadas et al., 2017a). Ethanolic extracts of *Centaurea bella*, *Centaurea daghestanica*, *Rhaponticum pulchrum*, and *Tanacetum vulgare* also exhibited amoebicidal and cysticidal activity. Other studies including the use of Tunisian *Thymus capitatus* essential oil (Saoudi et al., 2017), *Pericampylus glaucus* (Mahboob et al., 2017), and olive leaf extracts (Sifaoui et al., 2013; Sifaoui et al., 2017) all showed anti-

acanthamoebic activity. Using methanolic extracts of *Origanum syriacum* and *Origanum laevigatum* was also seen to exhibit dose-dependent amoebicidal activity on *A. castellanii* trophozoites and cysts (Degerli et al., 2012). *Teucrium polium* and *Teucrium chamaedrys* which have historic reputation as weight loss remedy in France have also been reported to exhibit amoebicidal action on *A. castellanii* trophozoites and cysts (Tepe et al., 2012). *In vitro* amoebicidal activity of four *Peucedanum* species on *A. castellanii* cysts and trophozoites were studied with their methanolic extracts, exhibiting time and dose-dependent amoebicidal action on the trophozoites and cysts (Malatyali et al., 2012). Acanthamoebic activity of shoots from *Eryngium alpinum in vitro* cultures and *in vivo* experiments exhibited notable time and dose-dependent amoebicidal action against *A. castellanii* trophozoites (Kikowska et al., 2020). Fractions of ethanolic extracts obtained from leaves and roots of *Eryngium planum* (*Apiaceae*) were evaluated *in vitro* for amoebicidal activity against *A. castellanii* with the phenolic acid fraction exhibiting amoebicidal activity on trophozoites (Derda et al., 2013). Evaluating the methanolic extract of *Peganum harmala* seeds on *A. castellanii* cysts and its encystment mechanism showed that it exhibited amoebicidal effects against *Acanthamoeba* cysts and inhibited encystation (Shohaib et al., 2016). Of all the listed experiments with natural products, there is yet to be a record of any of them transitioning into further studies earmarked as a mainstream candidate for final anti-acanthamoebic medication. The inability of the transition to *in vitro* experiments to the mainstream drug production can be caused by a number a factors which might include the inability of the most active chemical components of the screened natural products to exhibit anti-acanthamoebic activity outside its crude state which contains more compounds with synergistic potential to its activity.

1.9.7 *Camellia sinensis* use against infections

Of the scores of experiments and screenings of natural products for possible acanthamoebic activity, none of the studies have screened or tested *Camellia sinensis* (green tea) for its possible amoebicidal or cysticidal potential on *A. castellanii* trophozoites and cysts. *C. sinensis* originating from China is one of the many types of tea (Butt et al., 2014). *C. sinensis* is known

to contain bioactive compounds such as polyphenols including flavanols, flavandiols, flavonoids, and phenolic acids, which account for 30% of the dry weight of green tea leaves (Namal Senanayake, 2013; Zhong et al., 2014). It also contain catechins as well as (−)-epicatechin (EC), (−)-epicatechin-3-gallate (ECG), (−)-epigallocatechin (EGC), and (−)-epigallocatechin-3-gallate (EGCG) (Mukhtar and Ahmad, 2000) and caffeine which is its primary alkaloid and a CNS stimulant (Perva-Uzunalic et al., 2006), amino acids, sterols, vitamins and other components. Catechins are flavonoids with antioxidant and antiviral capability which is useful for disease prevention, and reduction of free radicals in the body, amongst other health benefits (Srichairatanakool et al., 2006; Sanlier et al., 2018; Yang et al., 2019; Katada et al., 2019; Liou, 2021). Reviews looking into different animal and clinical studies of *C. sinensis* and its catechins suggest that it is effective against metabolic syndrome, dyslipidaemia, obesity, diabetes and hypertension (Esmaeilpanah et al., 2021) and also against mouth bacteria. These range of bioactivities makes the *C. sinensis* catechins possible biochemical additives in mouthwash manufacture (Servin et al., 2021). In a quest to find cures for management of Alzheimer's disease using animal studies, it was reported that green tea extract suppressed amyloid β levels and alleviated cognitive impairment by inhibiting amyloid precursor protein (APP) cleavage, thus preventing neurotoxicity (Kan et al., 2021). In related study about cognitive function, the results suggested that high temperature processed-green tea extract could alleviate cognitive impairment by regulating synaptophysin expression and DNA methylation levels (Bae et al., 2020). Several studies have focused on extraction of the polyphenols of *C. sinensis* (Perva-Uzunalic et al., 2006; Namal Senanayake, 2013; Monsanto et al., 2014). *C. sinensis* extract has also been analysed and its anti-tumour activity investigated (Mukhtar and Ahmad, 2000; Adhami and Mukhtar, 2007; Dai and Mumper, 2010; Feitelson et al., 2015; Yang et al., 2019). To improve drug delivery, studies have shown that *C. sinensis* components conjugated into nanoparticles can be used for targeted prophylactic treatment without their bioactivity being lost during oral administration (Natarajan et al., 2019).

Studies have also shown anti-parasitic effects of *C. sinensis* by investigating its components against *Plasmodium falciparum* (Thipubon et al., 2015), where it reinforces the antimalarial effects of artemisinin without interfering with the folate pathway (Sannella et al., 2007; Thipubon et al., 2015). *C. sinensis* has also been tested against *Haemonchus contortus* for the reduction of worm burden (Zhong et al., 2014), *Leishmania braziliensis* against its promastigote and amastigote forms(Inacio et al., 2014), the inhibition of *Leishmania* (*Leishmania*) *amazonensis* arginase (dos Reis et al., 2013; Inacio et al., 2013), *Babesia* parasites (Aboulaila et al., 2010), the anticoccidial effect on *Eimeria* parasites (Jang et al., 2007), Anti-*Trypanosoma cruzi* activity (Paveto et al., 2004), and other parasites, thereby making it an important health benefit. In another study using Adult Motility Assay, *C. sinensis* exhibited *in vitro* anthelmintic activity against *H. contortus* (Zaheer et al., 2019). A study which looked at reducing cardiovascular disease risk factors related to high doses of anabolic androgenic steroids as seen in young athletes and non-athletes (Silva et al., 2019) showed that *C. sinensis* consumption by lab rats lessened inflammation and thickening of heart walls by reducing the expression of inflammatory cytokines. Of all the studies done so far, none has looked at the possibility of the anti-acanthamoebic or amoebicidal activity of *Camellia sinensis*. Furthermore, of all the experiments conducted with natural products few of them investigated the activities of extract fractions made up of phenolic compounds and saponins (Kikowska et al., 2020; Dodangeh et al., 2017; Derda et al., 2013). Also, only a few studies progressed further to identify and test the active component of the natural products which might possess anti-acanthamoebic capability. The investigation of Tunisian *Thymus capitatus* organic extracts revealed thymol and 2,3dihydroxy-p-cymene as its active molecules which exhibited anti-acanthamoebic activity *in vitro* in its naturally fractionated form (Saoudi et al., 2017). Another study investigating the activity of 24 chemically synthesized molecules of olive leaf extracts *in vitro* revealed that 4 of the molecules namely; vanillin, vanillic, syringic and ursolic acids possess an interesting amoebicidal activity (Sifaoui et al., 2017). As earlier mentioned, none of these studies progressed to *in vivo* experimentation.

1.10 RESEARCH AIMS AND OBJECTIVES

There are known chemotherapeutic agents for the treatment of *A. castellanii* but some of these require long term treatment, which can be complicated by secondary microbial infections, complexity of existing treatment regimen and the development of chemotherapeutic resistance. This has made the current therapeutic management of *A. castellanii* infections inadequate. With the waning of therapeutic studies focused on developing new anti-acanthamoebic drugs, suggestions have been made for the re-purposing of existing FDA-approved drugs as anti-acanthamoebic. The substances of choice are chosen based on their reported clinical efficacy. These drugs might not yield a sustainable degree of efficacy based on the dynamic nature of the organism. Furthermore, suggestions in therapeutic ventures have been made to target the cyst wall by understanding its chemical composition, but these *in vitro* discoveries have not led to desirable *in vivo* results, thereby preventing them from further consideration in conventional anti-acanthamoebic drug development. In the same vein, targeting the adherence mechanisms of the parasite without affecting host cell mortality is still being studied. Definitive chemotherapies which exhibit cytotoxicity against *A. castellanii* trophozoite and parasite-host cell adhesion have not been achieved. This frontier, if understood, will allow for development of effective chemotherapeutic protocols against the dynamic nature of *A. castellanii*.

1.10.1 Research hypothesis

This study assessed the hypothesis that the natural product *C. sinensis* (green tea) possesses acanthamoebicidal capabilities.

Thus, the overall aim of this research was to determine the possible acanthamoebic, trophocidal and cysticidal capability of *C. sinensis*. The objectives of this project were;

1. To investigate the inhibitory effects of *C. sinensis* forms on the growth kinetics of *A. castellanii* trophozoites and their ability to establish cysts and also to excyst from cysts to trophozoites.

2. To determine the intracellular and extracellular ultrastructural changes of *A. castellanii* when exposed to *C. sinensis*, using transmission electron microscopy (TEM) and scanning electron microscopy (SEM).
3. To determine the efficacy of *C. sinensis* analytes/ active ingredients vis-à-vis their industrial chemical standards counterpart on the growth of *A. castellanii* trophozoites, the cysts and encystation. The mechanism of action of each or a cocktail of specific active ingredients were determined.
4. To Determine changes in the protein expression of *A. castellanii* in response to exposure to *C. sinensis* brew and solvent extract using High performance liquid chromatography (HPLC), fluorescence assays, Data-independent acquisition mass spectrometry (DIA-MS), and Fourier-transform infrared spectroscopy (FTIR).

2 GENERAL MATERIALS AND METHODS

2.1 PREPARATION OF CULTURE MEDIA

2.1.1 Proteose-peptone-Glucose-Yeast Media

Standardized Proteose-peptone-Glucose-Yeast (PGY) media was prepared by dissolving 10g of 10% D-(+)- Glucose monohydrate (SIGMA-ALDRICH CHEMIE GmbH, France), 7.5g of Yeast Extract (SIGMA-ALDRICH CHEMIE GmbH, France) and 7.5g of Proteose-Peptone (SIGMA-ALDRICH CHEMIE GmbH, Spain) in 500mL of distilled water. This mixture was shaken vigorously, autoclaved for 2 hours and stored at 4^0C. The medium was warmed up in a water bath (Clifton: Scientific Laboratories Supplies, UK) at 37^0C prior to each use. PGY was used as the negative control medium for the duration of the study.

2.1.2 M199 complete medium with 20% foetal bovine serum

100 mL of foetal bovine serum (FBS), 5 mL of L-Glutamine (L-Glut) (Sigma-Aldrich, USA) and 5 mL of Antibiotic-Antimycotic (AbAm, Sigma-Aldrich, USA) were added to 500 mL of M199 (Sigma-Aldrich, UK) and mixed properly. After the preparation, aliquots were measured out into 50 mL centrifuge tubes (Falcon, Corning Science Mexico) by sterilising through a 0.22µm Millipore syringe filter (MILLEX®-HA, Ireland). The media was stored at 4^0C and warmed up in a water bath (Clifton: Scientific Laboratories Supplies, UK) at 37^0C prior to use.

2.1.3 Epilife Growth Medium

500 mL Epilife growth medium (Gibco Life Technologies, UK) was supplemented with 5 mL of Human Keratinocyte Growth Supplement (HKGS) (Invitrogen Life Technologies, UK) and 5 mL of AbAm (Sigma-Aldrich, USA). The medium was stored at 4^0C and warmed up in a water bath at 37^0C prior to use.

2.2 REAGENTS

2.2.1 10% Trichloroacetic acid

10% Trichloroacetic Acid (TCA) was prepared by dissolving 10gm of Trichloroacetic Acid (Fisher Scientific, Belgium) in 100 mL of distilled water. This was stored at 4^0C.

2.2.2 Tris Base

Tris-base buffer was prepared by addition of 1.21gm of Tris(hydroxymethyl)aminomethane (Fisher Scientific, Belgium) to 1000 mL of distilled water. The buffer was adjusted to 10nM with 1N NaOH and measured with a benchtop pH meter (Orion 3 Star, Thermo Electron, USA). The buffer was stored at 4^0C.

2.2.3 1% Acetic Acid

1% acetic acid was prepared by adding 10 mL of Glacial acetic acid (VWR Chemicals, France) to 990 mL of distilled water.

2.2.4 Sulforhodamine B dye

Sulforhodamine B dye (SRB) in 1% acetic acid was prepared by dissolving 4g of SRB dye (Sigma-Aldrich, USA) in 100 mL of 1% acetic acid in water

2.2.5 Acridine orange dye

Acridine orange dye (10mg/mL) was prepared by dissolving 1g of acridine orange crystals (ThermoFisher, UK) in 100 mL of distilled water.

2.2.6 Electron microscopy fixative

To prepare the primary electron microscopy (EM) fixative, 0.2M Cacodylate buffer (Tube B: 2.5mL) was added to 25% EM Glutaraldehyde (Tube G: 600µl) with a final concentration of 3% Glutaraldehyde. This was used immediately after preparation and stored at 4^0C if when not used immediately. The reagent 25% EM Glutaraldehyde comes pre-made as 600µl while 0.2M of Cacodylate comes in a pre-made volume of 2.5 mL and 1.9 mL of distilled water. The

fixative was used at the same temperature as the sample to be fixed to reduce physiological changes to the sample.

2.2.7 0.1M Cacodylate wash buffer

This was prepared by mixing equal volumes of 0.2M Cacodylate stock solution and distilled water.

2.2.8 3% Agarose (Low gelling)

This was prepared by adding 100 mL of distilled water to 3g of Agarose (low gelling) (Sigma-Aldrich, USA) and heated for approximately 1-2 minutes in the microwave to change its form from the liquid suspension to a gel. The solution was mixed properly and stored at 4^0C. The solution was heated in the microwave for about 5 seconds prior to use to liquefy it slightly.

2.2.9 Transmission Electron Microscopy Epoxy Resin

25 mL Araldite CY121 Resin (TAAB Laboratories, UK), 15 mL Agar 100 resin (Agar Scientific, UK), and 55 mL Dodecenyl succinic anhydrate (DDSA) (TAAB Laboratories, UK), respectively were weighed into a tripour beaker and stirred well with a wooden spatula. 2 mL Dibutyl phthalate (Agar Scientific, UK) and 1.5 mL Dimethylaminomethyl phenol (DMP-30) (TAAB Laboratories, UK) were weighed into the mixture and stirred well until there were no striations and the bubbles were evenly distributed. The mixture was stirred until the colour changed from red/orange to orange and was covered with a tin foil to limit exposure and spillage.

2.2.10 1% Osmium tetroxide

This was prepared by mixing 2% osmium tetroxide with 0.2M Cacodylate buffer stock solution at a 1:1 ratio.

2.3 BUFFERS

2.3.1 Standardised encystation buffer

Standardised encystation buffer (hyperosmotic medium) was prepared by dissolving 10g of glucose monohydrate, 0.48g of magnesium chloride (Sigma-Aldrich, UK) and one PBS tablet (Gibco®, Life technologies, UK) in 100 mL of distilled water. This suspension was filtered into a sterile bottle using a 0.45µl Millipore syringe filter (MILLEX®-HA, Ireland). The positive control included standardized encystation medium supplemented with 5% phenyl-methanesulfonyl fluoride solution (PMSF) (Sigma-Aldrich, Switzerland).

2.3.1 *C. sinensis* brew encystation buffer

C. sinensis encystation medium was prepared by dissolving 10g of glucose monohydrate, 0.48g of magnesium chloride (Sigma-Aldrich, UK) and one PBS tablet (Gibco®, Life technologies, UK) in 100 mL of already prepared sterile C. sinensis cold brew. This suspension was filtered into a sterile bottle using a 0.45µl Millipore syringe filter (MILLEX®-HA, Ireland).

2.3.2 1% sodium dodecyl sulfate buffer

Sodium dodecyl sulfate (SDS) (cyst digestion buffer) was prepared by dissolving 1g of Sodium dodecyl sulfate (Fisher Scientific, Japan) in 100 mL of distilled water.

2.4 PREPARATION OF *CAMELIA SINENSIS* (GREEN TEA)

2.4.1 Sterile *C. sinensis* brew solution

Dried *C. sinensis* (green tea) leaves used in the experiments were purchased off the shelf from different local tea stores in Lanzhou, Gansu Province, China. Sterile *C. sinensis* (green tea) brew was prepared in two forms: hot and cold brews. The hot brew was prepared by heating 550mL of distilled water in a loosely capped glass bottle (Fisher Scientific, UK) in the microwave for 5 min at high power. The volume was adjusted to 500mL and 5g of pulverised *C. sinensis* leaves were added. This mixture was shaken and left to stand for 10 min, then

filtered using a 500mL 0.22µl Stericup® vacuum filtration unit (Merck, UK). The cold brew was prepared by weighing 5g of pulverised *C. sinensis* leaves into a glass bottle containing 500mL of cold distilled water. The mixture was incubated at 4°C for 24 h and filtered as described for the hot brew. The solutions were stored at 4^0C and warmed up as previously described before being used. Samples of each of the tea purchased were tested in a pilot study to ensure all had the same or similar activity as they were all supposedly grown and processed with the same technique.

2.4.2 *C. sinensis* brew-PGY Media

C. sinensis-PGY medium was prepared by dissolving 10g glucose monohydrate, (Sigma-Aldrich, France), 7.5g of yeast extract (Sigma-Aldrich, France) and 7.5g of proteose-peptone (Sigma-Aldrich, Spain) in 500 mL of already prepared sterile *C. sinensis* brew. This was done to ensure that the base constituents of PGY media are also available in the *C. sinensis*-PGY media. This suspension was filtered as described above and stored in a glass bottle at 4°C. To make dilutions of *C. sinensis*-PGY medium, PGY medium was used a diluent to prepare lower concentrations of *C. sinensis*-PGY medium (25%, 50%, 75%, 100%).

2.4.3 *C. sinensis* brew encystation buffer

C. sinensis encystation medium was prepared by dissolving 10g of glucose monohydrate, 0.48g of magnesium chloride (Sigma-Aldrich, UK) and one PBS tablet (Gibco®, Life technologies, UK) in 100 mL of already prepared sterile C. sinensis cold brew. This suspension was filtered into a sterile bottle using a 0.45µl Millipore syringe filter (MILLEX®-HA, Ireland). The *C. sinensis* encystation medium was used in concentrations of 25%, 50%, 75% and 100% v/v with the standardised encystation buffer.

2.4.1 Solvent extraction of *C. sinensis*

The solvent extraction of *C. sinensis* was done using 2 solvents in a 2-step procedure. Methanol was used for step 1 and acetonitrile for step 2. The extraction was performed using the Soxhlet apparatus. Dried *C. sinensis* was ground to powder in a laboratory mill and

weighed into large sized Whatman® cellulose extraction thimbles (Sigma-Aldrich, UK) with 10 µm nominal particle retention, which was then plugged with cotton wool and placed in a Soxhlet apparatus. 500 mL of solvent was poured through the thimble into the 1 L round bottom flask allowing for an initial extraction of the sample prior to the commencement of the extraction cycles. The Soxhlet apparatus setup was placed on a hot plate (Radley's Tech, Germany) and the temperature set to 70^0C for methanol and 85^0C for acetonitrile, respectively. The solvent extraction was stirred at 25xg. The solvent extraction was carried out for 48 hours; 24 hours for each step. Both solvent extracts were pooled together and after cooling the combined extract was filtered using 0.22µl sterile cups (MILLEX®-HA brand, Ireland) under vacuum. The suspensions were evaporated to dryness in water bath set to 40^0C under vacuum with Rotavapor® R-300 rotary evaporator (BUCHI, Flawil, Switzerland). The solvent extracts were separated into active fractions using flash chromatography. LC-MS was used for the characterisation and identification of the components of the *C. sinensis* solvent extract and identified fractions.

2.4.1 *Camellia sinensis* solvent extract solutions

C. sinensis solvent extract solution was prepared at stock concentration of 10,000µg/mL containing 0.025% Dimethyl sulfoxide (DMSO). DMSO was used first to solubilize the solvent extract before addition of PGY as a homogenous solution could not achieved using only the water-based PGY. Firstly, 500mg of the sample was weighed into a 50 mL falcon tube and 2.5 mL of DMSO was added. This was placed in an ultrasonicator bath (Elma, Germany) for 15 minutes to form a homogeneous solution. Then, 47.5 mL of PGY media (which was used throughout the experiments as a negative control) was added to the initial solution to make up 50 mL of stock solution. The solution was filtered into a sterile 50mL falcon tube using a 0.22µl Millipore syringe filter (MILLEX®-HA brand, Ireland). Serial dilutions of 5000, 2500, 1250, 625, 312.5, and 156.25µg/mL were prepared from the stock solution using PGY as a diluent. In view of the possible cytotoxic effect of DMSO, which could erroneously increase sample anti-amoebic activity, additional wells containing the same 1:2 serial concentration of *C. sinensis*

to DMSO (5000-156.3 µg/mL) were prepared and accounted for during the final calculation of anti-acanthamoebic activity. For the cytotoxicity assays, *C. sinensis* serial dilutions (v/v) were prepared as described above using the respective cell culture medium as the diluent.

2.4.1 *C. sinensis* solvent extract encystation buffer

For *C. sinensis* solvent extract encystation medium, stock concentration of 10,000µg/mL was obtained by initially preparing a solvent extract solution as described above but using distilled water instead of PGY media. For the hyperosmotic encystation media, 10g of glucose monohydrate, 0.48g of magnesium chloride (Sigma-Aldrich) and one PBS tablet (Gibco®, Life technologies, ThermoFisher Scientific, UK) were dissolved in 100mL of the distilled water-*C. sinensis* solvent extract solution. This was stirred for 30 min and the suspension filtered into a sterile bottle using a 0.45µl Millipore syringe filter (MILLEX®-HA, Ireland).

2.4.1 *C. sinensis* chemical standards

The chemical standards of the 10 active components of *C. sinensis*, namely theogallin, theobromine, catechin, EC, EGC, ECG, EGCG, caffeine, kaempferol, myricetin. were purchased from Sigma-Aldrich (UK). These components were identified in *C. sinensis* by chromatography and HPLC profiling of the *C. sinensis* brew and solvent extract in this work as shown in sections 2.7.10, 2.7.11and 2.7.12. Stock solutions of each standard were prepared with PGY to a final concentration of 1,000µM.

2.4.1 *C. sinensis* chemical standards hyperosmotic buffer

To determine the possible inhibitory effect of specific chemical standards of *C. sinensis* on encystation dynamics, stock solutions of 1000 µM of EGCG and theobromine, respectively, were used as solvents for preparing serial dilutions of hyperosmotic solutions of each chemical standard for anti-encystation testing.

2.5 CULTURE CONDITIONS OF HUMAN CELL LINES

2.5.1 Corneal stromal cells

Corneal stromal cells (CSCs) were extracted from human corneal rims as described in another study (Sidney et al., 2015). The epithelial side of a corneal rim was placed down on a Petri dish and washed with some drops of phosphate buffered saline (PBS) fortified with Antibiotic-Antimycotic (AbAm, Sigma-Aldrich, USA). The sclera was carefully dissected with the aid of scalpel and forceps. The corneal rim was sectioned into 16 pieces and immersed in a collagenase solution in a 15 mL falcon tube (1 mg/mL collagenase, Sigma-Aldrich, UK). The immersed samples were incubated at 37^0C with 5% CO_2 for seven hours with a gentle agitation at the start of each hour. After the incubation, M199 (Sigma-Aldrich, UK) complete medium with 20% FBS was added to inhibit the action of collagenase. The solution was subsequently filtered with a 40µm cell strainer in a 50 mL falcon tube. The solution was centrifuged at 1,204xg for 5 minutes and the resultant pellet re-suspended in 5 mL of M199. The suspension was made homogenous by mixing with a tabletop vortex mixer (Thermo Scientific, Colchester, UK) and subsequently pipetted into a T-25 cm^2 tissue culture flask and incubated at 37^0C with 5% CO2. The culture media was refreshed every 2-3 days and the cells passaged at 80-90% confluency. CSCs used in the study at passages of 4-6.

2.5.2 Corneal cell passage

CSCs (passage 4-6) and iHCECs were harvested from T-75 flasks into 15 mL falcon tubes. This was done by pipetting previous media from the flasks, which was followed by the gentle but rapid washing of the cell monolayer with the addition of 5 mL of Dulbecco's PBS this was to wash off the culture media which might prevent the action of the dissociating agent to be used. 2 mL of TrypLE, an express dissociation reagent, was added into the culture flasks as a dissociation agent and they were incubated for 5-7 minutes at 37^0C temperature with 5% CO_2. The resulting physical representation showed the bottom of the flask being cloudy when observed under inverted light microscope showed dislodgement of cells from the flask surface.

The flask was also tapped gently on the countertop to ensure absolute detachment. 3 mL of FBS fortified respective media was added to the culture flasks and dispersed over the cell layer. The cell suspensions were transferred into 15 mL centrifuge tubes and centrifuged at 1,204xg for 5 minutes. Cell pellet was seen to form in the flask, the resultant supernatant was aspirated off and the pellet re-suspended in 3 mL of culture media. The cell suspension was dispersed in the tube by means of a pipette to ensure homogeneity of the suspension. Cell quantification was done using a Neubauer haemocytometer as earlier below().

2.5.3 SV40-Immortalised Human Corneal Epithelial Cell Line

Immortalised human corneal epithelial cell line (SV40-iHCEC) was constructed by infecting primary cultured human corneal epithelial cells with recombinant sv40-adenovirus vector. The infected cells were cloned thrice to obtain the immortalized cell line (Araki-Sasaki et al., 1995). The cells used for the experiments in this study were gifted by Felicity Rose (University of Nottingham, UK) to the academic ophthalmology department, University of Nottingham. They were maintained in 20 mL of Epilife growth medium supplemented with Human Keratinocyte Growth Supplement (HKGS) in T-75 cm^2 tissue culture flasks and incubated at 37^0C temperature with 5% CO2. The culture media was refreshed every 2-3 days and the cells passaged at 80-90% confluency of 10^4cell/cm^2 seeding density. iHCECs used in the study at passages of 30-35.

2.5.4 Madin-Darby Canine Kidney cells

The vial containing Madin-Darby Canine Kidney cells (MDCK) was removed from the liquid nitrogen and defrosted in a 37^0C water bath. After 2 minutes, the cell suspension had thawed, it was wiped down with 70% IMS and opened in the hood. Using a pipette, the contents of the vial (1.8ml of cell suspension) was transferred to a T25 flask and 20 mL of complete Dulbecco's Modified Eagle Medium (DMEM) supplemented with 20% FBS was added to the culture flask. The culture flask was gently swirled to ensure the cells were evenly distributed within the culture medium; this was confirmed under an inverted microscope and the flask

sprayed down with 70% IMS and placed in a humidified incubator at 37^0C with 5% CO_2. After 24 hours, the media was changed DMEM supplemented with 5% FBS and 2% Pen-Strep (details). The culture media was refreshed every 2-3 days and the cells passaged as described for corneal cells below at 80-90% confluency of 10^4 cells/cm^2 seeding density.

2.5.5 Measurement of viability of human cells

Host cell viability for the cells used in this study was determined prior to each experiment using the trypan blue exclusion method. Here, after the cells had been harvested and the trypsin or TrypLE (Gibco Life Technologies, UK) used as dissociation reagent had been removed by washing with the normal growth media, the cells were concentrated by spinning in a centrifuge and little volume of media added to the resultant pellet. The suspension was made homogenous and a sample of 10µl of cell suspension was mixed with 10µl of 0.4% Trypan Blue to make a 1:2 dilution in an Eppendorf tube. Suitable dilution factors were applied based on the concentrations of the suspension. The cell suspension/Trypan Blue was mixed gently, allowed to stand for 2 minutes and cell quantification was done using haemocytometer. Trypan blue stain is used to selectively colour dead cells blue which are identified by the dye's interaction with cells that have compromised cell membrane integrity (Mishell and Shiigi, 1980). Dark blue or faintly coloured cells are counted as dead (un-viable cells), while unstained cells are counted as live (viable cells). The percentage cell viability was determined with the formula below.

% Cell viability = Live cell count / total of cell count (stained + unstained cells) X 100

For the number of viable cells per mL of culture, the formular below was used.

Number of viable cells × 10^4 × dilution factor = cells/mL culture

2.5.1 Cytotoxicity of *C. sinensis* brews against corneal stromal cells

2.5.1.1 Cytotoxicity evaluations using SRB Assay

To determine the toxicity of cold and hot *C. sinensis* brew to corneal cells, CSC (passage 7-9) and iHCECs were used. After harvesting the respective cells and quantification as earlier described, 100ul of cell suspension was seeded into 96 well plates at 5×10^3 cells per well. The plates were incubated for 48 hours at 37^0C with 5% CO_2. After the incubation period, the media in the wells were aspirated out and the wells treated with graded concentrations of cold and hot *C. sinensis* brew. After treatment, the plates were re-incubated at 3, 24, 48 and 72 hours, respectively, based on the experimental design (see below). The experiment was designed to have treatment groups of 25%, 50%, 75% and 100% for hot and cold *C. sinensis* brew, respectively, in triplicates and a control group of M199 and Epilife growth medium (EPGM) for each respective corneal cell. After each incubation time, the viability of each treatment group was determined using SRB assay described in section 2.7.2.

2.5.1.2 Cytotoxicity evaluation by fluorometric quantification of RNA and DNA

Fluorometric quantification of RNA and DNA content in the CSCs post-treatment with both brews was achieved by using AO staining in a 96-well plate format. When AO binds to DNA, it exhibits an excitation at 502 nm (cyan) and an emission at 525 nm (green), and when it binds with RNA, the excitation is located at 460 nm (blue) and the emission is located at 650 nm. With the excitation and emissions from both nucleic acids, the level of fluorescent emitted can be proportionally related to the number of cells in each treatment sample

At each incubation time post-*C. sinensis* treatment as earlier stated, the media was aspirated from each well as earlier mentioned and the cells fixed with 30µl of methanol, which was left to stand for 15 minutes. After fixation, the wells were gently washed twice with distilled water. The wells were subsequently treated with 30µl of acridine orange dye, which was left to stand for 10 minutes and washed thrice with distilled water. 100µl of PBS was added to each well, and fluorometric quantification of RNA and DNA in the wells measured as relative fluorescent

unit (RFU) was done using a Varioskan Flash plate reader (Thermo Scientific, Finland). The excitation/emission was set at 460/650(nm) for ribonucleic acid (RNA) and 500/526 for deoxyribonucleic acid (DNA). SkanIt software 2.4.3 RE for Varioskan Flash was used.

2.5.2 Cytotoxicity of *C. sinensis* solvent extract on mammalian cells

2.5.2.1 Immortalised human corneal epithelial cells (iHCE-2s)

Cytotoxicity of the *C. sinensis* solvent extract was examined against immortalised human corneal epithelial cells (iHCE-2, CRL11135, ATCC, Manassas, Virginia, USA) using an established lactate dehydrogenase (LDH) assay (ThermoFisher Scientific, UK) as per the manufacturer's instructions. iHCE-2 cells were seeded into a Thermo Scientific™ Nunc MicroWell 96-well plate (ThermoFisher Scientific, Loughborough, UK), at 7.5 x 10^3 cells/well and grew to 80-90% confluency in the presence of growth media (consisting of keratinocyte serum free medium supplemented with human recombinant epidermal growth factor, bovine pituitary extract, hydrocortisone, and insulin). Cell cultures were incubated in a humidified atmosphere of 5% CO_2 at 37°C. iHCE-2 cells were subsequently incubated with graded concentrations of *C. sinensis* (1:2 serial concentration starting from 5000 µg/mL to 156.3 µg/mL) for 48 h. Appropriate controls were used, including 0.1% Triton X-100 as a positive control and growth media as a negative control. In view of the potential sedimentation of *C. sinensis* (which could erroneously increase the optical density (OD) reading, hence toxicity), additional wells containing the same 1:2 serial concentration of *C. sinensis* (5000-156.3 µg/ml), but without iHCE cells, were included so that the effect of sedimented *C. sinensis* solvent extract on the OD reading could be determined and accounted for during the calculation of cytotoxicity. At 24 and 48 h post-treatment, 50 µl of supernatant was obtained from each well and $OD_{490-680}$ was measured using BMG Clariostar microplate reader (BMG LABTECH Ltd., Aylesbury, United Kingdom). Cytotoxicity (%) was calculated using the following formula: [((Itreatment – INC) / (IPC – INC)) x 100; I=intensity]. The experiments were conducted in technical triplicate in two independent experiments.

2.5.2.2 Madin-Darby Canine Kidney cells

Madin-Darby Canine Kidney cells (MDCK) cultures were seeded in 96-well microplates at a density of 5×10^3 cells/well in 100 µl Gibco Dulbecco's Modified Eagle Medium (DMEM). Cell cultures were incubated in a humidified atmosphere of 5% CO_2 at 37°C. After 48 h of incubation, the medium was removed and the cultures were treated with *C. sinensis* solvent extract at the same above-mentioned concentrations and incubated and data collect at 3, 24, and 48 h experimental time. Parallel control wells contained MDCK cells with the respective medium only and without any exposure to *C. sinensis* solvent extract. At each time point of incubation, cell proliferation was determined using the SRB assay as described previously (Ortega-Rivas et al., 2016). The experiments were performed in technical triplicates in three biological settings.

2.6 *CULTURE CONDITIONS OF ACANTHAMOEBA CASTELLANII*

2.6.1 Cultivation of *Acanthamoeba castellanii*

The test organism *A. castellanii* strain of T4 genotype (American Type Culture Collection; ATCC 30011) was maintained in 20 mL of peptone-yeast-glucose (PGY) medium [proteose-peptone 0.75% (w/v), yeast extract 0.75% (w/v) and glucose 1.5% (w/v)] in T-75 Nunclon® cell culture flasks (ThermoFisher Scientific, Loughborough, UK) at 25°C in a humidified Stuart™ SI30H Hybridization bench top oven/shaker (Cole-Parmer Ltd, Staffordshire, UK) without rocking (Khan et al., 2000b). The culture medium was refreshed ~15 hrs before the commencement of each experiment to ensure that most of the culture was composed of vegetative trophozoites.

2.6.2 Quantification of *A. castellanii*

Before the commencement of any experiment, the *A. castellanii* trophozoites or cysts were quantified using a Neubauer haemocytometer (Neubauer-improved bright line, Marienfeld, Germany). For the adherent trophozoites, the culture flask(s) was placed on ice for 5-10 minutes, then tapped gently against the palm to dislodge adherent cells, and this suspension

was transferred into a 50 mL Falcon centrifuge tube. To ensure homogeneity of the suspension, it was mixed by placing the tapered based of the falcon tube on a vortex mixer set to medium speed for about 20 seconds. The haemocytometer was wiped with Kleenex and both sides of the counting chamber covered with haemocytometer coverslip. Both sides of the haemocytometer were loaded with 10µl of the suspension and the counting grid brought into focus at 10x magnification on an inverted microscope (CETI, Medline Scientific, UK). The average of the total count from each counting grid was taken and the cell concentration was calculated using the following formula:

Cell concentration (cells/ mL) = Total cells counted x dilution factor x 10,000

The number or trophozoites from the original sample was calculated by multiplying the cell concentration by the total volume from which the counted sample was obtained. The method described above was used in the course of the study for quantification of all the cell types prior to their use in respective experiments. The dilution factor aspect of the calculation was used for the host cell lines where viability of the cells was determined before seeding by using trypan blue exclusion method as described above (2.5.5).

2.6.3 Optimization of trophozoite seeding density

Here, we determined the optimal seeding density of *A. castellanii* trophozoites that were used in testing the anti-acanthamoebic activity of *C. sinensis*. Briefly, *A. castellanii* trophozoites at various numbers (1×10^3, 2.5×10^3, 5×10^3, 7.5×10^3 and $10x10^3$) were seeded in a volume of 100µl PGY medium/well in 96-well plates. Control wells included only 100µl PGY medium. The culture plates were checked under an inverted microscope (CETI, Medline, UK) to ensure the presence of trophozoites and incubated in a Stuart oven at 25°C. After 24, 48 or 72 h respectively, the plates were fixed and stained using the SRB assay as described below according to the protocol adapted for *A. castellanii* by Ortega-Rivas et al. (2016). The OD of each well was determined by measuring the colour absorbance spectrophotometrically at wavelengths of 450, 492 and 630nm using an L-T 4000 microplate reader (Labtech, UK). The

OD values of each seeding number were compared to the other seeding numbers and to the blank control at each of the examined time points (i.e., 24, 48 and 72 h).

2.7 EVALUATING EFFECTS OF *C. SINENSIS* ON *A. CASTELLANII*

2.7.1 Trophozoite growth inhibition evaluations using a haemocytometer

After determining the *Acanthamoeba* count, 1 mL of the suspension harvested earlier was pipetted into five 15 mL centrifuge tubes representing approximately 3.2 x 10^5 trophozoites in each tube. The tubes were labelled according to treatment group and centrifuged at 1,204xg for 5 minutes, the supernatant was discarded, and each resultant pellet was treated with 5 mL of the respective treatment media; *C. sinensis* brew or *C. sinensis* solvent extract. The respective suspensions were mixed using a vortex mixer aimed at ensuring homogenous mixture and also the detachment of adherent cells from the tube body. Each suspension was pipetted and seeded into its respective labelled T-25 Thermo Scientific™ Nunc tissue culture flask (ThermoFisher Scientific, Loughborough, UK), which were incubated at 25°C in a humidified Stuart™ SI30H Hybridization bench top oven/shaker without rocking. Controls included an equal number of trophozoites in PGY only (negative control) or in PGY supplemented with 0.02% Chlorhexidine (CHX) (positive control) and/ or 0.025% DMSO in PGY where needed. The flat base of the flasks had pre-divided and marked into 9 squares of which microscopic images will be recorded from 5 squares out of the 9. After 24, 48 and 72 hours respectively, trophozoites were counted using a haemocytometer and a CETI inverted microscope (Medline Scientific, UK) to determine the effect of each treatment group on the growth (numeric replication) of the trophozoites. For visual results of morphological changes, images were acquired semi-randomly from 5 squares out of 9 squares within the field of view with an inverted Leica DMIL CMS (Germany) inverted microscope running a Leica Application Suite (LAS version 4.3).

2.7.2 Evaluation of trophozoite growth inhibition using SRB assay

Without being able to analyse the cellulose, galactose and protein synthesis pathways being expressed during the in vitro anti-acanthamoebic activity of *C. sinensis* forms (brew or solvent extract) against trophozoites at this stage of the study, microplate based-SRB assay was used. SRB was used to assess the protein concentration in each of the treatment groups over time by determining the SRB dye absorbance of trophozoites exposed to *C. sinensis* at time intervals. SRB is a bright-pink aminoxanthene dye with two sulfonic groups that bind to basic amino acid residues under mild acidic conditions and dissociate under basic conditions (Vichai and Kirtikara, 2006). As the binding of SRB is stoichiometric, the amount of dye extracted from stained cells is directly proportional to the cell mass, hence SRB was used to determine trophozoite proliferation by assessing the protein quantity. After quantification of trophozoites as previously described, an approximate number of 2,500 trophozoites per well seeding density (Fakae et al., 2020) were seeded into 96-well microtiter plates in triplicates to achieve a final volume of 100µl/well per treatment group. The plates also incubated in a Stuart oven at 25^0C and SRB assay was conducted as described for *A. castellanii* (Ortega-Rivas et al., 2016). A spectrophotometer was used to quantify the OD of the wells after being treated with the dissociating agent tris-(hydroxylmethyl)-aminomethane. The recorded OD of the supernatant represents the spectrophotometric quantification of the protein concentration of the cells, which is directly proportional to the number of cells (e.g., increased OD correlates with increased protein content, which reflects an increase in the number of cells and vice versa).

After each incubation time, without removing respective media, 25µl of chilled 10% trichloroacetic acid (10% w/v) (TCA, Fisher, Belgium) was added per well and the plates were incubated for 1 h at 4^0C. The supernatant was discarded and the plates were washed gently with distilled water three times to remove TCA, PGY medium, and dead non-adherent cells, and were subsequently allowed to dry at ambient temperature. Then, 25µl of SRB solution (0.05% SRB dye dissolved in 1% acetic acid in water) was added per well and incubated for

15 min at ambient temperature. The plate was covered with aluminium foil to protect dye from light. After incubation, excess unbound SRB was removed by gently washing the plates with 1% acetic acid. After the plates had air-dried, cell protein-bound dye was solubilized by adding 150 µl of 10mM base solution (tris-(hydroxylmethyl)-aminomethane, pH 10.5) per well. The plates were subsequently placed on a see-saw oscillation rocker (Stuart, UK) for 7 min to achieve a homogenous suspension of the dye in the well's supernatant. The OD of each well was determined by measuring the colour absorbance spectrophotometrically at wavelengths of 450, 492 and 630nm using an L-T 4000 microplate reader (Labtech, UK). The OD values of each concentration were compared to the other concentrations and to the controls at each of the examined time points based on the experimental design (i.e., 3, 6, 24, 48 and 72 hr). All experiments were performed in triplicate, repeated independently at least three times and the mean values were also calculated.

2.7.3 Effect of transient exposure of *C. sinensis* on trophozoites

After determining the Acanthamoeba count, approximately 3.2 x 10^5 trophozoites from the suspension harvested earlier was pipetted into 15 mL falcon tubes. The tubes were labelled according to treatment groups and centrifuged at 1,204 xg for 5 minutes, the supernatant was discarded, and each resultant pellet was treated with 5 mL of the respective *C. sinensis* forms (brew or solvent extract). The negative and positive controls were the same as earlier mentioned. Each respective treatment group was seeded into a T-25 flask and incubated at 25^0C for 6 hours. The same procedure was conducted for 24 hours. At 6- and 24-hours post-treatment, the cells were harvested in 5 mL falcon tubes, washed with PBS and re-suspended in 5 mL of PGY, and incubated for 72 hours. At 24-, 48- and 72-hours post-incubation with PGY, haemocytometer count was conducted to determine the percentage of trophozoite growth inhibition.

With the number of trophozoites in the negative control determined as 100% growth, the growth of the treatment groups was calculated as follows;

Number of trophozoites in treatment / number of trophozoites in negative control x 100

2.7.4 Induction of encystation

T-75 flasks containing *A. castellanii* trophozoite culture were placed on ice for 5 minutes, tapped against the palm to dislodge adherent cells, and the suspension aspirated into a 50 mL centrifuge tube (Falcon, Corning Science Mexico). The suspension was centrifuged at 1,204xg for 5 minutes and the supernatant discarded. The resultant pellet was re-suspended in 20 mL of already prepared standardized encystation buffer (SEB). This was left for 72 h to ensure complete formation of cysts, which was confirmed by viewing under light microscopy. The cysts used for excystation experiments were taken from the T-75 flasks.

2.7.5 Inhibitory effect of *C sinensis* against trophozoite encystation

Approximately 6.2×10^5 *A. castellanii* trophozoites were pipetted into 15ml falcon tubes, which were labelled according to treatment groups. The tubes were centrifuged at 1,204 xg for 5 minutes, the supernatant was discarded, and each resultant pellet was treated with 6 mL of the treatment solution (brew or solvent extract). The negative control was an equal volume of standardized encystation buffer, while the positive control was standardized encystation buffer with 5% PMSF (Sigma life science, Switzerland). The suspension was mixed using the vortex mixer aimed at ensuring homogenous mixture and also the detachment of adherent cells from the tube body. Each suspension was pipetted into its respective T-25 flask. The flasks were labelled and placed into the Stuart oven at 25^0C. Using a haemocytometer, counting the number of trophozoites versus cysts for each concentration at 24, 48 and 72 h made it possible to determine the encystation rate of each treatment group. Images of each time course were taken with an inverted Leica DMIL CMS inverted microscope. All experiments were repeated three times and the mean values were calculated. After 72 hours, the respective treatment groups were centrifuged as described above, the resultant pellets were treated to an equal volume of 0.5% SDS and the samples were left for 60 minutes at room temperature to

solubilize any remaining trophozoites (Dudley et al., 2008). Then, pre- and post-SDS treatment counts were performed and the encystment percentage was determined using the formula:

% encystment = post digestion number / pre-digestion number × 100

2.7.6 Inhibitory effect of *C. sinensis* on trophozoite excystation

Approximately 2 × 10^5 *A. castellanii* cysts were seeded into 15 mL falcon tubes which were labelled according to treatment groups. The tubes were centrifuged at 1,204xg for 5 minutes, the supernatant was discarded, and each resultant pellet was treated with 5 mL of respective treatment media. The negative control included cysts in PGY only, while the positive control included cysts in PGY supplemented with 0.02% CHX. The suspensions were mixed using the vortex mixer aimed at ensuring homogenous mixture and each tube was capped slightly to ensure there was no build-up of CO_2 in the tubes. The tubes were placed in a rack and incubated in a Stuart oven at 25^0C. Using a haemocytometer, and a CETI inverted microscope, the count of each treatment group was done at 24-, 48- and 72-h post-treatment to determine the cyst to trophozoite excystation ratio. All experiments were repeated three times and the mean values were calculated. The treated cysts were also examined optically using a Leica DMIL CMS inverted microscope to identify any morphological alterations during excystation caused by exposure to *C. sinensis.*

2.7.7 Inhibitory effects of *C. sinensis* chemical constituents on trophozoites

Serial dilutions of *C. sinensis* chemical standards (200 µM, 100 µM, 50 µM, 25 µM, 12.5 µM, 6.25 µM and 3.12 µM) were used individually to investigate their inhibitory effect on the growth kinetics of trophozoites using the colorimetric SRB assay. For each chemical standard, *A. castellanii* trophozoites were seeded at 2.5×10^3 trophozoites/well in 96-well microtiter plates. Each well received 100 µl of the testing chemical standards. After testing each chemical standard individually, further evaluation the efficacy of all chemical standards combined together was done. Here, the 10 chemical compounds were mixed together using equal volumes to form one homogenous solution and evaluated for anti-acanthamoebic activity

using the colorimetric SRB assay at concentrations of 3.12 µM to 200 µM as previously described in General methods (Chapter 2, section 2.7.4.2). For each experiment, negative control wells received only 100 µl PGY medium/well, while positive control wells received 100 µl 3% SDS. The positive control was added 30 min before commencement of the SRB assay. The plates were incubated in a Stuart oven at 25°C. Then, at 3, 6, 24, 48 and 72 h post-incubation, the colour absorbance of each well was measured as previously described (Ortega-Rivas et al., 2016; Fakae et al., 2020). All experiments were performed in triplicate.

2.7.8 Inhibitory effect of *C. sinensis* chemical constituents on encystation

The stock solution of 1000 µM was used as solvent for preparing serial dilutions of hyper osmotic solutions for anti-encystation testing. Approximately 6.2×10^5 *A. castellanii* trophozoites, seeded in T25 tissue culture flasks, were treated with 500, 250, 125, and 62.5 µM of hyper osmotic solutions of three *C. sinensis* chemical standards: EGCG, theobromine and EGCG-theobromine combined. EGCG was chosen since it was the most efficacious chemical standard evaluated for its trophocidal effect, while theobromine though not as efficacious as EGCG was chosen to ascertain if the combination of a trophocidally efficacious chemical standard and another standard without the efficacy of ECGC combined in a 1:1 ratio, will be able to inhibit encystation. The anti-encystation ability of theobromine was also evaluated to ascertain if it was able to inhibit encystation even though it was not able to inhibit trophozoite growth as desired. The negative and positive controls were the same as described in the encystation experiments above. The experiments were performed in triplicate.

2.7.9 Ultrastructural analysis using electron microscopy

2.7.9.1 Transmission electron microscopy (TEM)

A. castellanii treatment samples (trophozoites or cysts) were harvested into capped 1.5 mL micro-centrifuge tubes (Eppendorf, UK) and were centrifuged at 1,204xg for 5 minutes using a Sigma 1-14 micro-tube centrifuge (Sigma, Germany). The supernatant was discarded and the resulting pellet washed with PBS by centrifugation and re-suspended in 3%

Glutaraldehyde in 0.1M Cacodylate buffer for 24 hours to ensure complete infiltration of fixative into the sample. After 24 hours, the samples were washed twice in 0.1M Cacodylate wash buffer and stored in the same solution prior to the post-fixative procedure. Before post-fixing, the samples were washed twice with distilled water to remove the cacodylate wash buffer which they were stored in. After centrifugation, the supernatant was discarded and resultant pellets were re-suspended in 1% osmium tetroxide for one hour. After post-fixing, the samples were washed twice in distilled water and embedded in 3% Agarose low gelling for 5 minutes; they were placed in the refrigerator for 5 minutes to accelerate solidification prior to en-bloc. The samples were transferred to a plastic sheet and cut into smaller chunks using a spatula and then en-bloced by submerging in 1% uranyl acetate (Agar Scientific, UK) for 30 minutes in a 30 mL glass bottle; this was done to enhance counterstaining for better contrast during imaging. After the en-blocing process, the waste uranyl acetate was discarded and the sample dehydrated in a graded ethanol series. At the addition of each ethanol dose at a 20:1 ratio of sample, the samples were capped and placed on a vari-speed rotator (TAAB, UK) to ensure gentle agitation for the specified time and the ethanol was aspirated out of the sample bottle. The dehydration process was done as follows; 50% ethanol for 10 minutes twice, 70% ethanol for 10 minutes twice, 90% ethanol for 10 minutes twice, 100% ethanol for 10 minutes thrice and 100% propylene oxide for 15 minutes twice. The propylene oxide served as a further dehydration medium and also as a transitional solvent between ethanol and epoxy resin.

After dehydration, the samples were infiltrated with a 3:1 propylene oxide-epoxy resin mixture for one hour and re-infiltrated with a 1:1 propylene oxide-epoxy resin mixture for 24 hours with the lids of the sample bottles open in a fume hood. After 24 hours, the samples were re-infiltrated with 100% epoxy resin for one hour in fresh bottles; this procedure was repeated once and the samples were embedded in plastic moulds in 100% epoxy resin and placed in an embedding oven (TAAB, UK) at 60^0C for 48 hours to polymerize.

After polymerization, the samples were sectioned for TEM using an ultra-microtome (Leica EM UC6, Germany). Before sectioning for TEM imaging, 500nm sections were cut and

collected onto 3-Aminopropyltriethoxysilane (APES) coated glass slides which were subsequently stained with a rapid morphological stain (toluidine blue in 1% sodium borate) for 60 s. The excess unabsorbed stain was washed off with 90% ethanol and distilled water, and the slide placed on a hot plate for 2 minutes to dry. After the slides were dried, they were viewed with an upright microscope (Leica DM 4000B, Germany). This rapid staining process was done to determine the area of interest and to direct any necessary or further trimming of embedded samples. After sectioning 90nm (ultra-thin) sections, 3.05nm Gilder copper grids (TAAB, UK) were used in picking up respective samples; these were subsequently stained for TEM.

For staining, staining stations were prepared by creating two hydrophobic surfaces by pasting parafilm strips on petri dishes, which allowed the staining reagents to form droplets and not run off. On one hydrophobic surface drops of Uranyl acetate were aspirated and dispensed through 0.45µl Millipore syringe filter (MILLEX®-HA brand, Ireland) and covered with a Petri dish. On the second surface drops of electron microscopy grade Reynold's lead citrate (TAAB, UK) were dispensed through 0.22µl Millipore syringe filter (MILLEX®-HA brand, Ireland) and surrounded with sodium hydroxide pellets (Fisher, UK) to mop up any CO_2 in the station. The sodium hydroxide pellets were introduced to prevent the formation of lead carbonate, which are heavy precipitates that can damage the samples. For rinsing the samples in between staining, one tripour beaker was filled with 200 mL of 50% ethanol and two beakers filled with sterile water for rinsing off the samples after staining. Using fine tipped forceps, the copper grid containing samples were placed facedown (sample side) on the uranyl acetate droplet for 5 minutes, then washed aggressively in 50% ethanol by dipping continuously in the solvent for about 10 seconds. The grids were subsequently rinsed in sterile water and placed sample face down in the lead citrate for 5 minutes. The grids were rinsed aggressively in sterile water twice, dried off on filter paper and stored for TEM imaging. Uranyl acetate was the primary stain while lead citrate was the counterstain. Forceps were rinsed and dried in between stations to prevent transferring reagents and solvents in between stations. Samples grids for

the control experiments were visualised using a Tecnai G2 T12 BioTwin transmission electron microscope (FEI, Eindhoven, The Netherlands), with an accelerating voltage of 100 kV and images of varying magnifications were captured using a MegaView II (Olympus) camera system. For each treatment sample, an average of 5 images captured, making it 60 images captured for the hot and cold *C. sinensis* brew experiments, while 40 images were captured for the solvent extract experiments. Without the presence of marked squares as seen while viewing samples with haemocytometer, these images were also acquired semi-randomly from different fields test samples to ensure some degree of objectivity.

2.7.9.2 Scanning electron microscopy (SEM)

A. castellanii treatment samples (trophozoites or cysts) were harvested, fixed and post fixed as previously described for TEM. After post fixing, the samples were washed twice in distilled water and dehydrated in a graded ethanol series. At the addition of each ethanol dose at a 20:1 ratio of sample, the suspension was mixed using a vortex mixer to ensure a homogenous mix and subsequently centrifuged to discard the supernatant without losing the sample. The dehydration process was done as follows; 50% ethanol for 10 minutes twice, 70% ethanol for 10 minutes twice, 90% ethanol for 10 minutes twice and 100% ethanol for 10 minutes thrice. After dehydration, the samples were infiltrated in hexamethyldisilazane (Acros, Germany) for 5 minutes twice to further enhance the drying of the samples without the risk of them collapsing. The samples were subsequently mounted on aluminium SEM stubs by the assistance of a double-sided carbon sticker. They were subsequently inserted into the coating crucible which allowed for them to be flushed with argon before they were coated with gold, making them ready for SEM imaging. Images were obtained with varying magnifications using a JEOL JSM-7100F LV Scanning Electron Microscope (JOEL, Tokyo, Japan) operating at an accelerating voltage of 10 kV and a working distance of 10 mm. Data was collected using the lower secondary electron detector. For each treatment sample, an average of 5 images captured, making it 60 images captured for the hot and cold *C. sinensis* brew experiments, while 40 images were captured for the solvent extract experiments. Without the presence of

marked squares as seen while viewing samples with haemocytometer, these images were also acquired semi-randomly from different fields test samples to ensure some degree of objectivity.

2.7.10 Liquid Chromatography-Mass Spectrometry of *C. sinensis* brews

Samples of hot and cold brew *C. sinensis* were characterised using Liquid Chromatography-Mass Spectrometry (LC-MS) to identify the components/analytes present in each of the brew forms. Two solvents (A and B) were used as mobile phase. A was 0.1% formic acid in water + methanol at a 90:10 ratio, while B was 0.1% formic acid in methanol. A Restek C18 Raptor™ column (Restek Thames, High Wycombe, United Kingdom) was used and the injection mode was by automatic liquid injection with an injection volume of 0.1 mL of *C. sinensis* brew. The flow rate was 0.25 mL/min with a run time of 15 minutes. The gradient elution of solvent B was 10% ramped to 95% over a period of 15 minutes, while that of solvent A was 95% ramped to 10% over a period of 15 minutes. The system used was Waters ultra-high performance liquid chromatography quadrupole time of flight tandem mass spectrometry (UHPLC-MS QTOF) (Waters, Milford, MA, USA).

2.7.11 Flash chromatography of *C. sinensis* solvent extract

After the solvent extraction of *C. sinensis*, a sample was taken out for flash column chromatography. A chromatography machine, Puriflash 5.125Plus (Interchim, Montluçon, France), was used to identify the active fractions in the *C. sinensis* solvent extract. To identify which method worked best to separate more fractions, two runs were conducted with different combinations of solvents as mobile phases. The first mobile phase (A + B) included (A) 0.1% formic acid in water and water at a 91:9 ratio + (B) 0.1% formic acid in methanol, while the second (A + B) included (A) 0.2 % acetic acid in water and acetonitrile at a 91:9 ratio + (B) water and acetonitrile at a 20:80 ratio. Rather than using a single HCC18 Flash Column, two flash columns were used; Puriflash C18HC spherical silica flash II column with particle size 50µm for high capacity weighing 40g, and puriflash C18HP spherical silica flash II column with

particle size 15µm for high performance weighing 12g. The injection mode was liquid with 1 mL of *C. sinensis* solvent extract, and the detection was 258 nm and 278 nm with a flowrate of 26 mL/min. The pressure was set to 9 bars and the auto gradient optimization mode was used. The elution profile for the first mobile phase (solvent A) was 5% to 95% holding gradient, while analytes showed their maximum absorbance over a run time of 60 min. The elution profile for the second mobile phase (solvent B) was also the auto gradient optimization holding gradient, while analytes showed their maximum absorbance over a run time of 59 minutes and only fractions of monitored peaks were collected.

2.7.12 High-performance liquid chromatography analysis of *C. sinensis* extracts

After collecting fractions of monitored peaks observed during flash chromatography of *C. sinensis* solvent extracts, the fractions collected were characterised using UHPLC-QTOF-MS (Waters, Milford, MA, USA) to identify the analytes present in these fractions. Two solvents (A and B) were used as mobile phase. A was 0.1% formic acid in water + methanol at a 90:10 ratio, while B was 0.1% formic acid in methanol. A Restek C18 Raptor^{TM} column (Restek Thames, High Wycombe , United Kingdom) was used. The injection mode was performed by automatic liquid injection with injection volume of 1 mL (50 µl crude solvent extract diluted in 950 µl LC-MS grade methanol). The flow rate was 0.25 mL/min with a run time of 15 minutes. The elution gradient of solvent B was 10% ramped to 95% over a period of 15 minutes, while that of solvent A was 95% ramped to 10% over a period of 15 min. The chromatographic data were analysed and the chemical composition of each component was confirmed by matching the chemical formula with references in the library using MassLynx® software (version 4.1, Waters, Milford, MA, USA).

2.7.13 Characterisation of *C. sinensis* activity using fluorescence assays

Qualitative characterisation of the effect of *C. sinensis* brew versus solvent extract on *A. castellanii* trophozoites was performed using two fluorescence-based 4′,6′-diamidino-2-phenylindole (DAPI) and Acridine orange (AO) staining assays. These two assays were used

to determine and confirm to which degree each of the *C. sinensis* forms (brew and solvent extract) were able to compromise the nuclear membrane integrity of the trophozoites during 24 hours of exposure in comparison to the positive control, CHX. The integrity of the nucleus was analysed by the fluorescence intensity of the trophozoite nucleus captured in the confocal micrographs. The DAPI staining assay was used to evaluate the level of apoptosis based on the appearance of nuclear morphology (e.g., condensation and fragmentation), while AO was used to quantify nucleic acids. In both assays, *A. castellanii* trophozoites were treated with 50% *C. sinensis* cold brew or 1250µg/mL *C. sinensis* solvent extract. PGY was used as negative control, and CHX as positive control. The concentrations of both *C. sinensis* forms were chosen for the 24 h experiment as it had been demonstrated via the trophozoites growth inhibitory experiments (Chapter 3 and Chapter 4) that though they exhibited some anti-acanthamoebic activity at 24 h, there were still some trophozoites alive. This will allow the evaluation of the protein content using fluorescence microscopy; the use of higher concentrations might leave little or no trophozoites to be evaluated. The intensity of fluorescence seen represents the nucleus of viable cells. Quantitative characterisation of the levels of fluorescence expressed as grey levels was also done by analysing the mean fluorescence intensities and the integrated fluorescence densities of the *C. sinensis* treated trophozoites that were exposed to the DAPI and AO dyes.

2.7.13.1 DAPI staining

The DAPI-treated trophozoites emit blue fluorescence when the nucleus of viable trophozoites absorbs the dye. This fluorescence is visible at an excitation peak of 359 nm and an emission peak of 457 nm. For DAPI staining, 24h post treatment, the trophozoites were washed with PBS and fixed with 4% paraformaldehyde for 10 min. The fixed trophozoites were washed twice with PBS and suspended in permeabilizing buffer (4% paraformaldehyde (PFA) and 0.5% Triton X-100) for 10 min. The permeabilized trophozoites were washed with bi-distilled water 3 times to remove the permeabilizing buffer and resuspended in 200 µL of bi-distilled water and two drops of the DAPI stain and incubated for 15 min. A few drops of the stained

trophozoite suspension were added to a microscope glass slide, covered with a coverslip and the edges sealed with transparent quick drying nail polish. Slides were viewed under an inverted Zeiss LSM 710 confocal microscope (Zeiss, Germany) running on ZEN 2011 software (Carl Zeiss microscopy, GmbH). Bright field and phase contrast images were acquired randomly using the respective fluorescence filters. The images were analysed using Carl Zeiss microscopy software (Zen Blue, version 3.3, Germany), and ImageJ (Public domain program).

2.7.13.2 Acridine orange staining

A fluorometric cell viability assay using AO stain was used to assess the viability via detecting changes in the levels of DNA and RNA of trophozoites in response to treatment, compared with the control groups. AO is a cell-permeant nucleic acid binding dye that emits green fluorescence by intercalation when it binds to double stranded DNA (dsDNA) and orange fluorescence by electrostatic attractions when it binds to single stranded DNA (ssDNA) or RNA. The interaction of AO with DNA by intercalation at a maximum excitation of 526 nm shows a green fluorescence which for confocal filters is FITC while at the maximum excitation of 650 nm, interaction with RNA via electrostatic attractions shows a red fluorescence (rhodomine). With the principle mentioned above, live trophozoites stained with AO fluoresce green and orange under fluorescence microscopy when the excitation wavelength range is switched between 500⁄526 for DNA and 460⁄650 for RNA.

For AO staining, following the removal of the treatment medium, trophozoites were washed, fixed, and stained with 1% AO for 15 min protected from light. The stained trophozoites were washed 3 times in bi-distilled water and the pellets were resuspended in 100 µl of PBS. A few drops of AO-stained trophozoite suspension were added to a microscope slide, covered with a coverslip and the edges sealed with transparent quick drying nail polish. Images were acquired randomly with rhodamine (red for RNA) and FITC (green for DNA) fluorescence filters using an inverted Zeiss LSM 710 confocal microscope (Zeiss, Germany) running on a ZEN 2011 software (Carl Zeiss microscopy, GmbH). The images were analysed using Carl Zeiss microscopy software (Zen Blue, version 3.3, Germany).

2.7.14 FTIR, spectra processing and multivariate data analysis

Here, FTIR Microspectroscopy was used to analyse the chemical changes that occurred in the trophozoites in response to treatment with *C. sinensis* brews and solvent extract.

2.7.14.1 FTIR sample preparation

To characterize the effect of *C. sinensis* on trophozoites treated with *C. sinensis* hot or cold brew, ~ 3.2 x 10^5 trophozoites were seeded in T25 tissue culture flasks and were treated with 50% *C. sinensis* brew. This was also done for trophozoites treated with 1250µg/mL *C. sinensis* solvent extract. The negative control included trophozoites treated with standardized PYG medium only, while the positive control was PGY with 0.02% CHX. After 48 hrs, the trophozoite suspension was harvested from the flasks and transferred to falcon tubes, then washed once with PBS by centrifugation at 1,204xg for 5 minutes, and resuspended in and washed once using bi-distilled water and centrifuged again as previously described. After the centrifugation, the pellets were fixed in 4% paraformaldehyde (PFA) for 24 hours and were left in the PFA until they were ready for use. Before measurements, samples were centrifuged as above to remove the PFA and washed twice in bi-distilled water and stored in isotonic saline solution at 4^{o}C until use. Before the spectral measurement, trophozoites and cysts were mounted on a 1 mm thick CaF_2 window by drop casting followed by gentle rinsing in bi-distilled water briefly to remove any remaining salt crystals and then thoroughly air-dried for ~30 min. Trophozoites and cysts were dispersed individually across the substrate when prepared in this way.

2.7.14.2 FTIR microspectroscopy

Single cell spectra were collected using a FTIR microscope (SpotLight^{TM} 400, Perkin Elmer, United States) combined with the ZnS hemispheres approach developed by Chan (Chan et al., 2018; Chan et al., 2020). Trophozoites and cysts were prepared by drop-casting on the flat surface of an upside-down ZnS hemisphere (32 mm radius, Crystran Ltd), drying in air at room temperature to adhere the cells to the ZnS surface, and then briefly rinsed in deionised water twice to remove the salt crystals. The cells on the ZnS were allowed to dry in air for 30

min. Another identical ZnS hemisphere was then placed on top of the upside-down ZnS hemisphere with a 12 µm spacer. The two hemispheres were held together with a lens-holder (Thorlab Ltd) before being centred on the microscope stage for single-cell analysis. The microscope aperture size was set to 30 µm x 30 µm, which is equivalent to ~13 µm x 13 µm (with 2.25x through the ZnS hemispheres). A clean area with no cells was used as the background location. The spectral resolution was set at 4 cm^{-1} with a spectral range of 4000-800 cm^{-1} and the number of scans was 64, with each spectrum taking approximately 1 min to acquire. Measurements of 35-37 randomly selected single amoeba cells were made for the control and each of the treatment conditions.

2.7.14.3 FTIR Data processing and analysis

The Spectrum software (PerkinElmer, United States) was used to perform interactive polynormal baseline correction with baseline points at 4000, 3725, 2380, 1800, 940 and 825 cm^{-1} followed by vector normalization calculated using Microsoft Excel™. The PyChem software version 3.0.5g Beta was then used to perform principal component analysis (PCA) on both the absorbance spectra and the second derivative spectra. Microsoft Excel™ t-test was used to calculate the p-values for the comparison between the control and the treatment groups.

2.7.15 Proteomics analysis via Data-independent acquisition mass spectrometry

Here, Data-independent acquisition mass spectrometry (DIA-MS) was used to analyse the proteomic changes that occurred in the trophozoites in response to treatment with *C. sinensis*. With the anti-acanthamoebic activity seen with *C. sinensis* from the brew phase of the study (Chapter 3), hot brew was used as the sample of choice for this proteomic analysis.

2.7.15.1 Protein quantification

Prior to proteomics analysis, protein concentration of the brews was quantified using a Pierce™ BCA protein assay kit (ThermoFisher, UK). Briefly, five 160µl dilutions of a bovine serum albumin (Merck, UK) representing the protein solution to be tested was prepared in

triplicate using a 96 well plate. The same triplicate dilutions were prepared for *A. castellanii* trophozoites treated with *C. sinensis* brew, as well as the blank *C. sinensis* brew sample. 40µl of dye reagent was added to each well and mixed with a multichannel pipette. The plates were incubated at room temperature for 5 minutes and the absorbance was measured at a wavelength of 595nm using an L-T 4000 microplate reader (Labtech, UK).

2.7.15.2 Sample preparations

To characterize the effect of *C. sinensis* on trophozoite proteins, ~ 3.2 x 10^5 trophozoites were seeded in T25 tissue culture flasks and were treated with 50% *C. sinensis* brew. The negative control included trophozoites treated with PYG medium only, while the positive control was PGY plus 0.02% CHX. After 48 hrs, prior to sample preparation, quantification of trophozoites was done as previously described. The trophozoite suspension was harvested from the flasks and transferred to falcon tubes which were embedded in dry ice to keep the temperature of the samples below 0°C. The samples were washed twice with cold PBS by centrifugation at 1,204xg for 5 minutes with the centrifuge set to 0°C, and snap frozen by immersing the sample point of the tube in liquid nitrogen. To maintain the cold-chain commenced at the start of sample preparation, the samples were stored in –80ºC freezer until they were ready to be analysed.

2.7.15.3 Proteomics analysis

All samples were buffer exchanged five times with 100 mM ammonium bicarbonate (pH 8.0) through a 3 kDa MWCO membrane (Amicon Ultra, Millipore, UK) after protein concentration was quantified, and in-solution trypsin digestion was performed. Briefly, *A. castellanii* trophozoites were reduced with 5 mM DTT at 56 °C for 60 min and alkylated with 20 mM iodoacetamide in the dark at 25 °C for 30 min. MS-grade trypsin (Pierce Thermo Fisher Scientific, UK) was added at 20:1 protein to enzyme ratio and the digestion mixture was incubated at 37°C overnight. The pH of the solution was lowered to 2 with 1% formic acid to quench the activity of trypsin. The digested samples were evaporated to dryness and the

samples were desalted with C18 fast-flow tips (Pierce Thermo Fisher Scientific, UK). Desalted peptides were dried in vacuum and stored at −20 °C for LC-MS/MS analysis. Before the data acquisition, retention time calibration iRT peptides (Biognosys, Switzerland) were spiked in all the samples at a 1:10 ratio for retention time normalization.

Protein profiling was performed by using LC–MS/MS. Briefly, the samples were injected by trap-elute (4 µL) using an Eksigent 425 LC system (trap: YMC triart C_{18} 0.3 × 5 mm, 300 µm ID. Analytical column: YMC Triart C_{18} 150 × 0.3 mm, 3 µm, 5 µL/min) coupled to a SCIEX TripleTOF 6600 mass spectrometer in Information Dependent Acquisition (IDA, top 30) mode via a gradient elution (mobile phase A: 0.1% formic acid; B: acetonitrile in 0.1% formic acid) over 87 min (2% to 30% B over 68 min; 40% B at 72 min followed by column wash and re-equilibration).

Mass spectrometry raw data were processed using ProteinPilot 5.02 (SCIEX, Warrington, UK) against the SwissProt mouse database (January 2019) and 1% false discovery rate (FDR) protein cut-off was applied. The SWATH method was run with the same source parameters as the IDA with a 50 ms TOFMS scan followed by 100 variable SWATH windows (optimized on an IDA datafile of the same samples) of 25 ms between 100 and 1500 m/z giving a cycle time of 2.6 s. A spectral library for SWATH data extraction was constructed using the output from ProteinPilot 5.0 (Sciex) searching against the SwissProt database (January 2015) with the addition of iRT peptides to the fasta file, combining IDA runs (pooled samples) and filtered and aligned to spike in iRT peptides (Biognosys, Switzerland) using PeakView 2.1 (Sciex). Proteins and peptides with at least 40% confidence ratio were considered and matched following ProteinPilot search against the SwissProt database.

2.8 SELECTIVITY INDEX

The *C. sinensis* brew and solvent extract concentration that caused 50% inhibition of host cell growth was expressed as 50% cytotoxic concentration (CC_{50}). The CC_{50} of *C. sinensis* brew on CSCs, and iHCECs were calculated by plotting dose-response curves followed by

performing simple linear regression analysis using Graph Pad Prism 9 software. The calculation of half-maximal inhibitory concentration (IC_{50}), which is the concentration of *C. sinensis* brew forms that caused a 50% decrease of *A. castellanii* trophozoite growth compared to the control, was performed using Graph Pad Prism 9.0's nonlinear regression (curve fit) built-in analysis tool of dose-response inhibition (three parameters). The selectivity index (SI), which represents the ratio of the CC_{50} for host cells to the IC_{50} for *A. castellanii*, was calculated by comparing the cytotoxicity of *C. sinensis* for host cells to that of *A. castellanii* trophozoites.

2.9 STATISTICAL ANALYSIS

One-way, two-way and randomized two-way analysis of variance (ANOVA) were conducted for the respective experiments, while post-test direct comparisons were done using Tukey's, multiple comparisons test based on the experimental plan and data. The descriptive statistics of data sets represented in tables and figures were expressed as mean±standard error of the mean (SEM), with all data represented at 95% confidence level. $p<0.05$ was considered as evidence of statistical significance. All statistical analysis were performed using GraphPad Prism Version 9.0 (GraphPad Software, Inc. USA).

2.10 ETHICAL APPROVAL

There was no need for ethical approval for extraction of human corneal cells as the cells used in all experiments were extracted by a research colleague in the academic ophthalmology department (University of Nottingham) while I observed, and gifted to me team for my research.

3 EFFECT OF *C. SINENSIS* BREWS ON *A. CASTELLANII*

3.1 SUMMARY

In this study, the effect of *Camellia sinensis* (green tea) on *A. castellanii* trophozoites and cysts were evaluated by subjecting both forms of *A. castellanii* to serial concentrations (100%, 75%, 50% and 25% v/v) of *C. sinensis* brews. After determining the optimal seeding density, the growth and replication of *A. castellanii* trophozoites was examined using a microplate based-Sulforhodamine B (SRB) assay. *C. sinensis* hot and cold brews at 75% and 100% concentrations significantly inhibited the growth of trophozoites. The ultrastructural alterations in *C. sinensis*-treated trophozoites and cysts were examined using transmission electron microscopy (TEM) and scanning electron microscopy (SEM). This analysis showed that *C. sinensis* brews compromised the cell membrane integrity and caused progressive destruction of trophozoites. *C. sinensis* brews also significantly inhibited the parasite's ability to form cysts in a dose-dependent manner and reduced the rate of excystation from cysts to trophozoites with 50%-100% cold and hot *C. sinensis* brews exhibiting 100% inhibition of *A. castellanii* cysts to trophozoites excystation as seen with chlorhexidine. Light microscopic evaluations corroborated the findings of the replication studies and the electron microscopic investigations. *C. sinensis* exhibited low cytotoxic effects on primary corneal stromal cells. However, cytotoxicity was more pronounced in SV40-immortalized corneal epithelial cells. This work demonstrated that *C. sinensis* has acanthamoebicidal activity against trophozoite and cystic forms of *A. castellanii*. Further studies are warranted to investigate the potential and potency of *C. sinensis* solvent extract in exhibiting trophocidal and cysticidal anti-acanthamoebic effect.

3.2 INTRODUCTION

Free-living amoebae are ubiquitously distributed in the environment and can be found in soil and water. One such organism is *A. castellanii*, which causes GAE and AK (Martinez and Visvesvara, 1997; Chomicz et al., 2010). The treatment for *A. castellanii* infection has been a challenge and is currently managed with drug combinations. Available therapies are lengthy and without a sustained effect, and their withdrawal allows for excystation of encysted trophozoites and a relapse of infection. The most routinely used chemotherapeutic agents, individually or in combination, are biguanides (e.g., polyhexamethylene [PHMB] or chlorhexidine gluconate [CHX]) and diamidines (propamidine isethionate and hexamidine). These anti-acanthamoebic drugs act by compromising the plasma membrane (biguanides) and interfering with DNA and protein synthesis (diamidines) of the amoeba (Kaya et al., 2019). However, they do not completely eradicate the parasite (Gooi et al., 2008), either due to delayed, misdiagnosis or resistance of the parasite to the treatment agent(s). Other therapies include the use of CHX in combination with diamidines and neomycin (Siddiqui et al., 2016a), a combination of antibiotics such as trimethoprim/sulfamethoxazole (Aichelburg et al., 2008), ketoconazole (Singhal et al., 2001), dicloxacillin, ciprofloxacin, voriconazole, amphotericin B (Walia et al., 2007), neomycin, metronidazole (Sun et al., 2006) fluconazole, rifampin, pentamidine and macrolide (Visvesvara et al., 2007; Maritschnegg et al., 2011). However, while effective against the trophozoites, these compounds are not highly effective against the cysts, which are made resistant by their cellulose-based double walls. Additionally, side effects and cytotoxicity are major concerns with the prolonged anti-acanthamoebic treatment regimens, which can cause damage of the host cells, with a possibility of re-infections (Visvesvara, 2010; Niyyati et al., 2010).

Given the challenges associated with the current treatment protocols, alternative approaches have been suggested in an effort to improve the treatment efficacy (Visvesvara et al., 2007; Gooi et al., 2008; Visvesvara, 2010; Maritschnegg et al., 2011; Kaya et al., 2019). Also, researchers have been delving into natural sources that might have therapeutic potential for

treatment of *A. castellanii* infection. These studies have shown anti-acanthamoebic activities of various plants *in vitro* and *in vivo* (Hadas et al., 2017a; Hadas et al., 2017b; Saoudi et al., 2017; Mahboob et al., 2017; Sifaoui et al., 2017; Dodangeh et al., 2018; Kaynak et al., 2018; Kaya et al., 2019).

Considering the need for more potent medications against *A. castellanii* infection and given the potential anti-infective properties of *C. sinensis*, the present study was performed to investigate the anti-acanthamoebic activity of hot and cold brews of *C. sinensis* against the trophozoite and cystic stage of *A. castellanii*. Also, the cytotoxicity of *C. sinensis* brews was evaluated on two human corneal cell lines.

3.3 RESULTS

3.3.1 Cytotoxicity evaluation of *C. Sinensis* brew

3.3.1.1 Cytotoxicity of corneal stromal cells using SRB Assay

The growth of primary corneal stromal cells was affected by cold and hot *C sinensis* brews in different ways. A two-way ANOVA of cold brew revealed a significant main effect of time ($F(3, 60) = 97.01$, $p < 0.0001$), concentration ($F(4, 40) = 8.084$, $p = 0.0005$), and time x concentration interaction ($F(12, 60) = 22.77$, $p < 0.0001$).

For cold brew, post-hoc comparisons showed increased optical density with all percentages of cold brew, compared to controls at 3 hours with a significant difference between the control and the treatment groups *(p<0.0001)*. The difference seen in the optical density indicated that there were more corneal cells in each of the *C. sinensis* cold brew treatment groups compared with the control. At 24 hours post treatment, while there was still no significant increase of OD between the control and 25%-75% cold brew treatment groups, while 100% cold brew showed a significant decrease to the OD of the control *(p=0.0064)*. At 48 hours post treatment, the OD of the control increased significantly in comparison to its 24-hour OD (*p = 0.0061*), and also showed significant increase to the cold brew groups ($p \geq 0.05$). At this time point the control group showed extensive cellular replication, with the OD higher than all the treatment groups. The treatment groups showed no difference between their 24-OD and their 48-hour OD. This indicates that the CSC in each treatment group may not have shown significant growth (replication) but at the same time the cold brew treatment was not toxic enough to bring about absolute cell death. At 72 hours, though there were significant increase in OD between the control and the cold brew treatment groups (*p<0.0001)*, there was equally increased OD in all cold brew treatment groups when comparing the 24 h and 48 h readings which indicated cell replication similar to the trend seen in the control (M199). The observation above shows that the arrested cellular replication phase was not sustained and thereby indicates that though

the cold brew exhibits toxicity to primary corneal stromal cells, it was not sustained. The chart suggests there was a slight cell replication at 72 h (Figure 3:1)

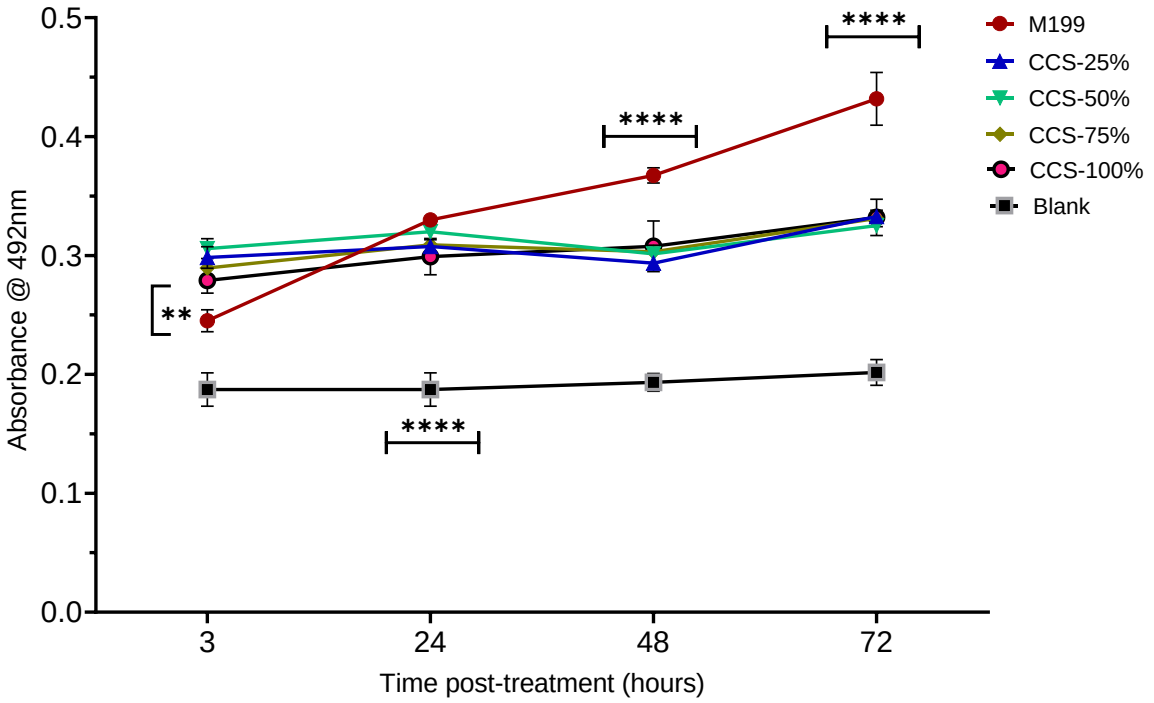

Figure 3:1: Cytoxicity of *C. sinensis* cold brew against CSC. At 3 h, the OD of M199 was significantly lower than the treatment groups. At 24 hours there was no significant difference between the OD of M199 and 25%-75% groups while the OD of 100% was significantly lower than the control. At 48 and 72 h, the OD of M199 was significantly higher than all the treatment groups. The highest concentration of cold brew (100%) allowed for CSC replication after 48 hours indicated by increased optical density. At all the time points, there was significant difference between the positive control and all the treatment groups (** $p \leq 0.01$;**** $p \leq 0.0001$; ns, non-significant).

The two-way ANOVA of hot brew revealed a significant main effect of time ($F(3, 60) = 93.98$, $p < 0.0001$), concentration ($F(4, 20) = 3.079$, $p < 0.05$), and time x concentration interaction ($F(12, 60) = 13.87$, $p < 0.0001$).

For hot brew, post-hoc comparisons between the control and all the treatment groups at 3 hours showed that the hot brew groups had more cells than the control. Within the hot brew groups, there were no significant increase ($p \geq 0.05$) between the 25%-75% hot brew group which showed higher OD than 100% and control ($p < 0.0001$). At 24-hour post treatment, there

were no significant increase between the control and all the hot brew groups ($p \geq 0.05$). The OD of the control had increased which indicted replication of cells to match the OD of the other treatment groups. At this phase there were no signs of toxicity of hot brew to CSC.

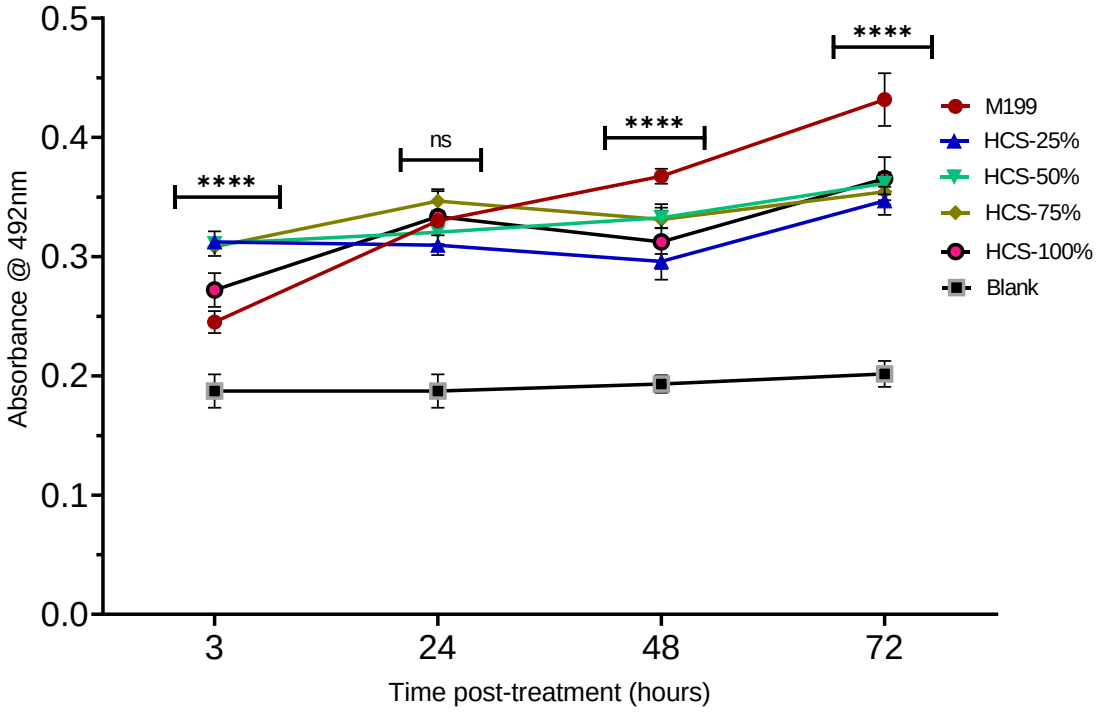

Figure 3:2: Cytoxicity of *C. sinensis* hot brew against primary corneal stromal cell. At 3 h post exposure, there was significant increase between the OD of control and 50%-100% treatment groups. At 24 hours, there was no significant increase or decrease between the cell replication for all treatment groups and the negative control. At the 48 h, there was no significant increase between the OD at 24 h and 48 h which suggested some form of arrested replication of CSC. The OD of negative control was significantly higher than all the treatment groups from 48 h to 72 h. As seen with the cold brew, all the treatment recorded a slight increase in their OD indicative of renewed CSC replication. At all the time points, there was significant difference between the positive control and all the treatment groups (**** $p \leq 0.0001$; ns, non-significant).

48 h post treatment, the OD of control increased significant between it all the hot brew groups 25%-100% (*p<0.0001*) . There was however no significant decrease or increases between the 24 h and 48 h OD which indicated a form of arrested replication or cellular death of CSC exposed to *C. sinensis* hot brew groups. At 72 hours post treatment, although there still was significant increase between both control groups and the treatment groups (*P<0.0001)*. The

increase in OD of all the hot brew groups by 72 hours indicates that the cells may have overcome the transient replication arrested phase or cellular death phase it may have encountered between 3 to 48 hours and by 72 hours normal cellular replication have commenced which may be similar to the trend observed in the control group (Figure 3:2). It is however important to note that the OD of the positive control was significantly lower when compared to all the treatment groups from 3 to 72 hours of the experiment.

In analysing the growth kinetics of primary CSCs treated with both cold and hot brews, the growth rate of all treated cells at 72 h was significantly higher than that of the same cells at 48h. However, the significant difference between the control and treated cells continued to increase in favour of control cells ($p < 0.0001$). The transient replication arrested phase observed at 24 and 48 h did not compromise the ability of the treated cells to resume their growth even at 100% concentrations of both brews.

3.3.1.2 Cytotoxicity of CSCs using AO staining

For further verification of the lack of sustained cytotoxicity of *C. sinensis* brew forms to CSCs seen with SRB assay by measuring cellular growth rate by replication, AO assay was used to quantify the RNA and DNA content in CSCs.

For RNA quantification, the two-way ANOVA of *C. sinensis* brew forms revealed a significant main effect of time ($F(3, 9) = 13.71$, $p = 0.0011$), concentration ($F(3, 9) = 35.07$, $p<0.0001$), and time x concentration interaction ($F(9, 27) = 1.830$, $p = 0.1086$). Post hoc comparisons of RNA fluorometric quantification at 6 h showed no difference between the CSCs RFU of the control and the brew forms ($p \geq 0.05$). At 24 h, the CSCs RFU for control and the brew forms still showed no significant increase or decrease though the RFU was significantly lower than 6 h. At 48 h post exposure, there was a significant increase in the RFU of control compared to both brew forms of *C. sinensis (p=0.0454).* At 72 h, the RFU of both treatment groups increased in with significant increase between 72 h and 48 h. However, the increase in control RFU was significantly higher than seen for both treatment groups. This result suggests that between 6 h to 48 h post treatment of CSCs with hot and cold brew forms of *C. sinensis*, the

RNA quantity of seen for both decreased continually indicating reduction of viable cells. But at 72 h post exposure, the action of the brew forms on the CSCs were no longer sustained as the CSCs started replicating as shown by the increase in RFU (Figure 3:3). For DNA quantification, the two-way ANOVA of *C. sinensis* brew forms revealed a significant main effect of time ($F(3, 9) = 12.40$, $p = 0.0015$), concentration ($F(3, 9) = 34.04$, $p<0.0001$), and time x concentration interaction ($F(9, 27) = 1.134$, $p = 0.3737$). Post hoc comparisons of DNA fluorometric quantification at 6 h showed no difference between the CSCs RFU of the control and the brew forms ($p \geq 0.05$). At 24 h, the CSCs RFU for control and the 100% cold brew form still showed no significant increase or decrease while there was a significant increase in the RFU of control compared to 100% hot brew form. For both brew forms and control, the 24 h RFU was significantly lower than 6 h. At 48 h post exposure, there was a significant increase in the RFU of control compared to both brew forms of *C. sinensis (p >0.9999).* At 72 h, there was no significant increase between the RFU of the control and 100% cold brew *(p= 0.0923)* while there was a significant increase between the control and the 100% hot brew form (*p= 0.*0192). As observed in with the RNA fluorometric quantification, the RFU of both treatment groups increased in with significant increase between 72 h and 48 h. However, the increase in control RFU was significantly higher than seen for both treatment groups. Again, this result suggests that between 6 h to 48 h post treatment of CSCs with hot and cold brew forms of *C. sinensis*, the DNA quantity of seen for both decreased continually indicating reduction of viable cells. But at 72 h post exposure, the 48-h cytotoxic action of the brew forms on the

CSCs were no longer sustained as the CSCs started replicating as shown by the increase in RFU (Figure 3:3).

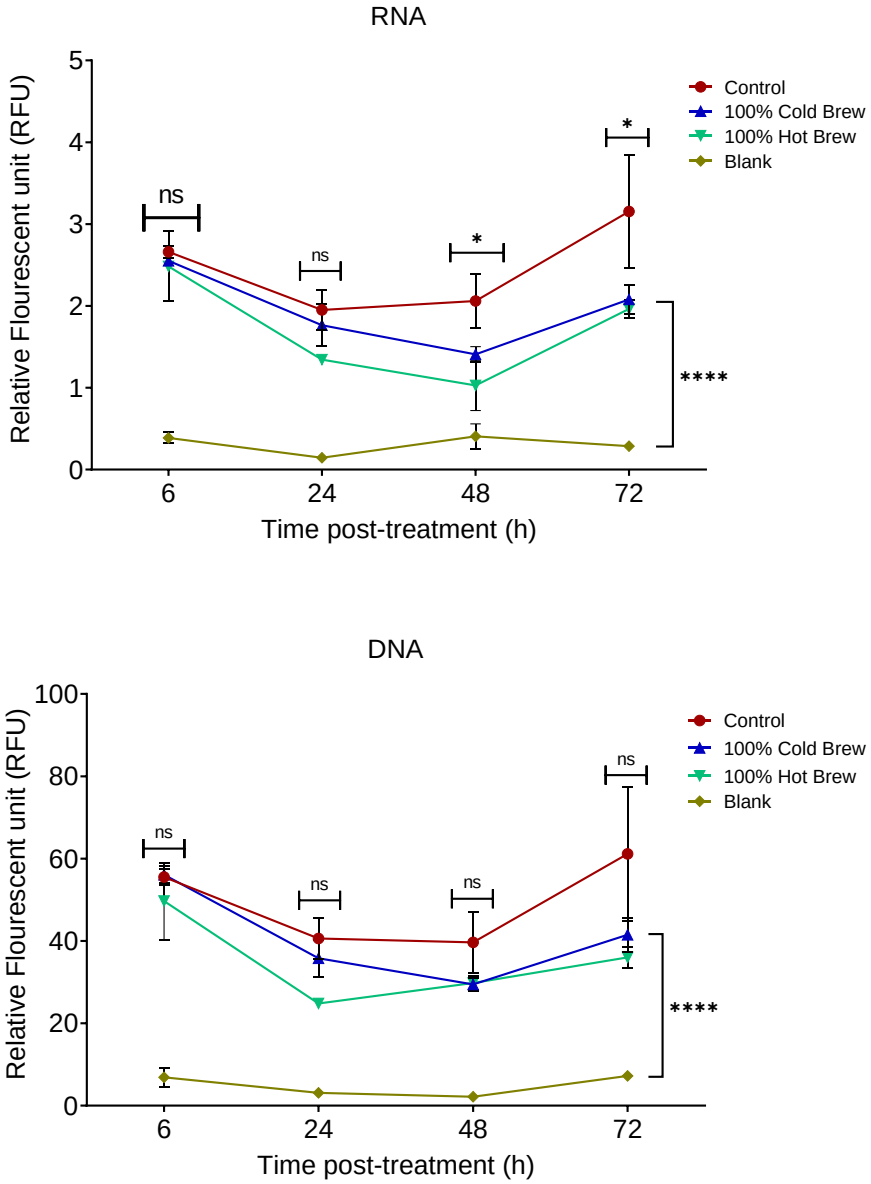

Figure 3:3: Fluorometric quantification of RNA and DNA to evaluate CSCs viability while exposed to 100% cold and hot *C. sinensis* tea brew. The replication kinetics of CSCs quantified with RNA shows that between 6 h to 24 h there was reduction of RFU for all the treatment groups including the negative control. Between 24 h to 48 h, the RFU of cold and hot brew reduced further while that of the negative control increased. Between 48 and 72 h, all treatment groups recorded different variations of RFU increase indicative of cell replication. The replication kinetics of CSCs quantified with DNA shows that between 6 and 24 h there was reduction of RFU for all the treatment groups including the negative control. This trend was also seen between 24 and 48 h. However, between 48 and 72 h, all treatment groups recorded different variations of RFU increase also indicative of cell replication. For both nuclei acid quantification, the positive control recorded significant decrease when compared with all the treatment groups at all the time points. (* $p \leq 0.05$; **** $p \leq 0.0001$; ns, non-significant).

3.3.1.3 SV40-iHCECs cytotoxicity with cold brew

In determining the toxicity of various concentrations of cold C. sinensis brew (25%, 50%, 75%, 100%; v/v) against iHCECs, a two-way ANOVA revealed a significant main effect of time ($F(4, 8) = 86$, $p < 0.0001$), concentration ($F(3, 6) = 14.33$, $p = 0.0038$), and time x concentration interaction ($F(12, 24) = 11.34$, $p < 0.0001$). Post-hoc comparisons at 3 h showed no significant difference between the control and treated cells ($p > 0.05$). At 24 h post-treatment, the OD values were increased for control cells compared to all treated cells ($p < 0.05$). Also, 100% cold brew caused a significant reduction in the cell growth compared to cells treated with lower concentrations ($p < 0.05$). Between 24 to 72 h, the control cells exhibited progressive increase in the growth rate compared to cells treated with all concentrations ($p < 0.0001$). The 100% *C. sinensis* brew continued to cause gradual decrease in cell growth with significant decrease between it and control ($p < 0.05$) . Interestingly, the growth rates of cells treated with 25, 50 or 75% *C. sinensis* maintained a similar trend (i.e., no increase or decrease) (Figure 3:4). This result indicates that cold *C. sinensis* brew does have a toxic effect against iHCECs particularly at 100% (highest) concentration.

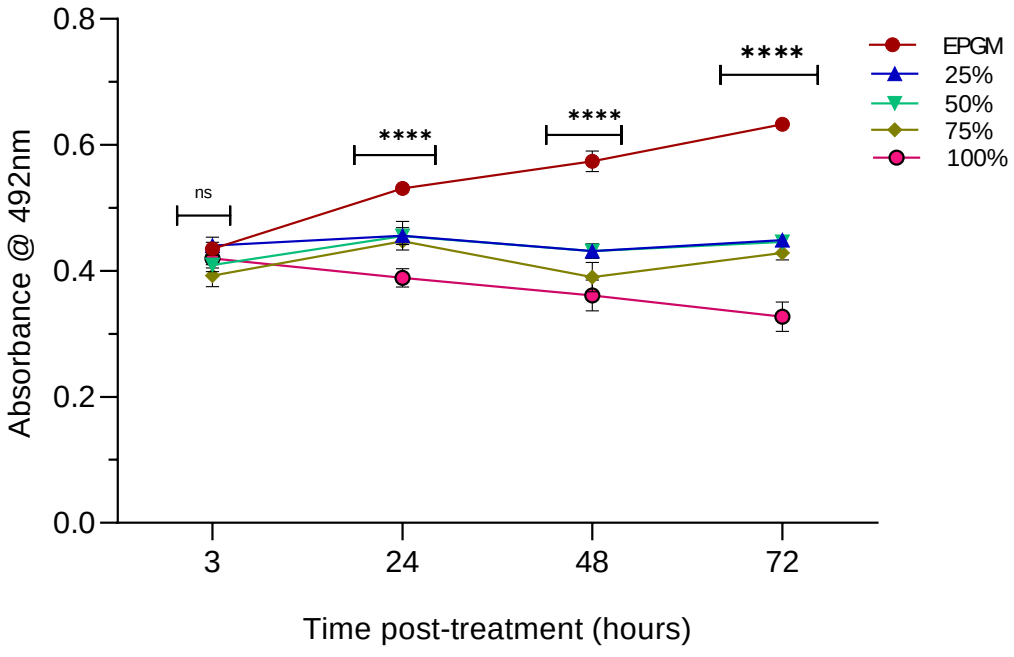

Figure 3:4: SV40-iHCECs cytotoxicity when exposed to cold *C. sinensis* brew. At 3 h there was no OD increase between the control and the treatment group. At 24 h there was significant difference increase the control OD and all the treatment groups. This trend of significant increase persisted till 72 h when the experiment was terminated. The OD of 25%-75% showed a form of arrested replication and or transient cellular termination with a sustained OD of iHCECs over the duration of 72 hours post exposure while 100% cold *C. sinensis* brew showed progressive decline of OD relating to cold *C. sinensis* brew toxicity to iHCECs (**** $p \leq 0.0001$; ns, non-significant).

3.3.1.4 Comparative corneal cytotoxicity of hot versus cold C. sinensis brew

The previous results showed that primary CSCs did not exhibit sustained cytotoxicity to 100% v/v concentrations of hot and cold *C. sinensis* brew after 72 hours of exposure compared to the control (Figure 3:1 & Figure 3:2), represented by increased optical density (OD) between 48 h and 72 h post treatment which is indicative of increased cellular replication. A comparative evaluation of cytotoxicity of the highest concentrations of hot and cold *C. sinensis* (75% and 100%) was done.

In determining comparative of cytotoxicity of the two highest concentrations of cold and hot *C. sinensis* brew (75% & 100%; v/v) against CSCs, a two-way ANOVA revealed a significant main effect of time ($F(3, 12) = 72.41$, $p < 0.0001$), concentration ($F(4, 16) = 28.18$, $p < 0.0001$), and time x concentration interaction ($F(12, 48) = 20.32$, $p < 0.0001$).

Post-hoc comparisons at 3 h showed a significant increase between the control and *C. sinensis* treated cells ($p< 0.0001$) while there was no significant increase or decrease between brew concentrations. At 24 h post-treatment, the OD values for the control and all the treatment concentration had no significant increase or decrease ($p > 0.05$). The lack of significant increase or decrease between the *C. sinensis* concentrations sustained till 72 h when the experiment was terminated. At 48 h, the OD value of the control was significantly increased in comparison to the OD of all treated cells ($p < 0.0001$), this trend was equally sustained till 72 h when the experiment was terminated. Despite the significant increase in OD of control compared to the *C. sinensis* treated cells, the OD of the treated indicated that there was no sustained cytotoxicity with *C. sinensis* (Figure 3:5)

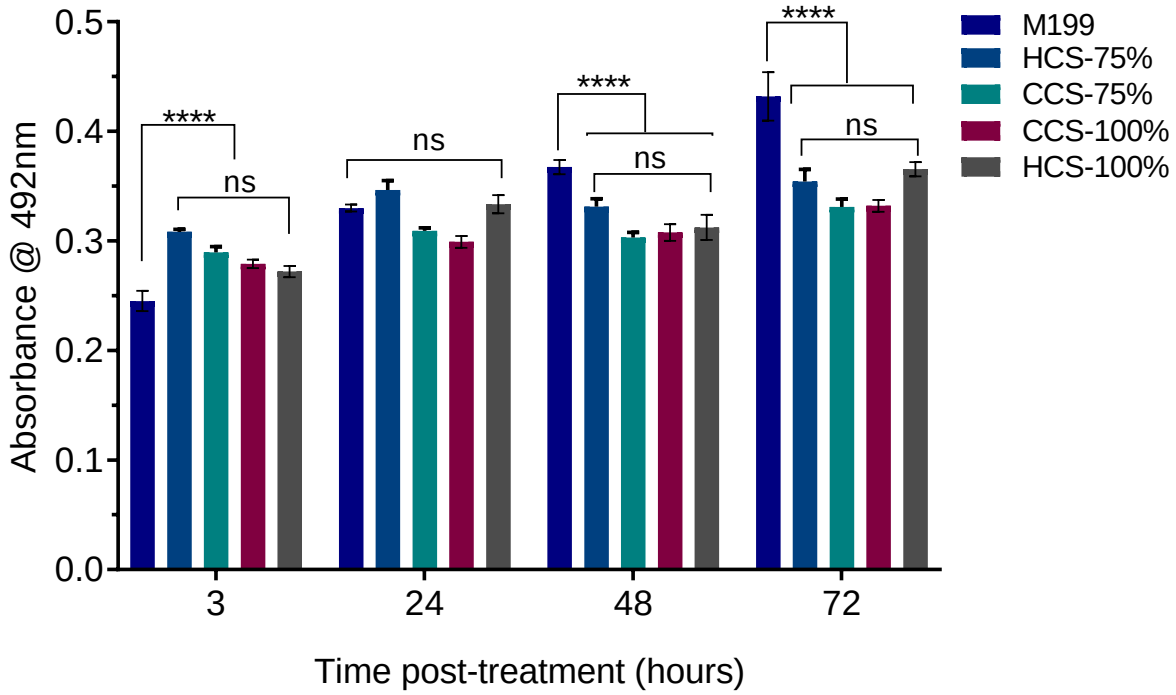

Figure 3:5: CSCs cytotoxicity showed no difference between highest concentration of cold and hot *C. sinensis* brew with between 3 to 72 hours post exposure. The control showed significant increase of OD compared to the treatment groups at 3, 48 and 72 h. At 48 h, there was not difference between the OD of control and all the treatment groups. (**** $p \leq 0.0001$; ns, non-significant).

3.3.2 Trophozoite optimal seeding density

The aim of this experiment was to examine whether initial seeding density and seeding time can influence trophozoite seeding efficiency, and consequently any subsequent analysis. While developing the colorimetric assay based on sulforhodamine B (SRB) dye protocol (Ortega-Rivas et al., 2016), BioTek's PowerWave XS absorbance microplate reader was used. Bearing this in mind and also considering that only the L-T 4000 microplate reader was available in our labs, there was a need for an experiment to optimize the seeding density of *A. castellanii* in 96 well plates. To determine the optimal seeding density, *A. castellanii* trophozoites at various concentrations (1×10^3, 2.5×10^3, 5×10^3, 7.5×10^3 and 10×10^3 trophozoites/well) were incubated over a period of 72 h. Apart from 1×10^3, all other concentrations grew to confluency by 72 h in 96-well plates. Two-way ANOVA revealed a significant main effect of time ($F(5, 10) = 580.9$, $p < 0.0001$), trophozoite number ($F(2, 4) =$

983, $p < 0.0001$), and time x trophozoite number interaction (F (10, 20) = 58.89, $p < 0.0001$). Using the quantitative colorimetric SRB assay for testing *A. castellanii* growth kinetics, it was deduced that the optimum seeding density for 96-well plates with the L-T 4000 microplate reader (Labtech, UK) is 2.5×10^3 trophozoites/well. During the experiment, the approximate number of trophozoites for each group was significantly increased between each time point of 24, 48 and 72 h, except for 1×10^3 which showed significant increase in cell numbers only between 48 h and 72 h (Figure 3:6).

At 24 h, 10×10^3 showed significant increase in OD ($p < 0.0001$) in comparison with the other concentrations. 5×10^3 and 7.5×10^3 were grouped together with no significant difference in their OD ($p > 0.05$), and the same was observed for 1×10^3 and 2.5×10^3 ($p > 0.05$) which were equally grouped together with no significant difference in their OD. At 48 h, there was no significant difference in cell number between 7.5×10^3 and 10×10^3 concentrations ($p > 0.05$). However, there was significant increase between the 7.5×10^3 and 10×10^3 concentrations and the 1×10^3, $2.5\times10^3$and 5×10^3 concentrations ($p < 0.0001$). At 72 h, there was no significant difference between the OD of 10×10^3, 2.5×10^3, 5×10^3 and 7.5×10^3 concentrations, the 1×10^3 concentration has a significant decrease of OD in comparison to the higher cell concentrations ($p < 0.0001$). Although, individual analysis of 2.5×10^3 and 5×10^3 concentrations showed significant increase at 24 and 48 h, there was no significant increase or decrease of their OD at the termination of the experiment (72 h). The growth curve of replication of 2.5×10^3 in relation to other seeding densities suggest that using 2.5×10^3 as an initial seeding density can clearly delineate the changes in the growth rate of trophozoites in response to treatment compared to the control at each time-point during the course of a 72-h experiment. After 48 hours post-incubation, the optical densities of trophozoite concentrations above 2.5×10^3 / well did not differ statistically from subsequent incubation times, which can be related directly to the possibility of cell confluency within the restricted parameters of the well, such as area available for further replication and presence of nutrients needed for replication.

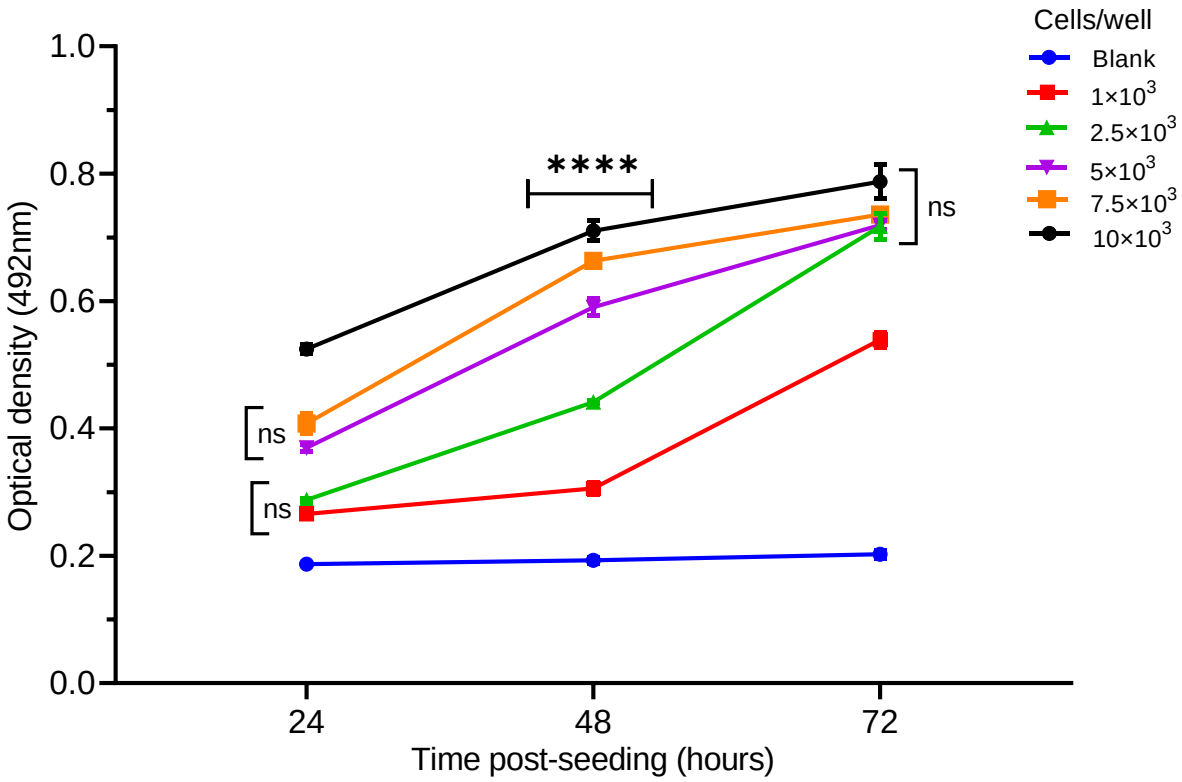

Figure 3:6: Calibration curves of SRB assay on *A. castellanii* trophozoites to determine optical density over 72 hours. Points are mean± S.D of six replicates from one plate. At 24 h post seeding . 5×10^3 and 7.5×10^3 were grouped together with no significant difference in their OD, same trend is seen for 1×10^3 and 2.5×10^3 . At 48 h, there is significant difference between all ODs. At 72 post seeding, OD of all the cell concentrations show no significant difference apart from the OD of 1×10^3 which shows a significant decrease in comparison with other cell concentrations.(**** $p \leq 0.0001$; ns, non-significant).

3.3.3 Inhibitory effects of *C. sinensis* brews on *A. castellanii* trophozoites

3.3.3.1 Microscopic analysis of C. sinensis effect on trophozoites

The direct anti-amoebic effects of hot brew on the morphology, structure, and differentiation stages during replication of *A. castellanii* trophozoites was observed using light microscopy. At 24 hours post treatment, visual results (Figure 3:7) showed extensive cytolysis with cytoplasmic contents expelled into the culture media in the form of extracellular vehicles (EVs). Large single walled cysts were formed by trophozoites in the 100% hot brew, indicative of immature cysts and incomplete or arrested encystation. At 48 hours, there was progressive cytolysis observed in 25%, 50% and 75% hot *C. sinensis* brew treatment groups with more

EVs observed in the culture. 100% hot *C. sinensis* brew treatment still showed large one walled cyst with cytoplasmic contents tapering to a corner of the cyst (Figure 3:8). Adhesion to flask surfaces was inhibited by all *C. sinensis* concentrations, which was observed with gentle agitation of the flasks from side to side. At 72 hours, the progressive cytolysis continued, with incomplete and arrested encystation seen in 50% and 100% hot brew groups (Figure 3:9). In the 50% hot brew group, the parasites got enlarged and had prominent and centrally located nuclei. On closer observation of the 100% hot brew treatment between 24 to 72 hours, the parasites got enlarged displaying a distinctively large nucleus in the presence of hot brew. Observing each time point between 24 hours to 72 hours, it appears as if the intracellular contents were pushed to one end of the cell after which they were subsequently expelled. This happened for all treatment group but the visual results were clearer in 100% hot brew. Also, in the 100% hot brew, the immature cysts were sustained in the form mentioned earlier from 24 to 72 hours followed by expulsion of cytoplasmic contents (EVs). These results illustrate that not only, were trophozoites significantly damaged when treated with 75% and 100% *C. sinensis*, but also the parasite's ability to counter the treatment by differentiating into cysts was inhibited at 100% *C. sinensis*. The CHX treatment group showed no trophozoites from 24 to 72 hours as they were totally destroyed. Similar visual results were for cold brew (not shown) microscopic examinations.

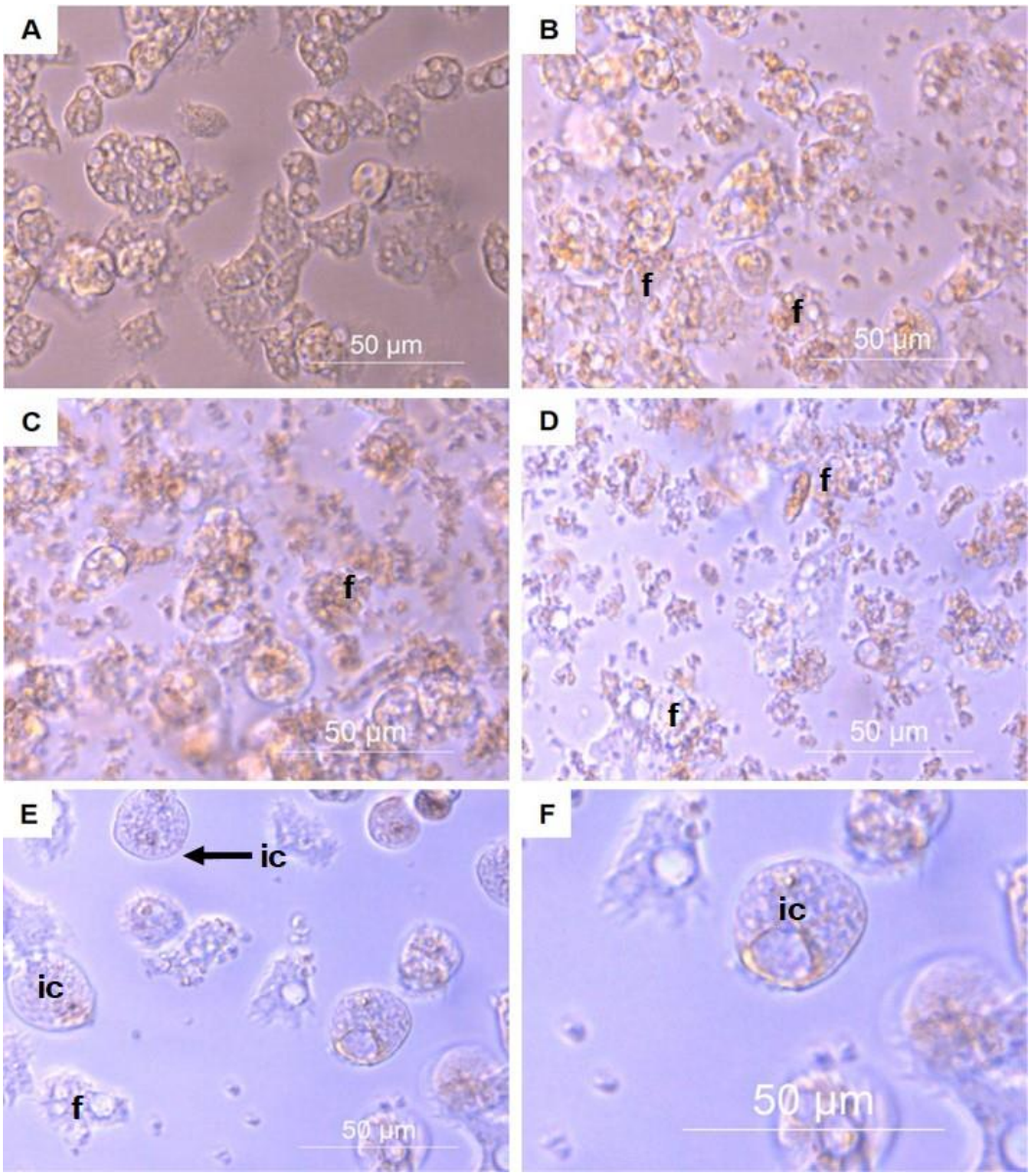

Figure 3:7: *A. castellanii* trophozoites at 24 hours post treatment with graded doses of hot *C. sinensis* brew. (A) control culture with PGY. (B to E) treatment groups with 25%, 50%, 75% and 100% hot *C. sinensis* brew respectively. (F) 100% hot *C. sinensis* brew showing formation of large one walled cysts with prominent nucleus. Distinctive cellular destruction observed in 25%, 50% and 75% *C. sinensis*. *Abbreviations*: (f) fragments of lysed cells depicted by presence of extracellular vesicles. (ic) incomplete encystation. X40 magnification. Scale bar = 50 µm.

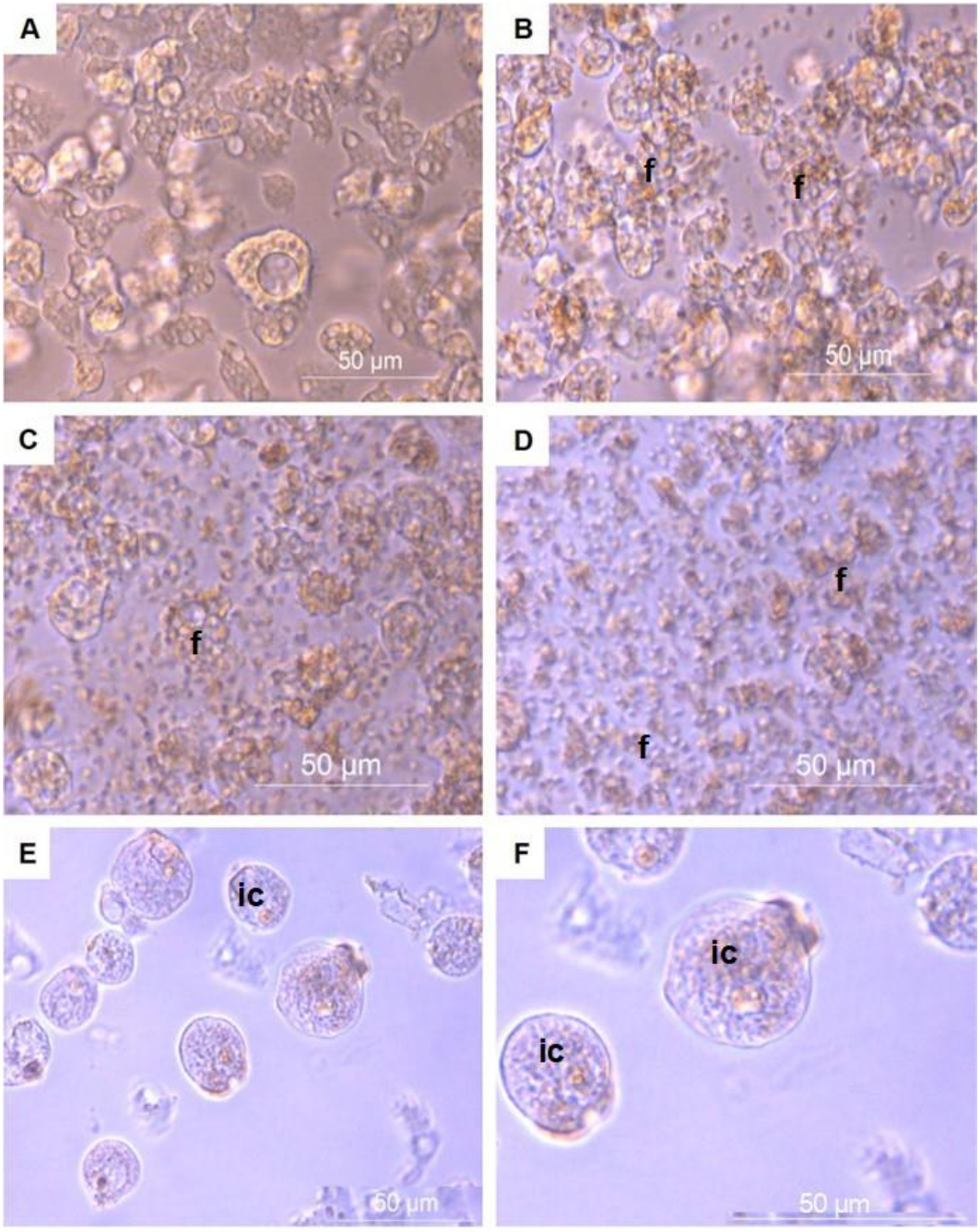

Figure 3:8: *A. castellanii* trophozoites at 48 hours post treatment with graded doses of hot *C. sinensis* brew. (A) Control culture with PGY. (B to E) treatment groups with 25%, 50%, 75% and 100% hot *C. sinensis* brew respectively. (F) 100% hot *C. sinensis* brew showing formation of large one walled cysts (ic) with cytoplasmic contents tapering to corner of the cyst. Progressive cytolysis observed in 25%, 50% and 75% *C. sinensis*. Adhesion to flask surfaces was inhibited by all *C. sinensis* treatment groups. *Abbreviations*: (f) Fragments of lysed cells. (ic) incomplete encystation. X40 magnification. Scale bar = 50 µm.

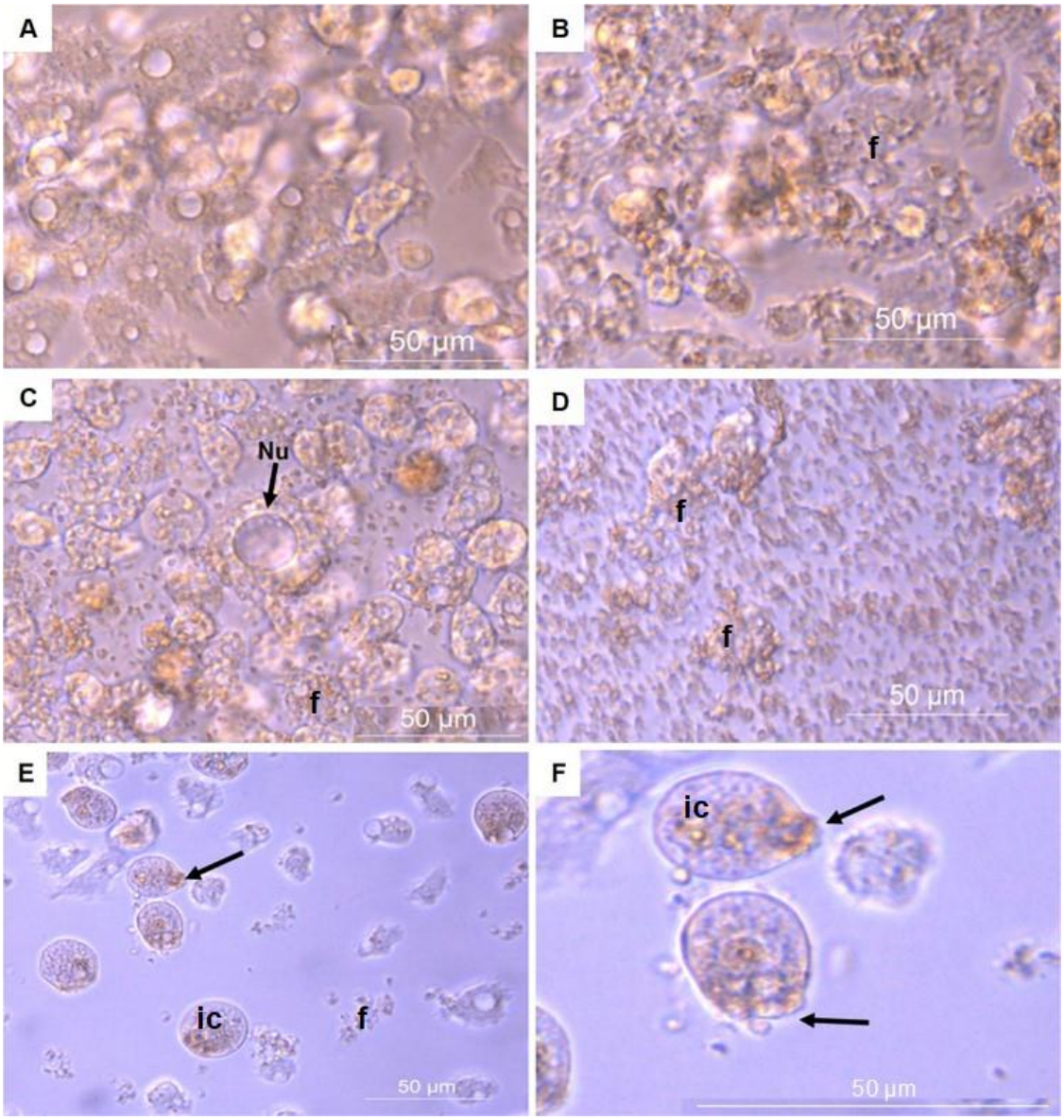

Figure 3:9: *A. castellanii* trophozoites at 72 hours post synchronised treatment with graded doses of hot *C. sinensis* brew. (A) control culture with PGY. (B to E) treatment groups with 25%, 50%, 75% and 100% hot *C. sinensis* brew respectively. (F) 100% hot *C. sinensis* brew showing formation of large one walled cysts with (arrows) expulsion of cytoplasmic contents depicted by presence of extracellular vesicles. (Nu) prominent centrally located nucleus seen on in treatment groups (B to E). *Abbreviations*: (f) Fragments of lysed cells. (ic) incomplete encystation. Progressive cytolysis observed in 25%, 50% and 75% *C. sinensis*. X40 magnification. Scale bar = 50 µm.

3.3.4 Determination of trophozoite replication and growth using SRB Assay

3.3.4.1 Hot brew C. sinensis against trophozoites

To determine the in vitro acanthamoebicidal activity of 25%, 50%, 75%, 100% concentrations v/v of hot *C. sinensis* brew, the SRB assay was also used, and the optical density readout analysed. The two-way ANOVA revealed a significant main effect of time ($F(5, 10) = 27.38$, $p < 0.0001$), concentrations of hot brew ($F(4, 8) = 22.95$, $p = 0.0002$), and the interaction between both factors ($F(20, 40) = 13.22$, $p < 0.0001$).

Post-hoc comparisons showed no significant differences between all the treatment groups between 3 to 6 hours. At 24-hour post treatment, comparisons between negative control (PGY) and the 25%-75% hot brew treatment groups showed no significant increase or decrease in OD ($p \geq 0.05$). However, comparisons between negative control (PGY) and the 100% hot brew and positive control showed a significant difference ($p < 0.05$ respectively). Interestingly comparisons between the OD of positive control (CHX) and all the hot brew treatments showed also showed no significant difference ($p \geq 0.05$). The differences above indicates that the cellular replication as represented by OD seen in the negative control group is not seen in the positive control and 100% group. At 48 hours, there were significant increase between the negative control OD and the rest of the hot brew treatment groups ($p < 0.0001$). Meanwhile the OD of the positive control showed no significant increase or decrease when compared to 75% and 100% hot brew. At 72 hours post treatment, the trend seen between the negative control as mentioned for 48 h persisted at 72 h with no significant increase in OD when compared with the hot brew treatment groups and positive control ($p < 0.0001$). Also, the trend seen in the comparisons between the positive control and 75%-100% hot brew showed no significant difference ($p \geq 0.05$) of OD.

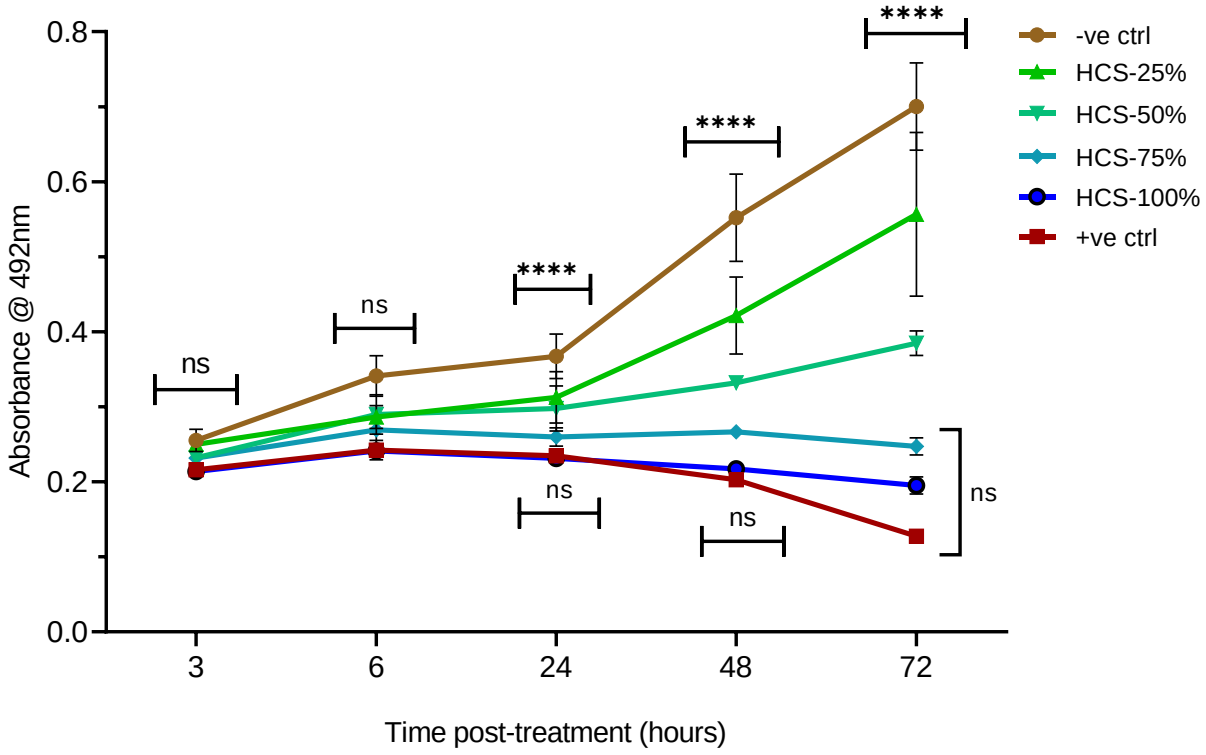

Figure 3:10: Acanthamoebicidal activity of hot brew *C. sinensis* on trophozoites. At 3-6 h post exposure, there significant increase or decrease between the negative or positive controls in comparison to the hot brew concentrations. At 24 h, the positive control showed no significant increase or decrease in comparison with 25%-75% groups, while it showed significant OD increase when compared to 100% treatment. Inversely, the OD of the positive control had no significant increase or decrease when compared with all the hot brew concentrations. At 48 h, the OD of negative control was significantly increased in comparison with all the treatment group, this trend persisted till the end of the experiment (72 h). For positive control comparisons at 48 h, there was no significant increase or decrease of OD when compared with 75% and 100% how brew. This trend also continued till the termination of the experiment (72 h) showing that 75% and 100% hot brew exhibited acanthamoebicidal activity mimicking that of Chlorhexidine (+ve ctrl), (**** $p \leq 0.0001$, ns; non-significant).

This result (Figure 3:10) further confirms that over a period of 72 hours post exposure of *A. castellanii* to hot *C. sinensis* brew, there was dose dependent acanthamoebicidal activity expressed as OD indicating inhibition of cellular growth (replication). 75% and 100% hot *C. sinensis* brew inhibited parasite growth and exhibited acanthamoebicidal activity between 6 to 72 hours mimicking the growth kinetic trajectory exhibited by Chlorhexidine gluconate (+ve ctrl).

3.3.4.2 Cold C. sinensis brew against trophozoites

The two-way ANOVA revealed a significant main effect of time F (5, 15) = 648.1, p <0.0001*)*, graded concentrations of cold *C. sinensis* brew*(v/v)* (F (4, 12) = 208.6, p <0.0001*)*, and the interaction between both factors (F (20, 60) = 103.9, p <*0*.0001*)*. Post-hoc comparisons between the treatments at 3 hours showed significant increase between the negative control (PGY) and the 100% cold brew (p <0.0001*)* with no significant increase in OD between control and 25%-75% cold brew (p ≥0.05). Inversely, comparison between the positive control and 25%-75% cold brew showed significant decrease in OD of control compared to the brews *(p* <0.0001*)* (Figure 3:11). The positive control however showed no significant difference in OD in comparison with 100% cold brew (p ≥0.05). At 6 hours post exposure, the comparison between the negative control OD and the cold brew showed no significant difference between it and 25%-75% cold brew (p ≥0.05), while it showed significant increase in OD compared to 100% cold brew (p<0.01). Comparisons of positive control OD with the cold brews showed no significant difference between it and 50%-100% brew (p ≥0.05), while there was a significant decrease in OD compared to 25% cold brew (p< 0.05). At 24 hours, with the exception of 25% cold brew, there was significant increase in OD in comparison with the 50%-100% cold brew *(p* <0.0001*)*, Inversely, except for 25% cold brew, there was no significant difference between the positive control OD and the 50%-100% cold brews.

At 48 hours, there were significant increases between the negative control and the rest of the treatment groups *(p*<0.0001 respectively*)*, with no significant decrease between the positive control and the 75% and 100% cold brew (p ≥0.05). This indicated that the level of Acanthamoebicidal activity shown by the positive control was similar to that of 75% and 100% cold *C. sinensis* brew.

At 72 hours post treatment, the negative control continued to show significant increases in OD when compared with the treatment groups 50%-100% (p<0.0001) with no significant difference of OD in comparison with 25% cold brew (p ≥0.05). The positive control equally showed significant decrease in OD when compared with 25% and 50% cold brew but showed

no significant difference when compared to 75% and 100% cold brew ($p \geq 0.05$). This result indicates that from 24 hours post exposure to cold *C. sinensis* brew, the 75% and 100% treatments had acanthamoebic activity which was progressive up to the end of the experiment (72 hours) with no significant difference with the positive control.

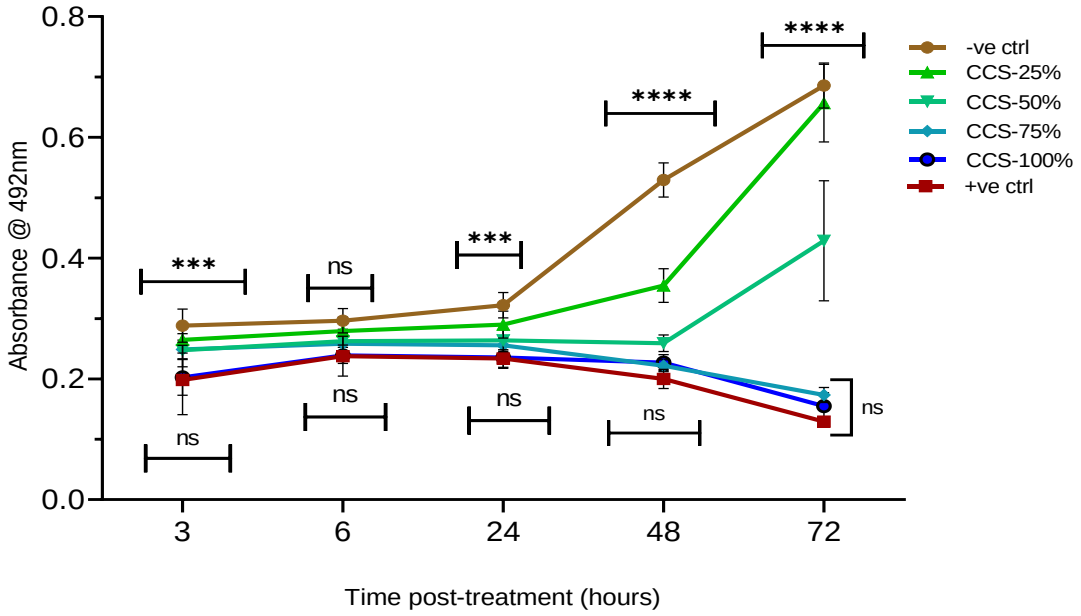

Figure 3:11: Acanthamoebicidal activity of cold brew *C. sinensis* on trophozoites. At 3h post exposure there was no significant differences between OD of negative control and 25%-75% cold brew, while there was also no significant difference between the positive control OD and the 100% cold brew. At 6 h, the trend persisted inversely when comparing the negative and positive controls to the cold brews. At 24 h, apart from the 25% cold brew, there was significant increase in OD when comparing negative control to the cold brews (50%-100%), inversely, this was also the case with positive control comparisons where apart from 25% cold brew there was no significant difference with the 50%-100% cold brews. At 48 h, there was significant increase in OD between the negative control and all the cold brews (25%-100%), while there was no significant difference between the positive control and the 75% and 100% cold brew. These trends persisted till the termination of the experiment (72 h). 75% and 100% hot brew exhibited acanthamoebicidal activity mimicking that of Chlorhexidine (+ve ctrl), (*** $p \leq 0.001$,**** $p \leq 0.0001$, ns; non-significant).

3.3.5 External ultrastructural changes of *C. sinensis* treated trophozoites

External ultrastructural characteristics of *C. sinensis* brew-treated trophozoites using SEM methods as described in General Methods revealed progressive morphological alterations and destruction of *A. castellanii* trophozoites treated with cold *C. sinensis* brew (Figure 3:12). At 24 h post treatment, trophozoites treated with *C. sinensis* brew showed loss of acanthopodia and also had lost their ability to adhere to each other.

.

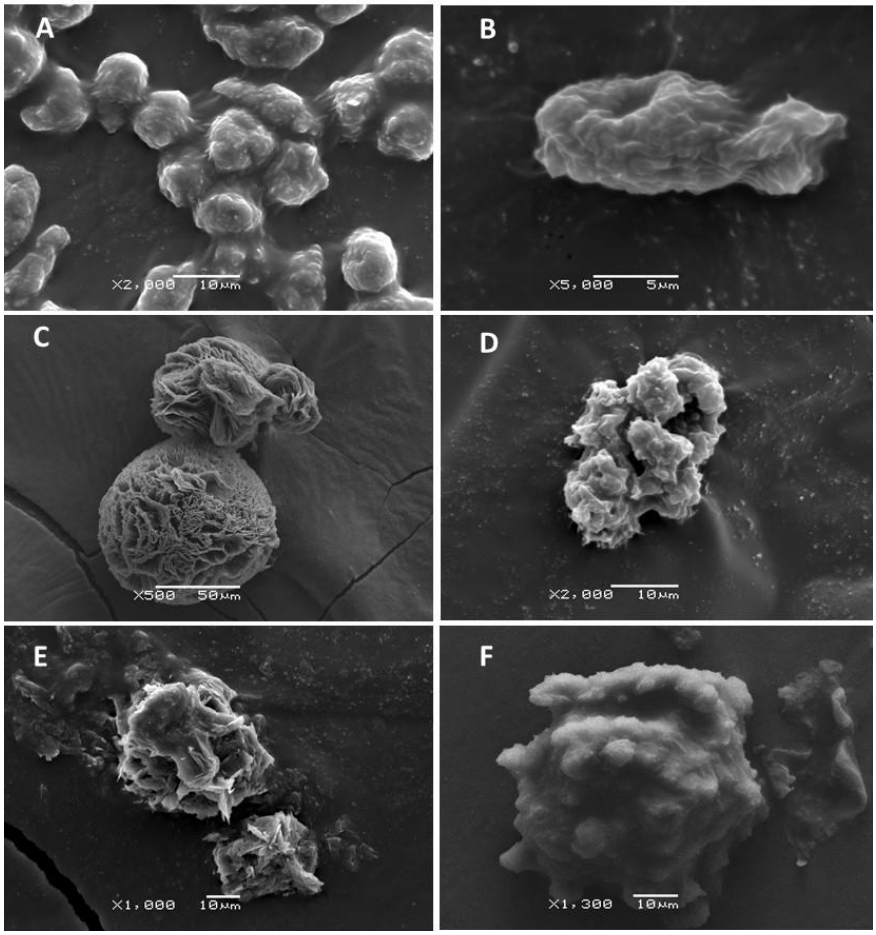

Figure 3:12: Scanning electron microscopy (SEM) micrographs showing loss of protective film of *A. castellanii* and shrinking of cell size possibly in the attempt to encyst. Continued exposure to both Chlorhexidine and *C. sinensis* brew shows loss of acanthopodia and progressive destruction of *A. castellanii* trophozoites. (A) Trophozoites in PGY (control) linked together by adhesin; (B) Single *A. castellanii* in PGY (C) Trophozoites in chlorhexidine at 24 hours showing loss of protective adhesin. (D) Trophozoites in *C. sinensis* brew at 24 hours showing loss of adhesion and misshaped; (E) Destruction of trophozoite in chlorhexidine at 72 hours; (F) Trophozoite in *C. sinensis* brew at 72 hours showing loss of adhesion, misshaped and shrunken. With increased duration of exposure to C. sinensis brew trophozoites shrivel and shrink in size as depicted by the decrease of magnification. Magnification: X2000, X5000, X500, X2000, X1000 and X1300 for A-F respectively; Scale bars: 10, 5, 50, 10, 10 and 10 µm for A-F respectively.

The trophozoites were seen to shrink in size possibly in an attempt to encyst and appear shrivelled, while the trophozoites in PGY were seen clumped together and linked with a protective layer which might be adhesin. The CHX treated trophozoites showed trophozoites that had lost their adhesive protection similar to the trophozoites seen in the *C. sinensis* brew. With increased exposure (72 hours), the trophozoites exposed to *C. sinensis* brew developed abnormal shape and finally become fragmented. Comparison with the results of trophozoites exposed to *C. sinensis* brew with CHX treated trophozoites showed the same or similar morphological ultrastructural changes.

3.3.6 Internal ultrastructural changes of *C. sinensis* treated trophozoites

The internal ultrastructural changes within the cold brew *C. sinensis*-treated trophozoites were examined using TEM methods as described in the General Methods. Intracellular ultrastructural damages were seen which confirms the microscopic examinations that showed expulsion of EVs after the loss of cell membrane integrity (Figure 3:13). At 24 hours post treatment, the 100% *C. sinensis* brew group was already showing loss of cellular membrane material, presumably acanthopodia, with the reduction and/or loss of intracellular organelles like the mitochondria, food vacuole and the normally centrally located nucleus. At 48 hours post exposure, the *C. sinensis* brew group showed progressive loss of cellular membrane integrity with continuous fragmentation of the trophozoites and expulsion of cellular vehicles. By 72 hours, TEM analysis of the ultrastructural changes within the *C. sinensis* brew-treated trophozoites showed evidence of complete trophozoite destruction characterised by the complete loss of cell membrane integrity, blotting out of the food vacuoles and mitochondria. For the CHX group, there were no visible images in the TEM micrographs from 24 hours to 48 hours post exposure to 0.02% CHX

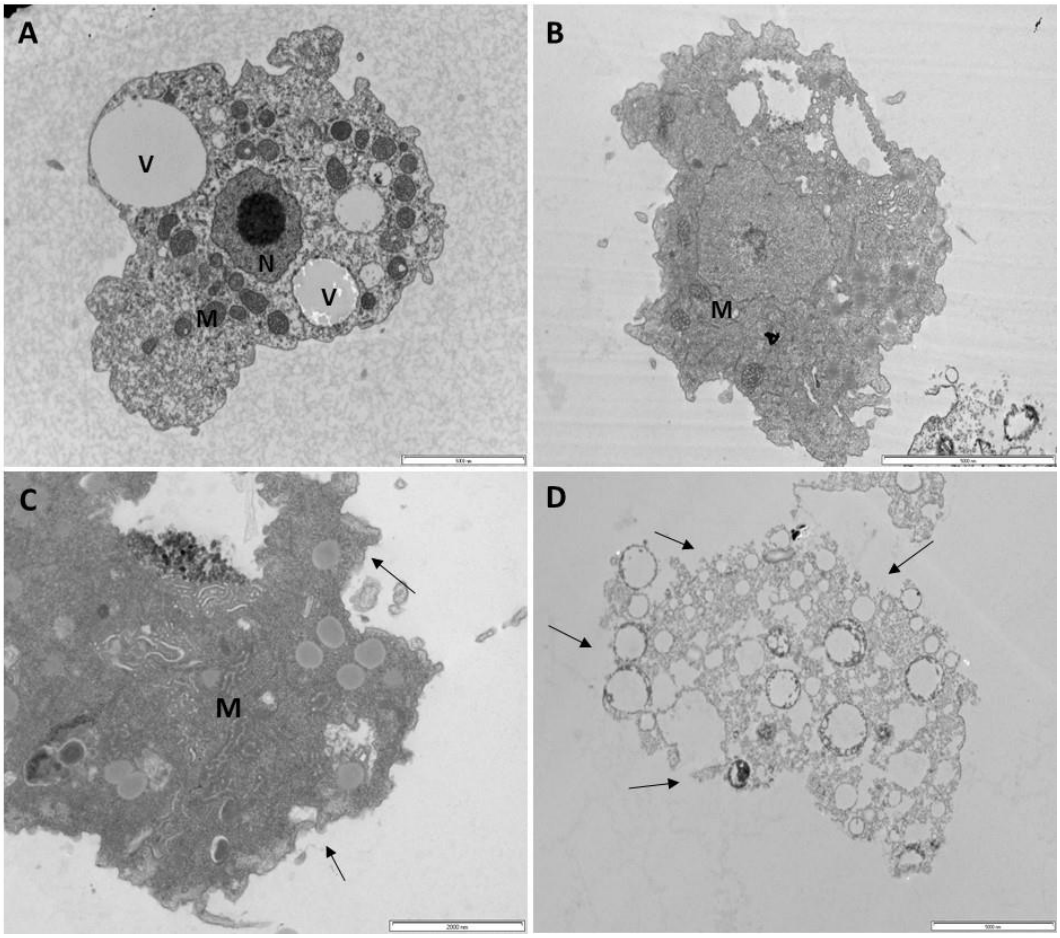

Figure 3:13: Transmission electron microscopy (TEM) micrographs showing progressive destruction of *A. castellanii* trophozoites exposed to *C. sinensis* brew. (A) Trophozoite in control media (PGY), (B) Trophozoites in 100% *C. sinensis* brew at 24 hours showing loss of cellular membrane material which are presumably acanthopodia, (C) Trophozoite at 48 hours showing loss of cellular membrane integrity (D) At 72 hours post exposure to C. sinensis trophozoite loses cellular membrane integrity. (V)food vacuole, (M)mitochondria, (N)Nucleus, (Arrow) loss of cellular membrane integrity. Magnifications: X6,000, X8,200, X16,500 and X4,200 for A-D respectively; Scale bars: 5,000 nm (A & B) 2,000 nm, (C) 1,000 (D) 5,000 nm.

3.3.7 Transient effect of *C. sinensis* brew against *A. castellanii* trophozoites

To determine the in vitro acanthamoebicidal transient activity of 100% hot and cold brew concentrations v/v, haemocytometer was used. The trophozoite growth inhibition percentage of each brew was evaluated.

The two-way ANOVA of 6 h transient exposure of *A. castellanii* to *C. sinensis* revealed a significant main effect of time ($F(2, 6) = 64.65$, $p < 0.0001$), concentration ($F(2, 3) = 677$, $p < 0.00001$), and a time x concentration interaction ($F(4, 6) = 32.11$, $p = 0.0003$). Post-hoc

comparisons for 6 h exposure showed no difference ($p > 0.05$) between the parasite growth inhibition caused by CHX and 100% *C. sinensis* cold brew (43% and 36%, respectively) at 24 h, with a significant increase ($p < 0.0001$) of growth inhibition between CHX and the hot brew. At 48 h, there was an increase of growth inhibition of 93% for the CHX with significant increase to cold and hot brews that had 44% and 41% growth inhibition, respectively ($p < 0.0001$). The trophozoite growth inhibition of CHX at 72 h was 97%, suggesting significant increase between growth inhibition caused by CHX compared to that of cold and hot brew *C. sinensis* ($p < 0.0001$), that caused 19% and 18% growth inhibition, respectively.

The two-way ANOVA of 24 h transient exposure revealed a significant main effect of time ($F(2, 6) = 233.4$, $p < 0.0001$), concentration ($F(2, 3) = 786.6$, $p < 0.00001$), and a time x concentration interaction ($F(4, 6) = 113.5$, $p < 0.0001$). Post-hoc comparisons for 24 h exposure showed parasite growth inhibition of 74.8%, 63.3%, and 86.4% for cold and hot brew *C. sinensis* and CHX, respectively. There was a significant increase in growth inhibition between the cold to hot brew and CHX ($p < 0.05$), and hot brew to CHX ($p < 0.0001$). The parasite growth inhibition for CHX increased at 48 h and subsequently at 72 h by 97.3% and 99.3%, respectively, while there was a sharp decline for the cold and hot brew *C. sinensis* at 48 and 72 h from 34.4% and 31% and 13.7% and 7.5%, respectively. The growth inhibitory effect of cold and hot brew had no significant difference ($p > 0.05$) with a significant decrease of inhibition ($p < 0.0001$) of both effects compared to that of CHX. These results (Figure 3:14) indicate that over a period of 72 h post-transient exposure of *A. castellanii* for 6 there was an increased inhibition of parasite growth for cold and hot brew between 24 and 48 h, which declined between 48 and 72 h. For 24 h post-transient exposure inhibition of parasite growth for cold and hot brew between declined progressively from 24-72 h. For both transient exposures CHX displayed progressive inhibition of parasite growth for 6 and 24 h exposure.

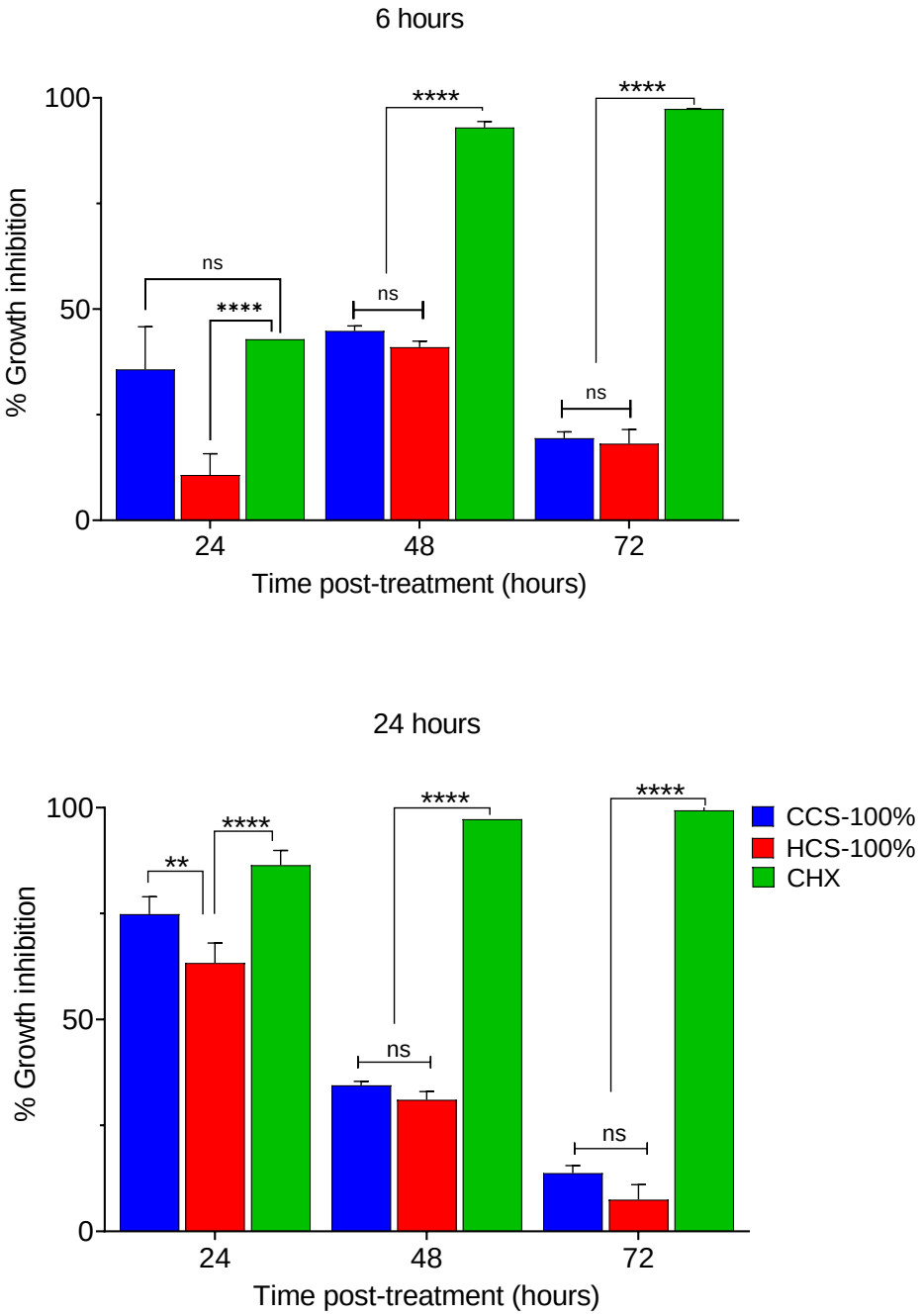

Figure 3:14: Percentage growth inhibition of trophozoites post transient exposure to cold and hot brew and Chlorhexidine for 6 and 24 hours. After 6 h transient exposure cold and hot brew growth inhibition increased between 24-48 h and decreased between 48-72 h. For 24 h transient exposure the growth inhibition percentage for both brews dropped progressively from 24-72 h. For both transient exposures there was significant increases between growth inhibition percentages of CHX and brew forms ($p < 0.0001$) at each time points. (**** p ≤0.0001, ns; non-significant).

3.3.8 Effect of *C. sinensis* brews on trophozoite encystation

3.3.8.1 Microscopic analysis of C. sinensis during encystation

Light microscopic observations showed that within 1 hour into the synchronised encystation process (Figure 3:15), the trophozoites in all the treatment groups had begun to show varying degrees of round shaped trophozoites, but it was too early to determine if encystation had commenced. The positive control (PMSF buffer) showed some trophozoites that seemed fragmented which was more pronounced in the 75% and 100% *C. sinensis* hot brew buffer treatment groups. The negative control also showed round shaped trophozoites but in addition there were *Acanthamoeba* aggregates which is seen most specifically in encysted *A. castellanii* where they are formed during encystation. At 2 hours post treated with the encystation buffers, the positive control group, 50%, 75% and 100% groups showed increased levels of cell destruction and by 4 hours all the treatment groups except the negative control showed signs of cellular destruction represented by EVs in form of fragments in the culture media.

At 12 hours post induction of encystation (Figure 3:16), cyst aggregates were observed in the negative control sample, while the positive control (PMSF) and *C. sinensis*-treated cultures showed signs of cellular degeneration characterised by the presence of particles in the encystation media. At 24 h, the control (untreated) showed normal encystation with well-defined cysts, and increased numbers of cyst aggregates, while the PMSF-treated culture and those treated with 25%, 50%, 75% and 100% *C. sinensis*, showed more damage (Figure 3:17). As seen in the negative control treatment, the *C. sinensis* treatment also showed cyst aggregates in which the aggregate sizes decreased as the concentration of C. *sinensis* increased. There were also different sizes of cysts with some approximately as large as 50µm. This trend progressed through 48 hours and by the end of 72 hours (Figure 3:18) there was clear cellular damage.

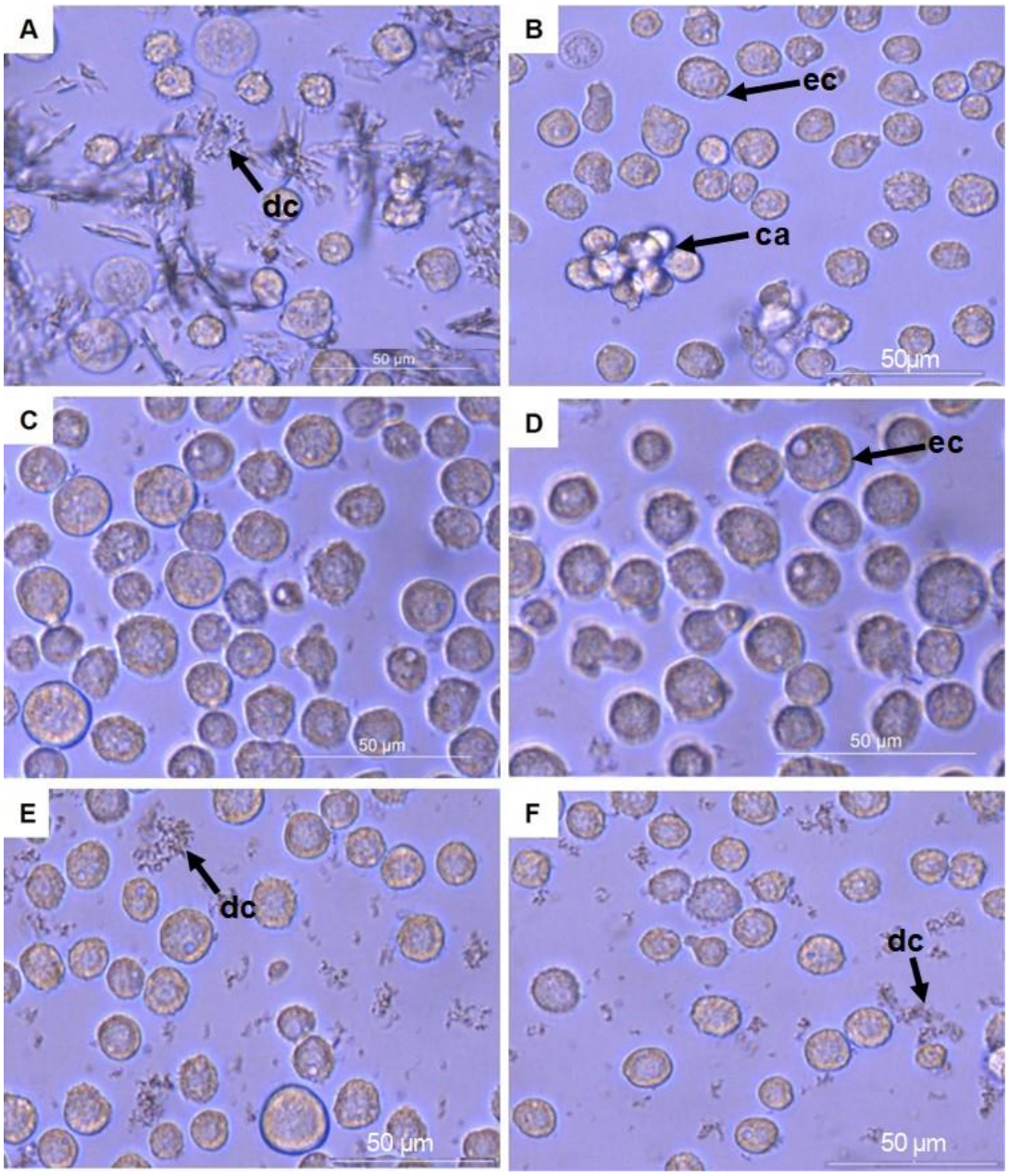

Figure 3:15: *A. castellanii* at 1 hour post induction of encystation. (A) Positive control culture with 5mM PMSF. (B) Control culture with 100% standardized encystation buffer. (C to F) treatment groups with 25%, 50%, 75% and 100% *C. sinensis* brew encystation buffer respective. Trophozoite destruction observed in 75% and 100% *C. sinensis* cultures with extracellular vesicles seen as fragments in the media. *Abbreviations*: (ec) encysted cells. (dc) destroyed cells. (ca) cyst aggregates. Scale bar = 50 µm. X40 magnification.

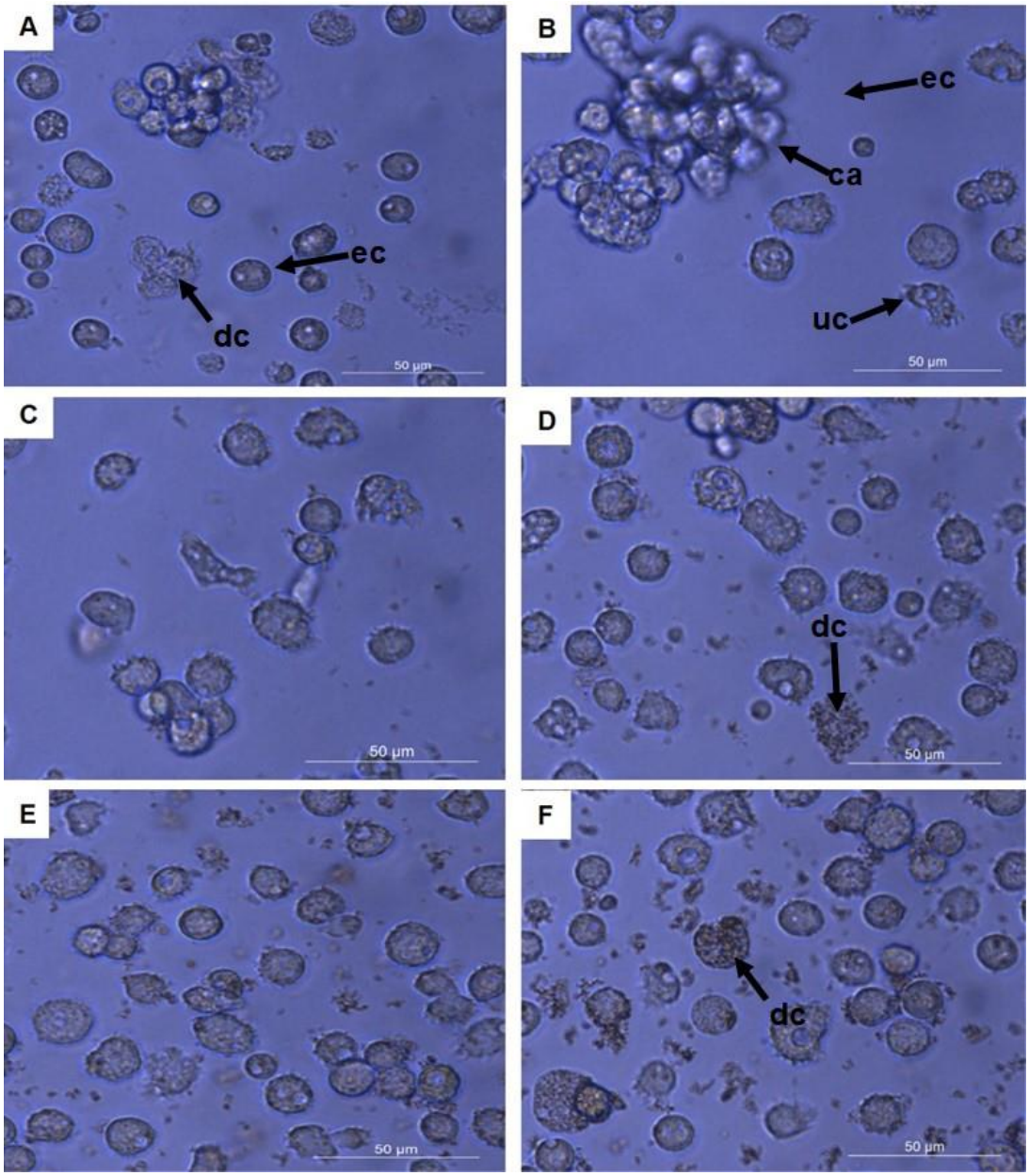

Figure 3:16: *A. castellanii* at 12 hours post induction of encystation. (A) positive control culture with 5mM PMSF. (B) negative culture with 100% standardized encystation buffer. (C to F) treatment groups with 25%, 50%, 75% and 100% *C. sinensis* encystation buffer respectively. Distinct cellular destruction observed in 50%, 75% and 100% *C. sinensis* encystation buffer cultures. *Abbreviations*: (ec) encysted cells, (dc) destroyed cells, (ca) cyst aggregates, (uc) unencysted cells. X40 magnification. Scale bar = 50 µm.

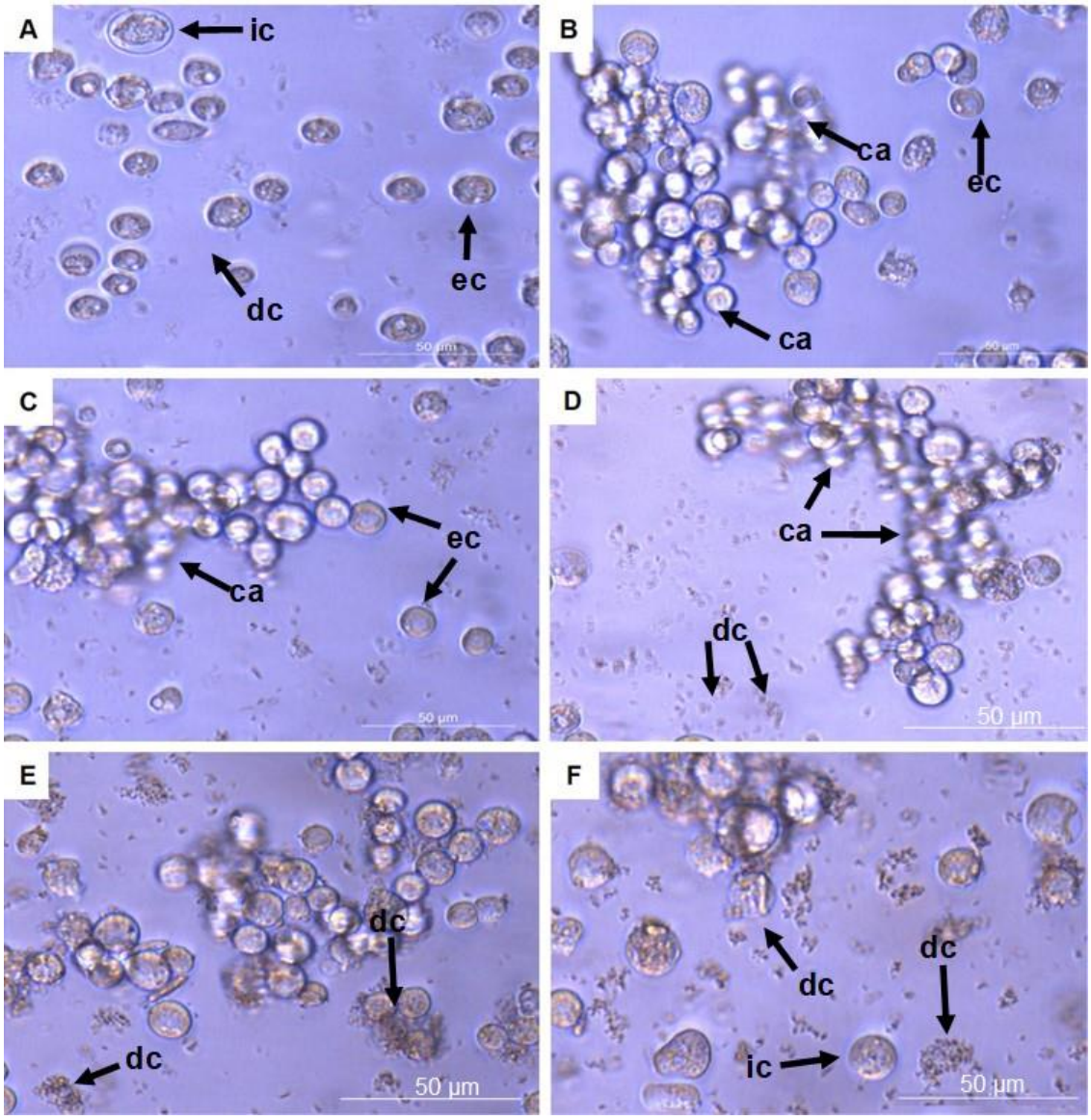

Figure 3:17: *A. castellanii* at 24 hours post induction of encystation. (A) positive control culture with 5mM PMSF. (B) negative control culture with 100% standardized encystation buffer. (C to F) treatment groups with 25%, 50%, 75% and 100% *C. sinensis* respectively. Increased cellular destruction observed in positive control group (A), 25%,50%, 75% and 100% *C. sinensis* encystation buffer cultures. Different degree of cyst aggregates in (B) negative control and (C) to (F) culture (B). *Abbreviations*; (ec) encysted cells. (dc) destroyed cells. (ca) cyst aggregates. (uc) unencysted cells. (ic) incomplete encystation. X40 magnification. Scale bar = 50 µm.

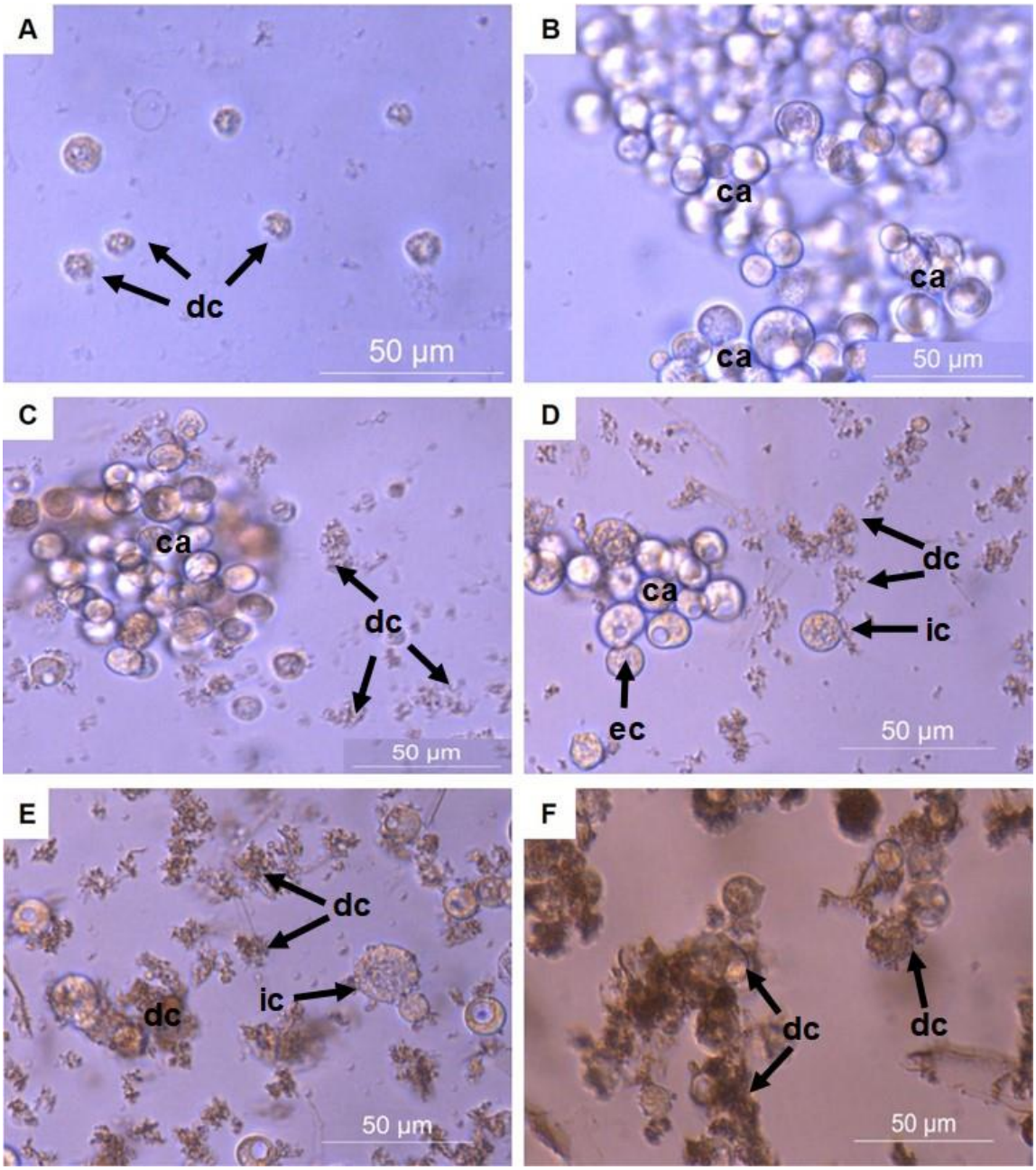

Figure 3:18: *A. castellanii* at 72 hours post induction of encystation. (A) positive control culture with 5mM PMSF. (B) negative control with 100% standardized encystation buffer. (C to F) treatment groups with 25%, 50%, 75% and 100% *C. sinensis* encystation buffer respectively. Increased cellular destruction observed in positive control group (A), 25%,50%, 75% and 100% *C. sinensis* encystation buffer cultures. Total cell destruction seen in positive control (A) and 100% C. sinensis encystation buffer (F). Different degree of cyst aggregates in control (B), (C) and (F) culture (B). *Abbreviations:* (ec) encysted cells. (dc) destroyed cells. (ca) cyst aggregates. (uc) unencysted cells. (ic) incomplete encystation. X40 magnification. Scale bar = 50 µm.

C. sinensis concentrations initially triggered encystation within the first few hours, which was sustained at subsequent time points of 12, 24, and 72 h, but subsequently cell death occurred which was more evident in sample treated with 100% *C. sinensis*. At 72 hours post induction of encystation, total destruction of the amoeba was evident in the positive control group. This damage was also detected in the 100% *C. sinensis* concentration with the destroyed cellular fragments bounded together. While cell destruction progressed from 48 h in 25%, 50% and 75% concentrations, cyst aggregates were observed in the negative control, 25% and 50% concentrations at varying degrees. Quantification of the approximate number of cysts per aggregate as displayed above showed that there was a progressive increase of cysts in the control (standardized encystation medium) whereas there was a progressive decrease of cysts in the *C. sinensis*-treated encystation samples (Table 3.1).

Time (h)	**Positive control [a]**	**Negative control [b]**	***C. sinensis* concentrations [c]**			
			25%	**50%**	**75%**	**100%**
24	0	4 - 100 (52 ± 28.15)	2 - 50 (26.02 ±14.26)	2 - 15 (8.50 ± 4.18)	2 - 10 (6 ± 2.74)	2 - 10 (6 ± 2.74)
48	0	4 - 500 (252 ± 143.62)	2 - 30 (16 ± 8.51)	2 - 10 (6 ± 2.74)	2 - 5 (3.50 ± 1.29)	2 (2 ± 0)
72	0	4 - 500 (252 ± 143.62)	2 - 30 (16 ± 8.51)	2 - 8 (5 ± 2.16)	2 - 3 (2.50 ± 0.71)	0

Table 3.1: Cyst aggregate formation by treatment groups during encystation of *A. castellanii* in 25% - 100% concentrations of *C. sinensis*. Values are mean± S.D of four replicates from three experiments. (a) Positive control with 5% PMSF, (b) negative control, (c) *C. sinensis* concentrations.

3.3.8.2 Percentage inhibition of encystation determined with SDS assay

In comparing the effect of hot brew *C. sinensis* before and after SDS digestion, Two-way ANOVA revealed a significant main effect of *C. sinensis* ($F(5, 12) = 862.2$, $p < 0.0001$) and of SDS ($F(1, 12) = 58.33$, $p < 0.0001$) with significant interaction of *C. sinensis* and SDS (F (5,

12) = 7.705, p =0.0019). Post-hoc comparisons revealed no significant difference between the pre-SDS effect of the positive control (5m PMSF) and 100% *C. sinensis* brew encystation buffer (p= 0.9980) while there was a significant increase between the pre-SDS effect of the positive control and the negative control, 25%, 50%, and 75% *C. sinensis* respectively (p = <0.0001). For post-SDS similar results were seen with no significant difference between the positive control and 100% *C. sinensis* (p >0.9999), while there was significant difference the positive control and the negative control, 25%, 50% and 75% *C. sinensis* brew encystation buffer respective (p = <0.0001). SDS had no significant decrease on encystation for positive control, negative control and 100% *C. sinensis* brew buffer respectively (p >0.9999, 0.5805, and 0.8884) (Figure 3:19). In analysing the pre vs post SDS effects for 25%-75% brew encystation buffer there was significant increase between the positive control and the brews (p = <0.0001 respectively). The negative control however had significant decrease in comparison with the 50%-100% brew with no difference with the 25% brew.

When comparing the effect of *C. sinensis* brew on inhibition of *A. castellanii* encystation, one-way ANOVA revealed a significant main effect of *C. sinensis* concentration ($F(5, 12) = 139.6$, $p < 0.0001$) on the inhibition rate. Post-hoc comparisons showed a significant increase in encystation inhibition between positive control (5 mM PMSF) and negative control, 25%, 50% and 75% *C. sinensis* groups ($p < 0.0001$). There was no significant difference between the positive control and 100% *C. sinensis* ($p > 0.9999$). The 100% *C. sinensis* concentration exhibited the same activity as the positive control. The positive control and the 100% concentration caused 100% inhibition of *A. castellanii* encystation. The control (untreated) and 25% concentration did not inhibit encystation (0%), while the 50% and 75% concentrations exhibited 28.6% and 42% inhibition of encystations, respectively (Figure 3:19). These results indicate that apart from the lowest concentration (25%), the treatment concentrations of *C. sinensis* brew encystation buffer caused dose dependent inhibition of *A. castellanii* encystation.

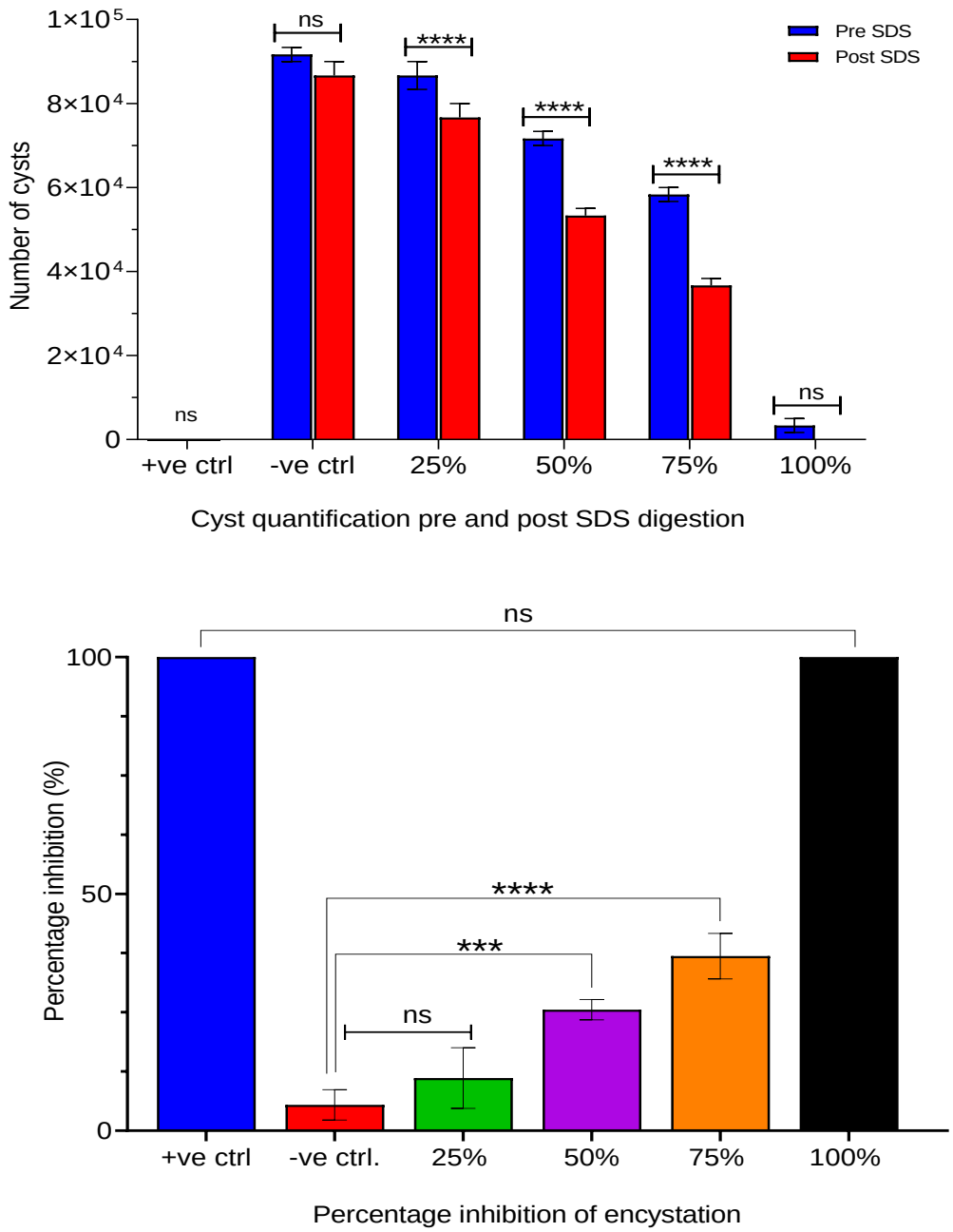

Figure 3:19: *A. castellanii* encystation pre and post SDS digestion and Percentage inhibition of encystation post-SDS digestion assay. 100% *C. sinensis* buffer displayed low encystation pre SDS and no encystation post SDS digestion. There was no significant difference between the pre-SDS and post-SDS effect of the positive control (5mM PMSF) and 100% *C. sinensis* encystation buffer. 100% *C. sinensis* encystation buffer exhibited inhibitory effect on encystation, with no significant difference between the positive control (5 mM PMSF) but with significant increase in comparison with negative control and 100% *C. sinensis* encystation buffer. (**** $p \leq 0.0001$, ns; non-significant).

3.3.9 External ultrastructural trophozoite to cyst changes examined with SEM

External ultrastructural analysis of trophozoite encystation using SEM as a confirmation of the microscopic analysis showed that at 24 hours post encystation, the negative control treatment group showed encysted *Acanthamoeba* linked together with a protective film which allows for the formation of aggregates as previously shown in the microscopic analysis (Figure 3:20). The cold *C. sinensis* brew treatment group showed cysts that were initially aggregated began to lose their adhesive ability, became shrunken and looked misshaped, which happened over the course of exposure to *C. sinensis* during encystation. At 72 h post-exposure to *C. sinensis* brew encystation buffer, there was a significant destruction of cysts. As observed in Figure 3:20, *C. sinensis* brew encystation buffer caused a progressive destruction of cysts (C-D), while in the control culture cysts remained in aggregates (A).

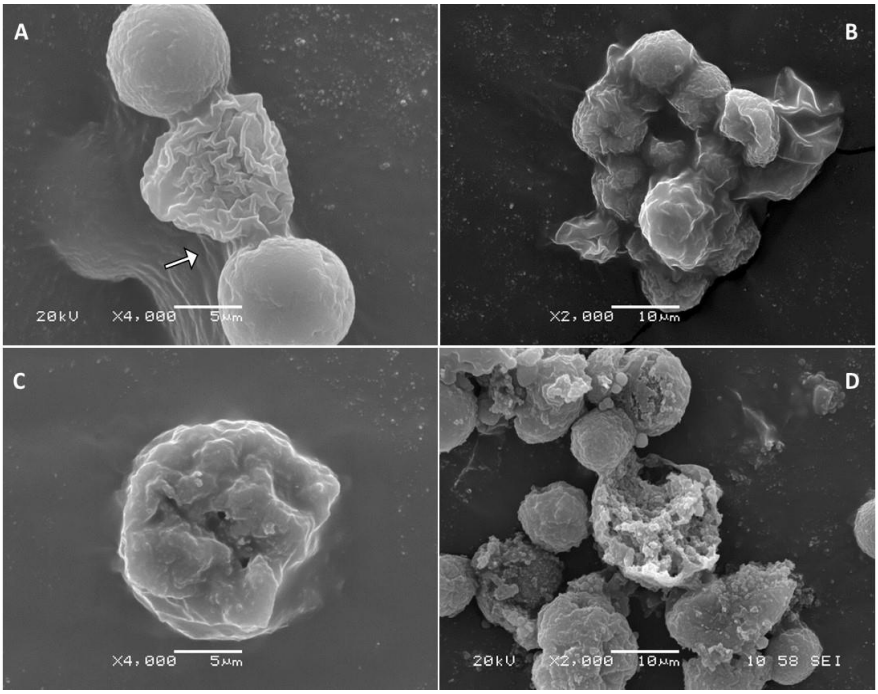

Figure 3:20: Scanning electron microscopy (SEM) micrographs showing progressive destruction of *A. castellanii* cysts exposed to *C. sinensis* brew encystation buffer during trophozoite to cyst encystation. (A) Cysts in negative control encystation buffer linked together by adhesin (arrow); (B) Aggregated cysts exposed to *C. sinensis* brew encystation buffer at 3 hours; (C) Cyst exposed for 24 hours showing loss of adhesion, misshaped and signs loss of membrane integrity; (D) Total destruction of cysts at 72 hours post exposure to *C. sinensis* brew encystation buffer. Magnification: X2,000 and X4,000; Scale bars = 5 µm (A and C) and 10 µm (B and D).

3.3.10 Internal ultrastructural trophozoite to cyst changes examined with TEM

TEM analysis of the internal ultrastructural alterations in the encysting *Acanthamoeba* showed time-dependent progressive destruction of the cysts. Compared to *A. castellanii* encysting in normal (control) encystation medium, trophozoites in cold *C. sinensis* brew encystation buffer showed a less intact membrane, fewer cytoplasmic vacuoles and condensation of the mitochondria at 3 h post-exposure (Figure 3:21B). These changes became more obvious in addition to abnormally condensed chromatin by 24 h (Figure 3:21C). At 72 h post-exposure, pronounced cellular destruction and loss of membrane integrity were detected together with the presence of fragments of the damaged cysts in the encystation medium (Figure 3:21D). Also, with increased duration of exposure to *C. sinensis*, a reduction in the volume of the cysts was observed. These ultrastructural alterations of the encysting trophozoites suggest that the presence of *C. sinensis* in the encystation medium induced some sort of stress and apoptosis-like death of the amoeba and disrupting the organism ability to form cysts.

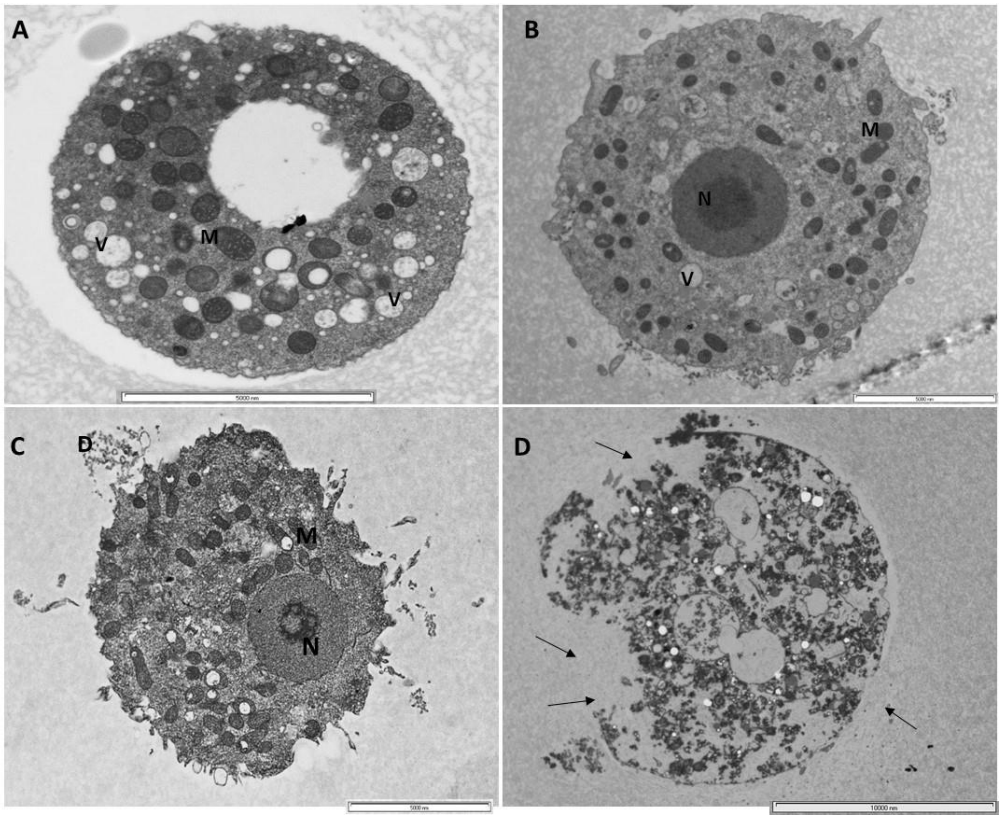

Figure 3:21: Transmission electron microscopy (TEM) micrographs showing progressive destruction of *A. castellanii* cysts exposed to *C. sinensis* brew encystation buffer during synchronized encystation. (A) Cyst in negative control encystation buffer; (B) Cysts exposed to *C. sinensis* brew encystation buffer at 3 hours; (C) Cyst exposed for 24 hours showing loss of cellular membrane material which are presumably acanthopodia; (D) At 72 hours post exposure to *C. sinensis* brew encystation buffer, cyst loses cellular membrane integrity. With increased duration of exposure to *C. sinensis*, cysts reduce in size as depicted by the decrease of magnification. *Abbreviations*: (V)food vacuole, (M)mitochondria, (N)Nucleus, (arrow) loss of cellular membrane integrity. Magnifications: X6,000, X4,200, X4,200 and X2,550 respectively; Scale bars: 5,000 nm (A,B,C) and 10,000 nm (D).

3.3.11 *C. sinensis* brews effects on excystation of *A. castellanii* cysts

In this experiment, the cysticidal, trophocidal and excystation capabilities of *C. sinensis* brews were investigated. The rate of cyst to trophozoite differentiation (excystation) as allowed by hot and cold *C. sinensis* brew concentrations was quantified by the number of trophozoites recorded at each time point post exposure to the treatment. The percentage inhibition of excystation by the *C. sinensis* brew concentrations was also determined. The direct effects of *C. sinensis* brew on the morphology and structure during differentiation was observed using light microscopy.

At 24 hours post treatment, visual results (Figure 3:22) showed that although there were cyst aggregates which form during encystation as earlier explained, cysts in the negative control treatment were excysting into trophozoites and were adherent to the flask surface than the hot *C. sinensis* brew treatments. 25% treatment showed the presence of some cyst aggregates but also showed extensive cytolysis with cytoplasmic contents expelled into the culture media in form of EVs. These EVs were also seen in the 50% and 75% treatment groups. The 100% treatment did not show as many EVs as the lower concentrations, instead there were large single walled cysts with measurements of approximately 100 µm. At 48 hours post exposure, most of the cyst aggregates in the negative control had excysted into vegetative trophozoites while the scenario seen in 24 hours of the treatment groups persisted. At 72 hours post exposure to hot *C. sinensis* brew (Figure 3:23), the treatment groups showed more EVs than earlier, clouding the observation fields of the microscope. This warranted washing of the

sample and subsequent quantification of the trophozoites visible in each treatment group for the determination of the excystation rate and the percentage inhibition of excystation.

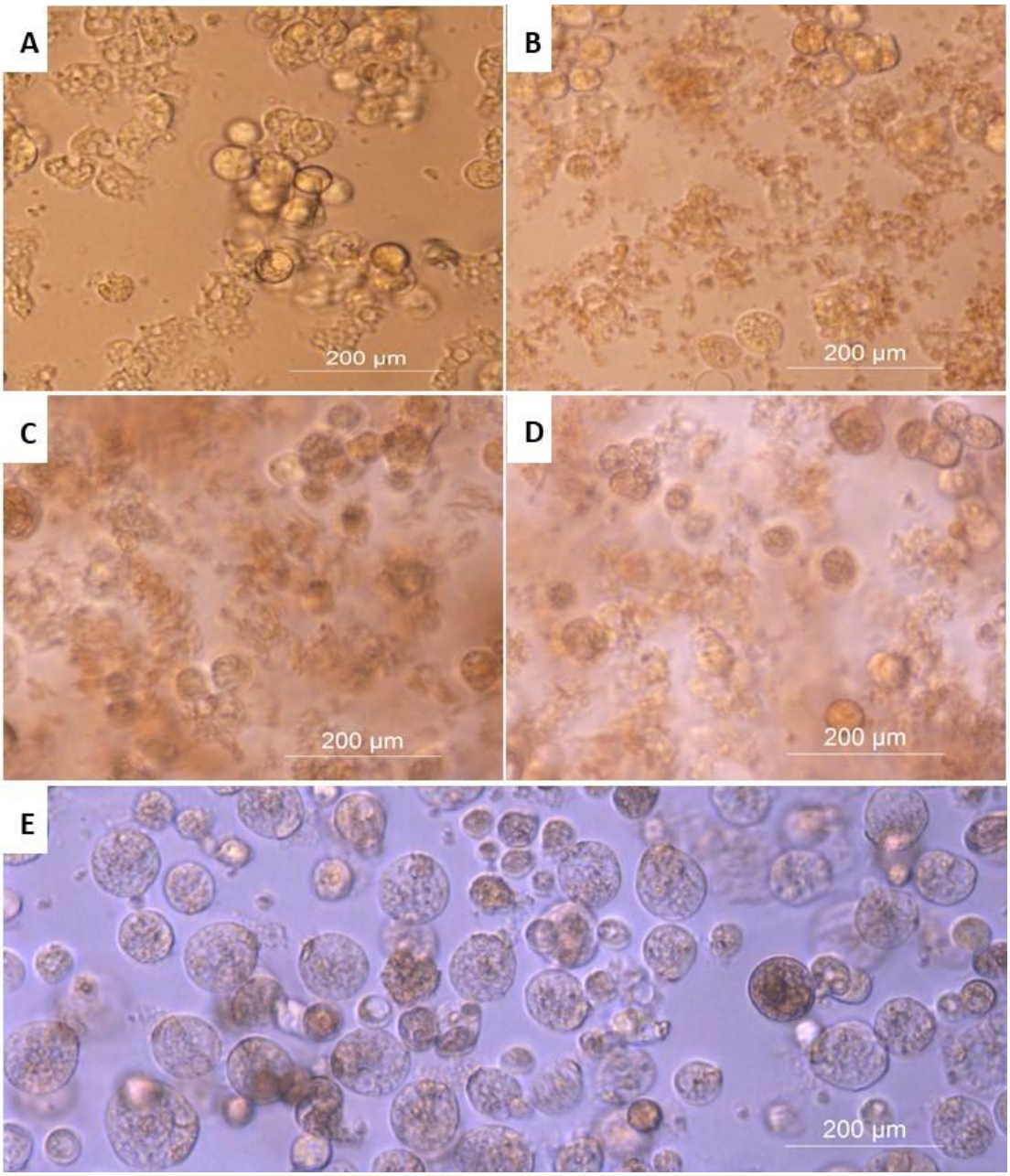

Figure 3:22: *A. castellanii* culture 24 hours post exposure of cysts to graded concentrations of hot *C. sinensis* brew to determine rate of excystation. (A) control culture with PGY. (B to E) treatment groups with 25%, 50%, 75% and 100% hot *C. sinensis* brew respectively. Extracellular vehicles seen in 25% to 75% *C. sinensis* brews (B to D); large single walled cysts seen in 100% *C. sinensis* brew. Scale bar = 200 µm.

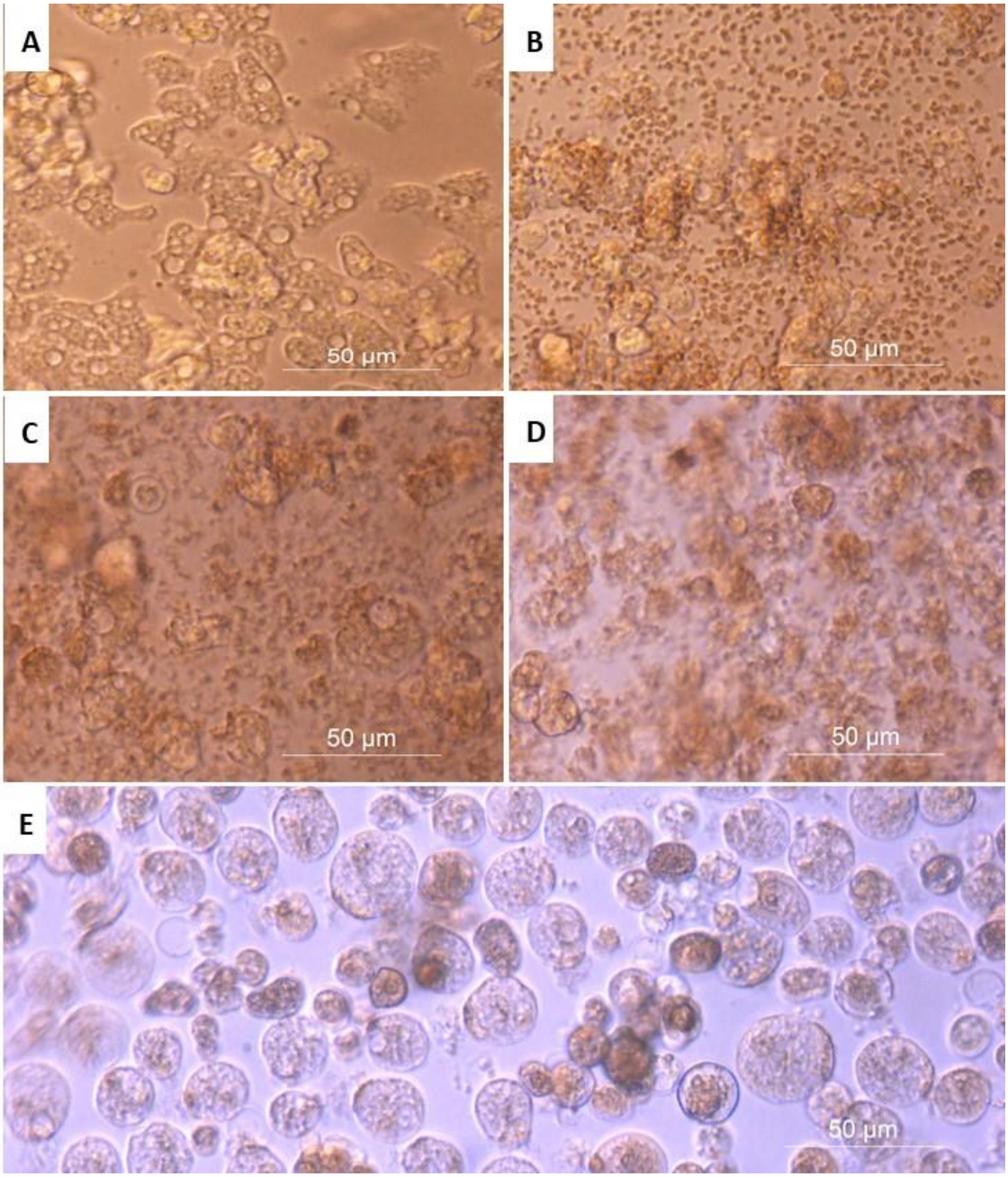

Figure 3:23: *A. castellanii* culture 72 hours post exposure of cysts to graded concentrations of hot *C. sinensis* brew to determine rate of excystation. (A) control culture with PGY. (B to E) treatment groups with 25%, 50%, 75% and 100% hot *C. sinensis* brew respectively. Extracellular vehicles seen in 25% to 75% *C. sinensis* brews due to progressive destruction of trophozoites when attempting to excyst (B to D), large single walled cysts seen in 100% C. sinensis brew. Scale bar = 50 µm.

For quantification of *A. castellanii* trophozoite excystation rates in the presence of hot and cold *C. sinensis* brew, two-way ANOVA revealed a significant main effect of time ($F(2, 4) = 809.9$, $p<0.0001$), treatment ($F(9, 18) = 1273$, $p<0.0001$) and significant interaction between time and treatment ($F(18, 36) = 66.60$, $p<0.0001$). Post-hoc comparisons of excysted trophozoite numbers 24-72 hours post excystation experiment showed significant increases between the negative control and all the cold and hot brew concentrations (25%-100%), and the positive control (CHX) as well (p <0.0001)(Figure 3:24).

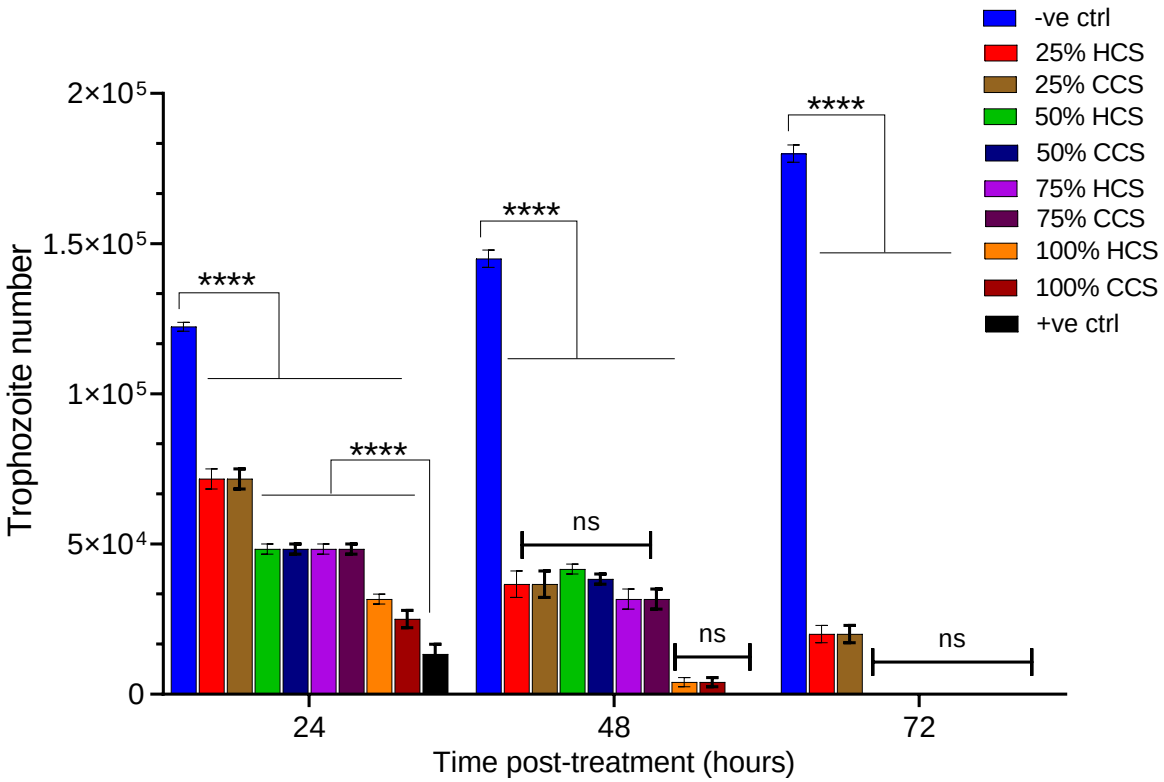

Figure 3:24: Excystation rate showing approximate trophozoite numbers when cysts are exposed to *C. sinensis* brew forms 72 hours. At 24 h there was significant increase in trophozoite number seen in the negative control compared to all the brew forms. This progressed till termination of experiment (72 h). The brews had progressive decrease of excysted trophozoites from 24 h to 72 h where only 25% hot and cold brew recorded any excysted trophozoites. From 48 hours post exposure there is no significant difference between the excysted trophozoite number for both brew forms of 100% and CHX, while at 72 hours post exposure, no difference is seen between 50% to 100% forms and CHX (**** $p \leq 0.0001$, ns: non-significant).

For comparisons of the treatment brews with and the positive control, 24 hours evaluation post-treatment showed that the excystation rates of the treatment groups were significantly higher than the positive control (p <0.0001) with higher trophozoite numbers recorded. At 48 hours, the number of excysted trophozoites decreased when compared to the trophozoite numbers recorded at 24 hours. There was however no significant difference between 25%-75% trophozoite number for both brew forms (hot and cold) (p > 0.05). Comparison with the positive control and 100% brew of both brew forms (hot and cold) indicated no significant difference between the trophozoite numbers (p > 0.05) indicating that 100% brew forms inhibited excystation of trophozoites to the same proportion as the positive control. negative control continued to increase while that of the treatment groups decreased. At 72 hours, excluding 25% hot and cold brew concentration, all the *C. sinensis* brew treatment groups effectively inhibited trophozoite excystation rate of *A. castellanii* cysts with no significant difference between them and the positive control (p > 0.05).

When determining the percentage inhibition of *A. castellanii* excystation when exposed to *C. sinensis* brew, one-way ANOVA revealed a significant main effect of *C. sinensis* brew concentration ($F(9, 20) = 3580$, $p < 0.0001$) on the percentage inhibition rate of cyst to trophozoite excystation. Post-hoc comparisons showed there was significant decrease between the percentage excystation inhibition of negative control in comparison with all the hot and brew concentrations (25%-100%), as well as with the positive control (p <0.0001) (Figure 3:25). Further comparisons between brew concentrations showed that there was also significant decrease between the percentage excystation inhibition of 25% hot and cold brew and the rest of the hot and brew concentrations (50%-100%) (p <0.0001). While comparing the positive control to the brews, there was no significant difference between the positive control and the 50%-100% hot and cold brews (p > 0.05). This result indicates that 50%-100% cold and hot *C. sinensis* brews exhibited 100% inhibition of *A. castellanii* cysts to trophozoites excystation as did the positive control treatment.

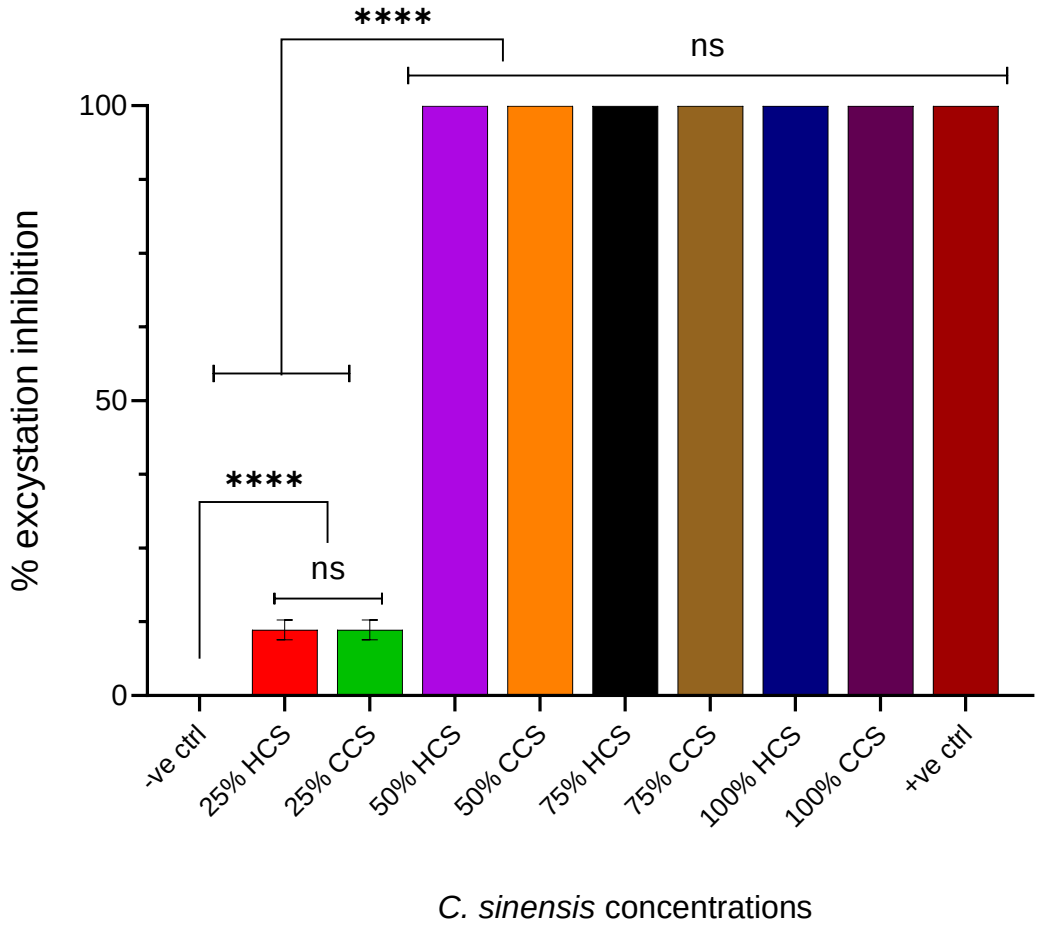

Figure 3:25: Percentage excystation inhibition rate of hot and cold brews rate at 72 hours post-excystation experiment. There was significant decrease of percentage excystation inhibition in comparison with negative control will all the hot and cold brew forms (25%-100%). 50%-100% hot and cold brew forms expressed no significant difference from positive control as they all exhibited 100% excystation inhibition rate. (**** $p \leq 0.0001$, ns: non-significant).

3.4 SELECTIVITY INDEX OF *C. SINENSIS BREW*

The half-maximal inhibitory concentration (IC_{50}), which is the concentration of *C. sinensis* brew that caused a 50% decrease of *A. castellanii* trophozoites growth compared to the control was determined to be 50.17% ± 1.118% *C. sinensis* brew v/v. (Figure 3:26). The IC_{50} of *C. sinensis* brew for iHCECs was determined to be 42.56% at 24 hours and 37% at 48 hours, while EC50 of *C. sinensis* brew for CSCs was 39.49% at 48 hours. This indicated that *C. sinensis* brew has time and dose dependent cytotoxicity for host cells as seen by the wide range of concentration allowed for CSCs and IHCECs.

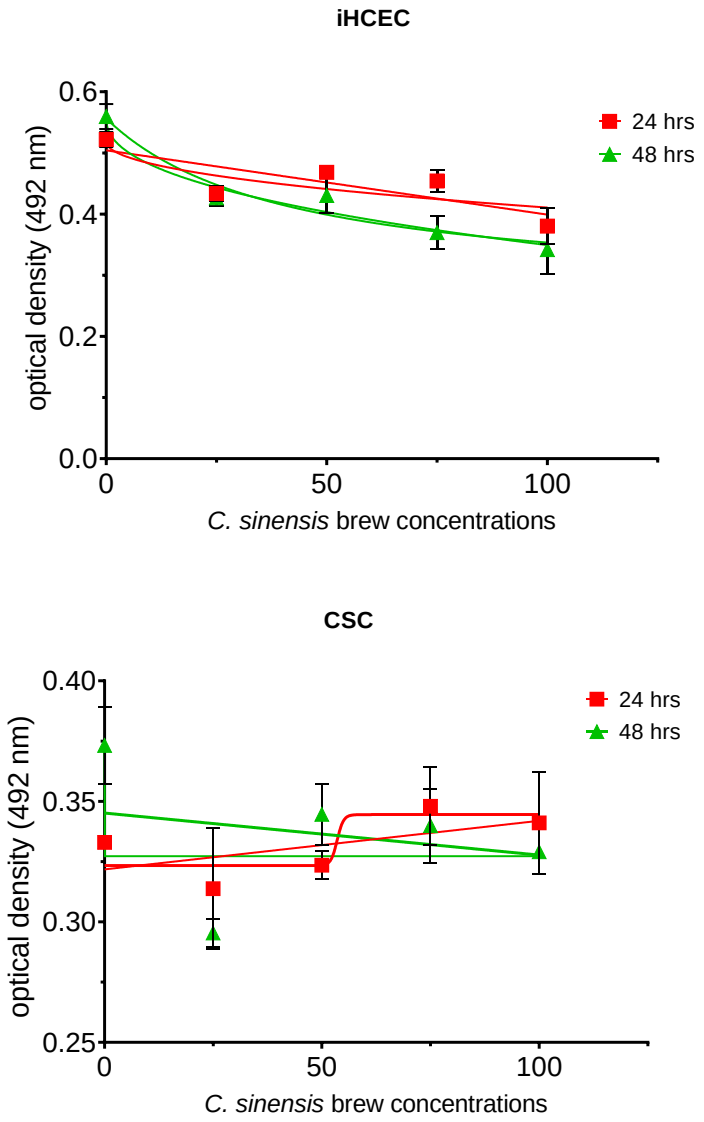

Figure 3:26: The half-maximal inhibitory concentration (IC_{50}) of *C. sinensis* brew for IHCECs was determined to be 42.56% at 24 hours and 37% at 48 hours, while EC50 for CSCs was 39.49% at 48 hours.

3.5 DISCUSSION

Considering the need for viable medications against *A. castellanii* infection and considering the extensive biological functions and pharmacological activities of *C. sinensis*, it was worthwhile to investigate the anti-acanthamoebic activity of *C. sinensis* hot and cold brews against the trophozoite and the cystic forms of this parasite. First, cytotoxicity assays using corneal cells were conducted, bearing in mind that the cornea is the predilection site for AK (Martinez and Visvesvara, 1997; Chomicz et al., 2010), for which CHX digluconate (0.02%) or PHMB (0.02%) drugs are often used. These reference drugs are known to exhibit toxicity when used individually at the regular concentrations, but when used synergistically in vitro, their toxic effect was not observed (Mafra et al., 2013). Interestingly, in our study, neither cold nor hot brew of *C. sinensis* at any tested concentrations had a persistent or sustained cytotoxic effect against primary corneal stromal cells according to the results obtained by SRB assay. Although high concentrations *C. sinensis* might cause initial inhibition of the growth rate of corneal stromal cells, this effect was not sustained as cells continue to grow to the end of the 72-h assay period. However, in the comparative cytotoxic testing of both *C. sinensis* brew forms, the cytotoxic effect of cold brew of *C. sinensis* was more pronounced in SV40-immortalized human corneal epithelial cells, than the hot brew *C. sinensis* especially at 100% concentration. It is not clear at this point of the study why there was a difference in cytotoxicity of two different types of corneal cells when exposed to *C. sinensis* brews.

CSCs are primary cells, whereas corneal epithelial cells are derived from an immortalized cell line. Corneal epithelial cells divide at a higher rate than the primary CSCs. The differential sensitivity of both cell types to treatment with *C. sinensis* brew might be attributed to the cell growth rate and culture conditions, or to cell type-specific innate properties that may have attributed to the observed corneal epithelial cell sensitivity. It is also possible that the results observed in long-term assays for the corneal epithelial cells might be influenced by altered sensitivity during progression through the cell cycle, however, this requires further investigation. The cytotoxicity results obtained by AO staining assay showed that despite the

reduced concentrations of RNA and DNA in 100% *C. sinensis* brew-treated CSCs, there was no sustained persistence of cytotoxicity up to 72 h of treatment as there was increased of RFU between 48 h and 72 h post exposure to the brew forms. The observations from the cytotoxicity evaluations of primary CSCs show that the arrested cellular replication phase was not sustained and thereby shows that though *C. sinensis* hot brew exhibited initial toxicity to primary corneal stromal cells, the toxicity either waned as the experiment progressed or the cells were able to overcome the toxicity over time. The temporary sluggishness in the growth rate of CSCs might be attributed to transient cytotoxicity because all treated cells managed to continue their growth till 72 h. The evaluations with SV40-immortalized human corneal epithelial cells, suggests that *C. sinensis* had a time and dose-dependent mild cytotoxic effect on human cells.

A. castellanii has a rapid growth rate especially under in vitro conditions (Siddiqui and Khan, 2012; Byers et al., 1991). Therefore, it was necessary to optimize the initial seeding density with respect to the assay design and equipment used under the experimental conditions implemented in the present study. We monitored the temporal changes in the proliferation of *A. castellanii* trophozoites with different initial seeding densities under normal culture conditions (i.e., without any treatment) for up to 72 h. A previous study (Ortega-Rivas et al., 2016) used the Sulforhodamine B (SRB) assay, and determined 500 trophozoites/well as an optimal seeding density. Using the same SRB assay, 2.5×10^3 trophozoites/well provided the optimal seeding density under the experimental conditions in our study.

With respect to the anti-acanthamoebic activity of *C. sinensis* brew against the trophozoites and cysts, our results demonstrated that *C. sinensis* brews are potent inhibitors of *A. castellanii* trophozoite replication in vitro. The level of acanthamoebicidal activity exhibited by 75% and 100% *C. sinensis* brew was comparable to that produced by CHX treatment (Figure 3:10, Figure 3:11). SRB dye was used in an assay to assess the protein concentration in each of the treatment groups over time. An increase in OD represented increase in cell growth by trophozoite proliferation, and its decrease represented decrease of trophozoite number. The

data suggest that the inhibitory effects of treatment with *C. sinensis* brew on trophozoite proliferation was dependent on the concentration of the brew and duration of treatment. Though both brew forms exhibited anti-acanthamoebic activity, comparatively, the cold brew had more effect than the hot brew as 75% and 100% of the cold brew effect on trophozoite growth kinetics were mirrored to the CHX with no significant difference from commencement of experiment till the termination (72 h). This effect of cold brew might have resulted from the preparation techniques (see General Methods) which allowed for the slow extraction of its anti-oxidant and phytochemical components from the tea leaves over a 24 h duration without degrading them, while the hot brew preparation done within 10 minutes might have resulted in the rapid extraction of more astringent properties of green tea (Lin et al., 2014; Safdar et al., 2016). Transient exposure to *C. sinensis* brew for 6 or 24 h was not sufficient to cause irreversible growth impairment of trophozoites (Figure 3:14). The cystic stage of *A. castellanii* presents a great challenge to anti-acanthamoebic therapy due to its innate resistance to most drugs. In this study, *C. sinensis* brews have shown a significant cysticidal activity by inhibiting the ability of *A. castellanii* trophozoites to differentiate into mature cysts. Additionally, *C. sinensis* brews have significantly reduced the excystment rate of the amoeba from cysts to trophozoites (Figure 3:18).

C. sinensis brew seems to have selective time and dose-dependent toxicity toward human corneal cells compared to *A. castellanii*. This result is anticipated because *A. castellanii* is a resilient organism and has a remarkable ability to adjust to changing environmental conditions and adapt to various stressors (Clarke et al., 2013). Additionally, *C. sinensis*-PGY medium used in anti-*A. castellanii* assays was prepared by dissolving the ingredients of PGY medium in *C. sinensis* brew. This has ensured that *A. castellanii* trophozoites have received all the nutritional needs that they normally obtain from PGY medium and thus can maintain homeostasis. By contrast, cytotoxicity testing against human cells involved the use of *C. sinensis* brew at 100% concentration or diluted with cell culture medium (M199 medium for CSCs and Epilife growth medium for iHCECs) to prepare lower concentrations. Maintaining of

mammalian cells *in vitro* depends on the presence of serum, growth factors and many other nutrients in the cell culture medium, which are essential for maintaining the physiology, metabolism and viability of cultured cells (Ishii et al., 2004; Yen et al., 2002; Kryczka et al., 2012) . Therefore, inhibition of the growth of corneal cells and their apparent sensitivity to 100% *C. sinensis* brew might have been confounded or aggravated by the scarcity of nutrients in the culture medium used in cytotoxicity testing.

EVs are known to be produced and secreted by *A. castellanii* (Gonçalves et al., 2018). In this study, the presence of EVs in cultures treated with 25%, 50% and 75% *C. sinensis* brew, and their absence from cultures treated with 100% *C. sinensis* brew deserves further reflection. *A. castellanii* secretes several proteins involved in protein metabolism, amino acid metabolism, oxidative metabolism, and cellular stress, which may play roles in the organism's adaptation to nutritional stress (Gonçalves et al., 2018). Also, *A. castellanii* secretes many proteases, which play roles in its virulence and pathogenesis (Khan et al., 2000a) and in the differentiation of the amoeba from trophozoites to cysts(Alsam et al., 2005; Dudley et al., 2008; Lorenzo-Morales et al., 2015). Therefore, the expulsion of cytoplasmic EVs might be a defense mechanism used by *A. castellanii* trophozoites to alleviate the stress caused by *C. sinensis* brew. On the other hand, exposure of trophozoites to 100% *C. sinensis* brew may have overwhelmed their capacity to adjust to the stress related to *C. sinensis* brew treatment by expelling these vehicles. Alternatively, the amoeba seemed to use another mechanism to defend its internal contents against such acute stress by rounding up soon after *C. sinensis* brew treatment as if they were trying to encyst to counter the toxic effect of the high concentration of *C. sinensis* brew. This observation is consistent with previous studies that have shown that *A. castellanii* trophozoites rapidly differentiate into pseudocysts upon exposure to organic solvents (Kliescikova et al., 2011b) or contact lens solutions (Kliescikova et al., 2011a), which enable *A. castellanii* to survive such lethal conditions. *A. castellanii* has many proteins that are involved in the modulation of the cellular response to external stimuli

(Clarke et al., 2013), providing more evidence to support the ability of this parasite to modify its response and adapt to cellular stress according to the external cues.

Our TEM and SEM analyses showed ultrastructural intracellular and surface changes in *A. castellanii* exposed to *C. sinensis*. Of interest is the inhibition of the amoeba's ability to encyst, which is facilitated by cellulose, galactose and protein synthesis (Anwar et al., 2018). It is possible that some of the *C. sinensis* brew components may not only inhibit protease secretion, but also inhibit synthesis of other components, such as M17 leucine aminopeptidase of *A. castellanii* (AcLAP), which is involved and expressed in the late stages of encystation during the formation of the cyst wall (Lee et al., 2015). Further evaluation of *C. sinensis* brews the efficacy vis-à-vis that of chlorhexidine (positive control) in relation to the trophozoite and cysts membrane, studies have shown that one of the known mechanisms of action of chlorhexidine is that it acts on the parasite membrane by gradual induction of pentose leakage. Pentose sugar is the deoxyribose in DNA and ribose in RNA. This action of pentose leakage leads to cell plasma damage and the loss of cell membrane integrity leading to parasite death (Khunkitti et al., 1996; Khunkitti et al., 1997). With the similarity of brew activity similar to that of chlorhexidine as exhibited by their effect on trophozoite growth kinetics, there is a possibility that *C. sinensis*'s mechanism of action on trophozoites might be similar to that of chlorhexidine.

In conclusion, *C. sinensis* brews possess amoebicidal activity against *A. castellanii* trophozoites and were highly effective at inhibiting the parasite's ability to encyst. Also, the *C. sinensis* brew forms interfered with the amoeba's ability to transform from cyst to trophozoites particularly at higher concentrations. These findings suggest that *C. sinensis* represents a source of potentially promising inhibitors of *A. castellanii* growth and encystation for the further development of topical complementary agents to support chemotherapeutic drugs currently used against *A. castellanii* infection. In light of the favourable discoveries made by evaluating the anti-acanthamoebic activity of *C. sinensis*, the subsequent section of this study will delve into the possible activity of the solvent extract of *C. sinensis.*

4 EFFECT OF *CAMELIA SINENSIS* SOLVENT EXTRACT ON *A. CASTELLANII*

4.1 SUMMARY

In this study, the trophocidal and cysticidal effect of *Camellia sinensis* (green tea) solvent extract was investigated by subjecting *Acanthamoeba castellanii* trophozoites and cysts to serial concentrations (5000, 2500, 1250, 625, 312.5, and 156.25µg/mL) of *C. sinensis* solvent extract. *C. sinensis* solvent extract exhibited a dose-dependent inhibition of encystation, with clear cysticidal activity at 2500 and 5000µg/mL concentrations. *A. castellanii* cytolysis and inhibition of trophozoite replication was detected within 24 to 72 hours of exposure to 5000, 2500, 1250, and 625 µg/mL of *C. sinensis* solvent extract. The ultrastructural alterations in *C. sinensis* solvent extract-treated trophozoites and cysts were examined using transmission electron microscopy (TEM) and scanning electron microscopy. Analysis of the EM micrographs revealed loss cellular membrane integrity of trophozoites with 2500 to 625 µg/mL concentrations. Light microscopic and haemocytometer evaluations revealed that the rate of cysts to trophozoites excystation with was significantly inhibited with 2500 to 5000 µg/mL exhibiting 100% excystation inhibition as seen with chlorhexidine, and the 312.5 and 625 µg/mL concentrations exhibited 78% and 87% excystation inhibition. Cytotoxicity analysis of *C. sinensis* against immortalised human corneal epithelial cells (iHCE-2s) and Madin-Darby Canine Kidney (MDCK) cells indicated that *C. sinensis* solvent extract concentrations of 156.25µg/mL to 2500µg/mL were not toxic to iHCE-2s, while 625µg/mL was not toxic to MDCK cells. This work demonstrated that *C. sinensis* solvent extract has anti-acanthamoebic activity against trophozoite and cystic forms of *A. castellanii*. Further studies are warranted to identify the exact substances in *C. sinensis* solvent extract that have the most potent anti-acanthamoebic effect.

4.2 INTRODUCTION

A wide range of studies have also evaluated and established the anti-parasitic capability of *C. sinensis* against *Haemonchus contortus* (Zhong et al., 2014)*, Leishmania braziliensis* (Inacio et al., 2014), *Leishmania amazonensis* (Inacio et al., 2013; dos Reis et al., 2013), *Trypanosoma brucei* (Vigueira et al., 2012), the zoonotic *Babesia* spp. (Batiha et al., 2019), and many more*.* With the continuous threat of malaria infections as transmitted by *Plasmodium falciparum* in the tropical climates, an evaluation of *C. sinensis* solvent extract *in vitro* has shown that it inhibits the growth of *Plasmodium falciparum* and might be an alternative source of anti-malarial drugs (Thipubon et al., 2015; Sannella et al., 2007).

Another study evaluating the antiviral potential of *C. sinensis* extract showed that the extract had antiviral efficiency against fowl adenovirus type 4 (FAdV-4) in broiler chickens (Aslam et al., 2014). The polyphenols of *C. sinensis* as antioxidants have also been known to possess inhibitory effect on the Reactive Oxygen Species (ROS) generation leading to abnormal metabolism in parasites (Liou, 2021). Evaluations against helminths which are causes of many parasitic infections of small and large ruminants with high mortality rates, also revealed that solvent extracts of *C. sinensis* possess *in vitro* anthelmintic activity against *H. contortus* (Zaheer et al., 2019).

Of all the studies done so far none has looked at the possibility of the anti-acanthamoebic or amoebicidal activity of *C. sinensis* solvent extract. Given the need for viable natural sources of anti-acanthamoebic substances, this study is an aspect of an intensive study into the possible anti-acanthamoebic activity of *C. sinensis.* In the results in the previous chapter, it showed that *C. sinensis* cold and hot brews possess amoebicidal activity against *A. castellanii* trophozoites and were highly effective at inhibiting the parasite's ability to encyst (Fakae et al., 2020*)*. In the present study, the activity of the crude solvent extract of *C. sinensis* in different concentrations (µg/mL) against the trophozoite and cystic stage of *A. castellanii* was investigated. In addition, its cytotoxicity against human corneal cell lines and Madin-Darby canine kidney cells (MDCK) was evaluated.

4.3 RESULTS

4.3.1 Cytotoxicity of *C. Sinensis* solvent extract

4.3.1.1 Cytotoxicity in iHCE-2

Cytotoxicity of *C. sinensis* solvent extract in serial dilutions of 156.25µg/mL, 312.5µg/mL, 625µg/mL, 1250µg/mL, 2500µg/mL, and 5000µg/mL were examined against iHCE-2 using LDH assay. The two-way ANOVA revealed a significant main effect of time ($F(6, 21) = 56.09$, $p < 0.0001$), concentration ($F(2, 21) = 25.49$, $p < 0.0001$), and time x concentration interaction ($F(12, 21) = 14.45$, $p < 0.0001$). Post-hoc testing indicated that by 24 h post-treatment there was no statistical difference between the control and the solvent extract concentrations of 156.25µg/mL-2500µg/mL ($p>0.05$) indicating that these range of concentration was not toxic iHCE-2 cells. Comparisons of the control with the 5000µg/mL concentration however, showed significant increase in cytotoxicity ($p<0.0001$). At 48 h post-treatment, 156.25µg/mL, 312.5µg/mL, 625µg/mL, 1250µg/mL, and 2500µg/mL also displayed no statistical difference compared with the control ($p>0.9999$), which also indicated that the concentrations were not toxic to iHCE-2. The highest concentration of 5000µg/mL continued to show statistically significant increase in the percentage cytotoxicity compared with the control ($p<0.0001$), indicating that *C. sinensis* solvent extract is toxic to iHCE-2 at 5000µg/mL (Figure 4:1). The cytotoxicity observed in 2500µg/mL at 24 h, could be attributed to transient cytotoxicity, because at the end of the experiment (48 h) the percentage toxicity had dropped with no statistical difference with the control ($p>0.05$) indicating that 2500µg/mL concentration of *C. sinensis* solvent extract is not toxic to iHCE-2.

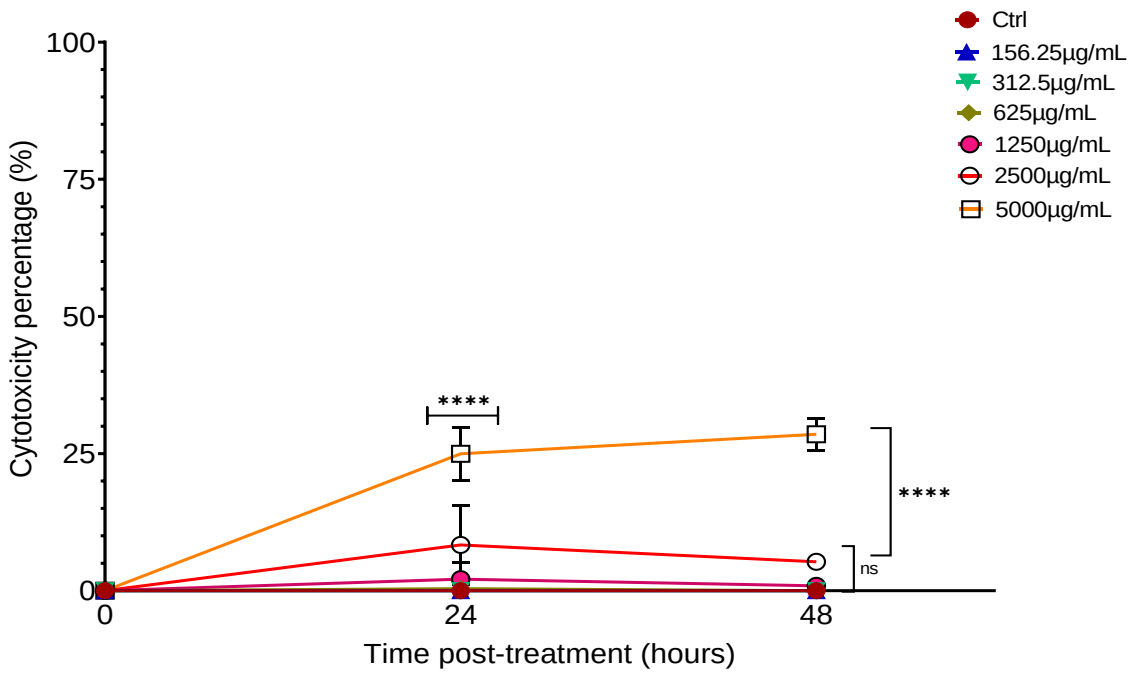

Figure 4:1: *C. sinensis* solvent extract cytotoxicity against iHCEs cells. At 24 h the result showed no significant difference between standardizes negative control cells and cells treated with the concentrations 156.25µg/mL, 312.5µg/mL, 625µg/mL and 1250µg/mL. 2500µg/mL and 5000µg/mL however exhibited significant increase in cytotoxicity in comparison to the control. At 48 hours post treatment concentrations of 156.25µg/mL to 2500µg/mL exhibited no cytotoxicity with no significant difference with control. There was however a significant difference between the control and 5000µg/mL treatment group at 48 hours post treatment (p<0.0001). This indicates that only the highest concentration is toxic to IHEC cells, with less than 30% cytotoxicity. (**** $p \leq 0.0001$; ns, non-significant)

4.3.1.2 Cytotoxicity in MDCK cells

Here, the toxicity of the *C. sinensis* solvent extract to MDCK cells was evaluated. The two-way ANOVA of *C. sinensis* solvent extract revealed a significant main effect of time ($F(7, 96) = 499.5$, $p < 0.0001$), concentration ($F(2, 96) = 440.4$, $p < 0.0001$), and time x concentration interaction ($F(14, 96) = 499.5$, $p < 0.0001$). Post-hoc testing found out that at 24 h post-treatment with 156.25µg/mL, 312.5µg/mL, and 625µg/mL, though there was cell replication, there was still a significant increase in their percentage cytotoxicity when compared with the negative control (p<0.0001). The cell replication rates for 1250µg/mL, 2500µg/mL and 5000µg/mL were much lower than the lower solvent extract concentrations and comparisons with the negative control also shower significant increase in cytotoxicity (p<0.0001).

Comparisons with the positive control inversely showed significant increase in cytotoxicity when compared with all the solvent extract concentrations (p<0.0001). At the 48 h post-treatment, the growth trends of the 156.25µg/mL and 312.5µg/mL solvent extract concentrations continued but halted the increase in cytotoxic readings with percentage cytotoxicity of 10% and 25% respectively. However, these growth trends were significantly lower than the negative control as their cytotoxicity were also significantly higher than the negative control (p<0.05 and p<0.0001 respectively). The 1250µg/mL, 2500µg/mL and 5000µg/mL solvent extract concentrations continued the same cytotoxicity trend as seen in 24 h with significant increase in cytotoxicity when compared to negative control. As witnessed with the comparisons in 24 h, all concentrations also showed significant decrease in cytotoxicity when compared with the positive control (p<0.0001) (Figure 4:2). These results indicates that only 156.25µg/mL and 312.5µg/mL concentrations showed the highest rate of cell replication hence the toxicity witnessed at 24 h can be said to be transient as it was not sustained at 48 h. 625µg/mL showed 45% cytotoxicity while the higher concentrations all exhibited cytotoxicity above 50%.

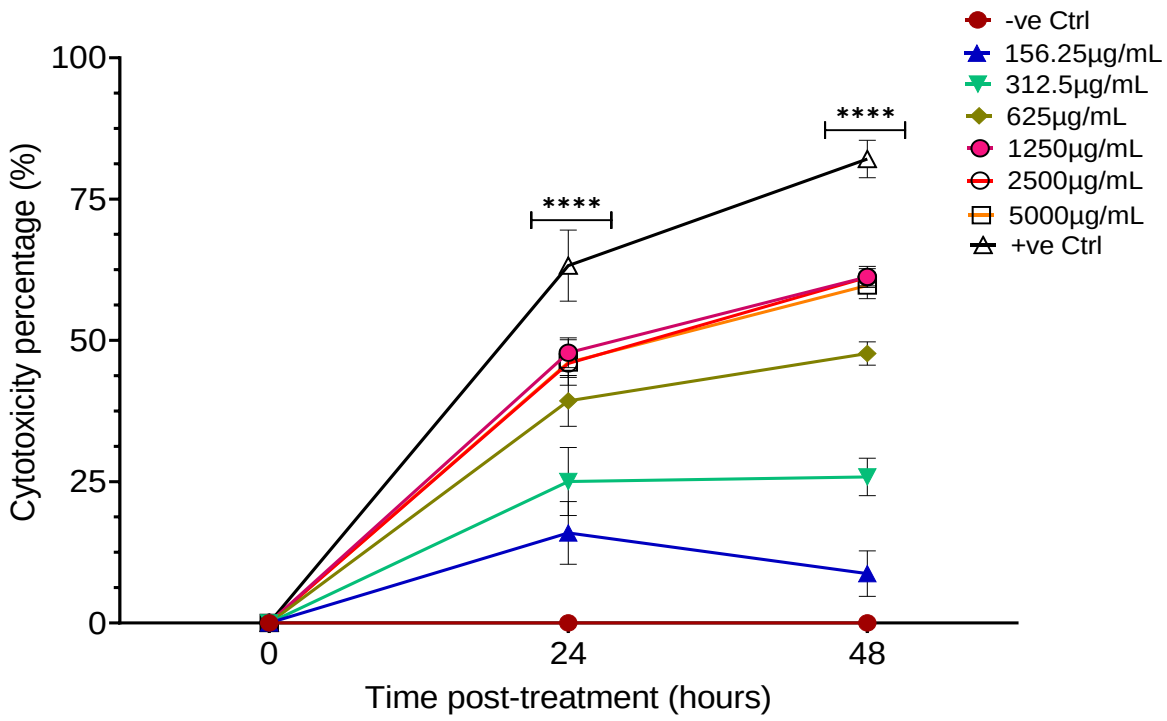

Figure 4:2: *C. sinensis* solvent extract cytotoxicity against MDCK cells. The result showed significant increase in cytotoxicity between the negative control (DMEM) and all the treatment groups at 24- and 48-hours post treatment. At 48 h 156.25µg/mL and 312.5µg/mL showed an average percentage cytotoxicity of 10% and 25% respectively, while 625µg/mL showed 45%. The higher concentrations exhibited percentage cytotoxicity above 50% (**** $p \leq 0.0001$, ns: non-significant).

4.3.2 Effects of *C. sinensis* solvent extract on *A. castellanii* trophozoites

4.3.2.1 Inhibitory effect of C. sinensis solvent extract against A. castellanii trophozoites

The effect of *C. sinensis* solvent extract on trophozoites was determined using the hemocytometer. The two-way ANOVA revealed a significant main effect of time ($F (3, 6) = 1148$, $p < 0.0001$), concentration (µg/mL) ($F (7, 14) = 26766$, $p < 0.0001$), and time x concentration interaction ($F (21, 42) = 2726$, $p < 0.0001$). At 24 h post- treatment, post hoc comparisons showed that all the solvent extract concentrations were able to decrease trophozoite growth with significant difference between their trophozoite number and the negative control ($p < 0.0001$). Comparisons with solvent extract concentrations and the positive control showed significant decrease in trophozoite number while compared with

312.5µg/mL, 625µg/mL and 1250µg/mL concentrations (p < 0.0001). Positive control comparisons with the 2500µg/mL and 5000µg/mL however showed no significant difference in trophozoite number (p>0.05) (Figure 4:3). At 48 h post treatment, the trend seen with the lowest concentration (312.5µg/mL) was reversed mimicking the negative control groups with an increase in the trophozoite number indicating that the concentration had no inhibitory effect on trophozoite growth, also there was no significant difference between the concentration and the negative control groups (p>0.05). The higher concentrations of *C. sinensis* solvent extract (625µg/mL to 5000µg/mL) continued their previous trend of continued reduction of approximate trophozoite numbers. Comparisons of the 625µg/mL solvent extract concentration however showed a significant decrease in trophozoite number between the positive control and the solvent extract concentration (p <0.0001). The trophozoite number reduction trend of 625µg/mL solvent extract continued at 72 h, but there was still a significant decrease of trophozoite number when comparing the positive control to 625µg/mL solvent extract (p <0.0001). Comparisons between the positive control and the 1250µg/mL, 2500µg/mL and 5000µg/mL *C. sinensis* solvent extract concentrations exhibited no significant difference between them and the positive control (p> 0.05). At 72 h post-treatment the trends witnessed at 48 hours post treatment with all the *C. sinensis* concentrations persisted. The lower *C. sinensis* solvent extract concentration of 312.5µg/mL still showed increase in approximate trophozoite number though with significant decrease of trophozoite number when compared to the negative control (p <0.0001). 2500µg/mL and 5000µg/mL solvent extract concentrations continuously mimicked the effect of positive control (CHX) and completely eradicated *A. castellanii* trophozoites with no statistical difference between the treatment groups and the positive control (p >0.05). The progressive reduction of trophozoite number by the concentrations higher than 312.5µg/mL suggests an inhibition of the parasite replication, and/or cytolysis.

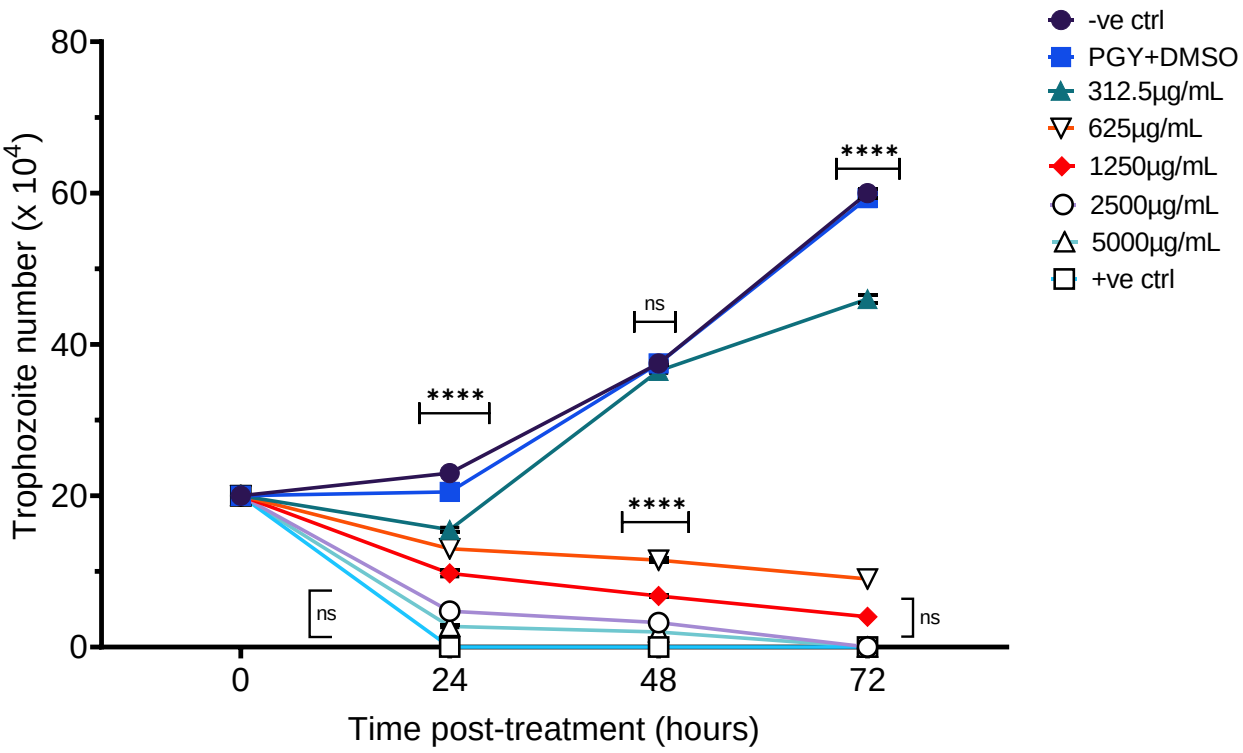

Figure 4:3: Growth inhibitory effect of *C. sinensis* solvent extract on *A. castellanii* at 24, 48, and 72h post treatment concentrations of 312.5µg/mL, 625µg/mL, 1250µg/mL, 2500µg/mL, and 5000µg/mL. At 24 hours, there was a decrease in trophozoite number for all the *C. sinensis* solvent extract treatment groups compared to negative control PGY+DMSO which showed increased trophozoite replication. The decrease seen was progressive for 625µg/mL, 1250µg/mL, 2500µg/mL, and 5000µg/mL concentrations till the end of the experiment (72 hours), while 312.5µg/mL allowed for trophozoite replication. At 72 hours post-treatment 2500µg/mL and 5000µg/mL mimicked the effect of the positive control (CHX) and completely eradicated *A. castellanii* trophozoites with no statistical difference ($p>0.9999$). (**** $p \leq 0.0001$, ns: non-significant).

4.3.2.2 External ultrastructural surface changes of C. sinensis solvent extract-treated trophozoites

Ultrastructural characteristics of *C. sinensis* solvent extract-treated trophozoites using SEM revealed progressive morphological alterations and destruction of *A. castellanii* trophozoites treated with *C. sinensis* (Figure 4:4). At 24 hours post exposure to 2500µg/mL *C. sinensis* solvent extract (Figure 4:4B), the SEM micrographs showed trophozoites that had lost their adhesive properties by equally losing their ability to secrete their adhesive and protective film when compared with the negative control treatment (PGY) which showed trophozoites in

aggregates linked together with adhesive films. Not only did the *C. sinensis* solvent extract allow for loss of adhesive film secretion ability, but there was also morphological alterations to trophozoites, with their sizes shrinking possibly in the attempt to encyst and fragmentation/ destruction of trophozoites. Continued exposure of trophozoites to the concentrations of *C. sinensis* from 24 hours post-exposure to 72 hours (Figure 4:4D) showed complete destruction of trophozoites treated with *C. sinensis* solvent extract. CHX showed similar morphological changes.

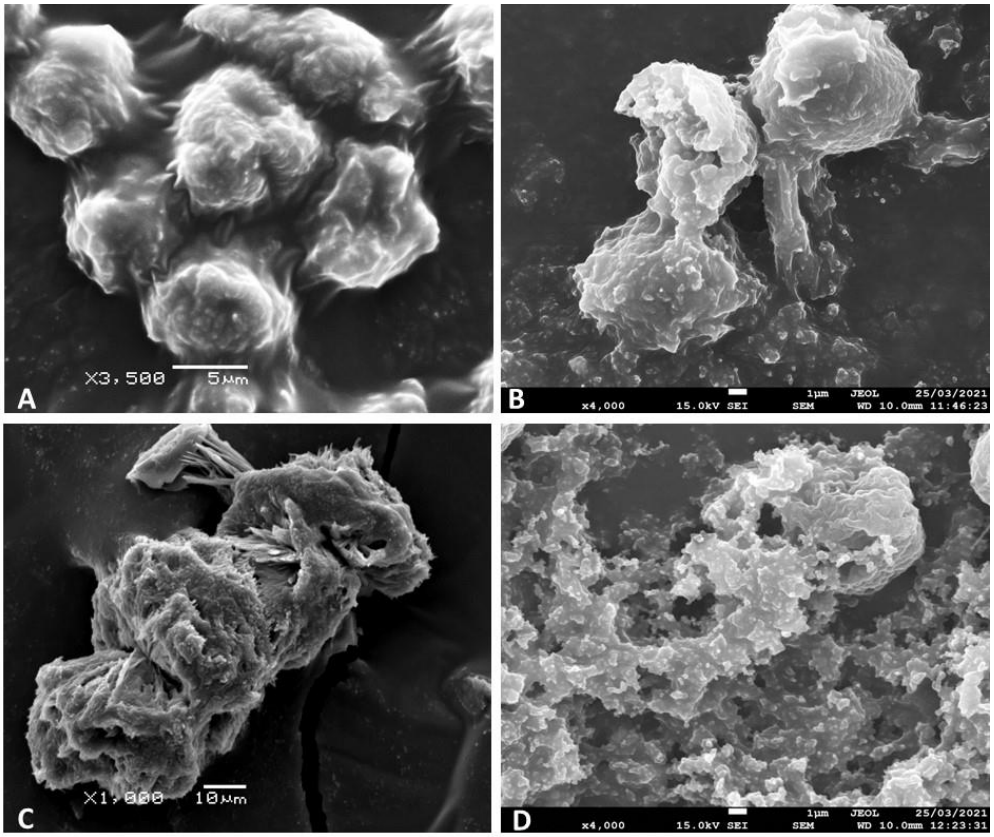

Figure 4:4: SEM micrographs of *A. castellanii* trophozoites showing loss of protective coat/layer of *A. castellanii* and shrinking of trophozoite size possibly in the attempt to encyst. Continued exposure to both *C. sinensis* solvent extract and Chlorhexidine shows loss of acanthopodia and progressive destruction of *A. castellanii* trophozoites. (A) Trophozoites in PGY (control) linked together by adhesin; (B) *A. castellanii* trophozoites in 2500µg/mL of *C. sinensis* solvent extract at 24 hours showing loss of protective adhesin and progressive destruction of the trophozoites. (C) Trophozoites in chlorhexidine at 24 hours showing loss of protective adhesin and shrinking/ destruction of the trophozoites. (D) Trophozoites in 2500µg/mL of *C. sinensis* solvent extract at 72 hours showing complete destruction of the trophozoites with dead parasite debris in the background. Magnification: X3500, X4000, X1000, X4000 respectively; Scale bars: 5, 1,10,1 µm respectively.

4.3.2.3 Internal ultrastructural changes of C. sinensis solvent extract-treated trophozoites

Ultrastructural changes within the *C. sinensis*-treated trophozoites were examined using TEM. TEM micrographs showing the intracellular organelles confirmed the progressive destruction of trophozoites exposed to *C. sinensis* as observed from the SEM micrographs (Figure 4:5). At 24 hours post-exposure, 2500µg/mL of *C. sinensis* treatment micrographs already showed loss of acanthopodia and rounded shape of the trophozoites, presumably in an attempt to encyst to protect itself from the action of *C. sinensis* (Figure 4:5B). At 72 hours post-exposure to *C. sinensis*, there was distinctive loss of cellular membrane integrity and expulsion of the EV cytoplasmic contents which indicates cell death, as well as the blotting out of the food vacuoles and mitochondria (Figure 4:5C). For the CHX group, there were no visible images in the TEM micrographs from 24 hours to 48 hours post exposure to 0.02% CHX.

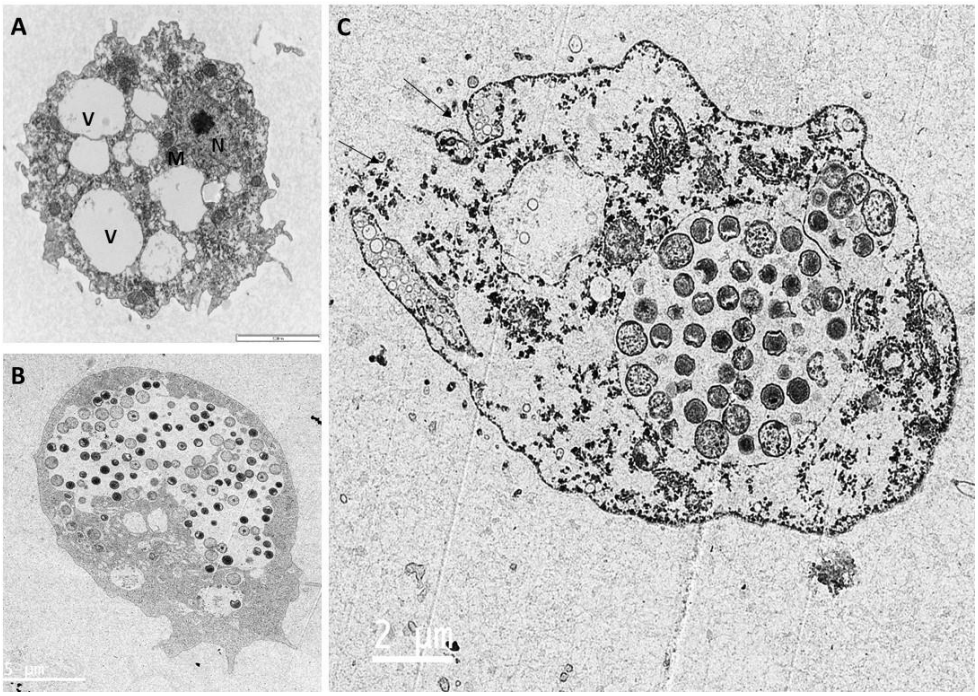

Figure 4:5: TEM micrographs showing progressive destruction of *A. castellanii* trophozoites exposed to *C. sinensis* solvent extract. (A) Trophozoite in control PGY medium; (B) Trophozoites in 2500µg/mL of *C. sinensis* solvent extract at 24 showing loss of acanthopodia and rounded shape of trophozoite in an attempt to encyst to protect itself from the action of *C. sinensis.* (C) At 72 h post-exposure to *C. sinensis*, trophozoite loses cellular membrane integrity (arrows). *Abbreviations:* (V) food vacuole, (M) mitochondria, (N) Nucleus. Magnifications: X6,000, X8,200, X16,500 & X4,200, respectively. Scale bars: 5,000 nm, 5µm, 2µm respectively.

4.3.2.4 Transient effect of C. sinensis solvent extract on A. castellanii trophozoites

The transient 2 and 24 h effect of *C. sinensis* solvent extract at 625µg/mL 1250µg/mL, and 5000µg/mL on trophozoites was determined using the hemocytometer. The two-way ANOVA of 2 h transient exposure of *A. castellanii* to *C. sinensis* revealed a significant main effect of time ($F(4, 12) = 656.9$, $p < 0.0001$), concentration ($F(2, 3) = 3993$, $p < 0.00001$), and time x concentration interaction ($F(8, 12) = 89.22$, $p < 0.0001$) (Figure 4:6).

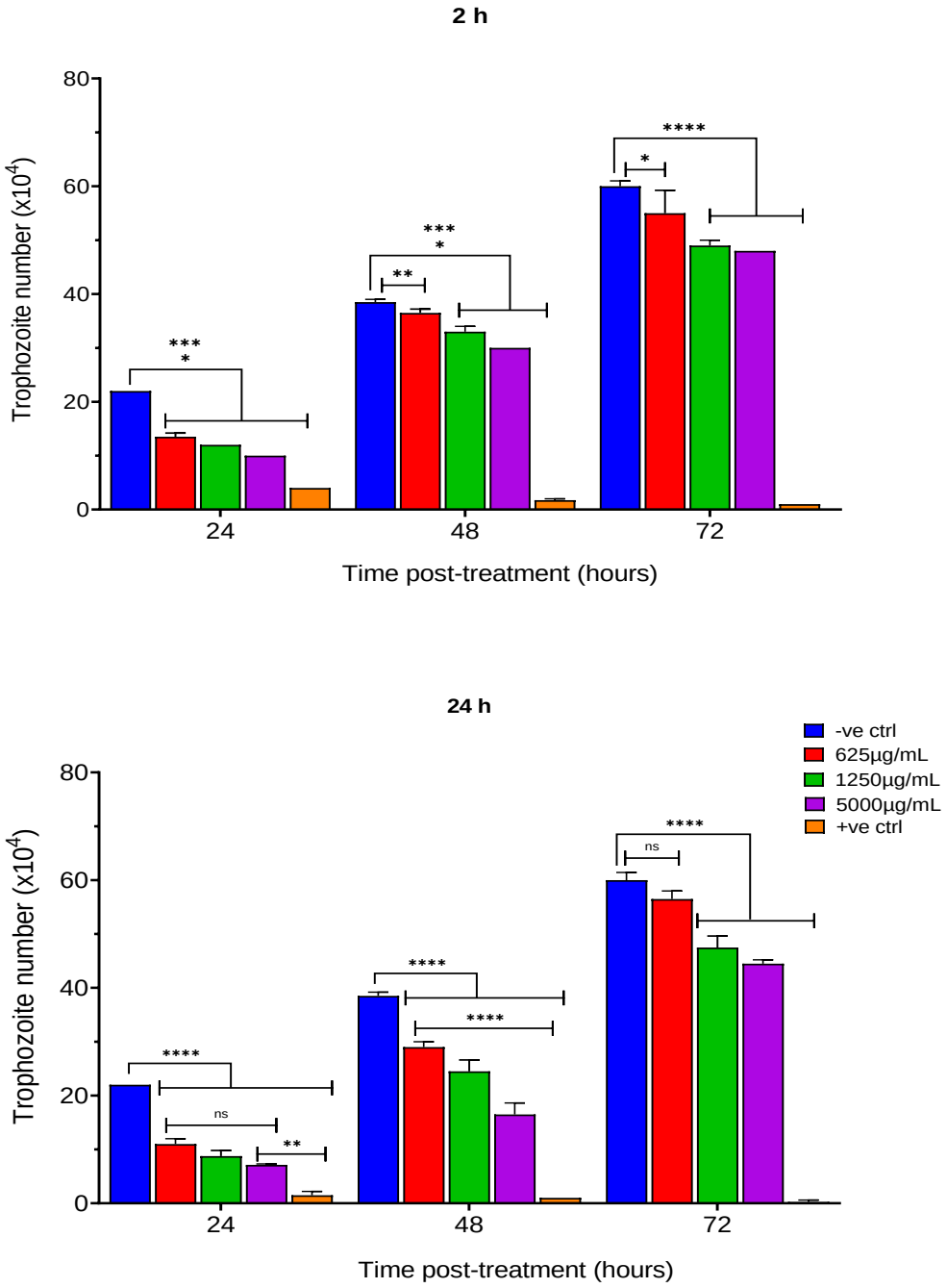

Figure 4:6: *C. Sinensis* solvent extract effect on growth kinetics of *A. castellanii* trophozoites post-transient exposure to 625µg/mL , 1250µg/mL, and 5000µg/mL of *C. sinensis* solvent extract and chlorhexidine (+ve ctrl) for 2 and 24 h. Significant increases were detected between the negative control and the solvent extract concentrations, however there was continued trophozoite replication for all the solvent extract concentrations. There was also continued inhibition of trophozoite replication by the positive control with significant increase in growth inhibition compared to all the *C. sinensis* solvent extract concentrations for the duration of the experiment 24-72 h exposure at both transient exposure time points. (**** $p \leq$ 0.0001, ns: non-significant).

Post-hoc comparisons for 2 h post transient exposure of trophozoites to solvent extract concentrations showed a significant increase in trophozoite replication ($p \leq 0.0001$) between the negative control and the solvent concentrations. Comparisons with the positive control also showed a significant increase in the trophozoite growth inhibition caused by the positive control (chlorhexidine) when compared with the *C. Sinensis* solvent extract concentrations of 625µg/mL, 1250µg/mL, and 5000µg/mL ($p < 0.00001$). at 48 h post treatment, there was increase in trophozoite replication for all the *C. Sinensis* solvent extract concentrations. There was however significant increase of growth in comparisons between the negative control and the solvent extract concentrations ($p < 0.00001$). Comparisons between the positive control and the solvent extract concentrations also showed significant increase in growth inhibition between the positive control and the solvent extract concentrations ($p < 0.00001$). The growth trends seen in 24 h and 48 h for all the solvent extract concentrations continued at 72 h. As seen in the previous time points, the comparisons between the positive and negative control when compared with the solvent controls showed significant increase in trophozoite growth for negative control and significant decrease in trophozoite growth for positive control ($p < 0.00001$).

The two-way ANOVA of 24 h transient exposure revealed a significant main effect of time ($F(4,12) = 1118$, $p < 0.0001$), concentration ($F(2, 3) = 601.3$, $p < 0.00001$), and a time x concentration interaction ($F(8,12) = 156.6$, $p < 0.0001$). Post-hoc comparisons for 24 h exposure also showed a significant increase ($p < 0.00001$) between the parasite growth inhibition caused by the positive control and the *C. Sinensis* solvent extract concentrations of 625µg/mL, 1250µg/mL, and 5000µg/mL for the duration of the experiment 24-72 h. As witnessed in the 2 h exposure, there was increased trophozoite number over time with treatment. Despite the significant difference between the treatment concentrations and the negative control ($p < 0.0001$), there was continuous replication of the trophozoites between 24 h to 72 hours. *C. sinensis* solvent extract concentrations at 625µg/mL 1250µg/mL, and

5000µg/mL were not able to exhibit any sustained inhibition on the growth kinetics of *A. castellanii* trophozoites after transient exposure at 2 and 24 h to *C. sinensis* (Figure 4:6).

4.3.3 Effect of *C. sinensis* solvent extract on trophozoite encystation

4.3.3.1 Inhibition of encystation

While determining the approximate number of cysts at 72 h pre- and post-SDS digestion, two-way ANOVA revealed a significant main effect of *C. sinensis* solvent extract concentrations ($F(6, 24) = 5926$, $p < 0.0001$), SDS effect ($F(1, 4) = 15123$, $p < 0.00001$) and a concentration x SDS interaction ($F(6, 24) = 171.4$, $p < 0.0001$) on encystation rate pre-SDS digestion and post-SDS digestion (Figure 4:7). Post hoc comparisons of the positive control with 2500µg/mL and 5000µg/mL *C. sinensis* solvent extract showed no significant difference ($p > 0.05$) as there were no cysts counted for those concentrations. The lower concentrations of 625µg/mL and 1250µg/mL showed some level of encystation but with significant decrease in encystation potential when compared with the negative control encystation buffer and the higher concentrations ($p < 0.0001$). This result indicates that not only did the *C. sinensis* solvent extract concentrations of 2500µg/mL and 5000µg/mL inhibition encystation, they also totally destroyed all the parasites in the medium which attempted to encyst.

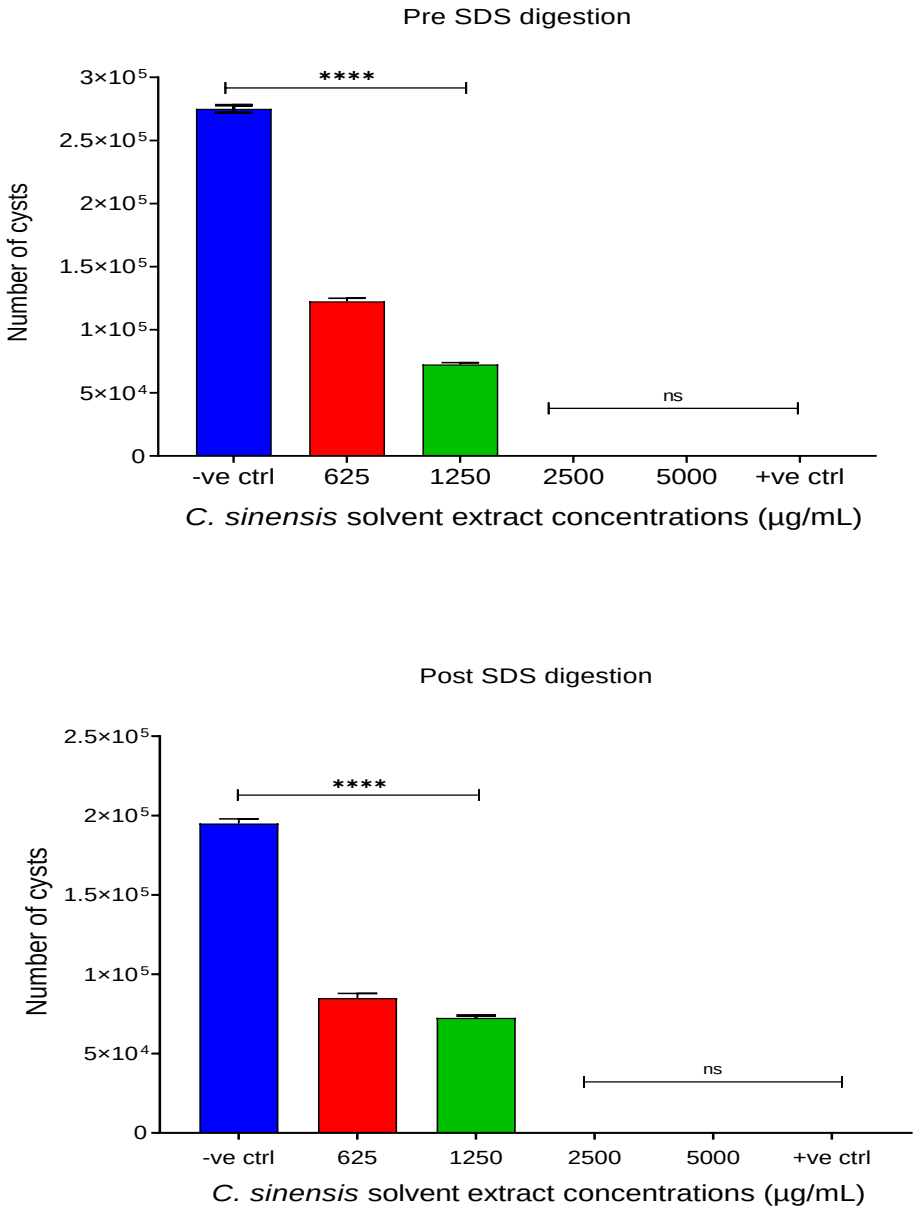

Figure 4:7: At 72 hours post encystation assay, pre- and post-SDS digestion, 2500µg/mL and 5000µg/mL *C. sinensis* solvent extract concentrations showed no cysts with no significant difference with the positive control (5 mM PMSF). The lower concentrations of 625µg/mL and 1250µg/mL showed some level of encystation but with significant difference with the negative control encystation buffer and the higher concentrations (**** $p \leq 0.0001$, ns; non-significant).

While comparing the encystation inhibitory percentage effect of *C. sinensis* solvent extract concentrations on *A. castellanii* trophozoites, one-way ANOVA revealed a significant main effect of *C. sinensis* solvent extract concentration ($F(5, 12) = 3149$, $p < 0.0001$) on the inhibition rate. Post hoc comparisons showed a 100% inhibition rate of 2500µg/mL and 5000µg/mL *C. sinensis* solvent extract encystation buffer with no significant difference between them and the positive control (5 mM PMSF) ($p < 0.0001$). Alternatively, the lower concentrations of 625µg/mL and 1250µg/mL *C. sinensis* solvent extract encystation buffers showed no significant difference between their inhibition rates of 30.67% and 35.57% respectively with the negative control encystation buffer of 29.10% ($p > 0.05$) (Figure 4:8). The results demonstrate that while the two lower concentrations did not inhibit encystation, the two higher ones did.

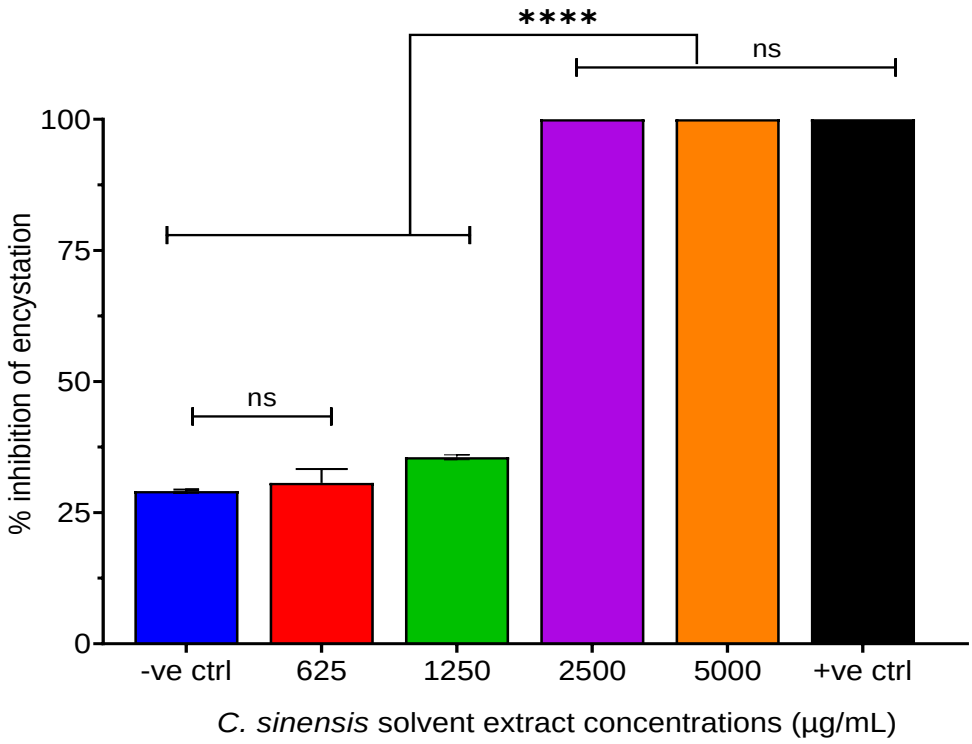

Figure 4:8: Percentage inhibition of encystation of *A. castellanii* by *C. sinensis* solvent extract encystation buffer 72 hours post exposure to treatment. 2500µg/mL and 5000µg/mL *C. sinensis* solvent extract encystation buffer displayed 100% inhibition of encystation with no significant difference between it and the positive control (5 mM PMSF). The lower concentrations of 625µg/mL and 1250µg/mL displayed less than 40% inhibition to encystation showing no significant difference with the negative control encystation buffer (**** $p \leq 0.0001$, ns: non-significant).

4.3.3.2 Ultrastructural surface changes of encysting trophozoites

SEM micrographs showed progressive destruction of the encysting *Acanthamoeba* trophozoites treated with *C. sinensis* encystation buffer during the 72 hours it took for the encystation experiment to be completed as represented by the reduction in cyst numbers pre- and post-SDS assay. The negative control shows that the encysting *Acanthamoeba* trophozoites encyst and the cysts were amassed in bunches and held together in the course of their encystation. Meanwhile, exposure of the encysting *Acanthamoeba* trophozoites to different concentrations of *C. sinensis* solvent extract led to the loss of their adhesive properties and the breaking up of the cysts, which was progressive for even a low concentration of 625µg/mL at 72 hours. At 72 hours post-exposure to *C. sinensis* encystation buffer, there was extensive destruction of the encysting and encysted *Acanthamoeba* (Figure 4:9).

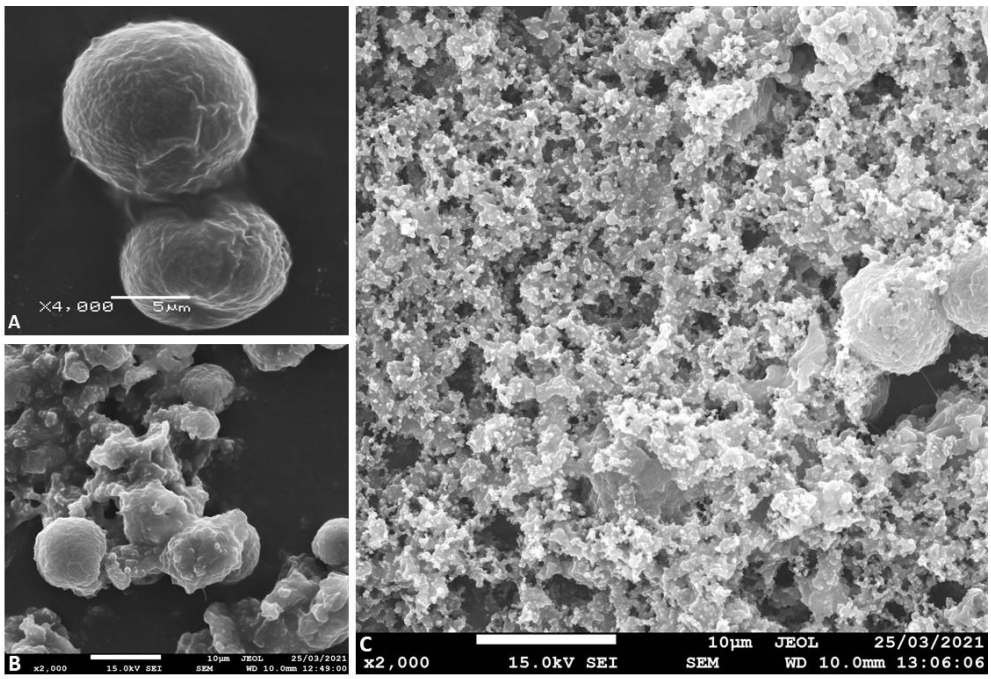

Figure 4:9: SEM micrographs showing progressive destruction of *A. castellanii* cysts exposed *to C. sinensis* solvent extract solvent extract encystation buffer during synchronized encystation. (A) Cysts in control encystation buffer linked together by adhesin (arrow); (B) Aggregated cysts exposed to *C. sinensis* buffer 625µg/mL at 72 hours. Shows a combination of or broken cysts, cyst debris and viable cysts; (C) Cyst exposed *C. sinensis* encystation buffer 2500µg/mL at 72 hours showing extensive destruction of cysts. Magnification: X4,000, X2,000 & X4,000; Scale bars: 5 (A) and 10 µm (B and C).

4.3.3.3 Internal ultrastructural changes of encysting trophozoites

TEM analysis of the internal ultrastructural alterations in the encysting *Acanthamoeba* showed time-dependent progressive destruction of the cysts (Figure 4:10). At 24 hours post-exposure there was increased condensation of the cellular contents and an abnormal increase in the quantity of food vacuoles in comparison to the negative control group; this change was seen even for the lowest *C. sinensis* encystation buffer concentration of 625µg/mL. At 72 hours post-exposure to *C. sinensis* encystation buffer, the *Acanthamoeba* cysts and encysting trophozoites lost their cellular membrane integrity and cysts seemed to have ruptured, leading to an extensive expulsion of the cellular contents as also represented in the SEM analysis (Figure 4:9).

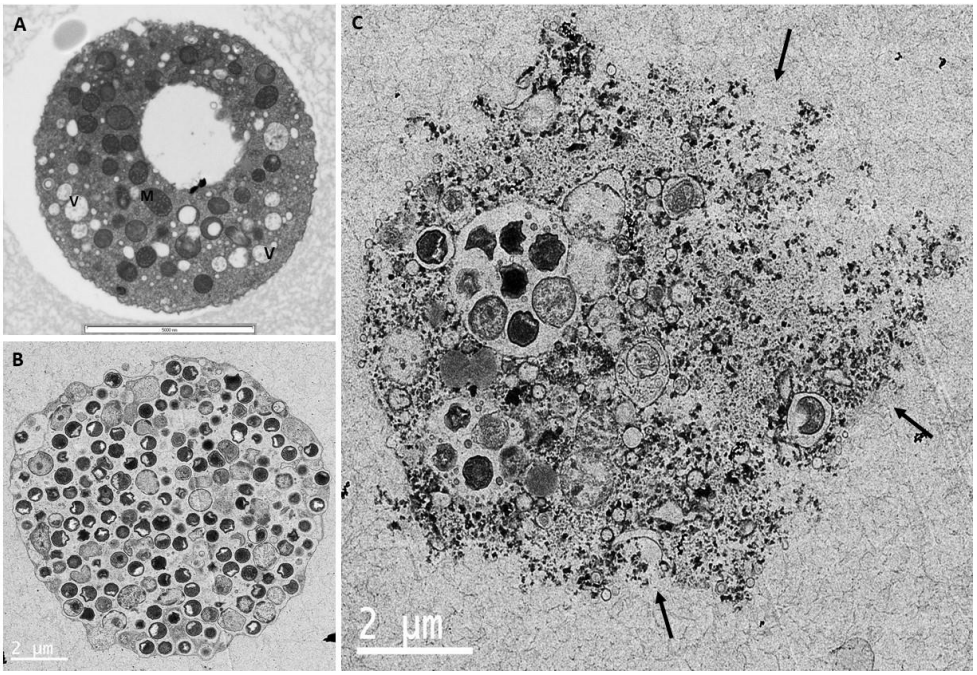

Figure 4:10: TEM micrographs showing progressive destruction of *A. castellanii* cysts exposed to *C. sinensis* solvent extract encystation buffer during synchronized encystation. (A) Cyst in control encystation buffer; (B) Cysts exposed to *C. sinensis* encystation buffer 625µg/mL at 24 hours; (C) Cyst exposed *C. sinensis* 2500µg/mL at 72 hours cyst loses cellular membrane integrity with debris seen in the background. (V)food vacuole, (M)mitochondria, (N)Nucleus, (Arrow) loss of cellular membrane integrity. Scale bars: 5,000 nm (A) and 2 µm (C, B)

As also speculated from the electron microscopic analysis of *C*. *sinensis* brew effect on *A. castellanii* in chapter 3 (Figure 3.21), the ultrastructural alterations of the encysting trophozoites suggest that the presence of *C. sinensis* solvent extract in the encystation medium induced some sort of stress and apoptosis-like death of the *Acanthamoeba,* thereby disrupting the organism's ability to form and maintain cysts.

4.3.4 *C. sinensis* effects on excystation of *A. castellanii* cysts

In this experiment, the cysticidal, trophocidal and excystation capabilities of *C. sinensis* solvent extract concentrations were assessed. The rate of cyst to trophozoite differentiation (excystation) as allowed by *C. sinensis* solvent extract concentrations was quantified by the number of trophozoites recorded at each time point post exposure to the treatment. The percentage inhibition of excystation by the *C. sinensis* solvent extract concentrations was also determined. The direct effects of *C. sinensis* solvent extract on the morphology and structure during the differentiation was observed using light microscopy.

4.3.4.1 Microscopic analysis of C. sinensis on A. castellanii cyst excystation

Microscopic observations of *A. castellanii* cyst culture 72 hours post exposure to *C. sinensis* solvent extract concentrations showed extensive excystation of the negative control treatment, while the *C. sinensis* solvent extract treatment concentrations showed a different picture with mild to extensive damage of the *A. castellanii* cysts (Figure 4:11).

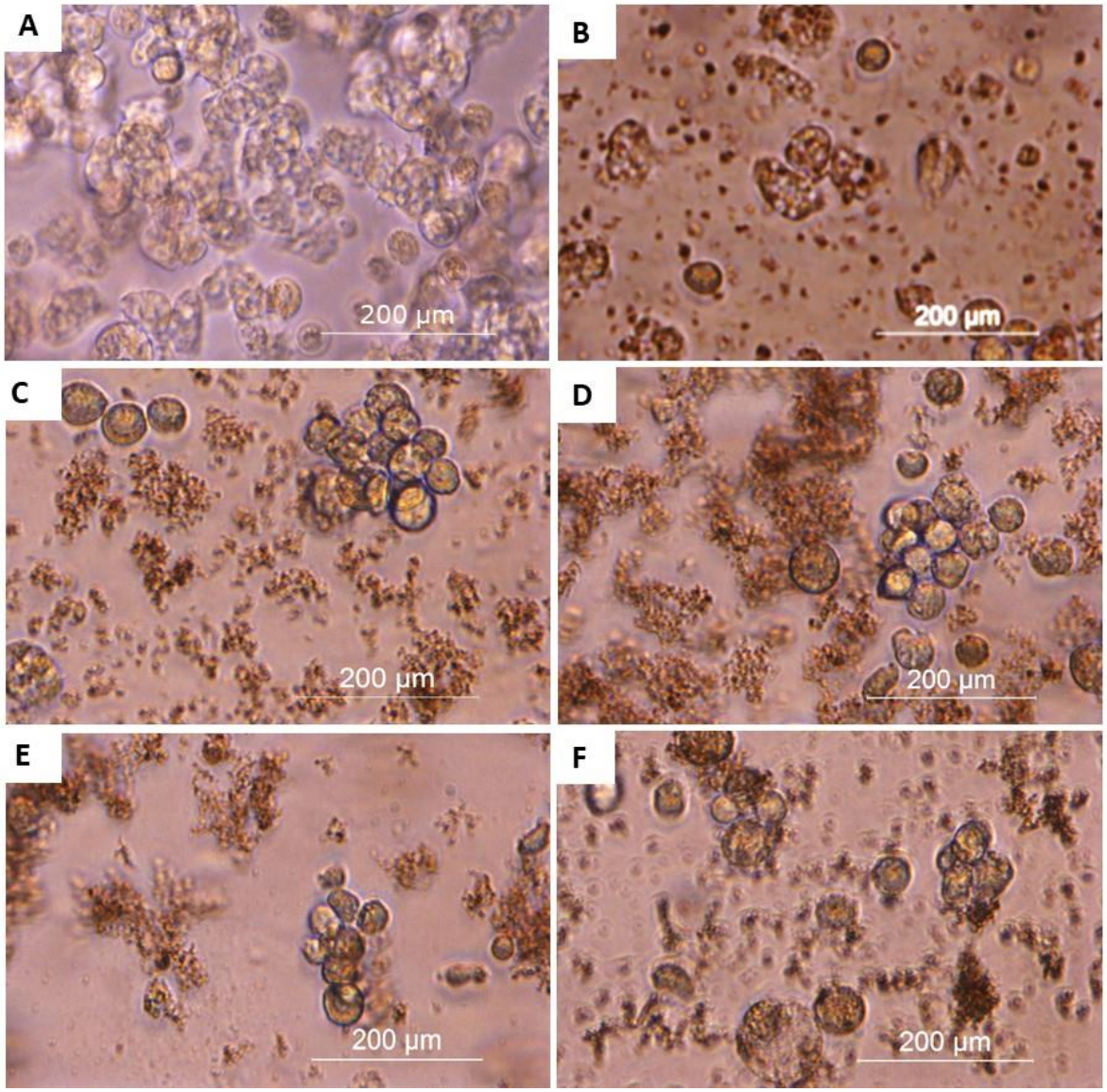

Figure 4:11: Morphological characteristics of *A. castellanii* cysts at 72 h post exposure to 312.5µg/mL, 625µg/mL, 1250µg/mL, 2500µg/mL, and 5000µg/mL *C. sinensis* solvent extract. (A) control cyst culture treated with PGY. (B-E) cysts treated with 312.5µg/mL, 625µg/mL, 1250µg/mL, 2500µg/mL, and 5000µg/mL C. sinensis, respectively. At 72 h, (D-F) 1250µg/mL, 2500µg/mL, and 5000µg/mL C. sinensis solvent extract shows the presence of broken up cysts, with cytoplasmic contents with cytolysis observed in all the culture media. Adhesion to flask surface was inhibited by all *C. sinensis* solvent extract treatment groups confirmed by the gentle rocking of the culture plates. 312.5µg/mL, 625µg/mL (B & C) culture plates also showed some debris and broken up cysts but not as extensive as seen in the higher concentrations. X40 magnification. Scale bar, 200 µm.

The images of *C. sinensis* solvent extract concentrations show the presence of broken up cysts, with cytoplasmic contents with cytolysis observed in all the culture media. The debris seen with 312.5µg/mL and 625µg/mL concentrations were not as extensive as the higher 1250µg/mL, 2500µg/mL, and 5000µg/mL concentrations, where fully damaged and improper cysts or trophozoites were observed. To confirm the presence or absence of trophozoites which adhered to the bottom of the flasks, the flasks were rocked gently during light microscopic imaging and the view of the entire flask bottoms showed varying degree of floating debris and improper cysts with no sign of adherent trophozoites. Subsequently, quantification of the approximate number of cysts per aggregate as displayed was impossible to achieve as the gentle rocking seemed to loosen the inter-cystic adherent properties seen in previous cyst related experiments.

4.3.4.2 C. sinensis inhibition of excystation of A. castellanii cysts

The effect of *C. sinensis* solvent extract on *A. castellanii* cysts exposed to 312.5µg/mL, 625µg/mL, 1250µg/mL, 2500µg/mL, and 5000µg/mL concentrations was determined using haemocytometer counting to check the cyst-trophozoite ratio at 72 hours post exposure. One-way ANOVA revealed a significant main effect of *C. sinensis* solvent extract concentrations ($F(7, 16) = 1001$, $p < 0.0001$) on the excystation rate of the cysts post exposure. Post hoc comparisons showed that the number of trophozoites excysted by the 312.5µg/mL and 625µg/mL concentrations were much lesser than the negative control groups with statistical increase in the excysted trophozoite number ($p < 0.0001$). Comparing the number of excysted trophozoites of 312.5µg/mL - 625µg/mL with the higher concentrations of 1250µg/mL - 5000µg/mL also showed significant increase in the excysted trophozoites of the lower band pf concentrations that the higher band ($p < 0.0001$). Further comparisons between the positive control and higher concentrations of 1250µg/mL, 2500µg/mL and 5000µg/mL displayed a high inhibition of trophozoite excystation represented by the absence of any trophozoites. This inhibition capability was same with the positive control where no excysted trophozoite were

seen, hence no statistical difference between the activity higher bands of *C. sinensis* solvent extract encystation buffer and the positive control ($p > 0.05$) (Figure 4:12).

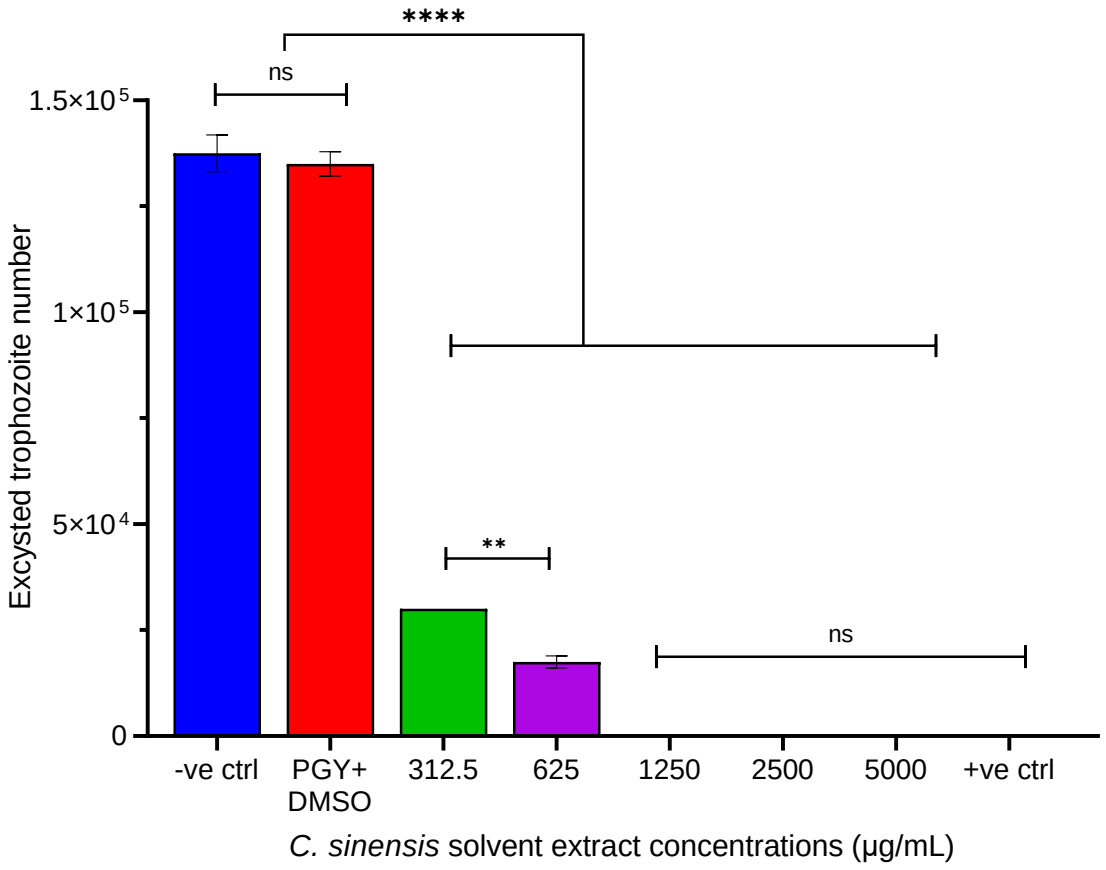

Figure 4:12: 72 hours post exposure to graded concentrations of *C. sinensis* solvent extract. 1250µg/mL, 2500µg/mL and 5000µg/mL exhibited 100% inhibition of excystation as seen with the positive control. Although there were significant differences between the higher concentrations and the lower concentrations of 312.5µg/mL and 625µg/mL, these low concentrations exhibited 78% and 87% inhibition of excystation respectively. (** $p \leq 0.01$, **** $p \leq 0.0001$, ns: non-significant).

In determining the percentage inhibition of excystation, one-way ANOVA revealed a significant main effect of *C. sinensis* concentrations (µg/mL) ($F(7, 16) = 10695$, $p < 0.0001$) on excystation inhibition percentage of the exposed cysts. Post hoc comparisons showed that 312.5µg/mL and 625µg/mL concentrations exhibited 78% and 87% inhibition of excystation respectively

with significant increase in inhibition potential compared to the negative control groups ($p<0.0001$). Similarly, the higher concentrations 1250µg/mL, 2500µg/mL and 5000µg/mL displayed 100% inhibition of excystation mimicking the activity of positive control ($p > 0.05$) (Figure 4:13). These high concentrations' inhibition capability was higher than those of the lower bands with significant increase in their excystation inhibition percentage ($p<0.0001$).

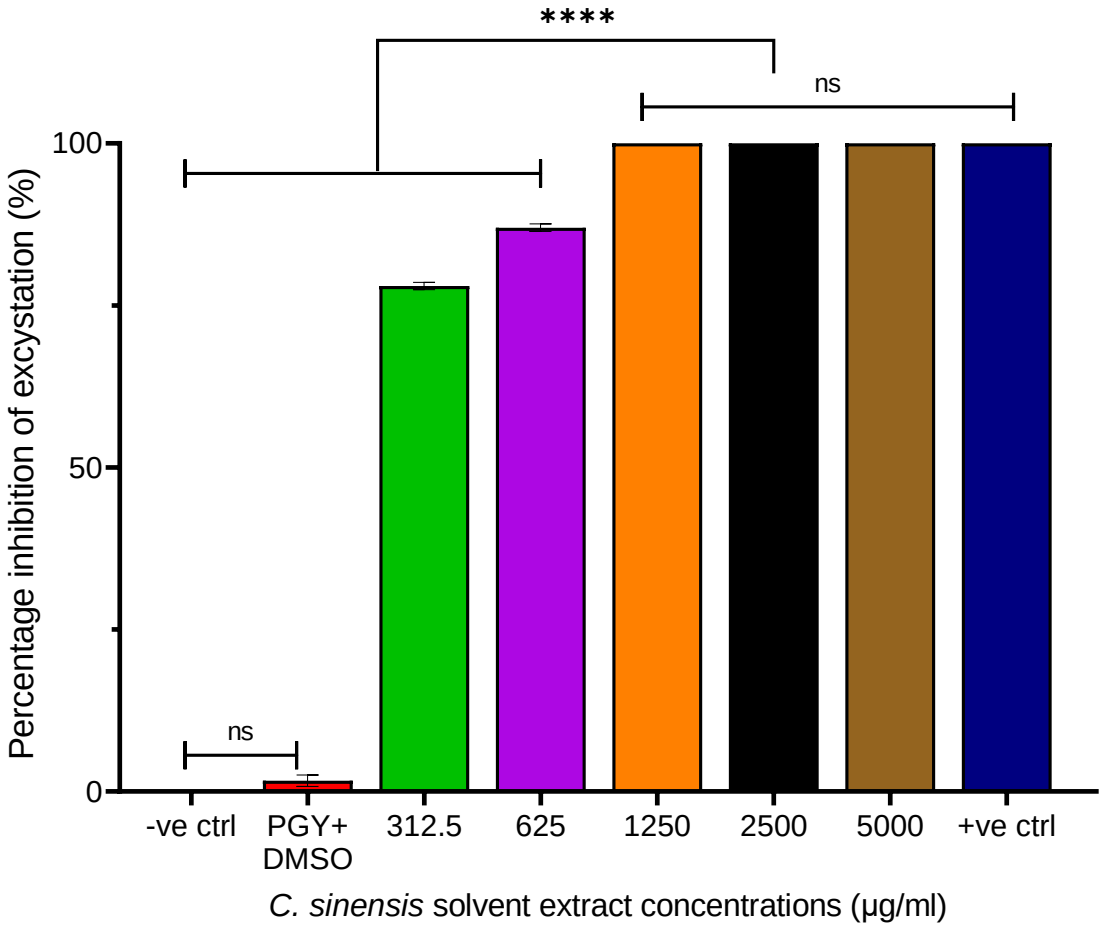

Figure 4:13: Percentage (%) inhibition of trophozoite excystation in *C. sinensis* solvent extract: 72 hours post exposure to graded concentrations of *C. sinensis,* 1250µg/mL, 2500µg/mL, and 5000µg/mL exhibited 100% inhibition of excystation as seen with the positive control. Although there were significant differences between the higher concentrations and the lower concentrations of 312.5µg/mL and 625µg/mL, these low concentrations exhibited 78% and 87% inhibition of excystation respectively. (**** $p \leq 0.0001$, ns, non-significant).

4.4 SELECTIVITY INDEX OF *C. SINENSIS* SOLVENT EXTRACT

The half-maximal inhibitory concentration (IC50), which is the concentration of C. sinensis solvent extract that caused a 50% decrease of *A. castellanii* trophozoites growth compared to the control was determined to be 1309 ± 517.1 µg/mL at 24 hours and 409 ± 8.089 µg/mL at 48 hours (Fig. 13). The CC50 for iHCE-2 and MDCK were determined to be 8891 ± 1135 µg/mL at 24 hours and 6916 ± 199 µg/mL at 48 hours, 222.1 ± 25.06 µg/mL at 24 hours and 346.3 ± 12.89 µg/mL at 48 hours respectively. This indicated that *C. sinensis* solvent extract has selective dose dependent cytotoxicity for host cells as seen by the wide range of concentration allowed for iHCE-2s and a lower range for MDCKs.

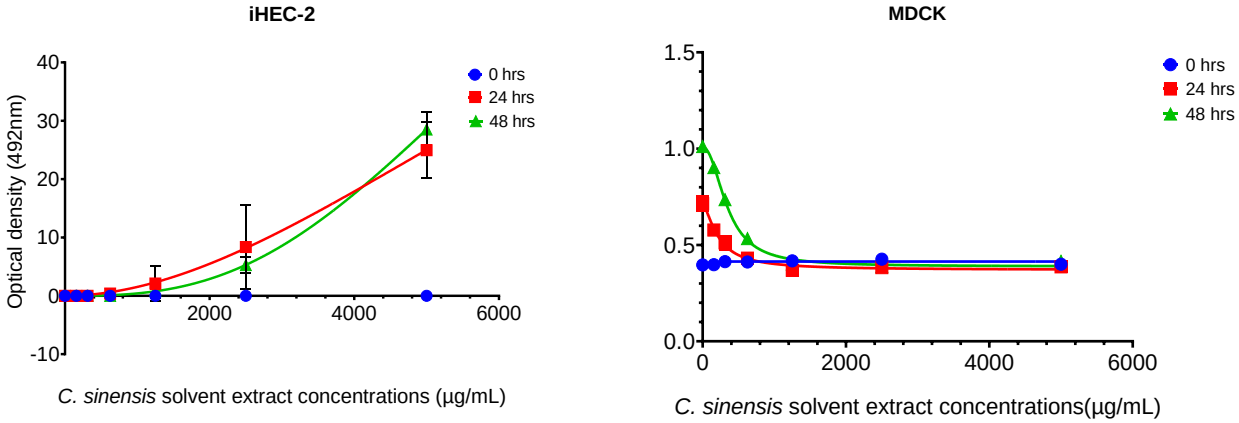

Figure 4:14: The half-maximal inhibitory concentration (IC50) of *C. sinensis* solvent extract for iHCE-2 and MDCK expressed as 50% cytotoxic concentration (CC50) were determined to be 8891 ± 1135 µg/mL at 24 hours and 6916 ± 199 µg/mL at 48 hours, 222.1 ± 25.06 µg/mL at 24 hours and 346.3 ± 12.89 µg/mL at 48 hours respectively.

4.5 DISCUSSION

Use of cationic antiseptics such as chlorhexidine and polyhexamethylene biguanide either as stand-alone or in combination, have been the most sought after choice with no sustained and satisfactory results (Kaynak et al., 2018). In a lot of the cases for these antiseptics and antifungals used, the extent of their amoebicidal or amoebistatic capabilities are equally commensurate to their cytotoxic effects in host cells when tested in vitro, and as such invalidates their usage as acanthamoebicides. In reality, there is still a need for alternative and more viable medications for treatment of *Acanthamoeba* infections, use of nutraceuticals seems to be an option for novel therapy sources. Plants have been known to produce metabolites which keeps them safe in biodiversity among animals, pathogens and insects (Tan and Zou, 2001), this encourages the rationale of natural products as probable novel sources of amoebicidal drugs, and a host of them have also been evaluated for their acanthamoebic capabilities post solvent extraction, olive leaf extract (Sifaoui et al., 2013), *Trigonella foenum graecum* (Dodangeh et al., 2018), *Ornithogalum sigmoideum* (Kaynak et al., 2018), *Ziziphus vulgaris* (Dodangeh et al., 2017), and many other solvent extracts of plant sources (Hadas et al., 2017a; Saoudi et al., 2017; Mahboob et al., 2017; Kikowska et al., 2020).

The preceding chapter (chapter 3) to the present study involved the use of *C. sinensis* tested in hot and cold brew forms in vitro to evaluate its acanthamoebicidal activity. That study led to the conclusion that *C. sinensis* brews possesses amoebicidal activity against *A. castellanii* trophozoites and were highly effective at inhibiting the parasite's ability to encyst .The present study entailed the use of *C. sinensis* solvent extract especially as literature showed anti-microbial and anti-protozoan capability of *C. sinensis* (Aslam et al., 2014; Servin et al., 2021). In this present study, *C. sinensis* solvent extract was tested against *A. castellanii* trophozoites and cysts with the presumption solvent extraction might yield higher concentration of bioactive properties of *C. sinensis* in comparison with brews. This may lead to more opportunities for

the development of better nutraceutical formulations with *C. sinensis*. It is however important to note that at this stage of the study there is no indices available in determining the concentration of the *C. sinensis* brews components as well as that of the solvent extract. As such, it is not possible to conduct a side-by-side evaluation to determine which of the forms possesses more anti-acanthamoebic capability. Knowing that reference drugs against acanthamoebiasis exhibit toxicity against corneal cells when used individually and also synergistically at the regular concentrations (Mafra et al., 2013), also resulted in the need for cytotoxic evaluations of *C. sinensis* solvent extract concentrations

Previous studies on solvent extractions of *C. sinensis* have presented data on the anti-microbial effects of *C. sinensis* and its components against gram-positive and gram-negative multi-drug resistant pathogens (Parvez et al., 2019). With regards to parasites, *C. sinensis* potentiated the antimalarial effect of artemisinin without interfering with the folate pathway (Thipubon et al., 2015; Sannella et al., 2007). Also, *C. sinensis* reduced the *Haemonchus contortus* worm burden (Zhong et al., 2014), inhibited promastigote and amastigote forms of *Leishmania braziliensis* (Inacio et al., 2014), and inhibited *Leishmania amazonensis* (dos Reis et al., 2013; Inacio et al., 2013). Additionally, *C. sinensis* had inhibitory activity against *Babesia* spp. (Aboulaila et al., 2010), *Eimeria* spp. (Jang et al., 2007) and *Trypanosoma cruzi* (Paveto et al., 2004). Given the recorded broad-spectrum antimicrobial activity of *C. sinensis*, and to potentiate the already known amoebicidal ability of *C. sinensis* brew forms*, C. sinensis* was subjected to extraction protocols using polar solvents (methanol and acetonitrile) to arrive at a crude extract aimed at consolidating the bioactive components of *C. sinensis* as previously done in literature (Atanasov et al., 2021)..

From the cytotoxic evaluations using iHCE-2s with a range of concentrations of 156.25µg/mL to 5000µg/mL, the second highest concentration of 2500µg/mL solvent extract had an initial approximate 7.5% cytotoxic effect at 24 hours exposure in comparison to the control, which was not sustained by 48 hours post exposure where the cytotoxicity percentage dropped to approximately 5%. Statistical analysis of both 24- and 48-hours cytotoxic evaluations with the

assay showed that there was no significant difference with the control treatment. Interestingly, the high concentration of 5000µg/mL solvent extract exhibited only 30% cytotoxicity at the termination of the cytotoxic evaluations. For an alternative and comparative cytotoxic evaluation in another mammalian cell, evaluations with MDCK cells painted a different picture with a sluggish cell replication, which indicated some level of cytotoxicity. The concentrations of 1250µg/mL, 2500µg/mL and 5000µg/mL, though showing cytotoxicity of up to 55% by the termination of the experiment, did not halt cell replication. The choice of continuing the experiment with the range of concentrations became dependent on the cytotoxicity level seen with the iHCE-2s (Figure 4:1), assuming that the application of possible final synthesis of *C. sinensis* being used as a topical agent against AK, which has the cornea as its predilection site (Siddiqui and Khan, 2012; Lorenzo-Morales et al., 2013b). In available literature, it has been impossible to determine what the safety margin of *C. sinensis* solvent extract is as no study has been conducted to determine *C. sinensis* solvent extract toxicity to host cells.

In available literature, there was no study on the amoebicidal effect of *C. sinensis* solvent extracts. With respect to the anti-acanthamoebic activity of *C. sinensis* solvent extract against the trophozoites and cysts, the results demonstrated that *C. sinensis* solvent extract inhibits trophozoite growth and replication and brings about cytolysis in vitro. While evaluating the growth inhibitory and trophocidal effects of *C. sinensis* solvent extract, it was shown that concentrations of 625µg/mL to 5000µg/mL exhibited sustained reduction of trophozoite numbers from 24 to 72 h post treatment confirming inhibition of trophozoite proliferation and/or cytolysis. For the encystation studies, there was similarity to the activity seen with *C. sinensis* brews, where trophozoites seemed to attempt to encyst as a counter to the toxic effect of *C. sinensis* solvent components, which could also be said to be consistent with previous studies that have shown that *A. castellanii* trophozoites rapidly differentiate into pseudocysts upon exposure to organic solvents (Kliescikova et al., 2011b; Kliescikova et al., 2011a). Also known is that when exposed to adverse conditions, cellulose synthesis with β1,4 glucans homopolysaccharide end point, 1,3-Galactose polymer synthesis with 1,3-galactopyranose

endpoint, and protein synthesis with fibrous cyst wall specific protein endpoint occur to form the cyst wall (Anwar et al., 2018). Apart from cellulose synthesis, glycogen phosphorylase formed during phosphorylation (Lorenzo-Morales et al., 2008) and xylose isomerase synthesis (Lloyd, 2014) are necessary during the encystation process.

In this study, the lower concentrations of 625µg/mL and 1250µg/mL were able to inhibit encystation to a certain degree, with the higher concentrations of 2500µg/mL and 5000µg/mL *C. sinensis* solvent extract hyperosmotic solutions completely inhibiting trophozoite to cyst differentiation (Figure 4:8) and destroying both life cycle stages of *A. castellanii*. Based on their concentrations of 2500µg/mL and 5000µg/mL *C. sinensis* solvent extract hyperosmotic solutions, they could be said to contain higher concentrations of bioactive compounds which might possess serine protease-like activity and cysteine-specific protease-like activity, like the phenyl-methanesulfonyl fluoride solution used for positive control that is known to inhibit the encystation of trophozoites (Dudley et al., 2008; Hirukawa et al., 1998; Leitsch et al., 2010). The bioactive compounds might also be capable of inhibiting cellulose and xylose isomerase synthesis, as well as inhibition of glycogen phosphorylation (Lloyd, 2014). In addition to the inhibition of encystation, concentrations of *C. sinensis* solvent extract hyperosmotic solutions also instigated the destruction of trophozoites in their attempt to encyst as the quantification of trophozoites and cysts pre and post SDS assay indicated absence of any of parasite forms (Figure 4:7). This confirms *C. sinensis* solvent extracts contain compounds that induce trophozoite membrane permeability which can also be said to be serine proteases-like in action (Alsam et al., 2005).

Ultrastructural changes of the trophozoites and cysts exposed to *C. sinensis* solvent extract confirms the results that the concentrations between 625µg/mL to 2500µg/mL caused progressive destruction of trophozoites. Firstly, this started possibly by inhibiting trophozoite protein synthesis which prevents it from secreting its 130 kDa MBP, 28.2kDa and 55kDa LBP, and a 207kDa adhesion protein which enables the adhesive capability of *A. castellanii* trophozoites (Siddiqui et al., 2012; Hong et al., 2004) (Figure 4:4). These parasite specific

adhesin proteins that allows the adhesion of trophozoites to surfaces also allows for cysts to bunch together in aggregates (Ahearn and Gabriel, 1997) when encystation process is complete (Siddiqui and Khan, 2012). With the loss of trophozoite adhesin follows the loss of cell membrane integrity and ultimately parasite death by phosphatidylinositol 3-kinase (PI-3k)-dependent mechanism (Figure 4:5). Although *A. castellanii* possesses the uncanny ability to differentiate to cysts when threatened by chemotherapy and hyperosmotic conditions (Anwar et al., 2018; Lloyd, 2014) as presented by *C. sinensis* solvent extract hyperosmotic solutions, their drug resistant and differentiational capability were inhibited by a dose-dependent action of *C. sinensis* solvent extract. As presumed with *C. sinensis* brew activity during encystation (chapter 3), it is also possible that some of *C. sinensis* solvent extract components may possess multifunctional capabilities of inhibiting protease secretion and also inhibiting synthesis of other components, such as M17 AcLAP, which is involved and expressed in the late stages of encystation during the formation of the cyst wall (Lee et al., 2015).

Interestingly, in evaluating the effect of *C. sinensis* solvent extract concentrations on the differentiation of *A. castellanii* from cysts to trophozoites, the low concentrations of 312.5µg/mL and 625µg/mL resulted in 78% and 87% inhibition of excystation of cysts, respectively. The higher concentrations of 1250µg/mL to 5000µg/mL completely inhibited trophozoite excystation (Figure 4:12, Figure 4:13). Light microscopic analysis of the culture at 72 hours post exposure showed extensive destruction of *Acanthamoeba* with presence of EVs in the culture (Figure 4:11). Although the reason for the ability of the lowest concentration of 312.5µg/mL to not only inhibit encystation but also to dramatically destroy the cysts and trophozoites during excystation might not be fully known, it is known that cysts are hardier and drug resistant when compared to trophozoites. Therefore, excystation will predispose *Acanthamoeba* to a more drug susceptible morphological form for which the inclusion of *C. sinensis* solvent extract during this process might have interfered with the transition leading to cyst and trophozoite destruction. While *A. castellanii* encysts when it is exposed to injurious conditions, it might not have the ability to halt and reverse its excystation process when it might

have sensed the presence of injurious compounds in the growth media, hence leading the excysting trophozoites to an apoptotic-style death. It is, however, intriguing and unexplainable at this point of the study that trophozoites exposed to the same low concentration of *C. sinensis* solvent extract during excystation experiments which inhibited excystation could not inhibit parasite replication during the *C. sinensis*-trophozoite growth inhibitory experiments. The excystation growth trajectory of the lower concentrations were seen to be similar to the growth trajectory of the negative control. In general, the solvent extract also exhibited similar anti-acanthamoebic activity in comparison with the positive control indicating that their activity and mechanism of action though not yet known might have mimicked that of the positive control.

Studies in literature have shown that *C. sinensis* contains bioactive compounds such as polyphenols including flavanols, flavandiols, flavonoids, and phenolic acids (Namal Senanayake, 2013; Zhong et al., 2014), and also catechins as well as (−)-epicatechin (EC), (−)-epicatechin-3-gallate (ECG), (−)-epigallocatechin (EGC), and (−)-epigallocatechin-3-gallate(EGCG)(Mukhtar and Ahmad, 2000), caffeine (Perva-Uzunalic et al., 2006), amino acids, sterols, vitamins and other components with antioxidant and antiviral capability (Sanlier et al., 2018; Yang et al., 2019; Katada et al., 2019; Srichairatanakool et al., 2006; Liou, 2021). A review of these compounds may give more insight on how *C. sinensis* solvent extract was able to inhibit trophozoite replication, inhibit encystation and excystation while also being trophocidal and cysticidal in dose dependent manner.

In conclusion, the results of this study demonstrated that *C. sinensis* solvent extract possesses amoebicidal ability against both trophozoite and cyst forms of *A. castellanii*. *C. sinensis* solvent extract demonstrated effectiveness in inhibiting encystation and a potential ability to quickly and effectively eliminate *A. castellanii* trophozoites *in vitro.* In evaluating the efficacy of *C. sinensis* solvent extract as a follow up to that of the *C. sinensis* brew forms, the *C. sinensis* solvent extract dose-dependent amoebicidal ability brings the evaluation of *C. sinensis* to a point where it can be recommended for further anti-acanthamoebic studies. Also, it is recommended that anti-acanthamoebic studies be carried out with the bioactive constituents

of *C. sinensis* solvent extract which might elicit more anti-acanthamoebic activity against trophozoites. They could also inhibit encystation and/or excystation of *A. castellanii.* The outcome of these studies can eventually contribute to the development of safe and effective therapeutic interventions against *A. castellanii* infection.

5 *C. SINENSIS* CHEMICAL PROPERTIES AND THEIR EFFECT ON *A. CASTELLANII*

5.1 SUMMARY

In this study, the trophocidal and cysticidal effect of *Camellia sinensis* chemical components was investigated by subjecting *Acanthamoeba castellanii* trophozoites and cysts to serial concentrations (200 µM, 100 µM, 50 µM, 25 µM, 12.5 µM, 6.25 µM and 3.12 µM) of the chemical components (EGCG, caffeine, EGC, ECG, EC, myricetin, theogallin, Kaempferol, theobromine and catechin). The components were identified with flash chromatography using a mobile phase of 0.1% formic acid in water and water + 0.1% formic acid in methanol, and also by UHPLC-QTOF-MS of *C. sinensis* solvent extract. Of the 10 chemical compounds identified, EGCG and caffeine mimicked the growth trajectory of SDS (positive control) by exhibiting dose-dependent anti-acanthamoebic activity inhibiting trophozoite replication within the safe concentration of 3.125µM to 200µM within 72 hours post treatment of *A. castellanii.* Evaluation of the chemical components' anti-encystational capability revealed that EGCG and theobromine possesses anti-encystational and cysticidal properties *in vitro* as each of them were tested individually and also at a 1:1 ratio combination of both components. They exhibited 100% inhibition of *A. castellanii* cyst to trophozoites encystation even at the lowest concentration of 6.25 µM. This work demonstrated that specific *C. sinensis* chemical components possess anti-acanthamoebic activity against trophozoite and cystic forms of *A. castellanii*.

5.2 INTRODUCTION

The treatment of *A. castellanii*-induced diseases using already known anti-acanthamoebic chemical compounds has not given the desired therapeutic outcome of parasite extermination with safe effects on host cells. The most potent FDA-approved anti-acanthamoebic chemical compounds are biguanides (Polyhexamethylene (PHMB) or chlorhexidine gluconate (CHX)), which have also been used alone and in combinations with antibiotics to improve their efficacy (Jones, 1997). Further studies for improved therapeutic outcomes of chemical compounds have employed the use of already existing and known anti-microbial drugs by re-purposing them as anti-acanthamoebics (Yousuf et al., 2016). Even with the use of biguanides and repurposed drugs, the *A. castellanii* cysts, which are largely resistant to safe concentrations of the used drugs, still manage to survive and excyst into infective trophozoites when their efficacy of the used drugs has waned. This knowledge has led to testing of a host of chemicals against both the trophozoite and cystic forms of *A. castellanii.* Acriflavine and proflavine are two among the host of antiseptic agents which have shown some anti-acanthamoebic activity against trophozoites and cysts. They act by disrupting the membrane integrity of the parasite forms (Henriquez, 2009). In another range of chemicals tested, 2,6-dichlorobenzonitrile, which is a herbicide, was shown to have disruptive capabilities to the trophozoite in the cyst differentiation process (encystation), indicative of its ability to inhibit cellulose synthesis required for the encystation process (Moon et al., 2018a). For anti-microbials, the efficacy of gatifloxacin, levofloxacin and gentamicin against *Acanthamoeba* cysts tested *in vitro* showed that these commercially available drugs may be of importance in the mainstream production of anti-acanthamoebic drugs (Thongseesuksai et al., 2019). A chlorhexidine and Na_2EDTA ocular gel combination tested *in vitro* exhibited more anti-acanthamoebic activity than when each was tested individually (Cucina et al., 2019). Among the host of alternative and experimental treatments for acanthamoebiasis, natural products and their bio-active components have also been tested *in vitro* and *in vivo* against *Acanthamoeba* diseases.

C. sinensis contains bioactive phenolic compounds, including polyphenolic flavanols (GTPs), catechins, caffeine and other alkaloids. The four major kinds of catechins present in *C. sinensis* are (−)-epicatechin (EC), (−)-epicatechin-3-gallate (ECG), (−)-epigallocatechin (EGC), and (−)-epigallocatechin-3-gallate(EGCG) (Sanlier et al., 2018; Yang et al., 2019; Katada et al., 2019; Srichairatanakool et al., 2006; Mukhtar and Ahmad, 2000). The primary alkaloid is caffeine, with other alkaloids such as theobromine and theophylline (Perva-Uzunalic et al., 2006; Chacko et al., 2010). *C. sinensis* also contains other polyphenols which are flavanols with their glycosides and theogallin (Graham, 1992). Other constituents of *C. sinensis* are proteins, amino acids such as theanine, carbohydrates, minerals and trace elements, as well as phenolic acids such as gallic acids (Graham, 1992; Chacko et al., 2010). *C. sinensis* also contains the two major classes of polyphenols, flavan-3-ols and flavanols and Quercetin, kaempferol and myricetin are the main flavanols in *C. sinensis* (Sekine et al., 1991; Hilal and Engelhardt, 2009).

Previous sections of this work focused on the use of different forms of *C. sinensis* as anti-acanthamoebic therapies from which the *in vitro* experiments conducted have yielded promising results. In another unrelated study, EGCG tested in combination with *C. sinensis* matcha against *A. castellanii* trophozoites showed they inhibited their growth *in vitro* (Dickson et al., 2020). Apart from these studies, the literature does not show any studies in which *C. sinensis* and/ or its bioactive components were evaluated for anti-acanthamoebic activity. This present section of the study will investigate the anti-acanthamoebic capability of major known *C. sinensis* chemical compounds. It is however importance to note that the activity of the individual bioactive ingredients and also in combinations do not really translate to the actual concentrations of the ingredients in a natural state such as the brews and solvent extract. Also, though not investigated at this stage of the study, one has to bear in that there are many other trace compounds in the brew forms and solvent state which might play a synergistic role to the anti-acanthamoebic activity of *C. sinensis.*

5.3 RESULTS

5.3.1 Identification of chemical ingredients in *C. sinensis* brews by UHPLC-MS

The chromatographic analysis showed that both *C. sinensis* brew forms contain the same number and type of chemical compounds though in slightly different concentrations but with the same mass-to-charge ratio (Table 5.1). UHPLC–QTOF–MS characterisation spectrographs of hot and cold *C. sinensis* identified the peaks of each chemical compounds in the brew forms (Figure 5:1and Figure 5:2)

UHPLC–QTOF–MS characterizations of hot & cold *C. sinensis* brew fractions		
Analyte(s)	**m/z ratio**	**Class of compound**
Caffeine	194.19	Methylxanthine alkaloid (CNS Stimulant)
Epicatechin Gallate (ECG)	442.37	Flavonoid
Epigallocatechin gallate (ECGG)	458.37	Polyphenol
Theogallin	344.27	Polyphenol
Quercetin	302.236	Flavonoid (Antioxidant)
Kaempferol	286.23	Flavonoid (Antioxidant)

Table 5.1: UHPLC–QTOF–MS characterisation of hot and cold *C. sinensis* brew showing the compounds in the samples. m/z: mass-to-charge ratio of the chemical compounds.

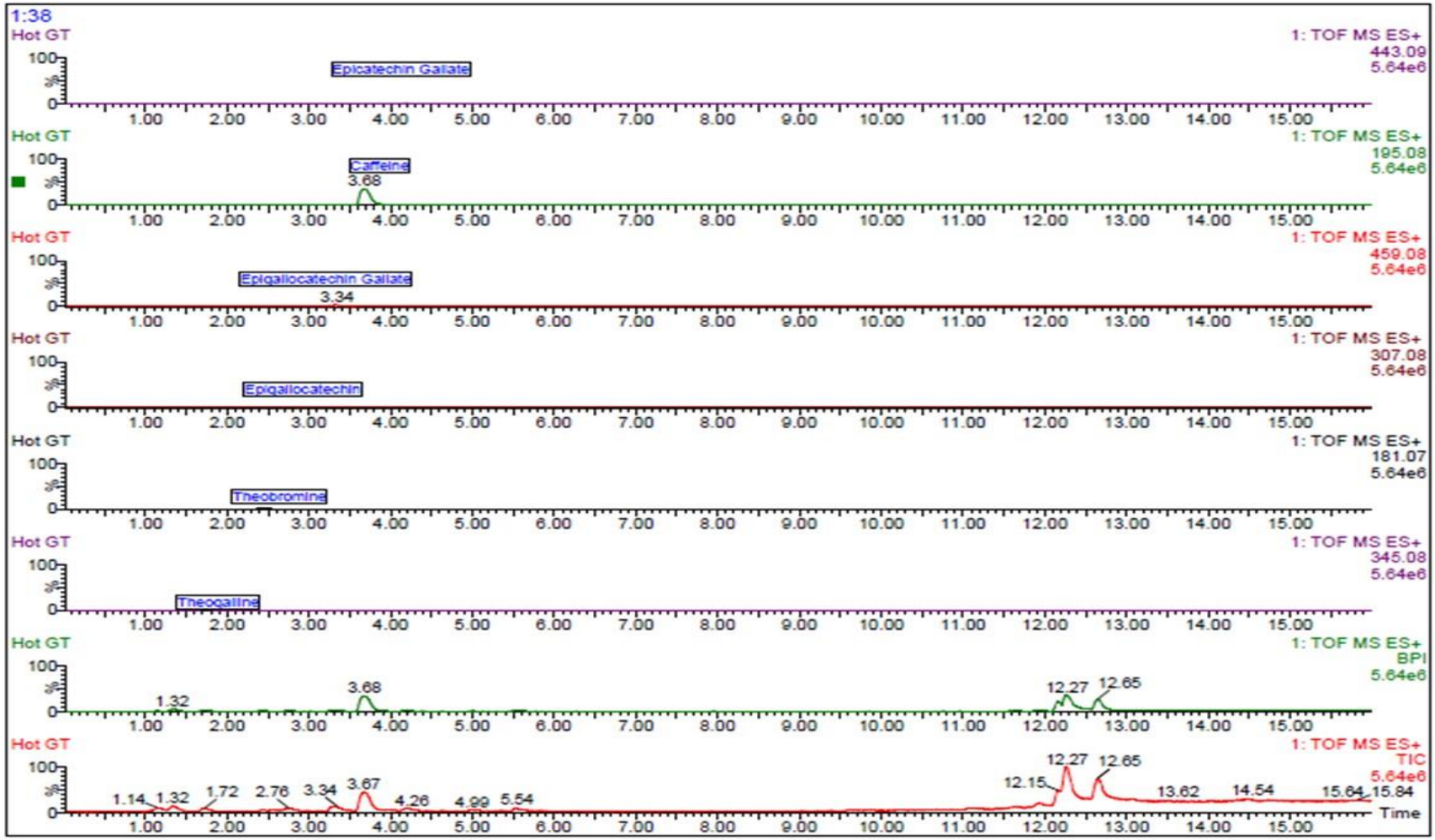

Figure 5:1: UHPLC–QTOF–MS characterisation spectrograph of hot *C. sinensis* brew showing Caffeine, EGCG, EGC, Theogallin, Kaempferol and Quercetin.

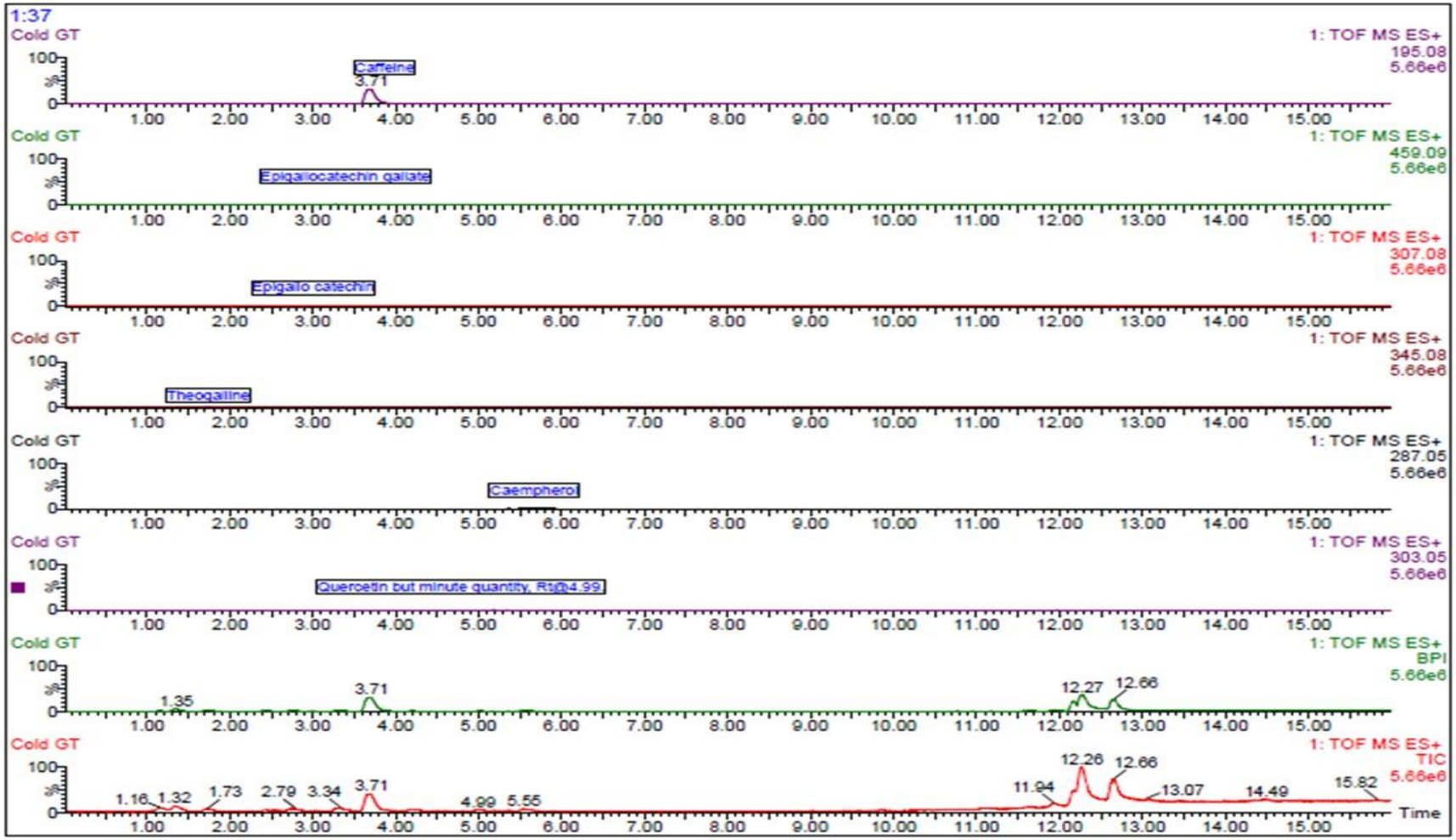

Figure 5:2: UHPLC–QTOF–MS characterisation spectrograph of cold *C. sinensis* brew showing Caffeine, EGCG, EGC, Theogallin, Kaempferol and Quercetin

5.3.2 Flash column chromatography of *C. sinensis* solvent extract

Two mobile phases were employed to identify which produced better results. At the end of the chromatography runs, there were 6 individual fractions collected from the first mobile phase (Figure 5:3), while from the second mobile phase (Figure 5:4), 10 fractions were collected, each fraction represented as peaks at different retention times.

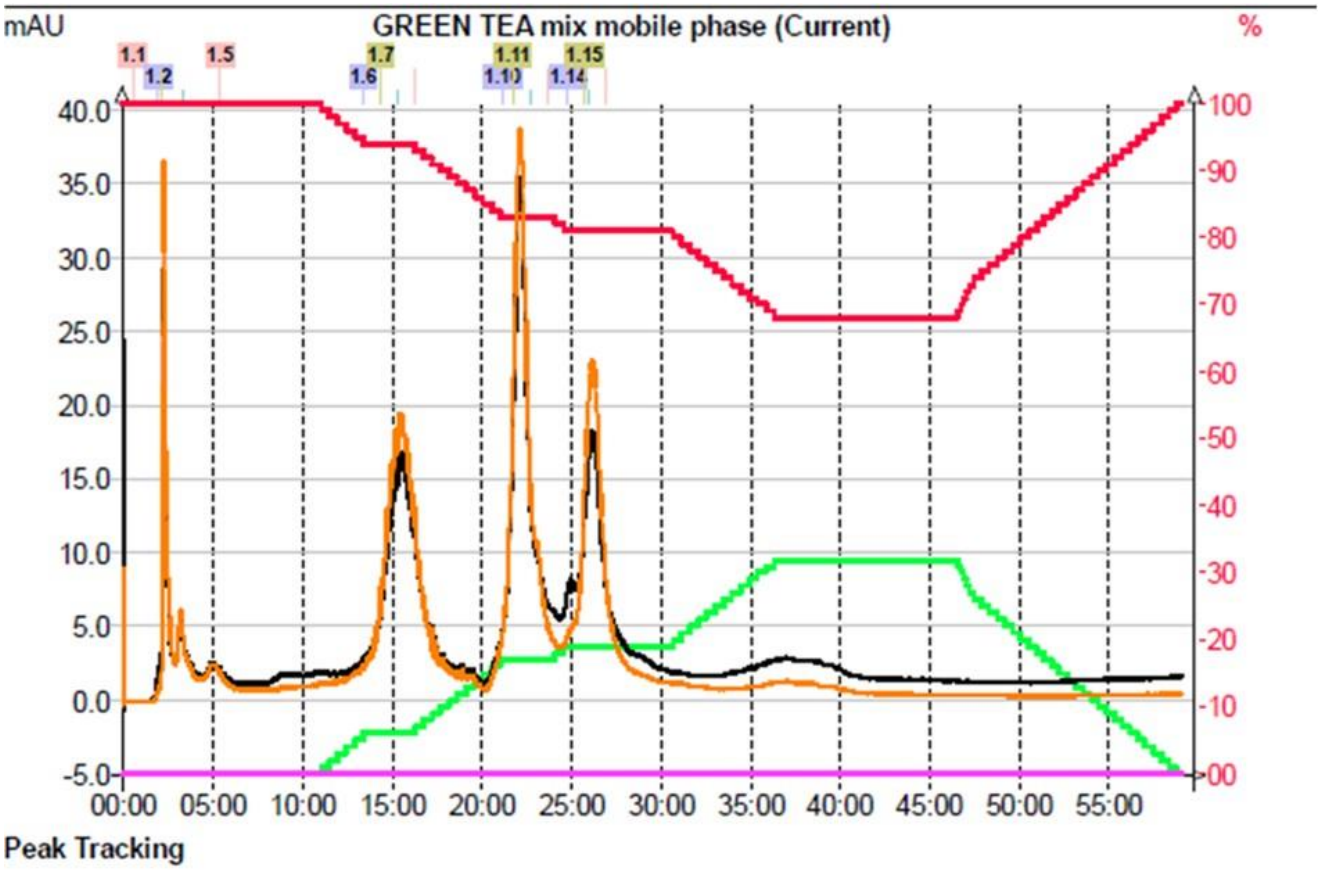

Figure 5:3: Flash column chromatography of *C. sinensis* solvent extract, Mobile phase 1. *C. sinensis* solvent extract Flash chromatograph with mobile phase 0.2 % acetic acid in water + acetonitrile at a 91:9 ratio and water + acetonitrile at a 20:80 ratio showing peaks representative of fractions with possible analytes present in *C. sinensis* solvent extract. Coloured lines: Red = Solvent A, Green = Solvent B, Black = Channel 1 (UV400:SIG1 ⇨ 254 nm), Orange = Channel 2 (UV400:SIG2 ⇨ 278 nm).

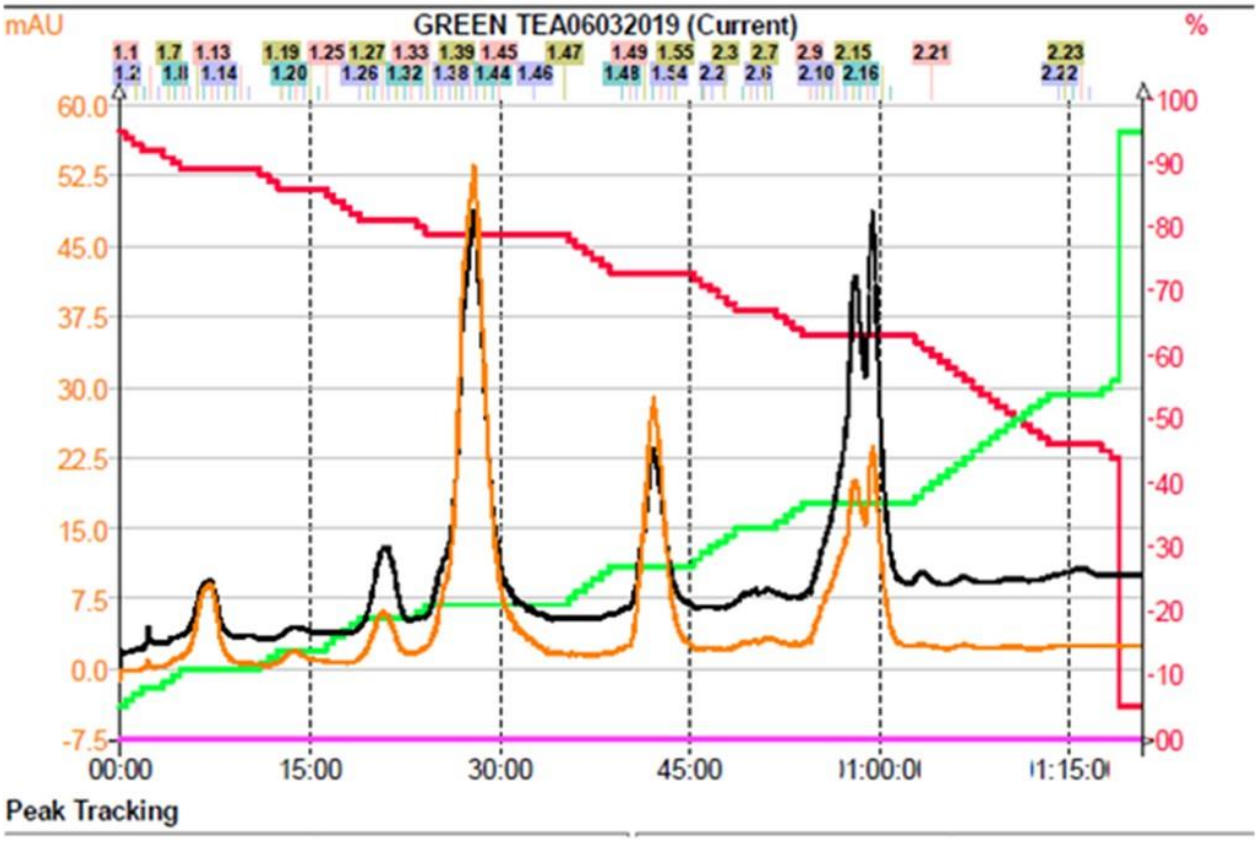

Figure 5:4: Flash column chromatography of C. sinensis Solvent extract, Mobile phase 2. *C. sinensis* solvent extract Flash chromatograph with mobile 0.1% formic acid in water and water + 0.1% formic acid in methanol showing peaks representative of fractions with possible analytes present in *C. sinensis* solvent extract. Coloured lines: Red = Solvent A, Green = Solvent B, Black = Channel 1 (UV400:SIG1 ⇨ 254 nm), Orange = Channel 2 (UV400:SIG2 ⇨ 278 nm).

The chromatograph with mobile phase 2 showed more individual peaks and another peak which showed coelution of two analytes at 1-hour retention time. To identify the analytes in the fractions seen in the chromatographs, samples of the fractions were characterized with HPLC, using Liquid Chromatography-Mass Spectrometry (LC-MS).

5.3.3 Identification of chemical ingredients in *C. sinensis* solvent extract

Ten fractions were separated during the flash column chromatography of *C. sinensis* solvent extract. Fraction 1 did not contain any identifiable components as the molecular weights seen there could not be identified against any database. The 9 remaining fractions showed 10 individual components with the 7th and 8th component showing as a coelution of 2 compounds (Catechin and Epicatechin) in one fraction, thereby making it a total of 10 components in the fractions. The coelution occurred due to similarity in their monomeric isotope mass and molar mass (Table 5.2).

Chemical constituents of *C. sinensis* solvent extract analyzed by UHPLC–QTOF–MS.

Fraction	Analyte(s)	m/z ratio	Class of compound
1	Non-Visible	-	-
2	Theogallin	344.27	Polyphenol
3	Theobromine	180.164	Xanthine Alkaloid
4	Epigallocatechin (EGC)	306.27	Flavonoid (Antioxidant)
5	Caffeine	194.19	Methylxanthine alkaloid (CNS Stimulant)
6	Epicatechin Gallate (ECG)	442.37	Flavonoid
7	Epigallocatechin Gallate (EGCG)	458.37	Polyphenol
8	Catechin/Epicatechin (EC)	290.27	Phenol & Antioxidant
9	myricetin	318.24	Flavonoid (Phenol)
10	Quercetin	302.24	Flavonoid (Polyphenol)

Table 5.2: UHPLC–QTOF–MS characterisation of *C. sinensis* solvent extract flash fractions showing the compounds in each fraction. Fraction 8 shows the coelution of two compounds with the same mass-to-charge ratio, and both are of similar compound class.

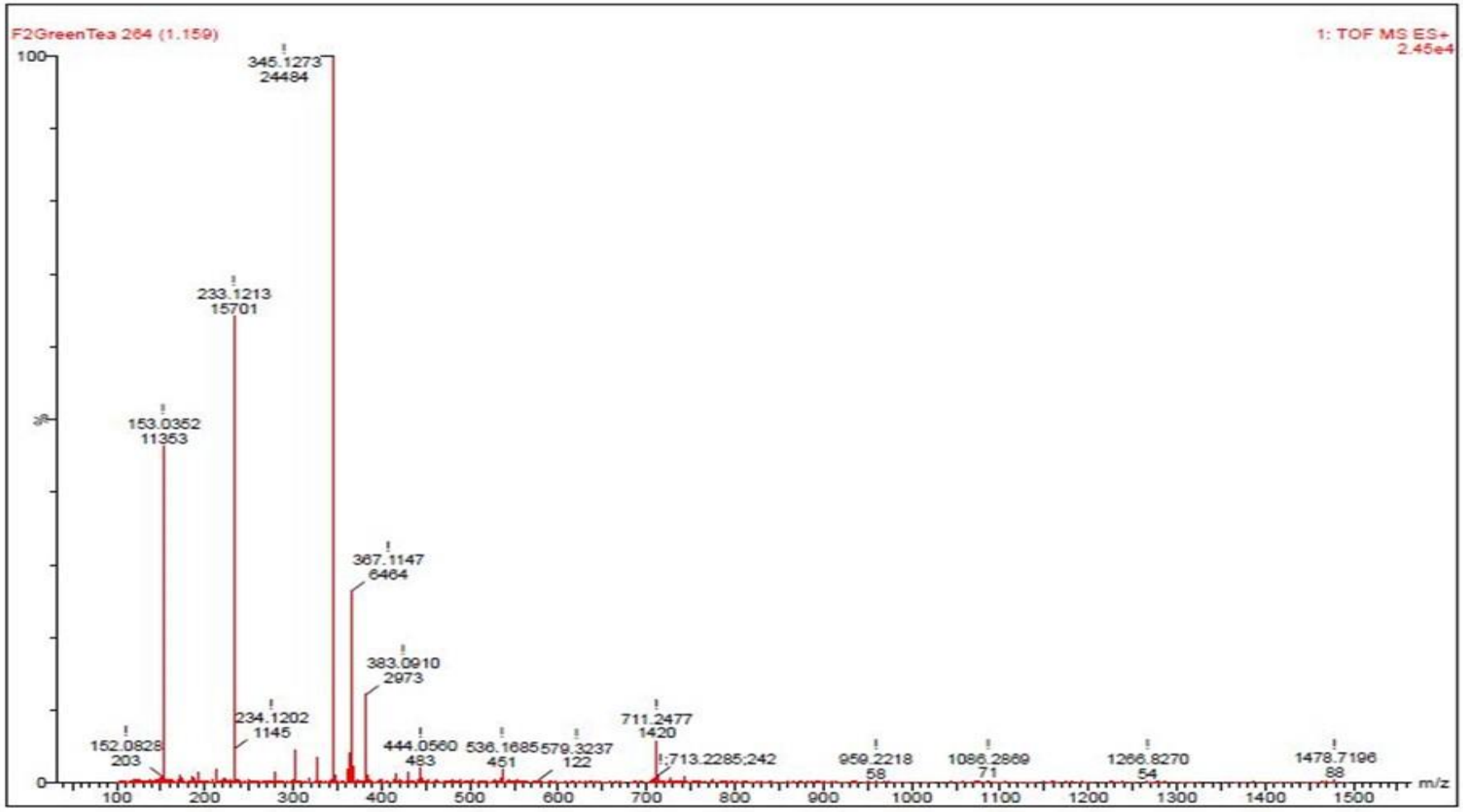

Figure 5:5: LC-MS characterisation spectrograph of *C. sinensis* solvent extract flash fraction showing Theogallin

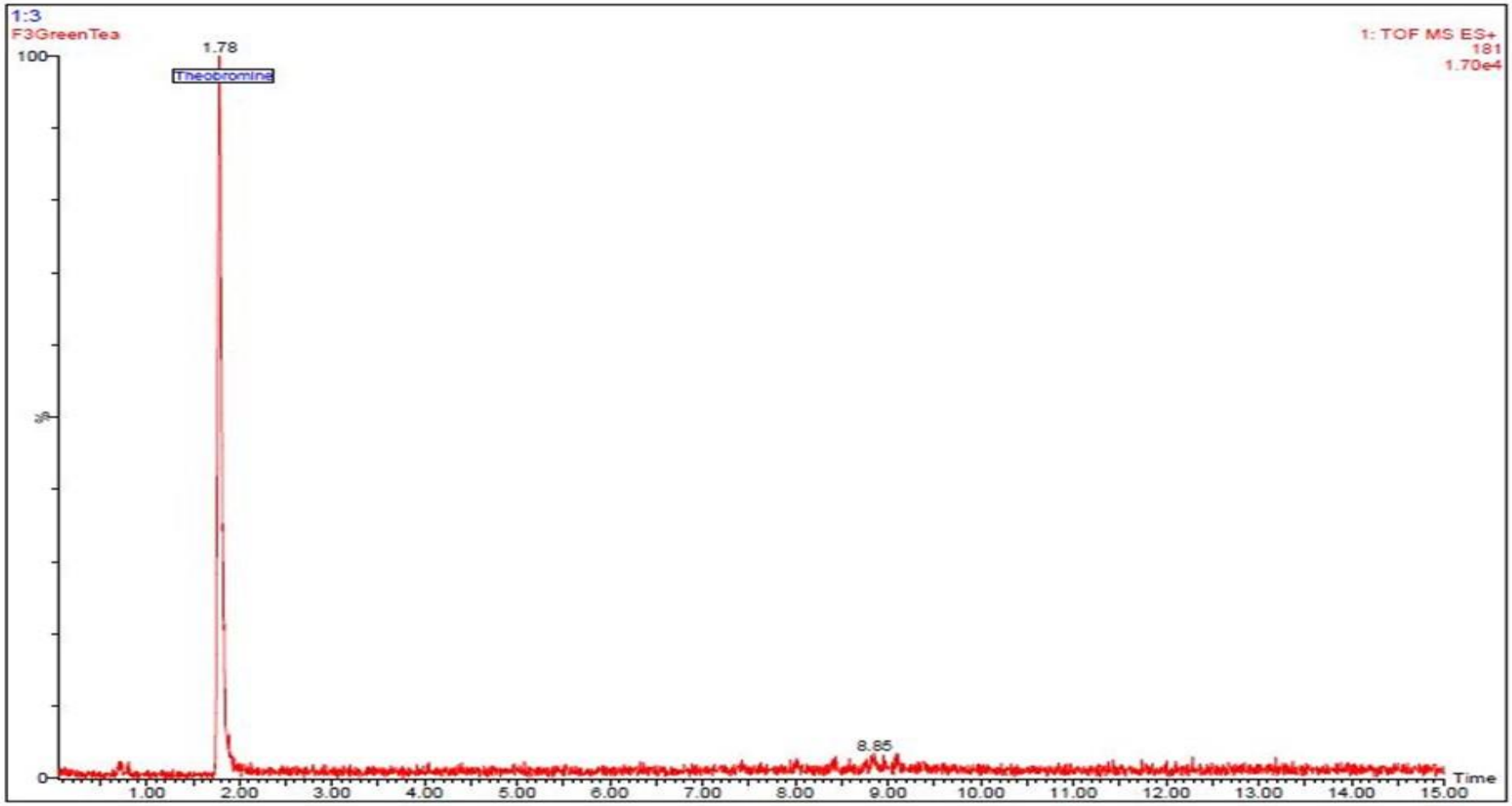

Figure 5:6: LC-MS characterisation spectrograph of *C. sinensis* solvent extract flash fraction showing Theobromine

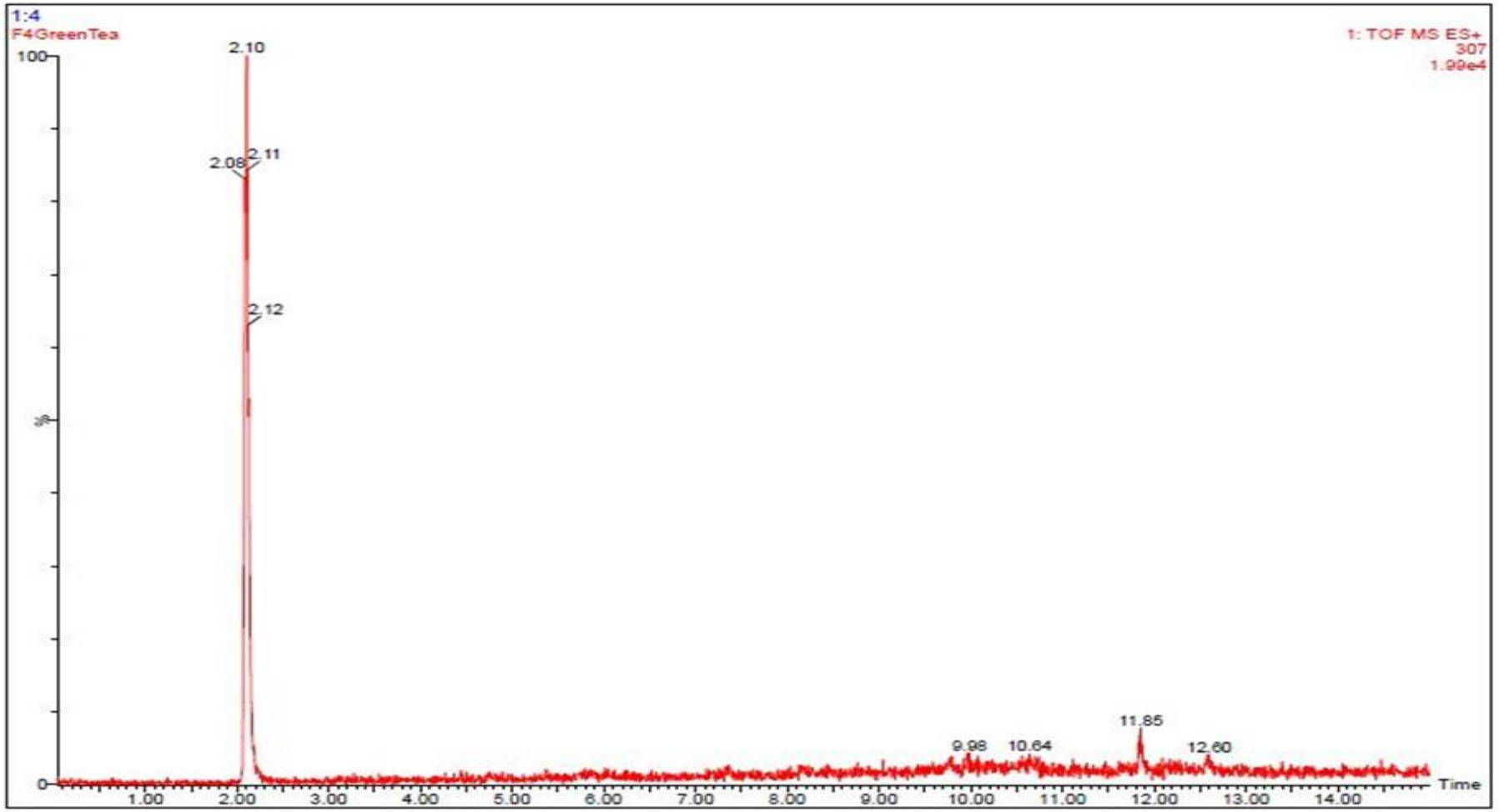

Figure 5:7: LC-MS characterisation spectrograph of *C. sinensis* solvent extract flash fraction showing Epigallocatechin

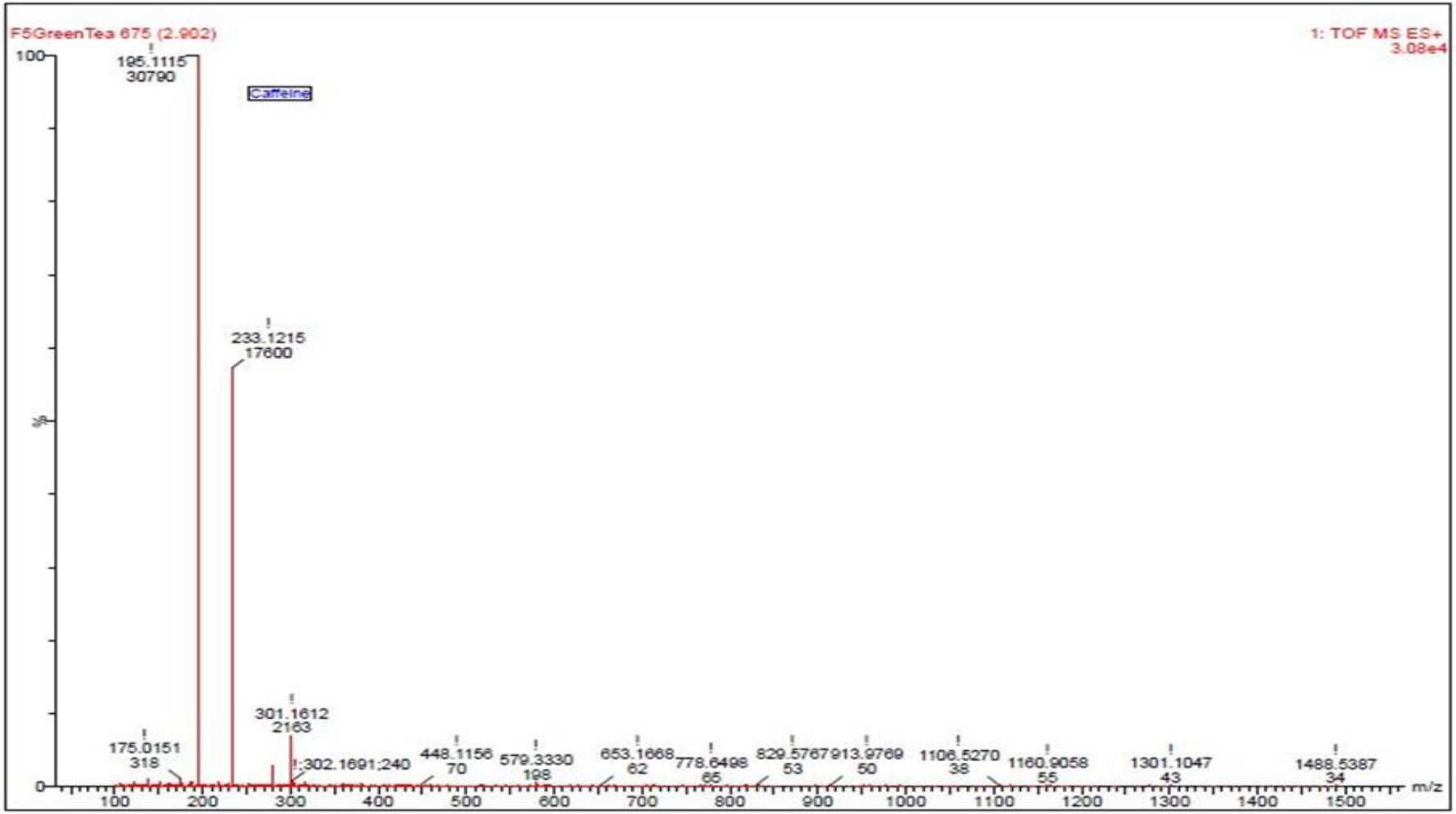

Figure 5:8: LC-MS characterisation spectrograph of *C. sinensis* solvent extract flash fraction showing Caffeine

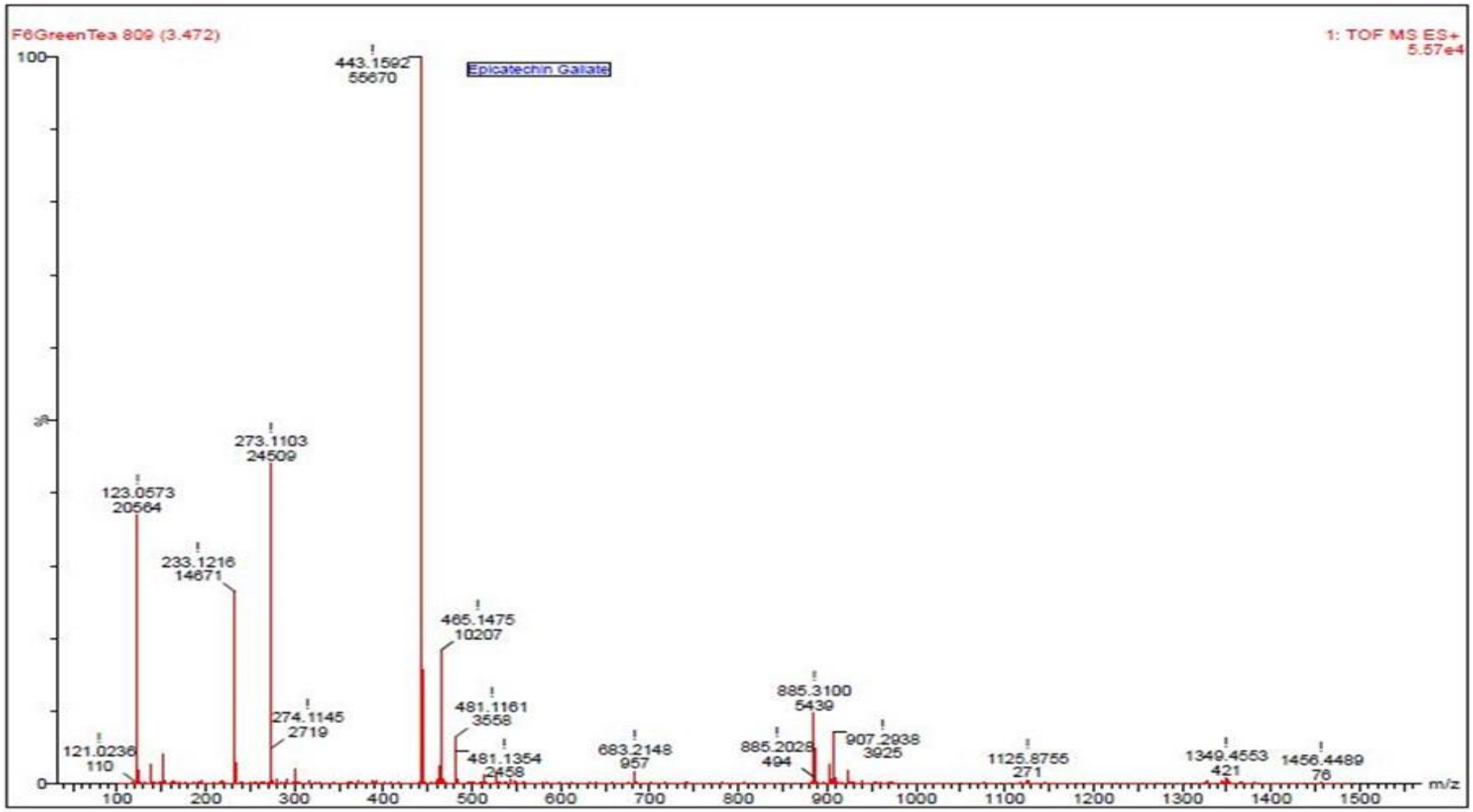

Figure 5:9: LC-MS characterisation spectrograph of *C. sinensis* solvent extract flash fraction showing Epicatechin Gallate

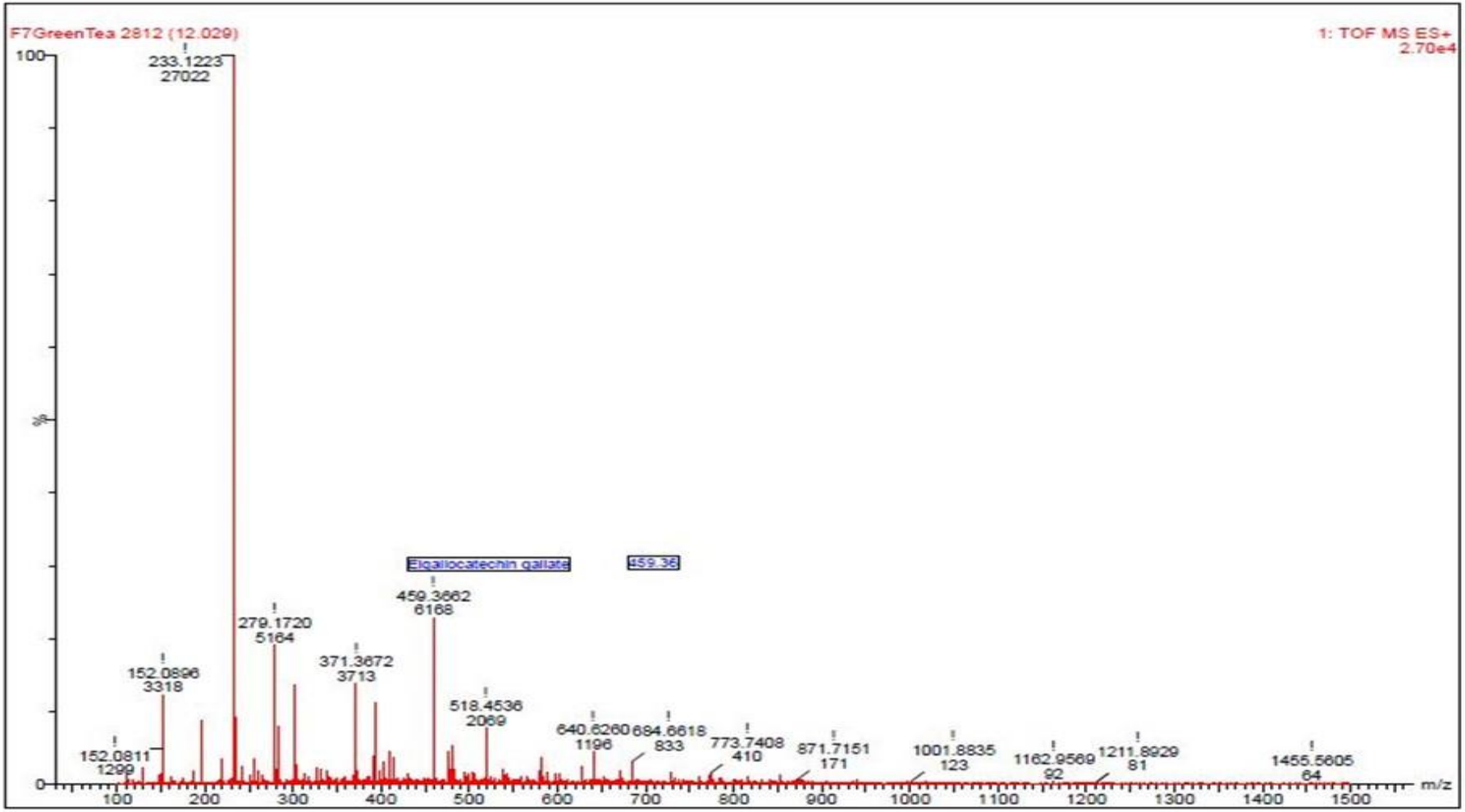

Figure 5:10: LC-MS characterisation spectrograph of *C. sinensis* solvent extract flash fraction showing Epigallocatechin Gallate

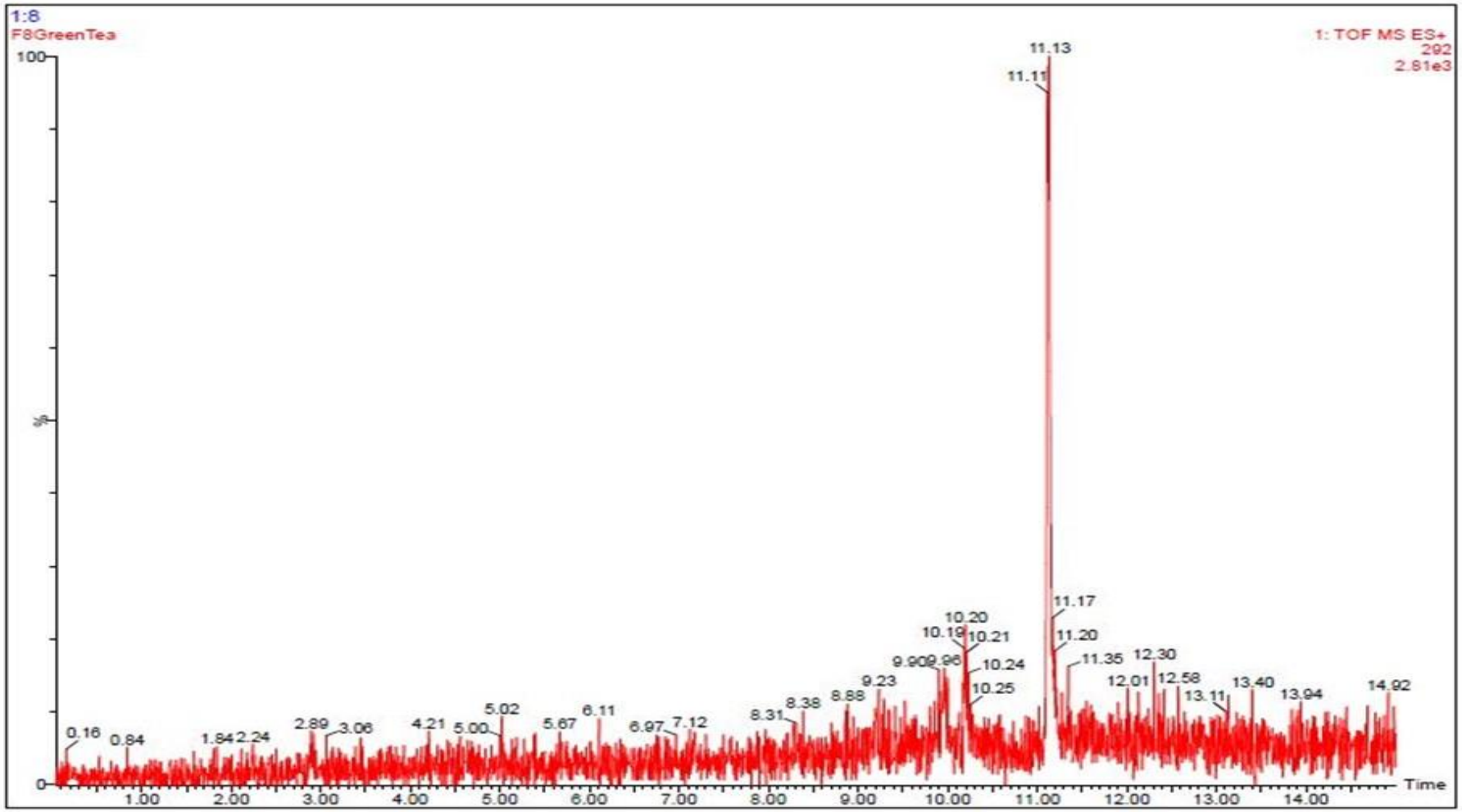

Figure 5:11: LC-MS characterisation spectrograph of *C. sinensis* solvent extract flash fraction showing Catechin and Epicatechin coelution

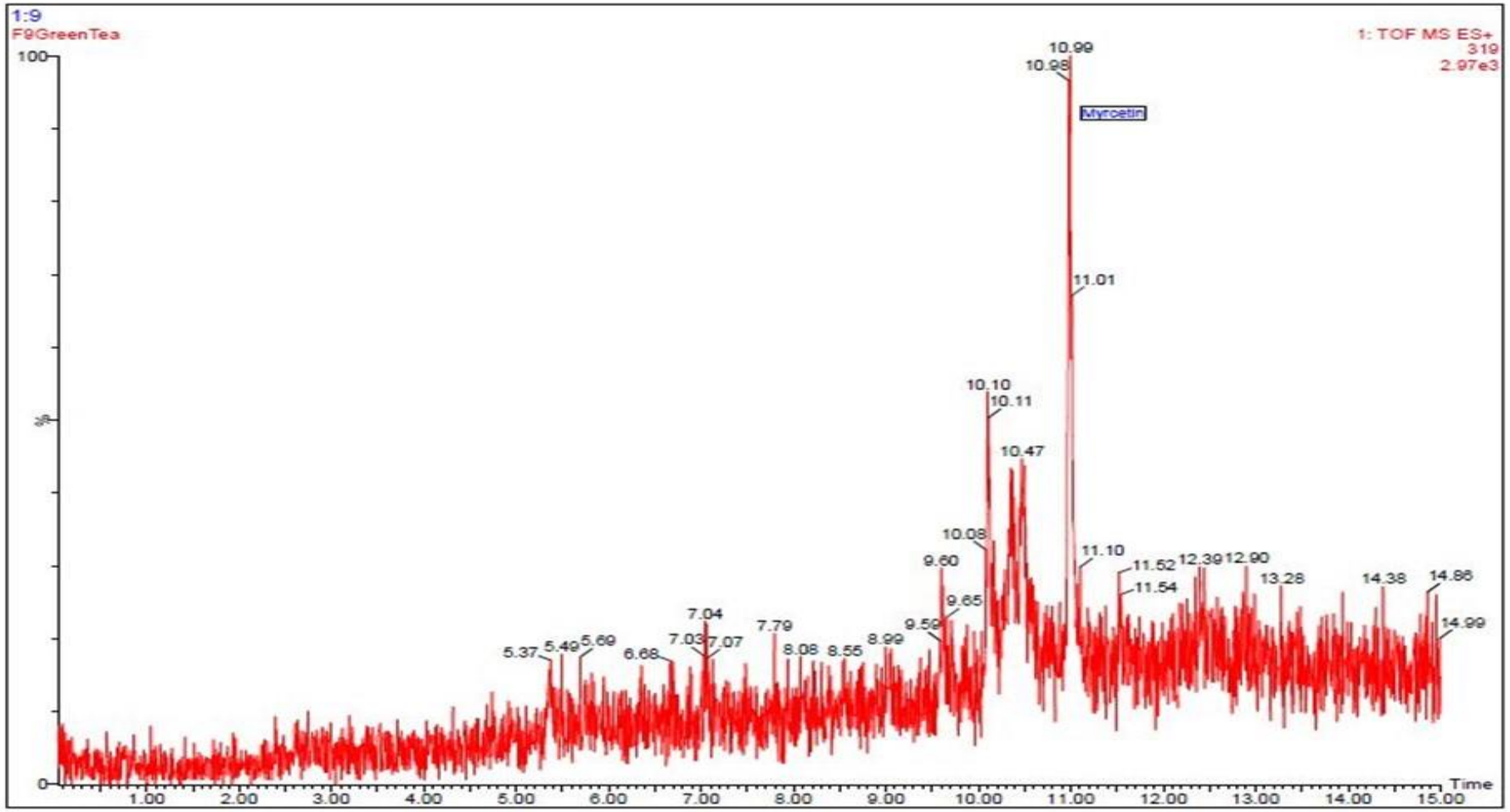

Figure 5:12: LC-MS characterisation spectrograph of *C. sinensis* solvent extract flash fraction showing myricetin

5.3.4 Inhibitory effects of *C. sinensis* chemical standards on trophozoites

After testing for the trophocidal and cysticidal capabilities of *C. sinensis* brews and *C. sinensis* solvent extract, a characterization of both test forms warranted the testing of the active fractions seen in the UHPLC–QTOF–MS analysis of both *C. sinensis* forms. The growth inhibitory effect of each *C. sinensis* industrial standards as indicated by the UHPLC–QTOF–MS analysis of solvent extract (Table 5.2) was tested against *A. castellanii* trophozoites. The *C. sinensis* solvent extract UHPLC–QTOF–MS analysis list of chemical ingredients was chosen as it had all the active chemical ingredients seen in the brew forms (Table 5.1) and more when compared with the brew forms of *C. sinensis*. Results from the trophocidal evaluation of all the industrial standards revealed EGCG and caffeine as the only components with noteworthy anti-acanthamoebic capability, while the remaining catechins and components did not exhibit any notable anti-acanthamoebic capability. As such, the results of EGCG and caffeine were described individually and that of the rest of the components grouped together.

5.3.4.1 EGCG

For EGCG, the two-way RM ANOVA revealed a significant main effect of time ($F(2, 4) = 36.64$, $p = 0.0027$), treatment ($F(8, 16) = 36.29$, $p < 0.0001$), and time x treatment interaction ($F(16, 32) = 6.880$, $p < 0.0001$). At 24 h post- treatment, post hoc comparisons showed that all concentrations of EGCG show significantly decreased absorbance, compared to the -ve control ($p < 0.05$), the +ve also showed less absorbance from the reading. Comparisons between the positive control and the EGCG concentrations showed no significant difference in their trophozoite quantity ($p > 0.05$). At 48 h post-treatment, comparisons between the negative control and the EGCG concentrations showed significant decrease in trophozoite replication for the EGCG concentrations represented by the decreased OD when compared to the negative control ($p < 0.01$). This trend persisted till the termination of the experiment (72 h). Comparisons between the positive control and the EGCG concentrations showed significant decrease of trophozoite number for the 25µM and 50µM concentrations between

48 h to 72 h, however, there a significant increase the OD when these concentrations were compared to the positive control ($p < 0.01$). Comparisons of the positive control and the 100µM and 200µM concentrations showed no significant difference between the control and concentrations ($p > 0.05$), this was witnessed at 24, 48 and 72 h where the experiment was terminated. The lesser concentrations of 3.125 µM, 6.25 µM and 12.5 µM showed continuous trophozoite growth though at a lesser rate than the negative control treatment with significant increase for the negative treatment group ($p < 0.01$) (Figure 5:13).

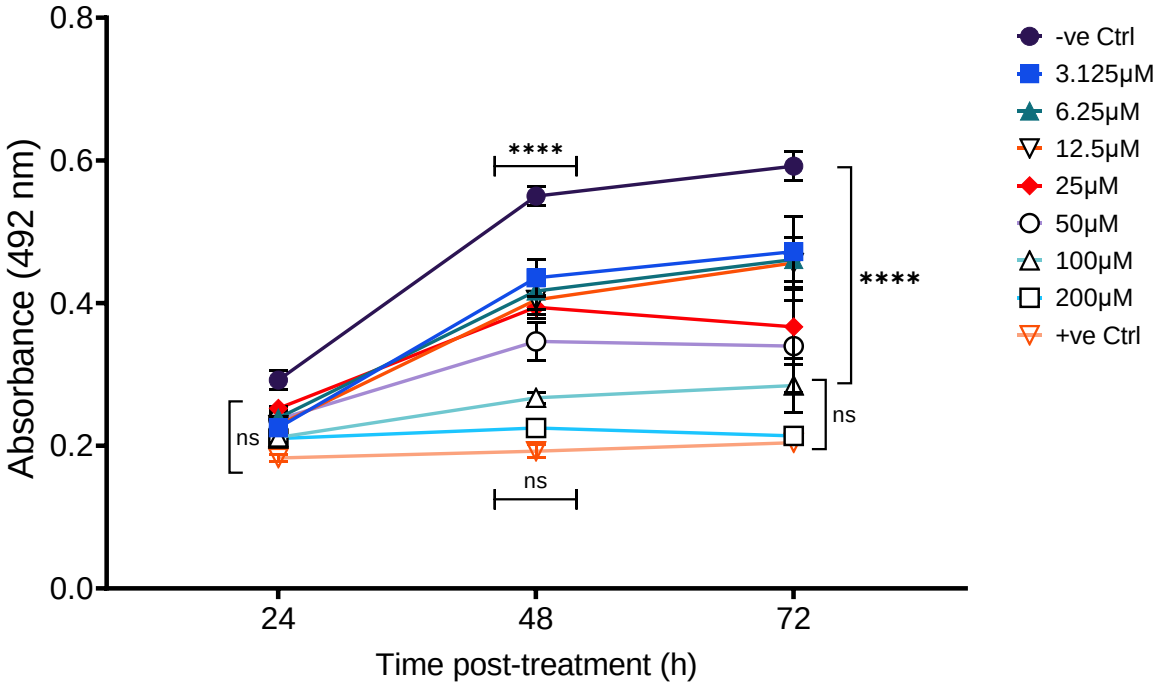

Figure 5:13: Growth inhibitory effect of EGCG, on *A. castellanii* trophozoites at 24, 48, and 72h post treatment at concentrations of 3.125µM, 6.25µM, 12.5µM, 25µM, 50µM, 100µM and 200µM. At 24 h, there was significant increase between trophozoite growth of the negative control and all the EGCG concentrations. The significant increase witnessed at 24 was also observed for all the subsequent time points. At 48 h post exposure the positive control showed significant decrease compared of 3.125µM, 6.25µM, 12.5µM, 25µM and 50µM with no significant difference between the positive control and 100µM - 200µM EGCG concentrations, this was also observed at 72 h (**** *p ≤ 0.0001, ns: non-significant*).

5.3.4.2 Caffeine

For caffeine, the two-way RM ANOVA revealed a significant main effect of time ($F(2, 6) = 5.154$, $p = 0.0498$, treatment ($F(8, 24) = 18.57$, $p < 0.0001$), and time x treatment interaction ($F(16, 48) = 4.810$, $p < 0.0001$). At 24 h post- treatment, post hoc comparisons of treatment groups with both controls (negative control, positive control (SDS 3%)) showed that only the negative control group exhibited any form of significant trophozoite growth ($p < 0.05$), while all the treatment groups showed no trophozoite growth with no significant increase in their trophozoite quantity when compared to the control group ($p > 0.05$). As seen with EGCG, the trend seen in 24 h however was not sustained for the 48 h post-treatment comparisons as all the concentrations showed growth of trophozoites though with significance decrease in growth ($p < 0.0001$) compared to the negative control growth rate. Comparisons between the positive control and the caffeine concentrations showed no significant difference between the trophozoite quantity of the 100µM and 200µM concentrations and the positive control ($p > 0.05$) at 24 h and 72 h. However, at 48 h, there was significant decrease of OD between the positive control and all the caffeine concentrations ($p < 0.01$). Comparisons with the lesser concentrations showed significant decrease in trophozoite growth between the positive control and those concentrations ($p < 0.0001$). Interestingly, between 48 h and 72 h, all the treatment concentrations with the exception of 3.125µM and 6.25µM exhibited halt of and decline of trophozoite growth with the 100µM and 200µM concentrations continuing to mirror the effect of positive control where post-treatment evaluation showed complete elimination of *A. castellanii* trophozoites with no statistical difference between the high controls and SDS ($p > 0.05$) (Figure 5:14). The lower concentrations with the exception of 3.125µM and 6.25µM still decreased the trophozoite growth but there was still statistical increase in their trophozoite number when compared to the positive control ($p < 0.0001$).

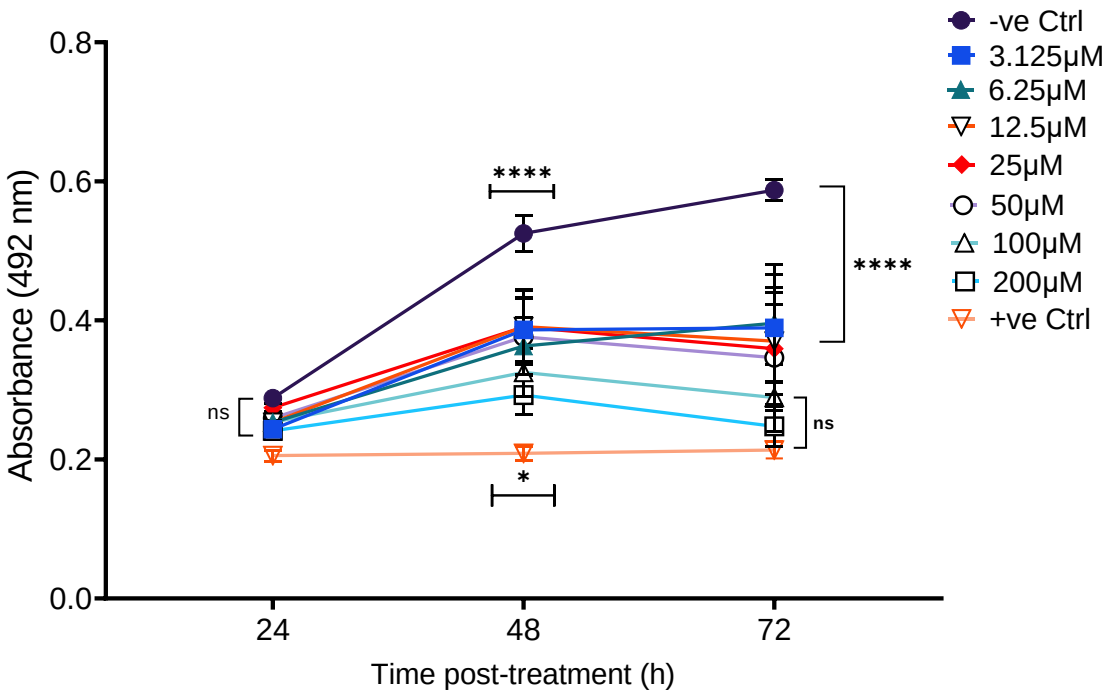

Figure 5:14: Growth inhibitory effect of Caffeine on *A. castellanii* at 24, 48, and 72h post treatment concentrations of 3.125µM, 6.25µM, 12.5µM, 25µM, 50µM, 100µM and 200µM. At 24 h, there was no significant difference between the negative control and the caffeine concentrations. At 48- and 72-hours post exposure the negative control showed significant increase in trophozoite proliferation, while all the treatment concentrations of caffeine allowed proliferation of trophozoites at 48. Post exposure showed that at 72 hours the concentrations except 3.125µM & 6.25µM showed inhibition of growth by reduction of the OD recorded for each concentration, but none were significantly significant with the SDS. At 72 hours, the 100µM and 200µM treatment groups showed no significant difference with the positive control (SDS) which indicated that both groups successfully inhibited trophozoite replication and growth. (**** $p \leq 0.0001$, ns: non-significant).

5.3.4.3 ECG, EGC, EC, and Catechin

For the other catechins, the two-way RM ANOVA of ECG revealed a significant main effect of time ($F(2, 6) = 104.6$, $p < 0.0001$, treatment ($F(8, 24) = 91.71$, $p < 0.0001$), and time x treatment interaction ($F(16, 48) = 11.86$, $p < 0.0001$). Post hoc comparisons of ECG treatment groups with both controls (negative control, positive control (SDS 3%)) showed that although there was continuous significance increase ($p < 0.0001$) between the OD of the negative control group and the ECG concentrations, the concentrations all exhibited little or no form of inhibition to the trophozoite growth from 24 h to 72 h (Figure 5:15A). The notable inhibition to trophozoite growth seen with ECG was with a selective range of low concentrations of

3.125µM, 6.25µM and 12.5µM. Although these concentrations did not destroy the trophozoites, they interestingly inhibited the trophozoite replication in sort of suspended animation resulting neither in the replication of the trophozoites or their depletion which was visualized by the OD recorded for the concentrations (Figure 5:15A). Statistical comparisons with the positive control showed that all ECG catechin concentrations exhibited significant increase in OD compared to the positive control ($p < 0.0001$).

For EGC anti-acanthamoebic evaluations, the two-way RM ANOVA revealed a significant main effect of time ($F (2, 6) = 152$, $p = 0.0002$, treatment ($F (8, 16) = 158.1$, $p < 0.0001$), and time x treatment interaction ($F (16, 32) = 63.21$, $p < 0.0001$). Post hoc comparisons of EGC treatment groups with both controls (negative control, positive control (SDS 3%)) showed that although there was continuous significance increase ($p < 0.0001$) between the OD of the negative control group and the EGC concentrations, the concentrations all exhibited little or no form of inhibition to the trophozoite growth from 24 h to 72 h (Figure 5:15B). Statistical comparisons with the positive control showed that all the EGC concentrations exhibited significant increase in OD compared to the positive control ($p < 0.0001$).

For EC anti-acanthamoebic evaluations, the two-way RM ANOVA revealed a significant main effect of time ($F (2, 6) = 40.45$, $p = 0.0003$, treatment ($F (8, 24) = 54.61$, $p < 0.0001$), and time x treatment interaction ($F (16, 48) = 22.95$, $p < 0.0001$). Post hoc comparisons of EC treatment groups with both controls (negative control, positive control (SDS 3%)) showed that although there was continuous significance increase ($p < 0.0001$) between the OD of the negative control group and the EC concentrations, the concentrations all exhibited little or no form of inhibition to the trophozoite growth from 24 h to 72 h (Figure 5:15C). Statistical comparisons with the positive control showed that all the EC concentrations exhibited significant increase in OD compared to the positive control ($p < 0.0001$).

For catechin anti-acanthamoebic evaluations, the two-way RM ANOVA revealed a significant main effect of time ($F(2, 4) = 14.65$, $p = 0.0144$, treatment ($F(8, 16) = 46.69$, $p < 0.0001$), and time x treatment interaction ($F(16, 32) = 8.277$, $p < 0.0001$). Post hoc comparisons of catechin treatment groups with both controls (negative control, positive control (SDS 3%)) showed that although there was continuous significance increase ($p < 0.0001$) between the OD of the negative control group and the catechin concentrations, the concentrations all exhibited little or no form of inhibition to the trophozoite growth from 24 h to 72 h (Figure 5:15D). Statistical comparisons with the positive control showed that all the catechin concentrations exhibited significant increase in OD compared to the positive control ($p < 0.0001$).

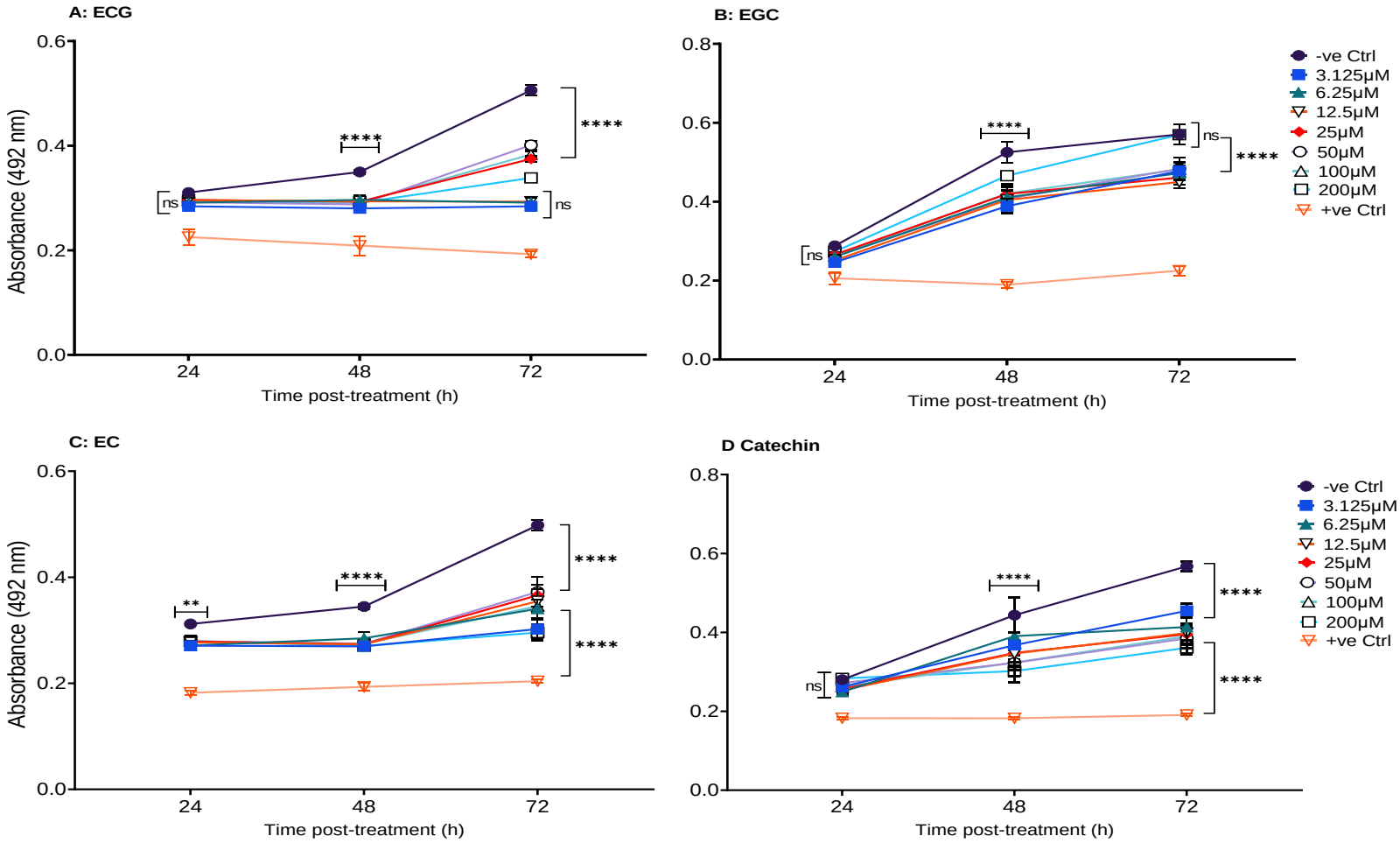

Figure 5:15: Growth inhibitory effect of catechins (A: ECG, B: EGC, C: EC, D: Catechin) on *A. castellanii* at 24, 48, and 72h post treatment concentrations of 3.125µM, 6.25µM, 12.5µM, 25µM, 50µM, 100µM and 200µM. All treatment groups showed significant decrease in OD between them and the negative control (PGY) and also between them and the positive control (SDS) at 48- and 72-hours post exposure. ECG & EC inhibited trophozoite replication and viability at 48 hours post treatment but were not able to sustain the effect and also could not match the anti-acanthamoebic/ growth inhibitory capability of SDS. (**** $p \leq 0.0001$, ns: non-significant)

5.3.4.4 Theobromine, Myricetin, Theogallin, Kaempferol

For the remaining *C. sinensis* chemical standards, the two-way RM ANOVA of theobromine revealed a significant main effect of time ($F(2, 6) = 952.2$, $p < 0.0001$, treatment ($F(8, 24) = 223.7$, $p < 0.0001$), and time x treatment interaction ($F(16, 48) = 52.50$, $p < 0.0001$). Post hoc comparisons of the theobromine treatment groups with both controls (negative control, positive control (SDS 3%)) showed that although there was interchangeable continuous significance increases of OD between the negative control group and the theobromine concentrations ($p < 0.0001$), Just like the 4 catechins previously tested (EGC, ECG, EC, Catechin), theobromine exhibited no inhibition to the trophozoite growth from 24 h to 72 h post treatment. There was equally significant decrease of OD ($p < 0.0001$) between the positive control and the theobromine concentrations (Figure 5:16 A).

For myricetin anti-acanthamoebic evaluations, the two-way RM ANOVA revealed a significant main effect of time ($F(2, 6) = 2224$, $p = 0.0002$, treatment ($F(8, 24) = 348.7$, $p < 0.0001$), and time x treatment interaction ($F(16, 48) = 32.99$, $p < 0.0001$). Post hoc comparisons of the myricetin treatment groups with both controls (negative control, positive control (SDS 3%)) also showed that although there was interchangeable continuous significance increases of OD between the negative control group and the myricetin concentrations ($p < 0.0001$), Just like the 4 catechins previously tested (EGC, ECG, EC, Catechin), myricetin exhibited no inhibition to the trophozoite growth from 24 h to 72 h post treatment. There was equally significant decrease of OD ($p < 0.0001$) between the positive control and the myricetin concentrations (Figure 5:16 B).

For theogallin, the two-way RM ANOVA revealed a significant main effect of time ($F(2, 6) = 20.47$, $p = 0.0021$, treatment ($F(8, 24) = 111.9$, $p < 0.0001$), and time x treatment interaction ($F(16, 48) = 15.86$, $p < 0.0001$). Post hoc comparisons of the theogallin treatment groups with both controls (negative control, positive control (SDS 3%)) also showed that although there was interchangeable continuous significance increases of OD between the negative control group and the theogallin concentrations ($p < 0.0001$), Just like the 4 catechins previously

tested (EGC, ECG, EC, Catechin), theogallin exhibited no inhibition to the trophozoite growth from 24 h to 72 h post treatment. There was equally significant decrease of OD ($p < 0.0001$) between the positive control and the theogallin concentrations (Figure 5:16 C).

For kaempferol, the two-way RM ANOVA revealed a significant main effect of time ($F (2, 6) = 90.28$, $p < 0.0001$, treatment ($F (8, 24) = 97.90$, $p < 0.0001$), and time x treatment interaction ($F (16, 48) = 46.7$, $p < 0.0001$). Post hoc comparisons of the analyzed treatment groups with both controls (negative control, positive control (SDS 3%)) showed that although there was interchangeable continuous significance increases of OD between the negative control group and the tested chemicals standards of *C. sinensis* ($p < 0.0001$). Just like the 4 catechins previously tested (EGC, ECG, EC, Catechin), kaempferol all exhibited no inhibition to the trophozoite growth from 24 h to 72 h post treatment. There was equally significant decrease of OD ($p < 0.0001$) between the positive control and the kaempferol concentrations (Figure 5:16 D).

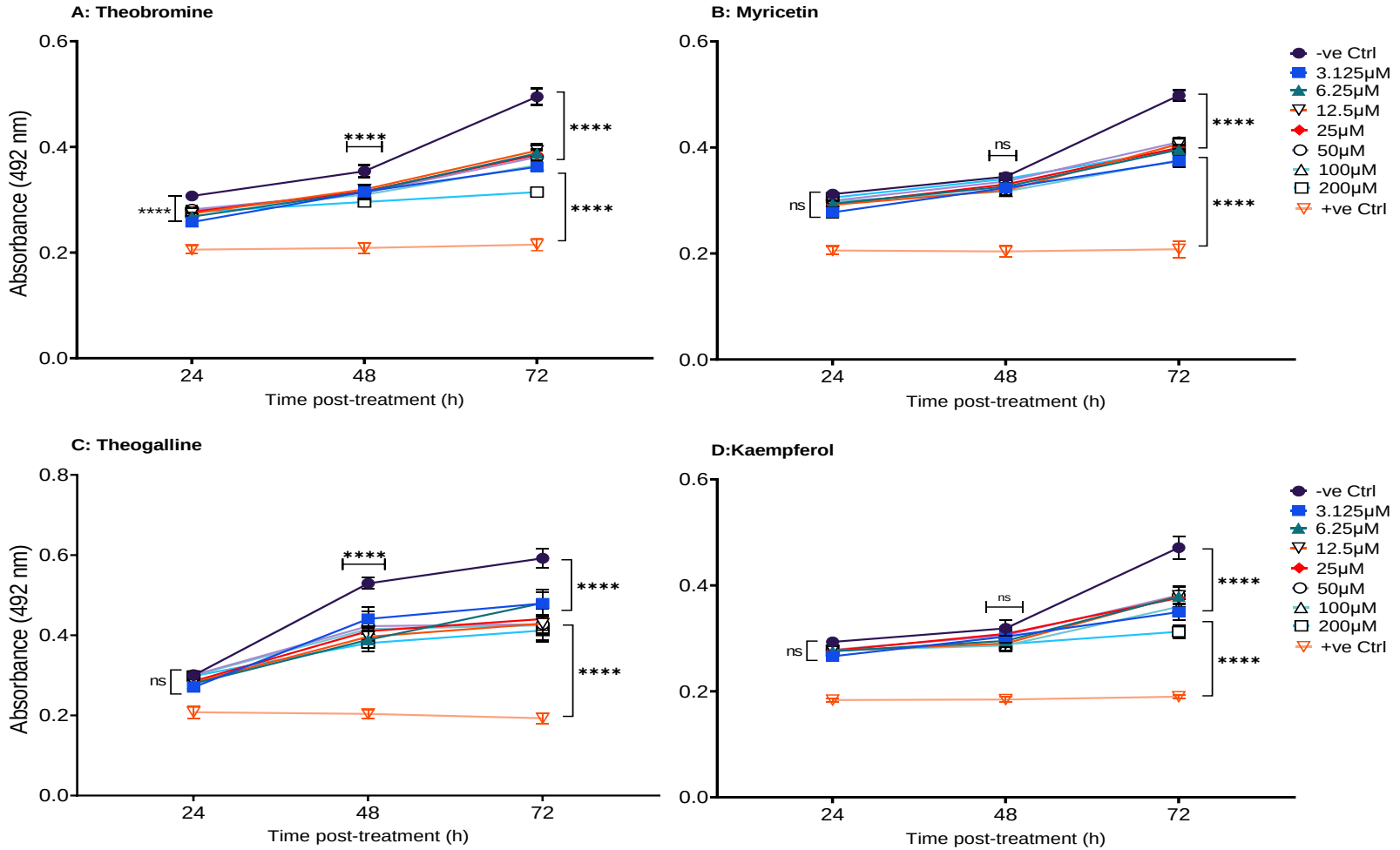

Figure 5:16: Growth inhibitory effect of Theobromine(A), Myricetin(B), Theogallin(C), Kaempferol(D) on *A. castellanii* at 24, 48, and 72h post treatment concentrations of 3.125µM, 6.25µM, 12.5µM, 25µM, 50µM, 100µM and 200µM. All treatment groups showed significant increase in OD between them and the positive control (SDS) from 24 - 72 h post exposure. The industrial standards did not exhibit any sustained anti-acanthamoebic/ growth inhibitory capability from for the duration of the experiment (72 h) (**** $p \leq 0.0001$, ns: non-significant).

From the testing of all the chemical standards, EGCG and caffeine were the only *C. sinensis* chemical standards that were able to inhibit trophozoite replication within the safe concentration of 3.125µM to 200µM with no significant difference with the efficacy exhibited by the positive control (SDS). It is also noteworthy that the trophocidal activity witnessed was expressed as early as 24 h post treatment for EGCG, while there was also noteworthy trophocidal activity for caffeine at 72 h after the 48-h treatment had exhibited significant difference between caffeine's OD and the positive control.

An analysis of all tested *C. sinensis* chemical standards combined together was done. A two-way RM ANOVA revealed a significant main effect of time ($F(2, 8) = 420$, $p < 0.0001$, treatment ($F(8, 32) = 99.29$, $p < 0.0001$), and time x treatment interaction ($F(16, 48) = 12.47$, $p < 0.0001$). Post hoc comparisons showed that despite the individually ranged efficacies of EGCG and caffeine, there was no form of activity as the complement exhibited no inhibition to trophozoite growth from 24 h to 72 h post treatment to all the complement doses (3.125µM to 200µM) of C. *sinensis* chemical standards (Figure 5:17).

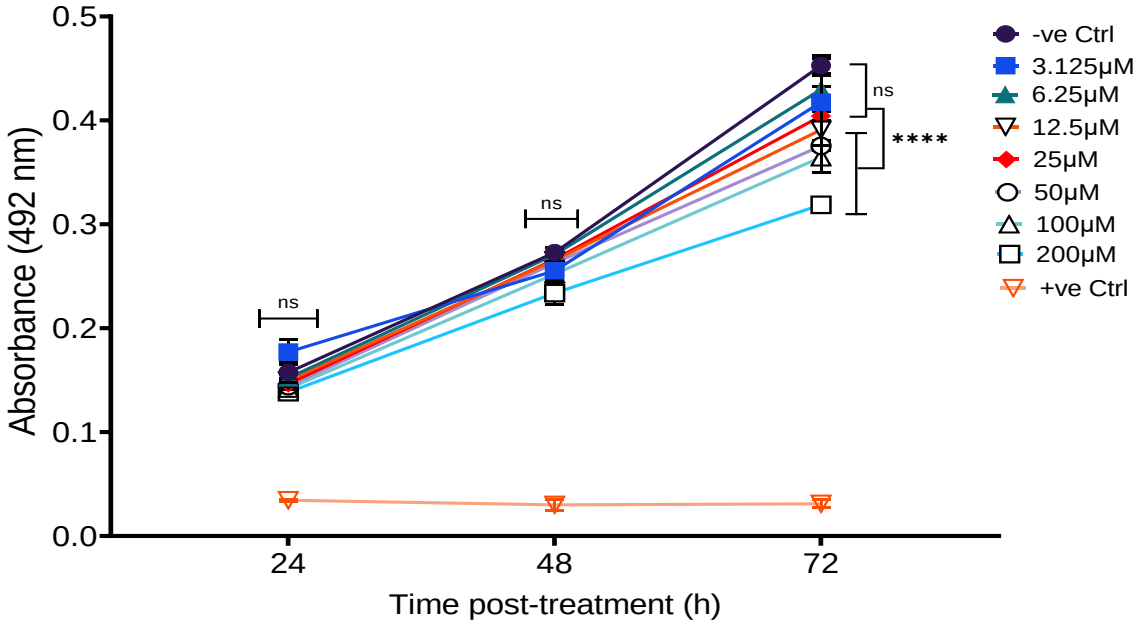

Figure 5:17: Growth inhibitory effect of *C. sinensis* chemical standards of all the earlier tested chemicals combined in equal volume to form a full complement. The complement is made up of EGCG, ECG, EGC, EC, Catechin, Caffeine, Theobromine, Myricetin, Theogallin, Kaempferol. At 24 h and 48 h, all treatment concentrations showed no significant difference

between them and the negative control. At 72 h, 12.5µM, 50µM, 100µM and 200µM concentrations showed significant difference their activity and negative control. Despite the differences seen for the later concentrations, the industrial standards combination did not exhibit any noteworthy anti-acanthamoebic/ growth inhibitory capability. For the duration of the experiment with significant difference between the treatment concentrations and the positive control (**** $p \leq 0.0001$, ns: non-significant).

5.3.5 Effects of *C. sinensis* chemical standards on trophozoite encystation

In this experiment, the cysticidal and anti-encystation ability of *C. sinensis* chemical standards on *A. castellanii* cysts was tested. To achieve this objective, hyperosmotic solutions of 2 *C. sinensis* chemical standards were chosen. From previous experiments in chapters 2, 3 and 4, *C. sinensis* concentrations that inhibited trophozoite growth/ replication were seen to also inhibit encystation. Therefore, it was presumed that either EGCG or caffeine might also inhibit encystation as they were able to inhibit trophozoite growth. To ascertain if there was a difference in the range of chemical standards, a random choice of chemical with low trophocidal activity was made to establish if those low trophocidal chemicals also did not possess anti-encystational capability. EGCG was chosen from the high-performance band and theobromine from the low-performance band. While determining the encystation inhibitory effect of *C. sinensis* industrial standards concentrations on *A. castellanii* cysts.

For EGCG, one-way ANOVA revealed a significant main effect of EGCG concentrations ($F(5, 12) = 3606$, $p < 0.0001$). Post hoc comparison between the positive control and the EGCG concentrations revealed no significant difference between the positive control and the concentrations as all of them exhibited 100% inhibition to *A. castellanii* encystation ($p > 0.05$). Comparisons between the concentrations and the negative control revealed significant decrease in the encystation inhibition capability of the negative control as opposed to the EGCG concentrations ($p \leq 0.0001$) (Figure 5:18).

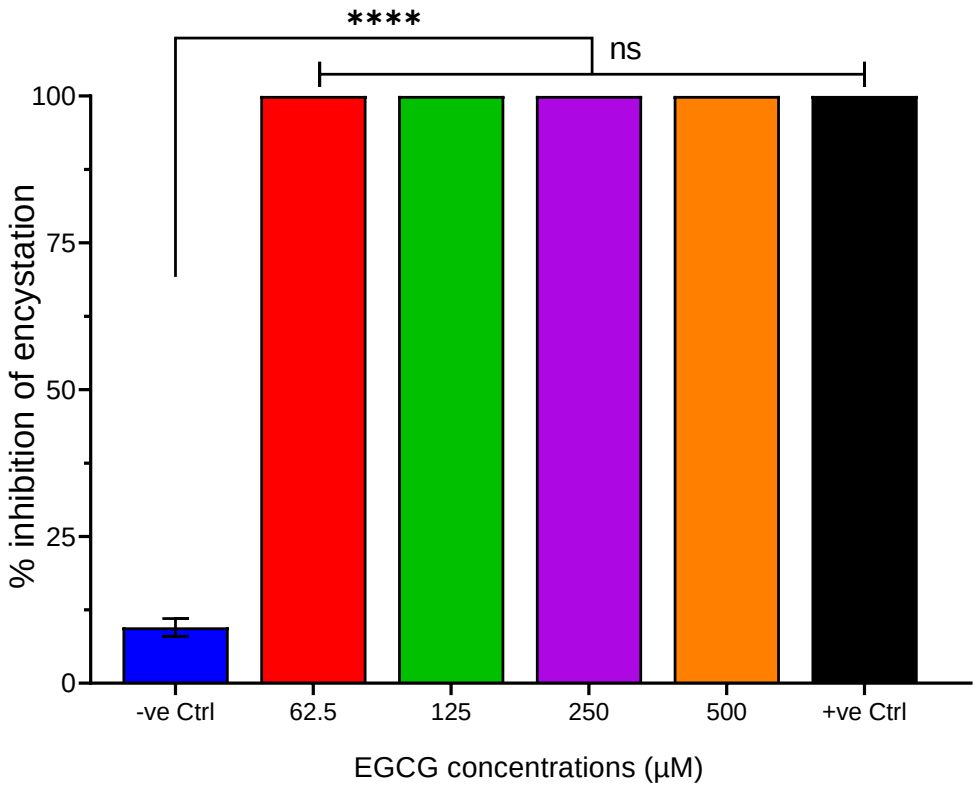

Figure 5:18: Percentage inhibition of encystation of *A. castellanii* exposed to EGCG hyperosmotic solution in doses of 62.5µM, 125µM, 250µM, and 500µM. All doses displayed 100% inhibition of encystation with no significant difference between them and the positive control (5 mM PMSF). (**** $p \leq 0.0001$, ns: non-significant).

For theobromine, one-way ANOVA revealed a significant main effect of theobromine concentrations ($F(5, 12) = 3606$, $p < 0.0001$). As observed with EGCG evaluation, post hoc comparison between the positive control and the theobromine concentrations revealed no significant difference between the positive control and the concentrations as all of them exhibited 100% inhibition to *A. castellanii* encystation ($p > 0.05$). Comparisons between the concentrations and the negative control revealed significant decrease in the encystation inhibition capability of the negative control as opposed to the theobromine concentrations ($p \leq 0.0001$) (Figure 5:19)

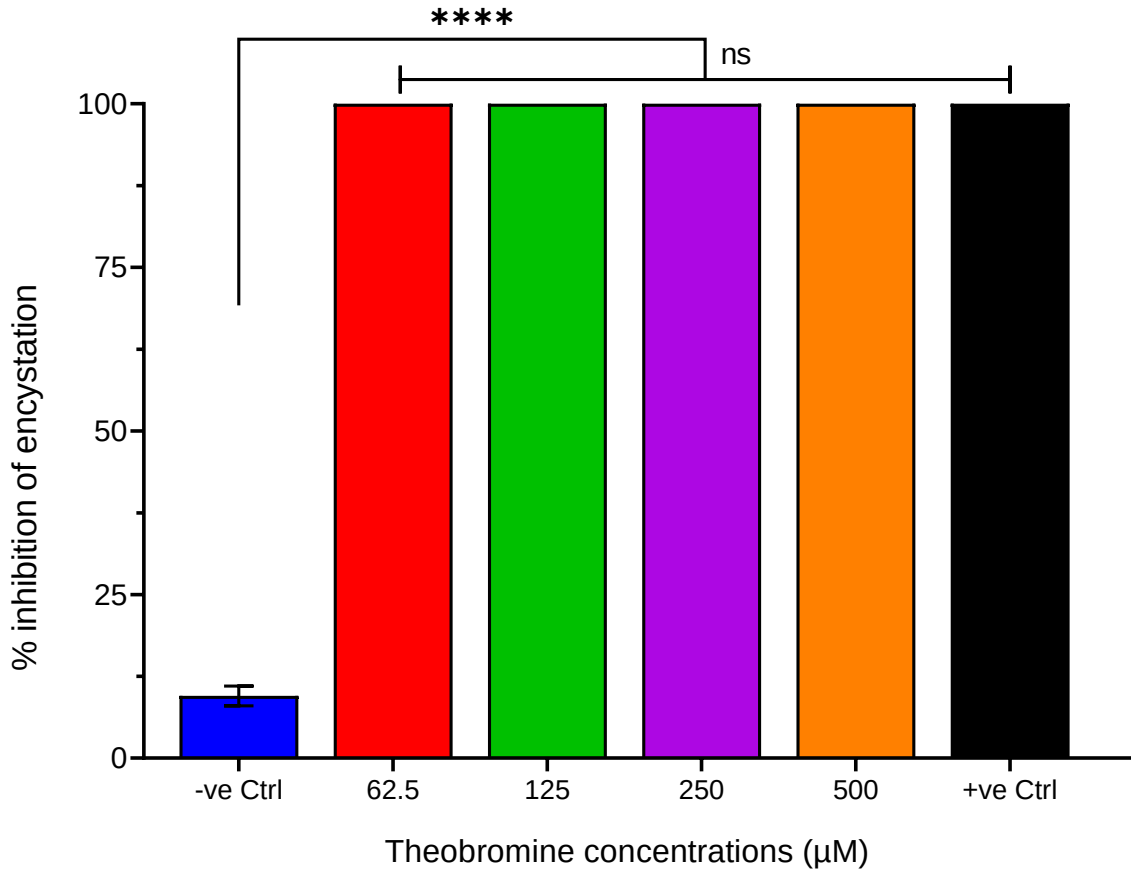

Figure 5:19: Percentage inhibition of encystation of *A. castellanii* exposed to theobromine hyperosmotic solution in doses of 62.5µM, 125µM, 250µM, and 500µM. All doses displayed 100% inhibition of encystation with no significant difference between them and the positive control (5 mM PMSF). (**** $p \leq 0.0001$, ns: non-significant).

In a different experiment, hyperosmotic solutions EGCG + theobromine chemical standards were combined together in a 1:1 ratio in doses of 62.5µM, 125µM, 250µM, and 500µM to also determine the percentage encystation inhibition rate (Figure 5:20). A one-way ANOVA revealed a significant main effect EGCG + theobromine concentrations ($F (5, 12) =3606$, $p < 0.0001$) on the inhibition rate. This was done to ascertain if the combination of both compounds will in any inhibit the encystational capability of the combination. Post hoc comparisons of all experiments showed a 100% trophozoites encystation inhibition rate of all selected concentrations of *C. sinensis* hyperosmotic chemical standards solutions with no significant difference between them and the positive control (5 mM PMSF) ($p <0.0001$).

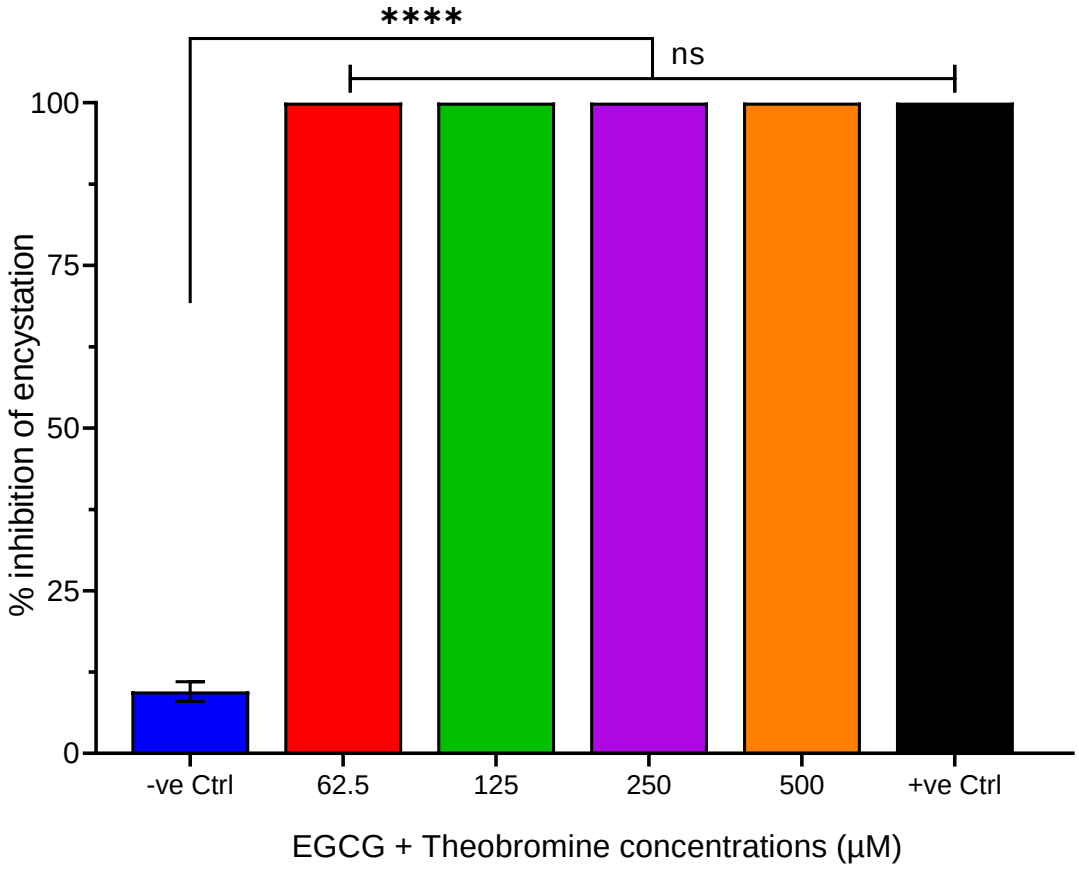

Figure 5:20: Percentage inhibition of encystation of *A. castellanii* trophozoites exposed to a combination of EGCG and Theobromine hyperosmotic solutions in a 1:1 ratio, in doses of 62.5µM, 125µM, 250µM, and 500µM. All doses displayed 100% inhibition of encystation with no significant difference between it and the positive control (5 mM PMSF). (**** $p \leq 0.0001$, ns: non-significant).

5.4 DISCUSSION

As a follow up to the earlier experiments conducted with *C. sinensis* brew and solvent extracts in the previous chapters of this research (chapters 3 and 4) which, it was worthwhile to identify the bio-active components of *C. sinensis* and to evaluate their anti-acanthamoebic activity to trophozoites and cystic forms of *A. castellanii*. This was done to determine if the purified identified chemical components would yield more efficacy than the already evaluated *C. sinensis* forms. First, identification of the chemical components was done using flash chromatography and UHPLC-QTOF-MS. The outcome of these evaluations revealed that EGCG and caffeine possess trophocidal capability, while EGCG and theobromine possess anti-encystational capability.

The most routinely used chemical agents, PHMB and CHX, are able to destroy the parasite membrane by inhibiting cellulose and DNA synthesis (Kaya et al., 2019) but still do not totally eliminate the parasite (Gooi et al., 2008; Kaya et al., 2019). Other therapeutic combinations using CHX with diamidines and neomycin (Siddiqui et al., 2016a), trimethoprim/sulfamethoxazole(Aichelburg et al., 2008), ketoconazole (Singhal et al., 2001), dicloxacillin, ciprofloxacin, voriconazole, amphotericin B(Walia et al., 2007), neomycin, metronidazole(Sun et al., 2006) fluconazole, rifampin, pentamidine and macrolide (Visvesvara et al., 2007; Maritschnegg et al., 2011) all yield the same therapeutic outcome. An alkylphosphocholine, miltefosine, has also been reported to cure a case of GAE, but rehabilitation of the patient did not improve the ataxic condition or hearing impairment (Aichelburg et al., 2008). Other compounds like heterocyclic alkylphosphocholines (APCs) (Garajova et al., 2014) demonstrate strong efficacy in vitro against *A. castellanii* trophozoites. These agents, while acting effectively against the parasite trophozoites, may not be equally effective against the cysts, which are made resistant by their cellulose based double walls. Despite reported success in some cases (Walia et al., 2007), long term treatments are toxic and also lead to destruction of host cells (keratocytes) with an imminent possibility of severe re-infections (Visvesvara, 2010; Niyyati et al., 2010).

The present study was preceded with a study evaluating the acanthamoebicidal capability of *C. sinensis* solvent extract, which showed that it possesses dose dependent amoebicidal activity against *A. castellanii* trophozoites and cysts. Although how *C. sinensis* exerts its anti-acanthamoebic inhibitory effects against *A. castellanii* remains to be elucidated, this study shows how *A. castellanii* fares against the chemical compounds identified in *C. sinensis.* The chromatographic analysis of *C. sinensis* brew form identified caffeine, ECG, EGCG, theogallin, quercetin, and kaempferol. Theobromine, EGC, EC, catechin, and myricetin were an additional five compounds identified in the chromatographic analysis of the solvent extract of *C. sinensis*.

In a recent study, the combination of EGCG with *C. sinensis* matcha tea displayed anti-acanthamoebic activity against trophozoites and cysts (Dickson et al., 2020). Against bacterial infections, EGCG has shown antifolate activity against *Stenotrophomonas maltophilia* (Navarro-Martínez et al., 2005), via inhibiting dihydrofolate reductase (DHFR), a key enzyme that catalyses the reduction of 7,8-dihydrofolate to 5,6,7,8-tetrahydrofolate, which is involved in nucleotide biosynthesis. Therefore, inhibition of DHFR can cause disruption of DNA synthesis. *A. castellanii* has DHFR and the antifolate trimethoprim drug has been shown to have amoebicidal activity (Siddiqui et al., 2016b). In a chemo-preventive study, EGCG also inhibited protein synthesis and the induced cellular apoptosis through multiple mechanisms (Shankar et al., 2007). It has also been seen as broad-spectrum attachment inhibitor of virus attachment to cells by regulating protein synthesis (Ciesek et al., 2011; Colpitts et al., 2014), Therefore, it is conceivable that EGCG, via its antifolate and protein synthesis inhibitory activity, might contribute to the anti-acanthamoebic effects of C. *sinensis*.

A. castellanii secretes an abundant amount of serine protease and metalloprotease (Khan, 2006b), which are known to compromise cell membrane integrity and cause cytolysis. In addition to being key determinants of the protozoan virulence (Dudley et al., 2008), these enzymes are also involved in regulating *A. castellanii* trophozoite differentiation into cysts (Lorenzo-Morales et al., 2015; Alsam et al., 2005). Interestingly, a study of *C. sinensis*

polyphenols showed that EGCG, appears to be a natural inhibitor of serine protease and metalloprotease (Benelli et al., 2002; Wyganowska-Świątkowska et al., 2018), and this inhibitory capability seems to be broad spectrum as it also inhibits 3 chymotrypsin-like protease (3CLpro) of SARS-CoV-2, resulting in inhibition of viral polyprotein processing and presumably inhibiting spread of coronavirus (Chiou et al., 2021). EGCG has also been seen to cause an overexpression of tissue factor pathway inhibitor-2 (TFPI-2), which is a Kunitz-type serine proteinase inhibitor (Gu et al., 2009). Therefore, *C. sinensis* components (e.g., 3-O-gallate group), through the interaction with or inhibition of these enzymes, might have caused the cytolysis of *A. castellanii* trophozoites and inhibition of encystation in the present study, with 100µM and 200µM concentrations of EGCG exhibiting anti-acanthamoebic activity from 48 h post-treatment.

Caffeine was also able to inhibit trophozoite replication. Caffeine had been identified for its capability to regulate the activation of cyclic AMP (cAMP) synthesis, which regulates chemotaxis and possibly gene transcription in the social amoeba *Dictyostelium discoideum* (Brenner and Thoms, 1984). A later study suggested that there were similarities between the cAMP-specific phosphodiesterase, RegA, found in both *A. castellanii* and *D. discoideum,* which plays an active role in regulating spore formation in *D. discoideum* and inhibiting encystation in *A. castellanii* by increasing cAMP levels (Du et al., 2014). With exposure of *A. castellanii* to harsh conditions, such as chemotherapy, the trophozoites will normally encyst to preserve themselves. It is therefore a possibility that in the presence of caffeine the regulation of the cAMP levels prevented encystation, leading to the dose-dependent extermination of the trophozoites 72 hours post-exposure to caffeine. Glucose-1-phosphate is a precursor of cellulose, which is one of the components of *A. castellanii* cyst walls. The breakdown of glycogen during encystation is enabled by the presence of the enzyme glycogen phosphorylase (Martín-Navarro et al., 2017). The expression of this enzyme is known to be inhibited by caffeine (Tsitsanou et al., 2000; Freeman et al., 2006), which leads to the inhibition of trophozoite replication and encystation in *A. castellanii.* Regarding protease inhibition,

caffeine has been seen to also inhibit poly (ADP-ribose) polymerase (PARP) expression, which is also inhibited by protease inhibition (Cleaver et al., 1986). Some of PARP's functions include cellular regeneration via DNA repairs, necrosis and apoptosis (Jagtap and Szabó, 2005). Therefore, caffeine may have inhibited trophozoite regeneration and also initiated apoptosis during the trophozoite replication experiments by interactions leading to PARP inhibition.

The anti-acanthamoebic inactivity of the identified chemical compounds evaluated in a mix of equal volume cannot be explained at this stage. It would seem, however, that that the combinations of all or some of the chemical compounds of *C. sinensis* outside its natural constitution may not have yielded desirable results as a host of other trace compositions of cellulose, proteins, amino acids and other compounds in the natural brew and solvent extract may not have been accounted for. It is also unclear at this point why there was trophocidal efficacy of 2 individual compounds (EGCG and caffeine), but yet in the combination of the rest of the non trophocidal components, they were not able to elicit any trophocidal activity; their activity might have been attenuated by the other components whose quantity exceeded them by an 8:2 ratio.

Contrary to the inability of theobromine to inhibit trophozoite replication as exhibited by caffeine and EGCG, interestingly, it was able to inhibit trophozoite to cyst differentiation during stimulation of excystation even at the lowest concentration (Figure 5:19). Also, a combination of theobromine and EGCG also inhibited the encystation of trophozoites suggesting that whatever phenomenon prevented the *C. sinensis* chemical cocktail from inhibiting trophozoite replication during normal trophozoite growth conditions did not occur when the trophozoites were subjected to encystation conditions. With this anti-encystation possibility, a combination of some or the rest of the other chemical compounds might possess the capability to interfere with trophozoite encystation process. The expression of serine protease and metalloprotease is one of the determinants of virulency and pathogenicity in A. castellanii (Khan et al., 2000a). Thereby, using PSMF which was the positive control in encystation and excystation

experiments as a reference point, the inhibition of protease by PMSF (Dudley et al., 2008) led to loss of cell membrane integrity in *A. castellanii* especially during parasite differentiation from trophozoites to cysts and cysts to trophozoites. This activity by PMSF can be relatable to the trophocidal and cysticidal activity expressed by EGCG, caffeine, theobromine identified in *C. sinensis*. Although a combination of equal volume of the identified *C. sinensis* bioactive compounds did not yield any favourable anti-acanthamoebic activity (Figure 5:17), some of these compounds exhibited sustained amoebicidal activity of *C. sinensis*. The individual evaluation of the bioactive compounds showed that EGCG (Figure 5:13) and caffeine (Figure 5:14) exhibited dose dependent anti-acanthamoebic activity at 72 h exposure to *A. castellanii* trophozoites.

In conclusion, the results of this study demonstrated that EGCG and caffeine possesses amoebicidal ability against both trophozoite forms of *A. castellanii.* For the rest of the chemical components, although there was interchangeable continuous significance increases of OD between the negative control group and those tested chemicals standards, they were not able to exhibit notable inhibitory activity to the trophozoite growth. In encystation and excystation experiments, these catechins and theobromine were also seen to possess cysticidal properties *in vitro*. The subsequent aspect of this study will attempt to characterise the action of *C. sinensis* on the protein components of *A. castellanii,* which will give more insight on how the tested compounds can contribute to the development of a safe and effective source of novel therapeutic approaches against *Acanthamoeba* infection.

6 CHARACTERISING ANTI-ACANTHAMOEBIC ACTIVITY OF *C. SINENSIS*

6.1 SUMMARY

In this study, the activity of *Camellia sinensis* (green tea) brew and solvent extract on *A. castellanii* was characterized by analysing the nuclear integrity and proteomic expressions after exposure of *A. castellanii* to both *C. sinensis* for 24 hours. Analysis of fluorescence intensity and nuclear membrane integrity of *A. castellanii* trophozoites exposed to 1250µg/mL *C. sinensis* solvent extract concentration and 50% hot brew using DAPI dye, caused the disruption of nuclear envelope leading to loss of nuclear membrane integrity and ultimately resulting to nuclear fragmentation, degradation of chromatin with low fluorescent intensity. Analysis with acridine orange dye showed that the trophozoites exposed to both forms of *C. sinensis* disrupted *A. castellanii* trophozoites' growth by disrupting the nuclear membrane integrity reducing the quantity of DNA and RNA indicating trophozoite death. Fourier-transform infrared spectroscopy revealed protein synthesis inhibition by the lack of amide I and II band peaks expression in the *C. sinensis* treated trophozoites. Proteomic analysis of trophozoites via Data-independent acquisition mass spectrometry (DIA-MS) approach identified 236 proteins, of which 150 and 91 proteins were exclusively identified in the treated and untreated trophozoites, respectively. Two proteins, 14-3-3 protein sigma and Keratin type I cytoskeletal 10 were not detected after *C. sinensis* treatment with the inhibition of 14-3-3 proteins isoforms and the expression of triosephosphate isomerase pointing to the inhibitory effect of *C. sinensis* on *A. castellanii* protein synthesis leading to trophozoite death. This work demonstrated that *C. sinensis* solvent extract has anti-acanthamoebic activity against trophozoite and cystic forms of *A. castellanii*.

6.2 INTRODUCTION

In the course of *A. castellanii* pathogenicity, there are many proteins, phospholipids, lipophosphonoglycans and sterols that are produced to enable it invade and infect host cells and tissue (Siddiqui and Khan, 2012). Specifically, a MBP (Siddiqui and Khan, 2012), a 28.2kDa and 55kDa LBP, and a 207kDa adhesion protein (Siddiqui and Khan, 2012; Hong et al., 2004), and a host of other unidentified proteins enables the adherence to the host cell. This induces the secretion of toxins and enzymes like serine proteases, resulting in an *A. castellanii*-mediated host cell death via a PI-3k-dependent mechanism (Sissons et al., 2005). All these components of *A. castellanii* presents a wide range of investigational and analytic possibilities when evaluating the source of apoptosis, encystation inhibition and ultimately parasite death.

A few proteomic characterisation studies and expression analyses of trophozoite proteins have been done. For example, two-dimensional polyacrylamide gel electrophoresis (2DE PAGE) and SDS-polyacrylamide gel electrophoresis (SDS-PAGE) (Behera and Satpathy, 2016; Carvalho-Silva et al., 2021), quantitative real-time PCR, Western blot analysis and peptide and protein identification using iTRAQ quantitative proteomic analysis (Deng et al., 2015). While these studies have not fully revealed the mechanisms of action of how the expression of *A. castellanii* proteins are inhibited, these analyses were only done for anti-acanthamoebic chemical compounds. There is currently no available literature showing any proteomic analysis from anti-acanthamoebic studies using natural products or their bioactive components, the ones that may have been done did not list or identify the specific proteins expressed by *A. castellanii* in vitro. For fluorescence analysis of biological samples, the ability of the dyes to permeate the cellular membranes for monitoring cell physiology, and the ability to employ multiple filters (Sanderson et al., 2014), allows for different nuclear content, proteins and nucleic acids to be tagged and analysed simultaneously. Fluorescence based dyes is measured in excitation and emission wavelengths with a range of 420 nm - 600 nm for most

of the fluorescent dyes used as cellular probes. Amongst all the dyes, acridine orange is probably the most widely used dye as stained cells fluoresce orange while the dye stains both live and dead cells by interacting with the DNA and protein components of cells (Bari and Yeasmin, 2021). Other methods of molecular characterisation employ the use of vibrational spectroscopy such as Fourier transform infrared spectroscopy (FTIR) (Faix, 1992), and Raman spectroscopy (Long, 1977). For FTIR, the imaging is label free using non-destructive and non-invasive methods (Chan et al., 2018), where chemical fingerprinting of samples are analysed based on their peaks and wavelengths measured in different bands. This technique uses infrared microscopy and synchrotron IR radiation making it possible to map cellular components (carbohydrates, lipids, proteins) to recognise and classify irregular cells (Berthomieu and Hienerwadel, 2009). Its use for proteomic analyses allows for the identification of molecular details of protein active sites during enzyme reaction (Siebert and Hildebrandt, 2008). RAMAN spectroscopy allows for spatial determination of the composition of compounds, thereby showing known changes in compounds due to a reaction as well as the properties of the bonds between molecules(Lyon et al., 1998).

From the preceding chapters of this study, it has been shown that *C. sinensis* possesses anti-acanthamoebic properties, though its mechanism of action is yet to be determined. The aim of this chapter is to characterise some aspects of *C. sinensis* mechanisms of action in *A. castellanii* by analysing the nuclear structure of treated trophozoites using fluorescence assays, and by proteomic and chemical fingerprinting analyses of *A. castellanii* in the presence and absence of *C. sinensis*. As the desired drug for *Acanthamoeba* infections is still yet to be discovered, the identification of specific proteins or other molecules in *A. castellanii* in response to exposure to *C. sinensis* may provide new insight on how *C. sinensis* inhibits *A. castellanii* proliferation and growth, which will be an invaluable contribution to the ongoing progress of anti-acanthamoebic drug discovery.

6.3 RESULTS

6.3.1 Characterisation of *C. sinensis* activity using fluorescence assays

6.3.1.1 DAPI fluorescence assay

In characterising the effect of *C. sinensis* brew and solvent extract on the integrity of *A. castellanii* nuclei, confocal imaging with DAPI showed a huge difference in the fluorescence intensity of the negative control trophozoites when compared with trophozoites treated with *C. sinensis* 50% brew and 1250µg/mL concentration of *C. sinensis* solvent extract for 24 hours (Figure 6:1). The fluorescent micrographs showed loss of nuclear membrane integrity of the trophozoites, ultimately resulting to nuclear fragmentation, and degradation of chromatin, with low fluorescent intensity. The fluorescence intensity shown by the negative control (PGY) was extensive, covering almost the whole view. When comparing this result with trophozoites treated with 50% *C. sinensis* brew and the 1250µg/mL *C. sinensis* solvent extract micrographs, the fluorescence intensity was low and dim, suggesting lesser nuclear content and lower number of trophozoites. Furthermore, the bright field and merged images of the 50% *C. sinensis* brew treatment showed less trophozoite clusters in comparison to the negative control. This also suggests that the quantity of trophozoites observed by light microscopy examination of *C. sinensis*-treated trophozoites does not necessarily mean that they are all viable. The same was observed for the 1250µg/mL *C. sinensis* solvent extract treated trophozoites, which showed even lesser trophozoite clusters, indicating that *C. sinensis* solvent extract has a higher anti-acanthamoebic capability than *C. sinensis* brew.

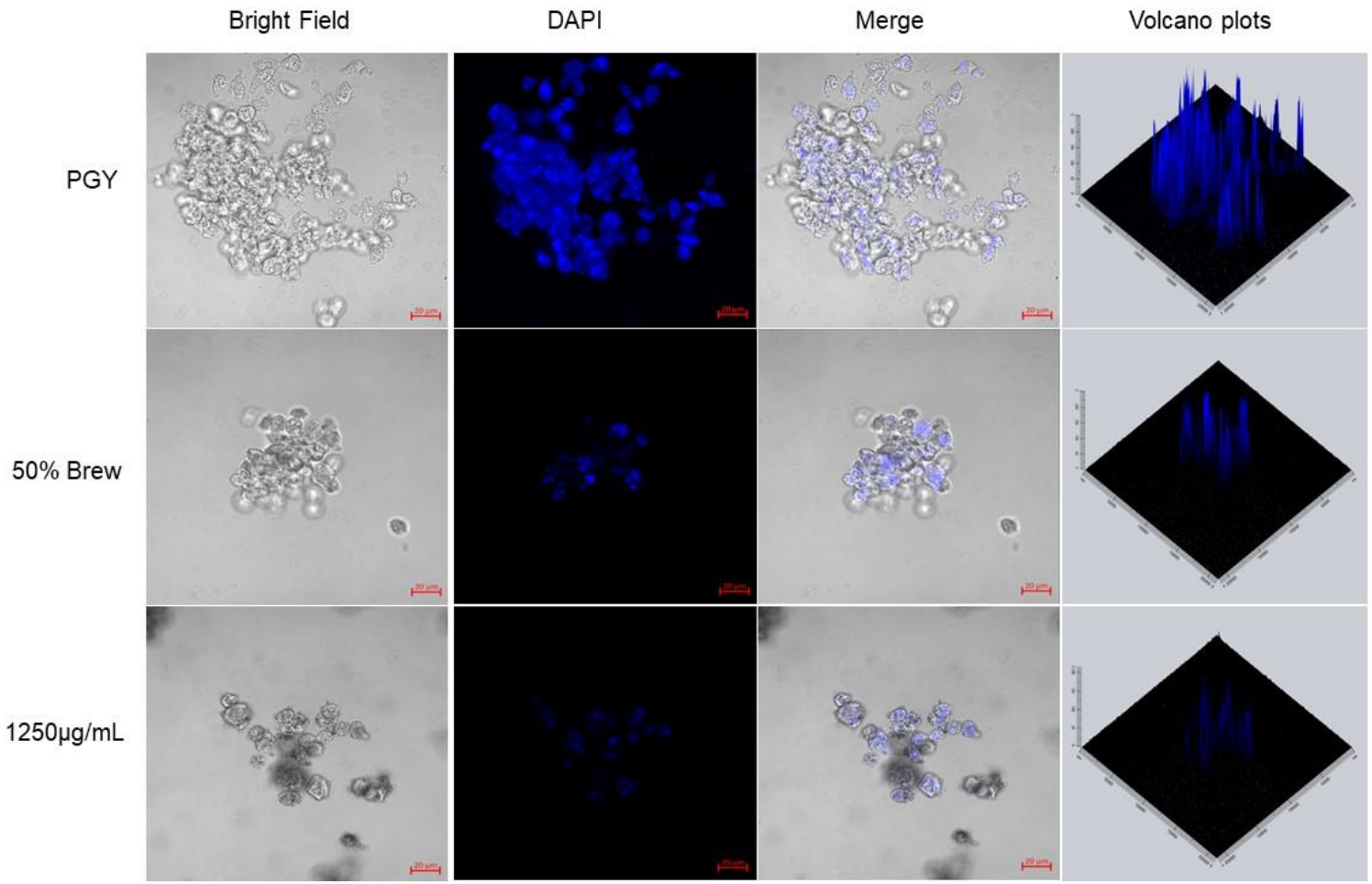

Figure 6:1: Staining using 4',6-diamidine-2'-phenylindole dihydrochloride (DAPI) shows a considerable difference in the fluorescent intensity between the PGY treated trophozoites and those treated with 50% *C. sinensis* brew and 1250µg/mL solvent extract. Volcano plots show clear differences between the fluorescence intensities. Scale bar = 20µM.

When determining the levels of fluorescence expressed when *A. castellanii* trophozoites treated with *C. sinensis* forms are exposed to DAPI dye, RM one-way ANOVA of the mean fluorescence intensity (Figure 6:2) revealed a significant main effect of *C. sinensis* forms ($F(1, 1) = 1316$, $p = 0.0175$). Post-hoc comparisons showed that there was no significant difference between the mean fluorescence intensity of the positive control and the *C. sinensis* forms (50% & 1250µg/mL) ($p > 0.05$). Further comparisons between the negative control and the *C. sinensis* forms showed that there was a significant increase in the mean fluorescence intensity of the negative control when compared to the *C. sinensis* forms ($p < 0.05$) (Figure 6:2). For integrated fluorescence density analysis, RM one-way ANOVA revealed a significant main effect of *C. sinensis* forms ($F(1, 1) = 1634403$, $p = 0.0005$). Post-hoc comparisons showed that there was a significant increase in the integrated fluorescence density of the positive control when compared with the *C. sinensis* forms ($p < 0.05$). Same results were observed when the negative control was also compared with the *C. sinensis* forms (Figure 6:2). This result corroborates the previous results that *C. sinensis* forms inhibits the growth and replication of *A. castellanii* trophozoites.

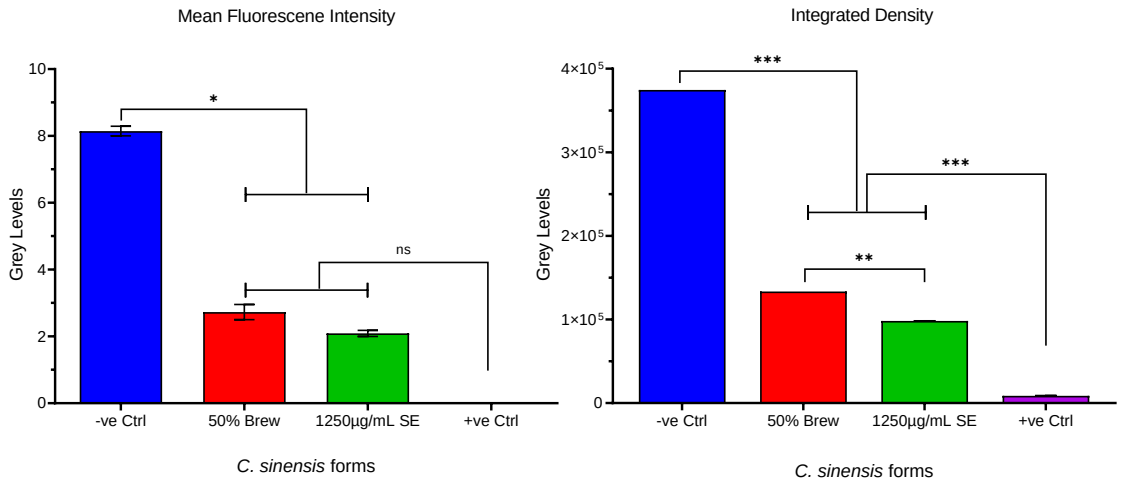

Figure 6:2: Quantitative analysis of fluorescence expressions after DAPI staining shows a considerable difference in the mean fluorescent intensity between negative control and the *C. sinensis* forms, and no significant difference between the positive control and the *C. sinensis* forms. There were also significant increases and decreases in the integrated fluorescence density of the negative and positive controls respectively when compared to the *C. sinensis* forms. (** $p \leq 0.05$, ** $p \leq 0.01$, *** $p \leq 0.001$, ns: non-significant*).

6.3.1.2 Acridine orange assay

By comparing to trophozoites treated with 1250µg/mL solvent extract of *C. sinensis,* negative control trophozoites showed yellow-to-reddish orange spots overlaying larger greenish spherical structures with a polygonal arrangement of the same reddish spots connecting the green spheres. Although seemingly same structures were observed in trophozoites treated with 1250µg/mL solvent extract of *C. sinensis*, these structures, which appeared much shrunken as indicated by the scale bars, were not pronounced as observed in the untreated trophozoites. AO staining also showed a significant difference in the fluorescence intensity of the negative control trophozoites when compared to trophozoites treated with 1250µg/ml solvent extract for 24 hours. At 24 hours post-treatment, 1250µg/mL solvent extract of *C. sinensis* disrupted *A. castellanii* trophozoites' replication by disrupting the nuclear membrane integrity, leaving sparse nucleic acids (DNA/RNA) available for interaction with the dye (Figure 6:3) when compared to the untreated trophozoites.

When determining the levels of fluorescence expressed when *A. castellanii* trophozoites treated with *C. sinensis* forms are exposed to AO dye, mean fluorescence analysis with two-way ANOVA revealed a significant main effect of AO dye ($F(1,) = 495.2$, $p = 0.0020$), *C. sinensis* forms ($F(3, 6) = 15870$, $p < 0.0001$), and AO dye x *C. sinensis* forms interaction ($F(3, 6) = 356.1$, $p < 0.0001$). Post-hoc comparisons showed that there was no significant difference between the mean fluorescence intensity of the positive control and the *C. sinensis* solvent extract (1250µg/mL) ($p > 0.05$) for both FITC and rhodomine channels, while there was significant decrease in mean fluorescence intensity of the positive control in comparison to the 50% *C. sinensis* brew ($p <0.05$). Further comparisons between the negative control and the *C. sinensis* forms showed that there was a significant increase in the mean fluorescence intensity of the negative control when compared to the *C. sinensis* forms ($p <0.05$) (Figure 6:4).

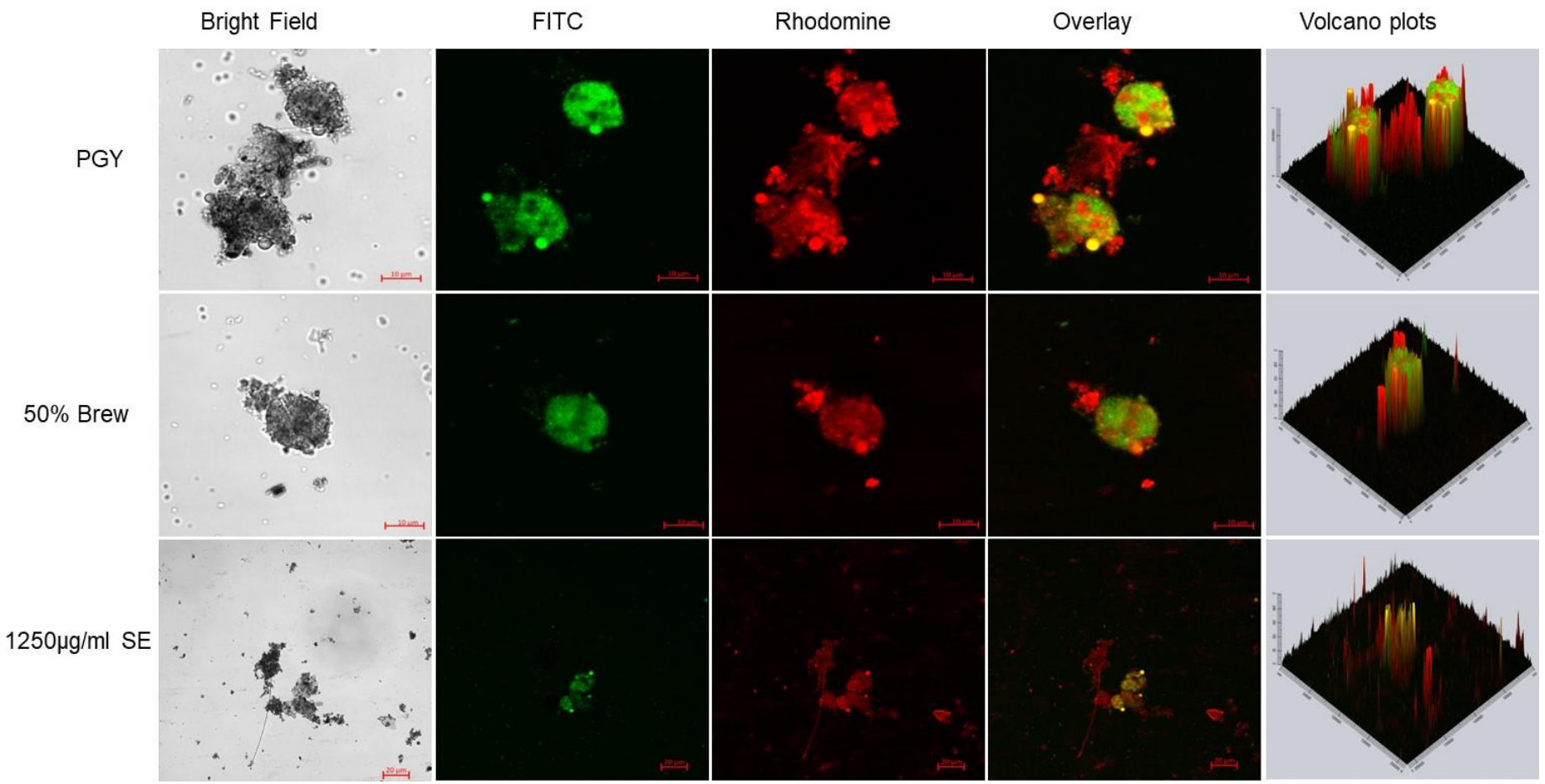

Figure 6:3: Staining with acridine orange dye shows a significant difference in the fluorescence intensity between the PGY treated trophozoites in comparison with trophozoites treated with *C. sinensis* 50% brew and the 1250µg/ml of solvent extract. The interaction of the dye with DNA at a maximum excitation of 525 nm shows a green fluorescence (FITC) while at the maximum excitation of 650 nm, interaction with DNA shows a red fluorescence (rhodomine). Volcano plots further supports this result. Scale bar = 10µM, 20µM,

For integrated fluorescence density analysis, two-way ANOVA revealed a significant main effect of AO dye (F (1, 2) = 4059074050, < 0.0001), *C. sinensis* forms (F (3, 6) = 120176471048, p < 0.0001), and AO dye x *C. sinensis* forms interaction (F (3, 6) = 2851851247, p < 0.0001). Post-hoc comparisons showed that there was a significant decrease in the integrated fluorescence density of the positive control when compared with the *C. sinensis* forms (p <0.05). Same results were observed when the negative control was also compared with the *C. sinensis* forms (Figure 6:4), there was significant increase in integrated fluorescence density of the negative control when compared with the *C. sinensis* forms (p <0.05). Although there was a significant decrease in integrated fluorescence density positive control when compared to the *C. sinensis* forms, the decrease in *C. sinensis* forms integrated fluorescence density also corroborates the previous results that *C. sinensis* forms inhibits the growth and replication of *A. castellanii* trophozoites.

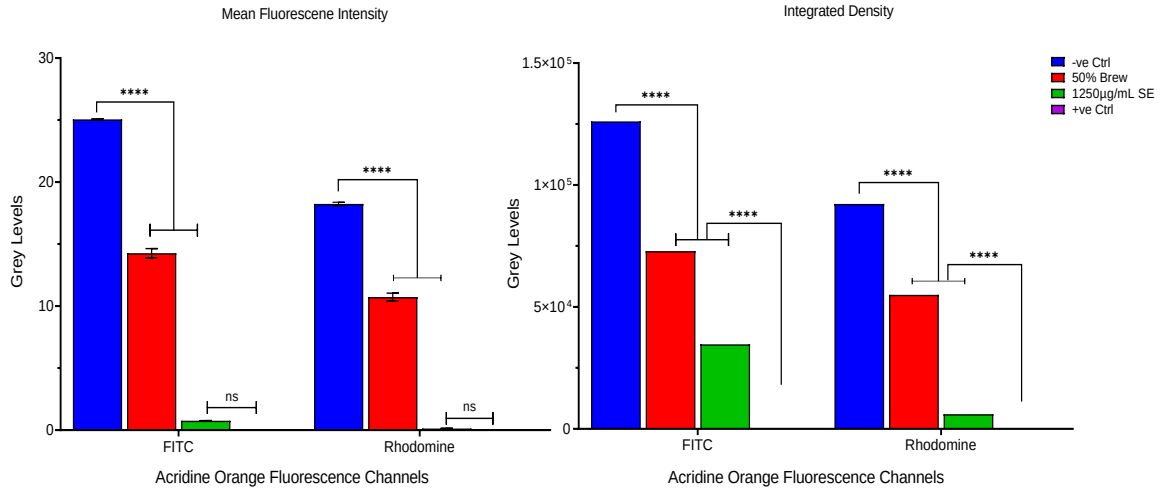

Figure 6:4: Quantitative analysis of fluorescence expressions after AO staining shows a considerable difference in the mean fluorescent intensity between negative control and the *C. sinensis* forms, and no significant difference between the positive control and the *C. sinensis* solvent extract. There were also significant increases and decreases in the integrated fluorescence density of the negative and positive controls respectively when compared to the *C. sinensis* forms. (*** $p \leq 0.001$, *ns: non-significant*).

6.3.2 FTIR spectroscopy micro-spectroscopy

FTIR spectroscopic imaging was performed on control *A. castellanii* trophozoites seeded on a flat CaF_2 substrate (Figure 6:5A) compared with imaging performed with trophozoites sandwiched between two ZnS hemispheres (Figure 6:5B). The results showed a marked improvement in the baseline distortion in the samples imaged using the two ZnS hemispheres approach. Therefore, all subsequent measurements of single trophozoites were made using the ZnS hemisphere lenses.

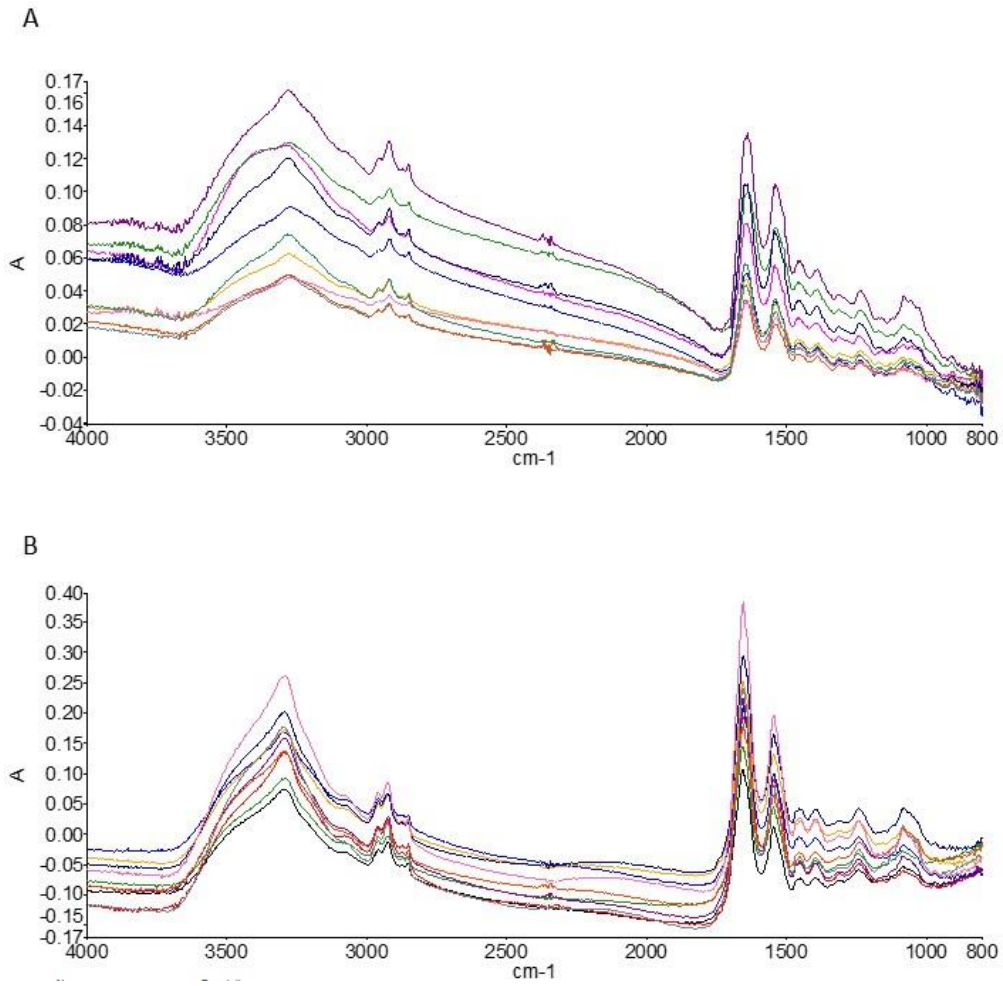

Figure 6:5: Randomly selected FTIR spectra of control *A. castellanii* trophozoites measured on (A) a flat CaF2 substrate and (B) in between two ZnS hemispheres. Both measurements were made with the same spectral resolution of 4 cm^{-1} and 64 scans.

The principal component analysis (PCA) results of the pair-wise comparison between the negative control (PGY) and the treatment with chlorhexidine (CHX, positive control) at 24 h and 48 h are shown in Figure 6:6. A near-identical score and loading plots can be observed for both time points with clear differences between the CHX-treated and control samples. The presence of CHX inside trophozoites was evidenced by the characteristic peak at 1492 cm^{-1}, suggesting a high concentration of CHX was absorbed by the trophozoites. Some of the peaks highlighted on the loading spectrum (1694 cm^{-1} and 1614 cm^{-1}) can also be the result of a change in the protein secondary structure with the treated trophozoites showing a higher content of beta-sheet protein.

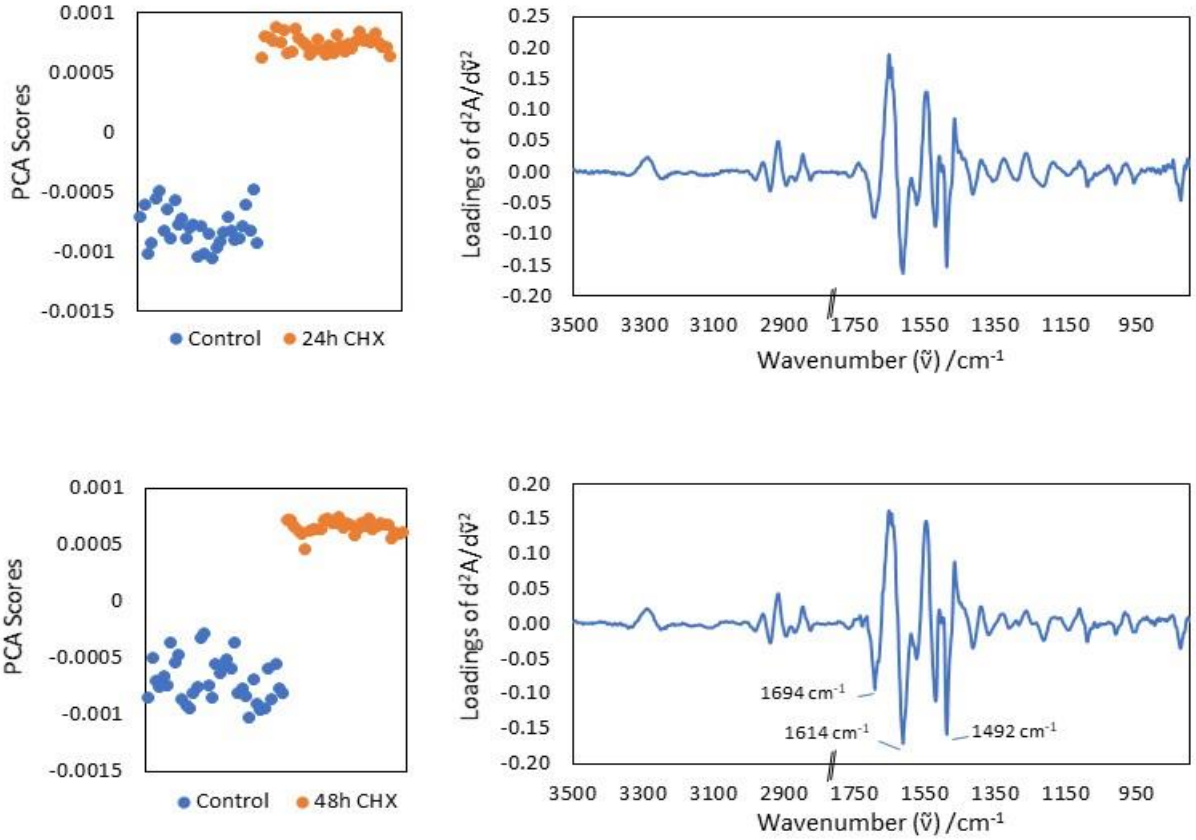

Figure 6:6: PCA of control trophozoites compared to trophozoites treated with chlorhexidine (CHX) for 24 h (top) and 48 h (bottom). Principal component (PC) score plots show how the trophozoites spectra are grouped together according to the variation between trophozoites and the PC loading vectors show what variants contribute to the grouping.

The PCA of the single trophozoite FTIR data for the comparison between control and *C. sinensis* hot brew-treated trophozoites are shown in Figure 6:7 and Figure 6:8. The data show that both principal component 1 (PC1) and PC2 produced statistically significant differences between the control and the treated trophozoites ($p < 0.0001$). For the 24 h treatment, PC1 mainly highlights the difference in the amide I and II regions, which suggests some of the treated trophozoites have changes in the protein composition when treated with *C. sinensis* hot brew. PC2 produced a loading vector that suggests some biochemical changes in the treated trophozoites. At 48 h after treatment, a similar PC1 loading vector is produced but the score plot does not associate this to the effect of the treatment ($p > 0.05$). The changes in the protein amide I and II peaks are likely to be attributed to intrinsic biological variations between trophozoites. Importantly, PC2 clearly differentiated between the control and treated trophozoites ($p < 0.0001$) with three characteristic peaks (1152 cm^{-1}, 1092 cm^{-1} and 1028 cm^{-1}), which are associated with increased glycogen content in *C. sinensis* brew treated trophozoites.

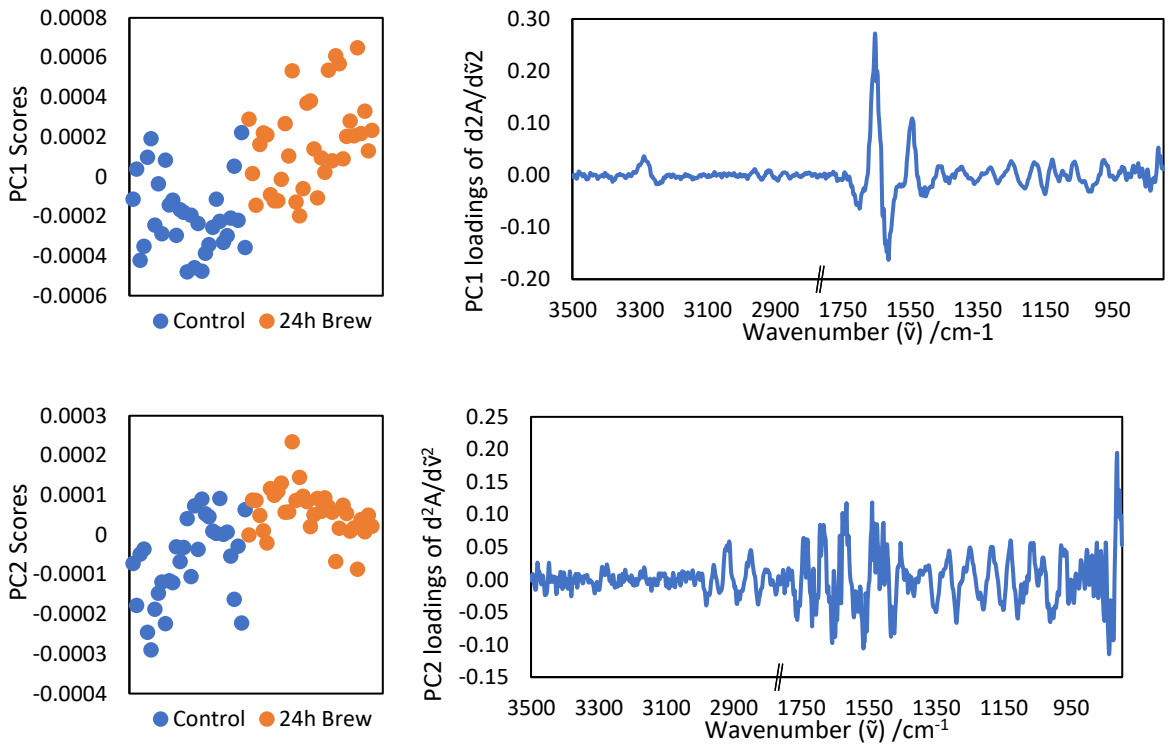

Figure 6:7: PC1 and PC2 of negative control compared with *C. sinensis* hot brew after 24 h, as detected in *A. castellanii* treated with *C. sinensis* hot brew.

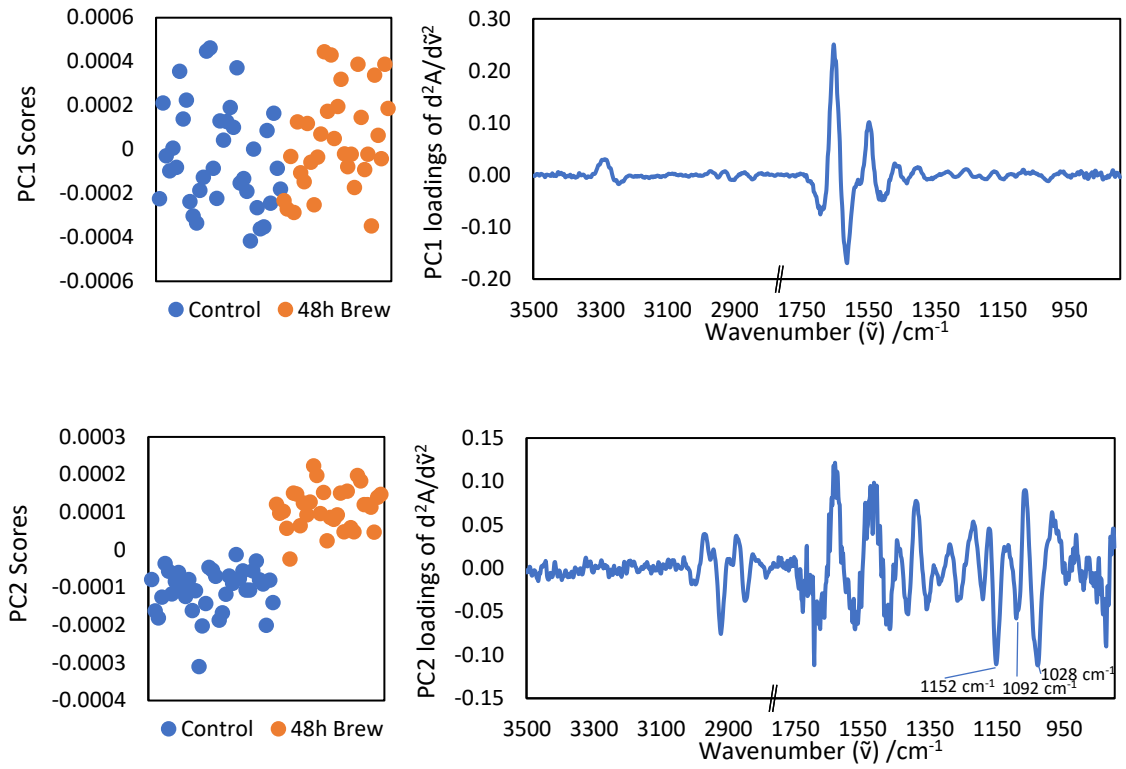

Figure 6:8: PC1 and PC2 of negative control compared to *C. sinensis* hot brew after 48-h, as detected in *A. castellanii* treated with *C. sinensis* hot brew.

PCA of trophozoites treated with solvent-extracted *C. sinensis* is shown in Figure 6:9. At 24 h after treatment, PC1 revealed some differences in the protein amide I and II region ($p < 0.05$). PC2, by contrast, produced a clear difference between control and treatment trophozoites ($p < 0.0001$) and similar to *C. sinensis* brew treatment, the changes are complex as shown by the multiple peaks over the analysed spectral regions. The 48 h treatment results have shown that PC1 highlights variations in the protein amide I and II peaks among trophozoites but with no association with the effect of treatment ($p > 0.05$). PC2 shows a clear effect of the treatment ($p < 0.0001$) and spectral changes are mostly found in the 1800-900 cm^{-1} region. However, the links to glycogen peaks are not as evident as observed by *C. sinensis* brew treatment at 48 h.

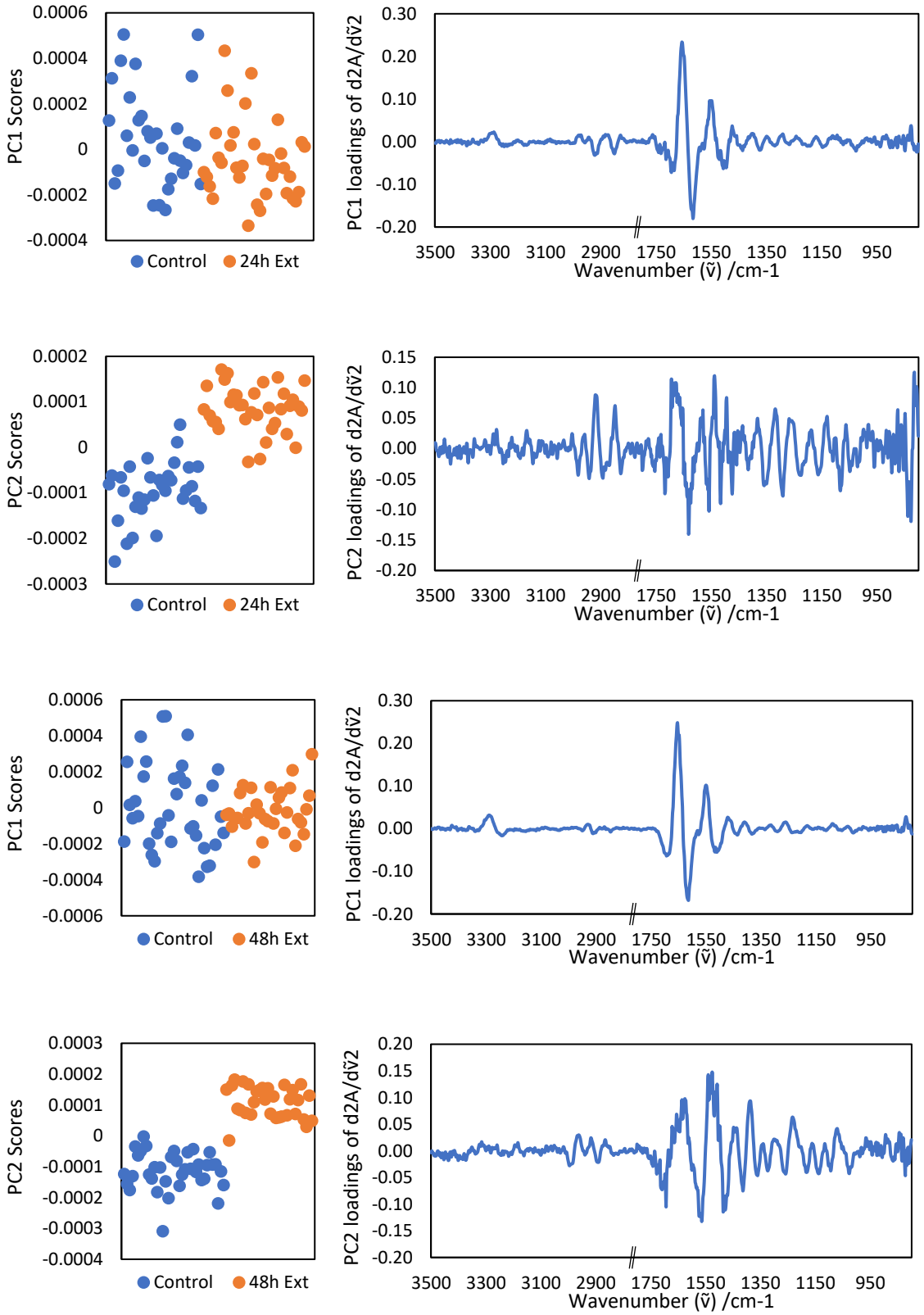

Figure 6:9: PC1 and PC2 of negative control trophozoites compared with *A. castellanii* trophozoites treated with *C. sinensis* solvent extract for 24 h (1st and 2nd spectrograph) and 48 h (3rd and 4th spectrograph).

6.3.3 Proteomics analysis of *C. sinensis* treated trophozoites

The protein content of *A. castellanii* culture before *C. sinensis* treatment after quantification with Pierce™ BCA protein assay kit (see section 2.7.15.1) was 0.59 mg/mL (Table 6.1, Figure 6:10). Desalted peptides along with calibration iRT peptides (Biognosys, Switzerland) were then analysed by LC–MS/MS, as a result of which multiple proteins were identified within each *C. sinensis* treated (appendix 1) and non-treated (appendix 2) *A. castellanii* trophozoites.

Table 6.1: Protein quantification of *C. sinensis* treated *A. castellanii* culture, and blank *C. sinensis* brew. *Abbreviations:* (Conc.) Concentration. (D.F) Dilution factor. (Abs) Absorbance. (FC) Final concentration.

						Conc.	D. F	FC
Sample Name	**Abs 1**	**Abs 2**	**Abs 3**	**Av Abs**	**Av-Blank**	**mg/mL**	**7.5**	**mg/mL**
A. castellanii culture before *C. sinensis* treatment	0.367	0.373	0.399	0.380	0.097	0.079	7.5	0.59
A. castellanii culture after *C. sinensis* treatment	0.390	0.377	0.380	0.382	0.099	0.081	7.5	0.60
C. sinensis hot brew	0.356	0.368	0.359	0.361	0.078	0.065	7.5	0.48

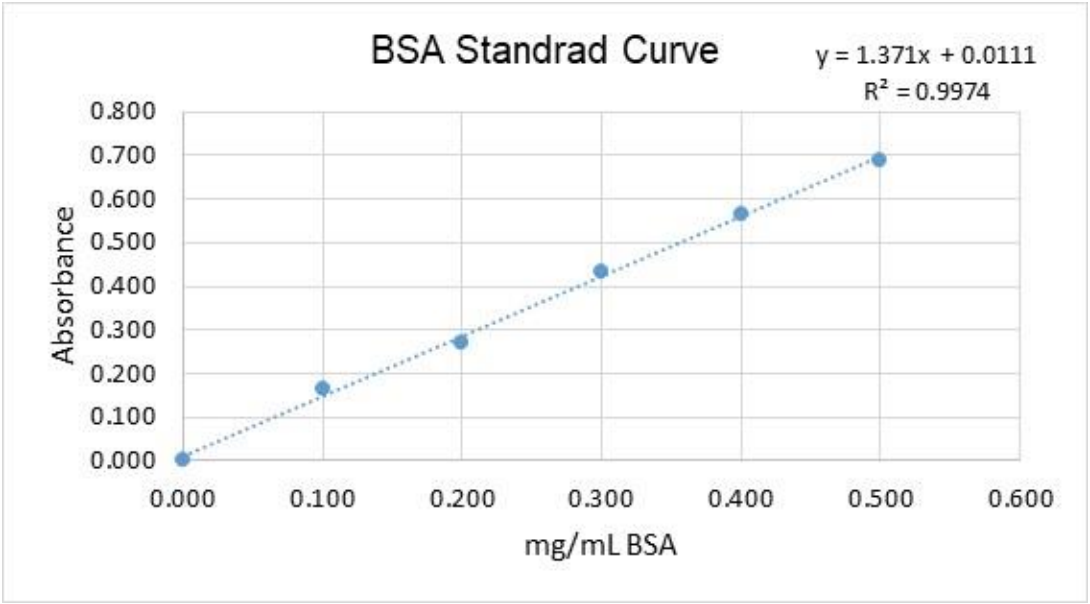

Figure 6:10: protein content of *C. sinensis* treated *A. castellanii* culture pre-proteomics analysis was determined using BSA standard curve and a dilution factor of 7.5.

The number of proteins and peptides expressed before and after treatment of *A. castellanii* with *C. sinensis* irrespective of the confidence ratio is listed below (Table 6.3: Major proteins expressed (40% confidence) between *C. sinensis*-treated and untreated *A. castellanii* trophozoites.). With a 1% false discovery rate (FDR) and at least 40% confidence ratio, 150 proteins and 485 peptides were identified in *A. castellanii* trophozoites before treatment, and 91 proteins with 244 peptides were identified after treatment.

Table 6.2: Summary of proteins and peptides expressed in *A. castellanii* following *C. sinensis* treatment evaluated in SWATH and IDA mode at 1% False Discovery Rate (FDR)

A. castellanii	**Run Method**	**Proteins at 1% FDR**	**Peptides at 1% FDR**	**Spectra at 1% FDR**
Before *C. sinensis* treatment	SWATH	N/A	N/A	N/A
After *C. sinensis* treatment	SWATH	N/A	N/A	N/A
Before *C. sinensis* treatment	IDA	150	485	685
After *C. sinensis* treatment	IDA	91	244	401
Before and after *C. sinensis* treatment (FDR)	IDA	236	1390	3839

More proteins were detected in *C. sinensis*-treated trophozoites compared with untreated trophozoites. Ten proteins were common between the treated and untreated trophozoites. Interestingly, two proteins (14-3-3 protein sigma and Keratin type I cytoskeletal 10) were not detected after *C. sinensis* treatment, whereas the expression of 3 proteins (triosephosphate isomerase, thioredoxin, and alpha-enolase) were expressed after *C. sinensis* treatment (Table 6.3).

Table 6.3: Major proteins expressed (40% confidence) between *C. sinensis*-treated and untreated *A. castellanii* trophozoites.

***C. sinensis* untreated trophozoites**	***C. sinensis* treated trophozoites**
Albumin	Albumin
Cystatin-A	Cystatin-A
Actin cytoplasmic 2	Actin cytoplasmic 2
Actin cytoplasmic 1	Actin cytoplasmic 1
Peptidyl-prolyl cis-trans isomerase	Peptidyl-prolyl cis-trans isomerase
Polyubiquitin-C	Polyubiquitin-C
Polyubiquitin-B	Polyubiquitin-B
Keratin type II cytoskeletal 1	Keratin, type II cytoskeletal 1
Fatty acid-binding protein 5	Fatty acid-binding protein 5
14-3-3 protein zeta/delta	14-3-3 protein zeta/delta
14-3-3 protein sigma	Triosephosphate isomerase
Keratin type I cytoskeletal 10	Thioredoxin
	Alpha-enolase

6.4 DISCUSSION

With a host of direct and indirect virulence factors contributing to the pathogenicity of *A. castellanii* (Lorenzo-Morales et al., 2015), one of the ways of determining the virulence of the pathogenic T4 *A. castellanii* is by the identification of proteins expressed at different stages of the parasite's life cycle especially during the encystation and excystation stages, where significant phenotypic differentiation occurs. In molecular studies, characterising *A. castellanii* pathogenicity focuses primarily on proteins (MBPs and adhesins) and enzymes, which induce cytopathic effects and mediate parasite-host adhesion (Garate et al., 2006). In anti-acanthamoebic studies, the inhibition of known virulence determinants of *A. castellanii* which may lead to parasite death can be examined by evaluating ultrastructural changes using electron microscopy techniques, fluorescence microscopy, and proteomic profiling by using mass spectrometric techniques, as well as by measuring the changes in the chemical composition of *A. castellanii.* The present chapter was preceded with a chapter that evaluated the anti-acanthamoebic effects of the biochemical analytes identified in *C. sinensis.* The present chapter attempts to describe how the different forms of *C. sinensis* evaluated throughout this study and their biochemical compounds might have inhibited *A. castellanii* trophozoite replication and growth, and also caused *A. castellanii* death.

The findings of this study from the DAPI fluorescence staining showed a qualitatively and quantitative decreased pattern of nuclear fluorescence intensities for trophozoites treated with *C. sinensis* brew and solvent extract in comparison with trophozoites treated with PGY. As a DNA-specific fluorochrome, the attachment of DAPI dye to AT-rich sequences of DNA allows viable cells to fluoresce (Kapuscinski, 1995; Eriksson et al., 1993), which was detected in the untreated trophozoites' PGY fluorescence micrographs. Similar confocal micrographs observed in studies where the condensation or fragmentation of the nuclear chromatin was used to determine apoptotic *A. castellanii* (Lee et al., 2006; Moon et al., 2018b), were also observed in this present study. When compared to the PGY, *C. sinensis* treated trophozoites showed a much fainter fluorescence which was not too luminated when compared to CHX

treatment, indicating chromatin condensation, nuclear DNA fragmentation, and reduced viability. DAPI dye has also been used as a direct counting method for protozoa quantification (Stevik et al., 1998), the findings of that study can be related to the present study as fluorescence imagery obtained showed a lesser quantity of trophozoite number from the *C. sinensis* treated trophozoites when compared to the PGY. The fluorescence imagery which indicates reduction of trophozoite numbers is directly proportional to the quantity of DNA and therefore the DNA synthesis functionality and ultimately the replicative capability of the trophozoites. The volcano plots of fluorescence intensity confirmed a progressive nucleic acid reduction from the PGY to 50% *C. sinensis* brew and to the *C. sinensis* solvent extract, with no expressed fluorescence seen for CHX treatments, this was corroborated with the quantitative analysis of the mean fluorescence intensity and integrated fluorescence density which confirmed the reduction in fluorescence intensity of *C. sinensis* treated trophozoites.

In an alternative staining assay using AO, bright yellow-to-orange fluorescence was used to identify apoptotic trophozoites and cysts as also identified in a study where corneal scrapes from an *Acanthamoeba* keratitis patient were obtained and also where *A. castellanii* trophozoites were cultured axenically in vitro (Hahn et al., 1998; Nakisah et al., 2012). In both cases, as also seen in this present study, there was shrinking of the trophozoites and cysts in the treatment groups with a display of condensation of cytoplasm and chromatin indicative of apoptotic trophozoites and/or cysts. Although a nonspecific stain, the cell-permeant and nucleic acid binding capability of AO allows for its binding to dsDNA with green fluorescence, ssDNA or RNA with red florescence, and also acid polysaccharides with bright red to orange fluorescence (Kasten, 1967; Rigler, 1969), for which their fluorescent intensity can be quantified or qualified. In the present study, based on the principles of AO's intercalation with DNA and electrostatic attractions with RNA, the confocal micrographs of the brightfield, FITC, rhodomine and their fluorescence overlay showed reductions in DNA and RNA quantities with the *C. sinensis* solvent extract fluorescence intensity being the least when compared to the 50% *C. sinensis* brew and PGY fluorescence intensities. Immunofluorescence AO studies of

DNA and RNA quantifications (Traganos et al., 1977), shows that the destruction of nucleic acid complexes which occurred in *C. sinensis* treatment inhibited or halted the transcriptional activity and terminally inhibited protein synthesis capability of the *A. castellanii* trophozoites. Further AO fluorescence intensity qualification as shown in the volcano plots, as earlier observed from the DAPI analysis, confirmed a progressive nucleic acid reduction from the PGY to 50% *C. sinensis* brew and to *C. sinensis* solvent extract, with no expressed fluorescence detected in trophozoites treated with CHX. As also mentioned with DAPI, AO quantitative analysis of the mean fluorescence intensity and integrated fluorescence density confirmed the reduction in trophozoite quantity which is proportion to the reduction in nucleic acid quantity further reflected in the nuclear fluorescence intensity recorded for *C. sinensis* treated trophozoites.

To understand the changes in chemical composition and protein composition in *C. sinensis* treated *A. castellanii*, FTIR was used. The FTIR is a non-invasive analytical technique used to provide data on chemical molecules of organisms (Yu and Irudayaraj, 2005; Jusman et al., 2009; Saravanakumar et al., 2012). FTIR measurement of single cells often produces strong scattering baseline effect when the shape of cells is round and, especially, when the size of the cells is in a similar length scale as the wavelength of mid-IR light (Hughes et al., 2015). In this study, the size of the fixed *A. castellanii* trophozoites was on the order of 10-15 μm and their largely round shape led to a challenge to obtain high quality single cell spectra with flat CaF_2 substrate. Therefore, ZnS hemispheres and FTIR microscopy were used in the present study. Previous work has shown that the hemisphere imaging approach has two main advantages: 1) it can suppress the scattering effect, and 2) increase the magnification and spatial resolution of the measurement (Chan and Kazarian, 2013). FTIR microscopy using two ZnS hemispheres was shown to be sensitive to differentiate the chemical changes in *A. castellanii* exposed to PGY and CHX, and the spectral profiles allowed the understanding of the chemical compositional modifications that occur in *A. castellanii* upon exposure to brew and solvent extract of *C. sinensis*.

Changes in protein composition as represented by protein amide I and II peaks, and the production of complex biochemical changes measured in wavenumber ranges of cm^{-1} are used to identify changes in FTIR data (Yu and Irudayaraj, 2005). FTIR data from treatment with *C. sinensis* brew showed differences in the amide I and II regions in *C. sinensis* brew treatment, suggesting that some of the treated trophozoites had changes in their protein structure and/or composition in the trophozoites (Gourion-Arsiquaud et al., 2008). The alterations of proteins in the amide I and II regions might also suggest that the trophozoites underwent oxidative stress, which led to apoptosis of the trophozoites (Woyda-Ploszczyca et al., 2011). Furthermore, there were characteristic differences between the PGY IR wavelengths and *C. sinensis* brew IR wavelengths regarding the absence of RNA, DNA, lipid, and protein bands, only the glycogen absorbance bands were elevated for *C. sinensis* brew with phosphate peaks of 1152 cm^{-1}, 1092 cm^{-1} and 1028 cm^{-1}. These bands were absence at 24 h treatments but present in 48 h treatment. This indicates that the presence of *C. sinensis* brew in *A. castellanii* samples inhibited proliferation of the trophozoites confirmed by the absence of protein and RNA absorbance bands (Mourant et al., 2003). For *C. sinensis* solvent extract *A. castellanii* treatments, there was a close similarity to the changes observed in amide I and II regions, which extended to the phosphate (glycogen) band region, all characteristic peaks relevant to the amide region and the carbohydrate region were all absent. This also indicates that exposure to *C. sinensis* solvent extract inhibited *A. castellanii* trophozoite proliferation and promoted trophozoite apoptosis.

Moving away from nucleic acid evaluation via fluorescence assays with DAPI, AO, and chemical changes detected by FTIR spectroscopy, DIA-MS proteomic analysis was performed to identify specific proteins whose synthesis might have been disrupted by exposure of *A. castellanii* to *C. sinensis.* DIA-MS employs proteomic methodology that produces digital proteome which enables reflective analysis of cells and biological samples by fragmenting all precursor ions. After the ions fragmentation, there is an integration post-acquisition *in silico* data processing steps, and interrogation of MS data with spectral libraries such as SwissProt

database (January 2015) after simplifying the resulting complex fragment ion spectra, and ultimately identifying specific proteins and number of peptides in the analysed sample (Krasny and Huang, 2021). In the present study, proteomics analysis of *A. castellanii* trophozoites treated with *C. sinensis* identified 150 proteins and 485 peptides in *A. castellanii* before treatment, and 91 proteins with 244 peptides after treatment. As mentioned earlier, proteins 14-3-3 protein sigma and Keratin type I cytoskeletal 10 were not detected in trophozoites after *C. sinensis* treatment, whereas 3 new proteins, namely triosephosphate isomerase, thioredoxin, and alpha-enolase were detected in trophozoites after *C. sinensis* treatment (Table 6.3: Major proteins expressed (40% confidence) between *C. sinensis*-treated and untreated *A. castellanii* trophozoites.& Table 6.3).

The 14-3-3 proteins are a group of conserved acidic proteins with at least seven different mammalian isoforms. These proteins are involved in cell cycle regulation, which probably happens when their isoforms bind or interact with specific proteins (Laronga et al., 2000; Ozoe et al., 2002). Studies suggest that 14-3-3 proteins play a role in defining the timing of mitosis as they are encoded by the *Rad24* and *Rad25* genes to play a role that is necessary for cell proliferation, including checkpoint and meiosis (Ford et al., 1994; Ozoe et al., 2002). Inhibiting the synthesis of these protein in *A. castellanii* by *C. sinensis* may have inhibited the differentiation and replication of *A. castellanii* trophozoites, leading to cell cycle arrest thereby leaving them in apoptotic state. Another important role of 14-3-3 proteins is their involvement in the RAS/MAPK cascade signalling in yeast and higher organisms (Ozoe et al., 2002). The RAS/MAPK pathway transduces signals from the extracellular setting to the cell nucleus where specific genes are activated for cell growth, division and differentiation, hence bringing about cell cycle regulation, tissue repair, integrin signalling and cell migration (Cary et al., 1999; Stacey, 2003; Molina and Adjei, 2006). The Ras/MAPK pathway also stimulates the formation of new blood vessels by cellular migration, growth, and differentiation of endothelial cells via the regulation of gene expressions, also making it a very important pathway in cellular functions (Kranenburg et al., 2004). In protozoa, the MAPK pathway regulates vital cellular

processes, such as parasite proliferation, immune defense, apoptosis, and stress regulation (Dong et al., 2002; Arthur and Ley, 2013; Soares-Silva et al., 2016). With these specialized functions of MAPK pathways in protozoan replicative and regenerative functions, the inhibition of 14-3-3 proteins caused by *C. sinensis* might also have led to the apoptotic and ultimate death of *A. castellanii* trophozoites as they might have been unable to proliferate or withstand the stress caused by exposure to *C. sinensis*. The lack of the above-described cellular functions in *A. castellanii* further corroborate the finding that *C. sinensis* inhibited the synthesis of important proteins in *A. castellanii.*

Keratins are cytoskeletal proteins which support the structural stability of cells during damage and stressful conditions in higher organisms (Reichelt et al., 2001; Saleh et al., 2021). Although the functions of intermediate filament proteins, under which Keratin type I cytoskeletal proteins fall, have not been determined in protists, with their function in higher organisms their role may not be far from maintaining structural integrity in protists since they are also present in them (Preisner et al., 2018). Although the significance of the absence of Keratin type I cytoskeletal 10 cannot be ascertained in *C. sinensis* treated *A. castellanii,* if they function the same way they do in higher organisms, then their loss might also pre-dispose treated trophozoites to certain death as they might lack the ability to withstand the stress caused by exposure to *C. sinensis.*

Of the three enzymes expressed in the post treatment trophozoites, triosephosphate isomerase (TPI) stands out as one of most importance. TPI is an effective metabolic enzyme with a side-product, methylglyoxal. The protein is inclusive in the sub pathway of D-glyceraldehyde 3-phosphate synthesis from glycerone phosphate. This sub pathway is a pathway of glycolysis which is equally a pathway of carbohydrate degradation (Rodriguez-Almazan et al., 2008). The reactive cytotoxic methylglyoxal can modify and alters proteins, DNA and lipids. With the aerobic metabolic capability of TPI, which its expression in *Trypanosoma brucei* inhibits cell growth (Helfert et al., 2001), the expression of the enzyme in the *C. sinensis* treated *A. castellanii* suggests how its presence might have affected the

protein, DNA, lipid and carbohydrate composition of trophozoites exposed to *C. sinensis*. With the knowledge of the molecular alteration ability of TPI, it is pertinent to remember that the structure of the trophozoite plasma membrane consists of 33% proteins, 25% phospholipids, 13% sterols (ergosterol and 7-dehydrostigmasterol), and 29% lipophosphonoglycan (Siddiqui and Khan, 2012). Also, the knowledge of TPI's carbohydrate degradation capability and the fact that the *A. castellanii* endocyst is made up of 33% proteins, 4-6% lipids, 35% carbohydrates, with cellulose as a major component (Neff and Neff, 1969; Weisman, 1976; Hirukawa et al., 1998), suggests that even though the trophozoite might attempt to encyst when exposed to *C. sinensis*, the expression of TPI might have contributed to inhibition of encystation.

Thioredoxin was the second protein found expressed in the *A. castellanii – C. sinensis* post-treatment culture. This enzyme and its isoforms are present in plants and animals. They function as electron donors for enzymes such as ribonucleotide reductases, thioredoxin peroxidases (peroxiredoxins) and methionine sulfoxide reductases, and they are essential in the redox regulation of protein function and signalling via thiol redox control (Arnér and Holmgren, 2000). This suggests that the presence of thioredoxin in *C. sinensis* may have contributed in regulating the expression of some gene-encoded proteins in *A. castellanii* contributing to the parasite's death. Although it is suggested that two types of thioredoxin reductases (TrxRases) are present in *Acanthamoeba* and involved in the parasite's response to oxidative stress and defense system (Andrade and Reed, 2015; Leitsch et al., 2021), it is not known at this stage of the study why they were not able to inhibit the *C. sinensis* thioredoxin activity. It is however suggestive that since both TrxRases in *A. castellanii* are localized in the cytoplasm (Leitsch et al., 2021), the action of *C. sinensis* on trophozoite membrane leading to loss of membrane integrity and rupture of the trophozoites are seen in qualitative evaluations using light microscopy and TEM (Chapters 3 and Chapter 4). The loss of containment and subsequent loss of the TrxRases by the ruptured trophozoite membrane may have also

allowed thioredoxin to operate unimpeded in conjunction with other *C. sinensis* proteins that led to trophozoite death.

Alpha-enolase is a multifunctional glycolytic enzyme involved in cellular stress. It is seen expressed during infections caused by fungal and parasitic agents and also involved in growth, development and reproduction of organisms (Ji et al., 2016). In this present study, proteomic evaluation of *A. castellanii* before exposure to *C. sinensis* did not show any expressions of alpha-enolase. However, post treatment, there was expression of alpha-enolase. This change in expression might be relatable to a study that suggests that alpha-enolase is one of the heat shock proteins (HSPs) expressed before and after stress exposure in mammalian cell (Ji et al., 2016). Another study with the genus *Saccharomyces* also showed that HSPs were induced upon exposure of the organism to high temperature stress, relating the HSP to temperature tolerance, growth regulation (Ji et al., 2016), stress protein and activator responsible for expressing hypoxia-inducible factor-1 (HIF-1) (Aaronson et al., 1995). Although alpha-enolase is also known to be present on the surface of bacterial cells, and also on the surface of anaerobic parasitic amoebozoan *Entamoeba histolytica* there is however no literature that has explained how it is found in *A. castellanii.* In *E. histolytica,* enolase is considered to act as a virulence factor which is also important in the encystation process of *E. histolytica* (Segovia-Gamboa et al., 2010), and also surface protein considered an adhesion protein (Biller et al., 2014). Bearing in mind that not all the components of the *A. castellanii* trophozoite and cyst wall have been identified, there is a possibility that the protein alpha-enolase might be a component of the parasite wall as it is on *E. histolytica,* but why it was expressed after treatment and not before treatment with *C. sinensis* cannot be explained at this stage of this study.

In conclusion, the results demonstrated that *C. sinensis* brew and solvent extract forms possesses amoebicidal ability against *A. castellanii* trophozoites. In the fluorescence assays, DNA and RNA quantification were reduced with *C. sinensis* treatment. The reduction of fluorescence intensity indicated the loss of replicative complexes and DNA synthesis.

Corroboration of *A.* castellanii protein synthesis inhibition expressed by the lack of amide I and II band peaks in FTIR spectroscopy, and also inhibition of 14-3-3 protein isoforms as seen in DIA-MS, and the expression of triosephosphate isomerase, all point to the inhibitory effect of *C. sinensis* on protein synthesis and ultimately causing apoptosis of *A. castellanii.* The knowledge gleaned from this study provides insight on how *C. sinensis* may have inhibited *A. castellanii,* which may help in the development and optimization of novel therapeutic approaches against *A. castellanii* infection.

7 GENERAL DISCUSSION AND CONCLUSION

7.1 GENERAL DISCUSSION

In this study, the anti-acanthamoebic activities of *C. sinensis* has been investigated. Prior to this study, available literature does not show any anti-acanthamoebic studies done with *C. sinensis.* The experiments commenced with investigations into the capabilities of *C. sinensis* cold and hot brew forms to inhibit the growth of *A. castellanii* trophozoites by inhibiting the parasite's replication and its protective ability seen in the form of differentiation where trophozoites encyst during harsh conditions. The next phase entailed the investigation of the solvent extract form of *C. sinensis* and how it was also able to inhibit trophozoite growth, encystation, and excystation. With favourable results from the solvent extract experiment, it was then necessary to identify the bioactive components of *C. sinensis* and to examine if they had the capability to individually inhibit trophozoite replication and inhibit excystation. This investigation suggested that although the brew and solvent extract forms of *C. sinensis* possess anti-acanthamoebic capability, not all of the potentially bioactive components had an anti-acanthamoebic capability. The final aspect of the study attempted to elucidate how the anti-acanthamoebic effect may have occurred by investigating changes in protein expression in *A. castellanii* in response to treatment.

The data from the *C. sinensis* brew studies revealed that 75% and 100% *C. sinensis* inhibited trophozoite replication, mimicking the reduced growth trajectory seen with chlorhexidine. These concentrations did not have sustained toxicity on CSCs as cellular replication, though lower than the CSCs in growth media, increased after an arrested replication phase, suggesting a transient cytotoxicity. The scenario observed with corneal epithelial cells was, however, different as there was greater toxicity with *C. sinensis* brew for this cell type. The disparity in sensitivity level of both cell types to treatment with *C. sinensis* brew might be due to the cell growth rate and culture conditions, or to cell type-specific inherent properties that may have contributed to the observed corneal epithelial cell sensitivity, especially as the growth rate of corneal epithelial cells is higher than CSC. The significance of the preparation conditions of the brew is an interesting discovery where the cold brews exhibited a higher level

of anti-acanthamoebic activity. It is noteworthy that the time and temperature of the preparation method may have made the difference as the cold brew was prepared by infusing the macerated *C. sinensis* leaves with room temperature water and stored for 24 hours at 4^0C. This would have allowed the slow and continuous leaching of the *C. sinensis* components into the water. The hot water preparation method may have rapidly extracted a given quantity of astringent components (Lin et al., 2014; Safdar et al., 2016), as it took approximately 10 minutes to complete the process. The heat applied to the leaves may have also denatured some of the components, making them less efficacious than the cold-generated components. Irrespective of the preparation conditions, both brew forms were able to inhibit trophozoite replication and inhibit encystation. However, they had no transient effect on *A. castellanii* as the withdrawal of the brew forms between 3-24 hours from the parasite allowed the dying trophozoite cultures to be resuscitated when exposed to PGY medium. A confirmation of the anti-acanthamoebic activity made use of EM studies, where TEM and SEM analyses showed ultrastructural intracellular and surface changes in *A. castellanii* exposed to *C. sinensis* brew. Although this study was done *in vitro*, the limitation of the *C. sinensis* brew form vis-a-vis pharmacology and drug production protocols bordered on the inability to definitively quantify the concentration and dosage needed, as each batch of brew prepared might have been affected by a number of physical or environmental factors.

Using solvent extracts of *C. sinensis* was a step to definitively quantity treatment concentrations, even though the test substance in this phase is still classified as a crude substance. This was also done with the hypothesis that solvent extraction might yield higher concentrations of bioactive properties of *C. sinensis* in comparison with brews. This was confirmed further when chromatographic analysis showed that both *C. sinensis* brew forms identified significant peaks representing 6 bioactive components, while chromatographic analysis of the *C. sinensis* solvent extract identified 10 significant bioactive components. The cytotoxic evaluation of the solvent extract painted a different picture, which was not surprising bearing in mind that more components were extracted from the *C. sinensis* leaves. Cytotoxic

evaluations using iHCE-2s exposed to solvent extract revealed that the second highest concentration had an initial concentration cytotoxic effect at 24 hours exposure in comparison to the control, which was not sustained by 48 hours post exposure. This means that this concentration was toxic to host cells with no difference between the control treatment. Alternatively, the data with MDCKs painted a different picture. The higher concentrations, though showing moderate cytotoxicity by the end of the experiment, did not halt cell replication. Not halting the experiment based on the cytotoxic data from MDCK experiments, was based on the fact that one the primary predilection site of *A. castellanii* is the cornea (Siddiqui and Khan, 2012; Lorenzo-Morales et al., 2013b), the solvent extract concentrations were not toxic to iHCE-2s. Thereby if applied topically, *C. sinensis* may not exhibit any site-specific toxicity. As seen with the *C. sinensis* brew evaluations, anti-acanthamoebic studies yielded similar results against the trophozoites and cysts, the results demonstrated that *C. sinensis* solvent extract inhibits trophozoite growth/replication which was demonstrated by cytolysis of *A. castellanii*. For anti-encystation evaluations, the higher concentrations completely inhibited trophozoite-to-cyst differentiation. This form of *C. sinensis*, which contain higher concentrations of bioactive compounds that might possess serine protease-like activity and cysteine-specific protease-like activity, might have inhibited the encystation of trophozoites mimicking the activity of PMSF (Dudley et al., 2008; Hirukawa et al., 1998; Leitsch et al., 2010). From the later aspect of this study, it is presumed that *C. sinensis* brew and solvent forms interfered with cellulose and protein synthesis of *A. castellanii.* This is based on the evidence that the cyst wall of *A. castellanii* is made up of cellulose, galactose and protein and the inhibition of these components will inhibit the parasite's ability to encyst (Anwar et al., 2018). The bioactive compounds may also have inhibited xylose isomerase synthesis, as well as inhibition of glycogen phosphorylation (Lloyd, 2014). As seen with the brew form, the confirmation of these results with EM studies reveals that lower to middle concentrations caused progressive destruction of trophozoites.

After establishing the anti-acanthamoebic capability of *C. sinensis* brew and solvent extract forms, we investigated which of the bioactive components possessed this activity. The investigation also determined if the components could act individually or in combination. EGCG, caffeine, EGC, ECG, EC, myricetin, theogallin, Kaempferol, theobromine and catechin were identified as the most prominent bioactive components of *C. sinensis.* Prior to this study, only one study was found to have tested the anti-acanthamoebic activity of any of the identified *C. sinensis* components. In that study, the combination of EGCG with *C. sinensis* matcha tea displayed anti-acanthamoebic activity against trophozoites and cysts (Dickson et al., 2020). EGCG had also been tested in against *Stenotrophomonas maltophilia* (Navarro-Martínez et al., 2005) and also in an anti-viral study investigating EGCG's broad-spectrum inhibition of virus attachment to cells by regulating protein synthesis (Ciesek et al., 2011; Colpitts et al., 2014).

This current study showed that this component possesses more capability by inhibiting *A. castellanii* trophozoite replication and also inhibiting encystation. This study also tested all the identified bioactive components for their anti-acanthamoebic activity and results showed that only EGCG and caffeine possessed effective trophocidal activity. Caffeine had been identified for its capability to block the activation of cyclic AMP (cAMP) synthesis, thereby regulating chemotaxis and possibly gene transcription in the social amoeba *Dictyostelium discoideum* (Brenner and Thoms, 1984); the regulation of cAMP levels may have prevented encystation. With regards to the anti-encystational capability of caffeine, the expression of the enzyme glycogen phosphorylase leads to the breakdown of glycogen during encystation (Martín-Navarro et al., 2017). However, caffeine is known to inhibit the expression of glycogen phosphorylase, making it one of the possible ways caffeine may have inhibited trophozoite differentiation into cysts while killing off the parasite. The evaluation of the combination of all the identified components in equal quantity did not yield any favourable results suggesting that the individual active components may have been inhibited by the presence of the non-active ones. Also, as the concentration of each bioactive component as seen in the solvent extract

was not determined, the use of the complete components in the same ratio might suggest that the components with recorded anti-acanthamoebic activity were not up to the concentration they were in the solvent extract, hence attenuating their activity. There also might have been a scenario where some unidentified components like proteins and other trace elements may have had a contributing or synergistic force to the mixed compound as seen in the brew and solvent extract forms, where they were tested as one compound and not as fractions. For encystation studies, EGCG inhibited encystation and interestingly theobromine, which was not seen to possess any activity against trophozoites, also inhibited encystation even at the lowest concentration. This suggests that the rest of the non-active components could possess more activity than detected with further investigations probably in 1:1 combinations.

The concluding aspect of this study focused on characterising the activity of *C. sinensis* on a molecular level, where the protein expressed was evaluated. The pathogenicity of *A. castellanii* commences with their surface proteins, which allow for adhesion to host cells. The MBPs, LBP and adhesins induce cytopathic effects by mediating parasite-host adhesion (Garate et al., 2006). Therefore, the lack of and reduction of these proteins post-treatment of *A. castellanii* with forms of *C. sinensis* indicated a successful first step in preventing or reducing the parasite's virulence. Fluorescence microscopy with dyes using DAPI, showed a decreased pattern of nuclear fluorescence intensities qualitatively for trophozoites treated with *C. sinensis* brew and solvent extract in comparison with trophozoites treated with PGY. This suggests that there was reduction of trophozoite numbers and ultimately the replicative capability of the trophozoites were inhibited or halted by *C. sinensis*. As seen with DAPI evaluations, AO dye evaluations also showed that the qualitative and quantitative intensity of the fluorescence was greatly reduced for trophozoites treated with both forms of *C. sinensis.*

Beyond the fluorescence of the nucleic acids, determining the chemical composition of treated and untreated trophozoite cultures was evaluated with FTIR technique. Changes in protein composition as represented by protein amide I and II peaks, and the production of complex biochemical changes suggested that some of the treated trophozoites had changes in their

protein composition. These changes also might have been a fallout of oxidative stress, leading to apoptosis of the trophozoites (Woyda-Ploszczyca et al., 2011). The absence of protein and RNA absorbance bands indicates that the presence of *C. sinensis* brew in *A. castellanii* samples inhibited proliferation of the trophozoites. In addition to that the solvent extract treated trophozoites did not display any characteristic peaks relevant to the amide and carbohydrate regions suggesting that *C. sinensis* solvent extract inhibited *A. castellanii* trophozoite proliferation and promoted trophozoite apoptosis.

To round up the proteomic evaluations, we identified specific proteins which were expressed before and after *C. sinensis* treatment of *A. castellanii* trophozoites to determine how *C. sinensis* actually inhibited trophozoite replication and possibly how it may have also inhibited encystation. 150 proteins and 485 peptides were identified in *A. castellanii* before *C. sinensis* treatment, and 91 proteins with 244 peptides were identified after *C. sinensis* treatment. Proteins 14-3-3 protein sigma and Keratin type I cytoskeletal 10 were not detected in trophozoites after *C. sinensis* treatment, while triosephosphate isomerase, thioredoxin, and alpha-enolase were detected after *C. sinensis* treatment. The 14-3-3 proteins are involved in cell cycle regulation, which probably happens when their isoforms bind or interact with specific proteins (Laronga et al., 2000; Ozoe et al., 2002). These proteins also play a role in defining the timing of mitosis as they are encoded by the *Rad24* and *Rad25* genes which are necessary for cell proliferation, including checkpoint and meiosis. Inhibition of these proteins leads to cell cycle arrest (Ford et al., 1994; Ozoe et al., 2002). From this study, it is presumed that inhibition of the synthesis of these proteins in *A. castellanii* by *C. sinensis* may have inhibited the differentiation and replication of *A. castellanii* trophozoites, leading to trophozoite death. With the 14-3-3 proteins involvement in the RAS/MAPK cascade signalling in yeast and higher organisms (Ozoe et al., 2002), It is also assumed that *C. sinensis* inhibited the functions of the Ras/MAPK pathway which regulates vital cellular processes, such as parasite proliferation, immune defense, apoptosis, and stress regulation (Dong et al., 2002; Arthur and Ley, 2013; Soares-Silva et al., 2016).

While taking a closer look at the structural integrity of *A. castellanii*, TEM analysis from this study indicated that its membrane integrity was lost with exposure to *C. sinensis*. Keratins support the structural stability of cells and protists (Reichelt et al., 2001; Preisner et al., 2018; Saleh et al., 2021), hence the loss of *A. castellanii* membrane integrity might in part be related to the absence of Keratin type I cytoskeletal proteins, which were not expressed post-treatment with *C. sinensis.* Also, the carbohydrate degradation capability of TPI might also have contributed to the loss of structural integrity of the parasite when exposed to *C. sinensis*. Apart from the proteins and lipids seen in the endocyst of *A. castellanii*, the membrane consists of 35% carbohydrates, with cellulose as a major component (Neff and Neff, 1969; Weisman, 1976; Hirukawa et al., 1998) and TPI is inclusive in the glycolysis pathway which is a pathway of carbohydrate degradation (Rodriguez-Almazan et al., 2008). In this study, TPI was seen expressed in the parasite culture after treatment, suggesting that the protein might have contributed to inhibiting encystation. While dealing with the actions of TPIs, the presence of TrxRases, which are essential in the redox regulation of protein function and signalling via thiol redox control (Arnér and Holmgren, 2000), may have been involved in the parasite's response to oxidative stress and compromise of its defense system (Andrade and Reed, 2015; Leitsch et al., 2021). Furthermore, alpha-enolase, which is a multifunctional glycolytic enzyme involved in cellular stress, growth, development, and reproduction of organisms (Ji et al., 2016), was expressed post-*C. sinensis* treatment. Collectively, these results suggest that treatment of *A. castellanii* with *C. sinensis* might have led to the parasite's death via apoptosis.

7.2 CONCLUSIONS AND RECOMMENDATIONS

Overall, the data presented in this study increases the possibility of the use of natural products as a novel source for anti-acanthamoebic therapeutic compounds in the future. The understanding gleaned from this study reveals that *C. sinensis* and its bioactive components might be a valuable candidate for anti-acanthamoebic drug development. In future studies, the effects of *C. sinensis* forms (brew and solvent extract) on the mechanisms of protein inhibition, and specific pathways for these purposes which were not understood at this stage but revealed as being possible in the experiments with trophozoites, could help to understand how to develop targeted treatment to combat *A. castellanii*. The same thing goes for the parasite cyst which is realized post-encystation. The mechanism of inhibition for cellulose, galactose and other components which make up the drug-resistant cyst wall is a subject that could be investigated since the literature already shows that serine proteases and a reference compound used in this study (PMSF), inhibit the encystation process (Hirukawa et al., 1998; Khan, 2006b; Dudley et al., 2008; Leitsch et al., 2010) as did *C. sinensis* brew and solvent extract. Quantitative studies focused on apoptotic markers (e.g., expression of apoptosis-related genes / proteins) could be carried out to complement the data obtained using DAPI and AO staining assays. Other fluorescence dyes such as Calcofluor-white, Sytox green, Sytox red and other can also be used to evaluate and quantify the nucleic acid integrity of trophozoites exposed to natural anti-acanthamoebic agents. It is hoped that the data presented in this study reveals additional and invaluable knowledge in combatting acanthamoebiasis which might be rare but have a high mortality rate.

REFERENCES

Aaronson, R. M., Graven, K. K., Tucci, M., McDonald, R. J. & Farber, H. W. 1995. Non-neuronal Enolase Is an Endothelial Hypoxic Stress Protein (*). Journal of Biological Chemistry, 270**,** (46), 27752-27757. https://doi.org/10.1074/jbc.270.46.27752.

Aboulaila, M., Yokoyama, N. & Igarashi, I. 2010. Inhibitory effects of (-)-Epigallocatechin-3-gallate from green tea on the growth of *Babesia* parasites. Parasitology, 137**,** (5), 785-791. 10.1017/s0031182009991594.

Adhami, V. M. & Mukhtar, H. 2007. Anti-Oxidants from Green Tea and Pomegranate for Chemoprevention of Prostate Cancer. Molecular Biotechnology, 37**,** (1), 52-57. 10.1007/s12033-007-0047-8.

Adl, S. M., Simpson, A. G. B., Farmer, M. A., Andersen, R. A., Anderson, O. R., Barta, J. R., Bowser, S. S., Brugerolle, G., Fensome, R. A., Fredericq, S., James, T. Y., Karpov, S., Kugrens, P., Krug, J., Lane, C. E., Lewis, L. A., Lodge, J., Lynn, D. H., Mann, D. G., McCourt, R. M., Mendoza, L., Moestrup, O., Mozley-Standridge, S. E., Nerad, T. A., Shearer, C. A., Smirnov, A. V., Spiegel, F. W. & Taylor, M. 2005. The new higher level classification of eukaryotes with emphasis on the taxonomy of protists. Journal of Eukaryotic Microbiology, 52**,** (5), 399-451. 10.1111/j.1550-7408.2005.00053.x.

Ahearn, D. G. & Gabriel, M. M. (1997). Contact Lenses, Disinfectants, and *Acanthamoeba* Keratitis. *In:* NEIDLEMAN, S. L. & LASKIN, A. I. (eds.) *Advances in Applied Microbiology.* Academic Press.

Aichelburg, A. C., Walochnik, J., Assadian, O., Prosch, H., Steuer, A., Perneczky, G., Visvesvara, G. S., Aspock, H. & Vetter, N. 2008. Successful Treatment of Disseminated *Acanthamoeba spp.* Infection with Miltefosine. Emerging Infectious Diseases, 14**,** (11), 1743-1746. 10.3201/eid1411.070854.

Alsam, S., Kim, K. S., Stins, M., Rivas, A. O., Sissons, J. & Khan, N. A. 2003. Acanthamoeba interactions with human brain microvascular endothelial cells. Microbial Pathogenesis, 35**,** (6), 235-241. https://doi.org/10.1016/j.micpath.2003.07.001.

Alsam, S., Sissons, J., Jayasekera, S. & Khan, N. A. 2005. Extracellular proteases of *Acanthamoeba castellanii* (encephalitis isolate belonging to T1 genotype) contribute to increased permeability in an in vitro model of the human blood-brain barrier. Journal of Infection, 51**,** (2), 150-156. https://doi.org/10.1016/j.jinf.2004.09.001.

Anderson, I. J., Watkins, R. F., Samuelson, J., Spencer, D. F., Majoros, W. H., Gray, M. W. & Loftus, B. J. 2005. Gene Discovery in the Acanthamoeba castellanii Genome. Protist, 156**,** (2), 203-214. https://doi.org/10.1016/j.protis.2005.04.001.

Andrade, R. M. & Reed, S. L. 2015. New drug target in protozoan parasites: the role of thioredoxin reductase. Frontiers in Microbiology, 6. 10.3389/fmicb.2015.00975.

Anwar, A., Khan, N. A. & Siddiqui, R. 2018. Combating *Acanthamoeba spp.* cysts: what are the options? Parasites & Vectors, 11**,** (1), 26. https://doi.org/10.1186/s13071-017-2572-z.

Anwar, A., Numan, A., Siddiqui, R., Khalid, M. & Khan, N. A. 2019a. Cobalt nanoparticles as novel nanotherapeutics against Acanthamoeba castellanii. Parasites & Vectors, 12**,** (1), 280. 10.1186/s13071-019-3528-2.

Anwar, A., Siddiqui, R., Hameed, A., Shah, M. R. & Khan, N. A. 2019b. Synthetic Dihydropyridines as Novel Antiacanthamoebic Agents. Medicinal chemistry (Shariqah (United Arab Emirates)), 10.2174/1573406415666190722113412. 10.2174/1573406415666190722113412.

Anwar, A., Siddiqui, R., Raza Shah, M. & Khan, N. A. 2019c. Antidiabetic drugs and their nanoconjugates repurposed as novel antimicrobial agents against Acanthamoeba castellanii. J Microbiol Biotechnol, 10.4014/jmb/1903.03009. 10.4014/jmb/1903.03009.

Araki-Sasaki, K., Ohashi, Y., Sasabe, T., Hayashi, K., Watanabe, H., Tano, Y. & Handa, H. 1995. An SV40-immortalized human corneal epithelial cell line and its characterization. Investigative Ophthalmology & Visual Science, 36**,** (3), 614-621. https://doi.org/

Arnér, E. S. J. & Holmgren, A. 2000. Physiological functions of thioredoxin and thioredoxin reductase. European Journal of Biochemistry, 267**,** (20), 6102-6109. https://doi.org/10.1046/j.1432-1327.2000.01701.x.

Arthur, J. S. C. & Ley, S. C. 2013. Mitogen-activated protein kinases in innate immunity. Nature Reviews Immunology, 13**,** (9), 679-692. https://www.nature.com/articles/nri3495

Aslam, A., Mahmood, M. S., Hussain, I. & Khan, M. N. 2014. Evaluation of Antiviral Effect of Epigallocatechin Gallate, Epigallocatechin, Epicatechin Gallate and Green Tea Extract Against Fowl Adenovirus-4. Pakistan Journal of Zoology, 46**,** (5), 1283-1294. <Go to ISI>://WOS:000344443900013

Atanasov, A. G., Zotchev, S. B., Dirsch, V. M., Orhan, I. E., Banach, M., Rollinger, J. M., Barreca, D., Weckwerth, W., Bauer, R., Bayer, E. A., Majeed, M., Bishayee, A., Bochkov, V., Bonn, G. K., Braidy, N., Bucar, F., Cifuentes, A., D'Onofrio, G., Bodkin, M., Diederich, M., Dinkova-Kostova, A. T., Efferth, T., El Bairi, K., Arkells, N., Fan, T.-P., Fiebich, B. L., Freissmuth, M., Georgiev, M. I., Gibbons, S., Godfrey, K. M., Gruber, C. W., Heer, J., Huber, L. A., Ibanez, E., Kijjoa, A., Kiss, A. K., Lu, A., Macias, F. A., Miller, M. J. S., Mocan, A., Müller, R., Nicoletti, F., Perry, G., Pittalà, V., Rastrelli, L., Ristow, M., Russo, G. L., Silva, A. S., Schuster, D., Sheridan, H., Skalicka-Woźniak, K., Skaltsounis, L., Sobarzo-Sánchez, E., Bredt, D. S., Stuppner, H., Sureda, A., Tzvetkov, N. T., Vacca, R. A., Aggarwal, B. B., Battino, M., Giampieri, F., Wink, M., Wolfender, J.-L., Xiao, J., Yeung, A. W. K., Lizard, G., Popp, M. A., Heinrich, M., Berindan-Neagoe, I., Stadler, M., Daglia, M., Verpoorte, R., Supuran, C. T. & the International Natural Product Sciences, T. 2021. Natural products in drug discovery: advances and opportunities. Nature Reviews Drug Discovery, 20**,** (3), 200-216. 10.1038/s41573-020-00114-z.

Bacon, A. S., Frazer, D. G., Dart, J. K. G., Matheson, M., Ficker, L. A. & Wright, P. 1993. A review of 72 consecutive cases of Acanthamoeba keratitis, 1984–1992. Eye, 7**,** 719. 10.1038/eye.1993.168.

Bae, H. J., Kim, J., Jeon, S. J., Kim, J., Goo, N., Jeong, Y., Cho, K., Cai, M., Jung, S. Y., Kwon, K. J. & Ryu, J. H. 2020. Green tea extract containing enhanced levels of epimerized catechins attenuates scopolamine-induced memory impairment in mice. J Ethnopharmacol, 258**,** 112923. 10.1016/j.jep.2020.112923.

Baig, A. M., Iqbal, J. & Khan, N. A. 2013a. In vitro efficacies of clinically available drugs against growth and viability of an Acanthamoeba castellanii keratitis isolate belonging to the T4 genotype. Antimicrob Agents Chemother, 57**,** (8), 3561-7. 10.1128/aac.00299-13.

Baig, A. M., Iqbal, J. & Khan, N. A. 2013b. In vitro efficacies of clinically available drugs against growth and viability of an Acanthamoeba castellanii keratitis isolate belonging to the T4 genotype. Antimicrob Agents Chemother, 57. 10.1128/aac.00299-13.

Baig, A. M., Katyara, P., Khaleeq, A. & Nazim, F. 2019. Repurposing drugs: Ca2+ ion dependency that can be exploited to treat keratitis caused by Acanthamoeba castellanii. Eye, 33**,** (11), 1823-1825. 10.1038/s41433-019-0597-6.

Band, R. N. & Mohrlok, S. 1973. The Cell Cycle and Induced Amitosis in Acanthamoeba*. The Journal of Protozoology, 20**,** (5), 654-657. 10.1111/j.1550-7408.1973.tb03592.x.

Bari, M. L. & Yeasmin, S. (2021). Microbes Culture Methods. *Reference Module in Biomedical Sciences.* Elsevier.

Batiha, G. E.-S., Beshbishy, A. M., Tayebwa, D. S., Shaheen, H. M., Yokoyama, N. & Igarashi, I. 2019. Inhibitory effects of Syzygium aromaticum and Camellia sinensis methanolic extracts on the growth of Babesia and Theileria parasites. Ticks and Tick-borne Diseases, 10**,** (5), 949-958. https://doi.org/10.1016/j.ttbdis.2019.04.016.

Behera, H. S. & Satpathy, G. 2016. Characterisation and expression analysis of trophozoite and cyst proteins of Acanthamoeba spp. isolated from Acanthamoeba keratitis (AK)

patient. Molecular and Biochemical Parasitology, 205, (1), 29-34. https://doi.org/10.1016/j.molbiopara.2016.03.009.
Benelli, R., Venè, R., Bisacchi, D., Garbisa, S. & Albini, A. 2002. Anti-Invasive Effects of Green Tea Polyphenol EpiGalloCatechin-3-Gallate (EGCG), a Natural Inhibitor of Metallo and Serine Proteases. Biological Chemistry, 383, (1), 101-105. https://doi.org/10.1515/BC.2002.010.
Berthomieu, C. & Hienerwadel, R. 2009. Fourier transform infrared (FTIR) spectroscopy. Photosynthesis Research, 101, (2), 157-170. 10.1007/s11120-009-9439-x.
Biller, L., Matthiesen, J., Kühne, V., Lotter, H., Handal, G., Nozaki, T., Saito-Nakano, Y., Schümann, M., Roeder, T., Tannich, E., Krause, E. & Bruchhaus, I. 2014. The Cell Surface Proteome of Entamoeba histolytica*. Molecular & Cellular Proteomics, 13, (1), 132-144. https://doi.org/10.1074/mcp.M113.031393.
Bonkowski, M. 2004. Protozoa and plant growth: the microbial loop in soil revisited. New Phytologist, 162, (3), 617-631. 10.1111/j.1469-8137.2004.01066.x.
Bowers, B. & Korn, E. D. 1969. The fine structure of Acanthamoeba castellanii (Neff strain). J Cell Biol, 41. 10.1083/jcb.41.3.786.
Bowers, B. & Korn, E. D. 1973. Cytochemical identification of phosphatase activity in the contractile vacuole of *Acanthamoeba castellanii*. The Journal of Cell Biology, 59, (3), 784-791. http://www.ncbi.nlm.nih.gov/pmc/articles/PMC2109120/

http://jcb.rupress.org/content/jcb/59/3/784.full.pdf
Brenner, M. & Thoms, S. D. 1984. Caffeine blocks activation of cyclic AMP synthesis in *Dictyostelium discoideum*. Developmental Biology, 101, (1), 136-146. https://doi.org/10.1016/0012-1606(84)90124-6.
Brindley, N., Matin, A. & Khan, N. A. 2009. Acanthamoeba castellanii: High antibody prevalence in racially and ethnically diverse populations. Experimental Parasitology, 121, (3), 254-256. https://doi.org/10.1016/j.exppara.2008.11.009.
Bryant, K., Chang, T., Chen, S. & Rosenberg, J., Hammond, R, McConnell, K, Sanderson, R, Elm, J, Nakata, M, Wakida, C, Austin, C, Bestudik, J, Bordson, MG, Conover, C, Granzow, L, Pelletier, A, Rea, V, Chu, A, Luckman, E, Signs, K, Harper, J, Damrow, T, Mosher, E, Kruger, K, Saheli, E, Cassidy, M, Hatch, J, Weltman, A, Garcia Rivera, EJ, Garcia, Y, Kainer, MA, Archer, J, Joslin, C, Cernoch, P, Jones, D, Hamill, M, Matoba, A, Pflugfelder, S, Wilhelmus, K, Beavers, S, Chen, T, Christian, K, Cooper, M, Dufficy, D, Gershman, M, Glenshaw, M, Hall, A, Holzbauer, S, Huang, A, Langer, A, Moore, Z, Patel, AS, Carpenter, LR, Schaffzin, J, Su, J, Trevino, I, Weiser, T, Wiersma, P, Lorick, S & Verani, JR 2007. Acanthamoeba keratitis multiple states, 2005-2007. Morbidity and Mortality Weekly Report,, 56, (21), 532-4.
Burger, G., Plante, I., Lonergan, K. M. & Gray, M. W. 1995. The mitochondrial-DNA of the ameboid protozoan, *Acanthamoeba castellanii* - complete sequence, gene content and genome organization. Journal of Molecular Biology, 245, (5), 522-537. 10.1006/jmbi.1994.0043.
Butt, M. S., Imran, A., Sharif, M. K., Ahmad, R. S., Xiao, H., Imran, M. & Rsool, H. A. 2014. Black Tea Polyphenols: A Mechanistic Treatise. Critical Reviews in Food Science and Nutrition, 54, (8), 1002-1011. 10.1080/10408398.2011.623198.
Byers, T. J., Kim, B. G., King, L. E. & Hugo, E. R. 1991. Molecular aspects of the cell cycle and encystment of *Acanthamoeba*. Rev Infect Dis, 13 Suppl 5, S373-84. 10.1093/clind/13.supplement_5.s373.
Carnt, N., Hoffman, J. J., Verma, S., Hau, S., Radford, C. F., Minassian, D. C. & Dart, J. K. G. 2018. *Acanthamoeba* keratitis: confirmation of the UK outbreak and a prospective case-control study identifying contributing risk factors. British Journal of Ophthalmology, 102, (12), 1621. 10.1136/bjophthalmol-2018-312544.
Carvalho-Silva, A. C., Coelho, C. H., Cirelli, C., Crepaldi, F., Rodrigues-Chagas, I. A., Furst, C., Pimenta, D. C., Toledo, J. S. d., Fernandes, A. P. & Costa, A. O. 2021. Differential expression of Acanthamoeba castellanii proteins during amoebic keratitis in rats.

Experimental Parasitology, 221, 108060. https://doi.org/10.1016/j.exppara.2020.108060.
Cary, L., Han, D. & Guan, J. 1999. Invited Reviews-Integrin-mediated signal transduction pathways. Histology and histopathology, 14, (3), 1001-1009.
Cerva, L. 1989. Acanthamoeba culbertsoni and Naegleria fowleri: occurrence of antibodies in man. Journal of hygiene, epidemiology, microbiology, and immunology, 33, (1), 99-103. http://europepmc.org/abstract/MED/2723426
Chacko, S. M., Thambi, P. T., Kuttan, R. & Nishigaki, I. 2010. Beneficial effects of green tea: A literature review. Chinese Medicine, 5, (1), 13. 10.1186/1749-8546-5-13.
Chan, K. A., Fale, P. L., Atharawi, A., Wehbe, K. & Cinque, G. 2018. Subcellular mapping of living cells via synchrotron microFTIR and ZnS hemispheres. Analytical and bioanalytical chemistry, 410, (25), 6477-6487. https://www.ncbi.nlm.nih.gov/pmc/articles/PMC6132686/pdf/216_2018_Article_1245.pdf
Chan, K. L. A., Altharawi, A., Fale, P., Song, C. L., Kazarian, S. G., Cinque, G., Untereiner, V. & Sockalingum, G. D. 2020. Transmission Fourier transform infrared spectroscopic imaging, mapping, and synchrotron scanning microscopy with zinc sulfide hemispheres on living mammalian cells at sub-cellular resolution. Applied spectroscopy, 74, (5), 544-552. https://journals.sagepub.com/doi/10.1177/0003702819898275?url_ver=Z39.88-2003&rfr_id=ori%3Arid%3Acrossref.org&rfr_dat=cr_pub%3Dpubmed&
Chan, K. L. A. & Kazarian, S. G. 2013. Correcting the Effect of Refraction and Dispersion of Light in FT-IR Spectroscopic Imaging in Transmission through Thick Infrared Windows. Analytical chemistry, 85, (2), 1029-1036. 10.1021/ac302846d.
Chiou, W.-C., Chen, J.-C., Chen, Y.-T., Yang, J.-M., Hwang, L.-H., Lyu, Y.-S., Yang, H.-Y. & Huang, C. 2021. The inhibitory effects of PGG and EGCG against the SARS-CoV-2 3C-like protease. Biochemical and Biophysical Research Communications, 591, 130-136. https://doi.org/10.1016/j.bbrc.2020.12.106.
Chomicz, L., Padzik, M., Graczyk, Z., Starosciak, B., Graczyk, T. K., Naprawska, A., Oledzka, G. & Szostakowska, B. 2010. *Acanthamoeba castellanii:* In vitro effects of selected biological, physical and chemical factors. Experimental Parasitology, 126, (1), 103-105. https://doi.org/10.1016/j.exppara.2010.01.025.
Ciesek, S., von Hahn, T., Colpitts, C. C., Schang, L. M., Friesland, M., Steinmann, J., Manns, M. P., Ott, M., Wedemeyer, H. & Meuleman, P. 2011. The green tea polyphenol, epigallocatechin-3-gallate, inhibits hepatitis C virus entry. Hepatology, 54, (6), 1947-1955. https://doi.org/10.1002/hep.24610.
Cirillo, J. D., Cirillo, S. L. G., Yan, L., Bermudez, L. E., Falkow, S. & Tompkins, L. S. 1999. Intracellular growth in Acanthamoeba castellanii affects monocyte entry mechanisms and enhances virulence of Legionella pneumophila. Infection and Immunity, 67, (9), 4427-4434. <Go to ISI>://WOS:000082138600017

https://www.ncbi.nlm.nih.gov/pmc/articles/PMC96761/pdf/ii004427.pdf
Cirillo, J. D., Falkow, S., Tompkins, L. S. & Bermudez, L. E. 1997. Interaction of Mycobacterium avium with environmental amoebae enhances virulence. Infection and Immunity, 65, (9), 3759-3767. <Go to ISI>://WOS:A1997XT42000038

http://iai.asm.org/content/65/9/3759.full.pdf
Clarholm, M. 2002. Bacteria and protozoa as integral components of the forest ecosystem their role in creating a naturally varied soil fertility. Antonie Van Leeuwenhoek International Journal of General and Molecular Microbiology, 81, (1-4), 309-318. 10.1023/a:1020543424098.
Clarke, D. W. & Niederkorn, J. Y. 2006a. The immunobiology of Acanthamoeba keratitis. Microbes and Infection, 8, (5), 1400-1405. https://doi.org/10.1016/j.micinf.2005.12.009.

Clarke, D. W. & Niederkorn, J. Y. 2006b. The pathophysiology of Acanthamoeba keratitis. Trends in Parasitology, 22, (4), 175-180. https://doi.org/10.1016/j.pt.2006.02.004.
Clarke, M., Lohan, A. J., Liu, B., Lagkouvardos, I., Roy, S., Zafar, N., Bertelli, C., Schilde, C., Kianianmomeni, A., Bürglin, T. R., Frech, C., Turcotte, B., Kopec, K. O., Synnott, J. M., Choo, C., Paponov, I., Finkler, A., Heng Tan, C. S., Hutchins, A. P., Weinmeier, T., Rattei, T., Chu, J. S. C., Gimenez, G., Irimia, M., Rigden, D. J., Fitzpatrick, D. A., Lorenzo-Morales, J., Bateman, A., Chiu, C.-H., Tang, P., Hegemann, P., Fromm, H., Raoult, D., Greub, G., Miranda-Saavedra, D., Chen, N., Nash, P., Ginger, M. L., Horn, M., Schaap, P., Caler, L. & Loftus, B. J. 2013. Genome of Acanthamoeba castellanii highlights extensive lateral gene transfer and early evolution of tyrosine kinase signaling. Genome Biology, 14, (2), R11. 10.1186/gb-2013-14-2-r11.
Cleaver, J. E., Banda, M. J., Troll, W. & Borek, C. 1986. Some protease inhibitors are also inhibitors of poly(ADP-ribose) polymerase. Carcinogenesis, 7, (2), 323-325. 10.1093/carcin/7.2.323.
Colpitts, C. C., Schang, L. M. & Hutt-Fletcher, L. 2014. A Small Molecule Inhibits Virion Attachment to Heparan Sulfate- or Sialic Acid-Containing Glycans. Journal of Virology, 88, (14), 7806-7817. https://journals.asm.org/doi/abs/10.1128/JVI.00896-14
Coven, S. L., Song, E., Steward, S., Pierson, C. R., Cope, J. R., Ali, I. K., Ardura, M. I., Hall, M. W., Chung, M. G. & Bajwa, R. P. S. 2017. Acanthamoeba granulomatous amoebic encephalitis after pediatric hematopoietic stem cell transplant. Pediatric Transplantation, 21, (8), 6. 10.1111/petr.13060.
Cucina, A., Filali, S., Risler, A., Febvay, C., Salmon, D., Pivot, C., Pelandakis, M. & Pirot, F. 2019. Dual 0.02% chlorhexidine digluconate – 0.1% disodium EDTA loaded thermosensitive ocular gel for Acanthamoeba keratitis treatment. International Journal of Pharmaceutics, 556, 330-337. https://doi.org/10.1016/j.ijpharm.2018.12.016.
Dai, J. & Mumper, R. J. 2010. Plant Phenolics: Extraction, Analysis and Their Antioxidant and Anticancer Properties. Molecules, 15, (10), 7313-7352. http://www.mdpi.com/1420-3049/15/10/7313

https://res.mdpi.com/molecules/molecules-15-07313/article_deploy/molecules-15-07313.pdf?filename=&attachment=1
Dart, J. K. G., Saw, V. P. J. & Kilvington, S. 2009. Acanthamoeba Keratitis: Diagnosis and Treatment Update 2009. American Journal of Ophthalmology, 148, (4), 487-499.e2. https://doi.org/10.1016/j.ajo.2009.06.009.
Debnath, A., Tunac, J. B., Galindo-Gómez, S., Silva-Olivares, A., Shibayama, M. & McKerrow, J. H. 2012. Corifungin, a New Drug Lead against Naegleria, Identified from a High-Throughput Screen. Antimicrobial Agents and Chemotherapy, 56, (11), 5450-5457. doi:10.1128/AAC.00643-12.
Debnath, A., Tunac, J. B., Silva-Olivares, A., Galindo-Gómez, S., Shibayama, M. & McKerrow, J. H. 2014. In vitro efficacy of corifungin against Acanthamoeba castellanii trophozoites and cysts. Antimicrob Agents Chemother, 58, (3), 1523-8. 10.1128/aac.02254-13.
Degerli, S., Tepe, B., Celiksoz, A., Berk, S. & Malatyali, E. 2012. In vitro amoebicidal activity of Origanum syriacum and Origanum laevigatum on Acanthamoeba castellanii cysts and trophozoites. Exp Parasitol, 131, (1), 20-4. 10.1016/j.exppara.2012.02.020.
Deng, Y., Ran, W., Man, S., Li, X., Gao, H., Tang, W., Tachibana, H. & Cheng, X. 2015. Artemether Exhibits Amoebicidal Activity against Acanthamoeba castellanii through Inhibition of the Serine Biosynthesis Pathway. Antimicrobial Agents and Chemotherapy, 59, (8), 4680-4688. doi:10.1128/AAC.04758-14.
Derda, M., Thiem, B., Budzianowski, J., Wojt, W. J. & Wojtkowiak-Giera, A. 2013. The evaluation of the amebicidal activity of Eryngium planum extracts. Acta Pol Pharm, 70, (6), 1027-34.
Dickson, A., Cooper, E., Fakae, L. B., Wang, B., Chan, K. L. A. & Elsheikha, H. M. 2020. In Vitro Growth- and Encystation-Inhibitory Efficacies of Matcha Green Tea and

Epigallocatechin Gallate Against *Acanthameoba Castellanii*. Pathogens, 9, (9), 763. https://doi.org/10.3390/pathogens9090763.

Dodangeh, S., Niyyati, M., Kamalinejad, M., Lorenzo-Morales, J., Haghighi, A. & Azargashb, E. 2017. The amoebicidal activity of *Ziziphus vulgaris* extract and its fractions on pathogenic *Acanthamoeba* trophozoites and cysts. Tropical Biomedicine, 34, (1), 127-136. <Go to ISI>://WOS:000398580600018

Dodangeh, S., Niyyati, M., Kamalinejad, M., Lorenzo morales, J., Moshfe, A., Haghighi, A. & Azargashb, E. 2018. In vitro activity of *Trigonella foenum graecum* seeds against a clinical strain of *Acanthamoeba* genotype T4. Iranian Journal of Pharmaceutical Research, 17, (2), 661-667. http://ijpr.sbmu.ac.ir/article_2192_c532349635931fb199eadf6e1ebae4c7.pdf

Dong, C., Davis, R. J. & Flavell, R. A. 2002. MAP kinases in the immune response. Annual review of immunology, 20, (1), 55-72.

dos Reis, M. B. G., Manjolin, L. C., Maquiaveli, C. D., Santos, O. A. & da Silva, E. R. 2013. Inhibition of *Leishmania (Leishmania*) *amazonensis* and Rat Arginases by Green Tea EGCG, (+)-Catechin and (2)-Epicatechin: A Comparative Structural Analysis of Enzyme-Inhibitor Interactions. Plos One, 8, (11), 9. 10.1371/journal.pone.0078387.

Du, Q., Schilde, C., Birgersson, E., Chen, Z. H., McElroy, S. & Schaap, P. 2014. The cyclic AMP phosphodiesterase RegA critically regulates encystation in social and pathogenic amoebas. Cell Signal, 26, (2), 453-9. https://doi.org/10.1016/j.cellsig.2013.10.008.

Dudley, R., Alsam, S. & Khan, N. A. 2008. The role of proteases in the differentiation of Acanthamoeba castellanii. Fems Microbiology Letters, 286, (1), 9-15. 10.1111/j.1574-6968.2008.01249.x.

Elsheikha, H. M., Siddiqui, R. & Khan, N. A. 2020. Drug Discovery against Acanthamoeba Infections: Present Knowledge and Unmet Needs. Pathogens (Basel, Switzerland), 9, (5), 405. 10.3390/pathogens9050405.

Eriksson, S., Kim, S. K., Kubista, M. & Nordén, B. 1993. Binding of 4',6-diamidino-2-phenylindole (DAPI) to AT regions of DNA: evidence for an allosteric conformational change. Biochemistry, 32, (12), 2987-98. 10.1021/bi00063a009.

Esmaeilpanah, E., Razavi, B. M. & Hosseinzadeh, H. 2021. Green tea and metabolic syndrome: A 10-year research update review. Iranian Journal of Basic Medical Sciences, 24, (9), 1159-1172. 10.22038/ijbms.2021.52980.11943.

Faix, O. (1992). Fourier Transform Infrared Spectroscopy. *In:* LIN, S. Y. & DENCE, C. W. (eds.) *Methods in Lignin Chemistry.* Berlin, Heidelberg: Springer Berlin Heidelberg.

Fakae, L. B., Stevenson, C. W., Zhu, X.-Q. & Elsheikha, H. M. 2020. In vitro activity of *Camellia sinensis* (green tea) against trophozoites and cysts of *Acanthamoeba castellanii*. International Journal for Parasitology: Drugs and Drug Resistance, 13, 59-72. https://doi.org/10.1016/j.ijpddr.2020.05.001.

Feitelson, M. A., Arzumanyan, A., Kulathinal, R. J., Blain, S. W., Holcombe, R. F., Mahajna, J., Marino, M., Martinez-Chantar, M. L., Nawroth, R., Sanchez-Garcia, I., Sharma, D., Saxena, N. K., Singh, N., Vlachostergios, P. J., Guo, S., Honoki, K., Fujii, H., Georgakilas, A. G., Bilsland, A., Amedei, A., Niccolai, E., Amin, A., Ashraf, S. S., Boosani, C. S., Guha, G., Ciriolo, M. R., Aquilano, K., Chen, S., Mohammed, S. I., Azmi, A. S., Bhakta, D., Halicka, D., Keith, W. N. & Nowsheen, S. 2015. Sustained proliferation in cancer: Mechanisms and novel therapeutic targets. Seminars in cancer biology, 35 Suppl, (Suppl), S25-S54. 10.1016/j.semcancer.2015.02.006.

Ferro, S., Coppellotti, O., Roncucci, G., Ben Amor, T. & Jori, G. 2006. Photosensitized inactivation of *Acanthamoeba palestinensis* in the cystic stage. Journal of Applied Microbiology, 101, (1), 206-212. https://doi.org/10.1111/j.1365-2672.2006.02893.x.

Ford, J. C., al-Khodairy, F., Fotou, E., Sheldrick, K. S., Griffiths, D. J. F. & Carr, A. M. 1994. 14-3-3 Protein Homologs Required for the DNA Damage Checkpoint in Fission Yeast. Science, 265, (5171), 533-535. doi:10.1126/science.8036497.

Fouque, E., Trouilhé, M.-C., Thomas, V., Hartemann, P., Rodier, M.-H. & Héchard, Y. 2012. Cellular, biochemical, and molecular changes during encystment of free-living amoebae. Eukaryotic cell, 11, (4), 382-387. 10.1128/EC.05301-11.

Freeman, S., Bartlett, J. B., Convey, G., Hardern, I., Teague, J. L., Loxham, S. J. G., Allen, J. M., Poucher, S. M. & Charles, A. D. 2006. Sensitivity of glycogen phosphorylase isoforms to indole site inhibitors is markedly dependent on the activation state of the enzyme. British Journal of Pharmacology, 149, (6), 775-785. https://doi.org/10.1038/sj.bjp.0706925.

Gabriel, S., Rasheed, A. K., Siddiqui, R., Appaturi, J. N., Fen, L. B. & Khan, N. A. 2018. Development of nanoparticle-assisted PCR assay in the rapid detection of brain-eating amoebae. Parasitology Research, 10.1007/s00436-018-5864-0. 10.1007/s00436-018-5864-0.

Garajova, M., Mrva, M., Timko, L., Lukac, M. & Ondriska, F. 2014. Cytomorphological changes and susceptibility of clinical isolates of *Acanthamoeba spp*. to heterocyclic alkylphosphocholines. Experimental Parasitology, 145, S102-S110. https://doi.org/10.1016/j.exppara.2014.05.015.

Garate, M., Cao, Z. Y., Bateman, E. & Panjwani, N. 2004. Cloning and characterization of a novel mannose-binding protein of Acanthamoeba. Journal of Biological Chemistry, 279, (28), 29849-29856. 10.1074/jbc.M402334200.

Garate, M., Marchant, J., Cubillos, I., Cao, Z., Khan, N. A. & Panjwani, N. 2006. In Vitro Pathogenicity of Acanthamoeba Is Associated with the Expression of the Mannose-Binding Protein. Investigative Ophthalmology & Visual Science, 47, (3), 1056-1062. 10.1167/iovs.05-0477.

Goh, J. W. Y., Harrison, R., Hau, S., Alexander, C. L., Tole, D. M. & Avadhanam, V. S. 2018. Comparison of In Vivo Confocal Microscopy, PCR and Culture of Corneal Scrapes in the Diagnosis of Acanthamoeba Keratitis. Cornea, 37, (4), 480-485. <Go to ISI>://WOS:000429590300024

https://insights.ovid.com/pubmed?pmid=29256983

Gomart, G., Denis, J., Bourcier, T., Dory, A., Abou-Bacar, A. & Candolfi, E. 2018. In vitro amoebicidal activity of Titanium dioxide/UV-A combination against Acanthamoeba. Invest Ophthalmol Vis Sci, 59. 10.1167/iovs.18-25003.

Gonçalves, D. d. S., Ferreira, M. d. S., Liedke, S. C., Gomes, K. X., de Oliveira, G. A., Leão, P. E. L., Cesar, G. V., Seabra, S. H., Cortines, J. R. & Casadevall, A. 2018. Extracellular vesicles and vesicle-free secretome of the protozoa Acanthamoeba castellanii under homeostasis and nutritional stress and their damaging potential to host cells. Virulence, 9, (1), 818-836. https://www.ncbi.nlm.nih.gov/pmc/articles/PMC5955443/pdf/kvir-09-01-1451184.pdf

Gooi, P., Lee-Wing, M., Brownstein, S., El-Defrawy, S., Jackson, W. B. & Mintsioulis, G. 2008. *Acanthamoeba* keratitis - Persistent organisms without inflammation after 1 year of topical chlorhexidine. Cornea, 27, (2), 246-248. 10.1097/ICO.0b013e31815b82a2.

Gourion-Arsiquaud, S., West, P. A. & Boskey, A. L. (2008). Fourier Transform-Infrared Microspectroscopy and Microscopic Imaging. *In:* WESTENDORF, J. J. (ed.) *Osteoporosis: Methods and Protocols.* Totowa, NJ: Humana Press.

Graham, H. N. 1992. Green tea composition, consumption, and polyphenol chemistry. Preventive Medicine, 21, (3), 334-350. https://doi.org/10.1016/0091-7435(92)90041-F.

Gu, B., Ding, Q., Xia, G. & Fang, Z. 2009. EGCG inhibits growth and induces apoptosis in renal cell carcinoma through TFPI-2 overexpression. Oncol Rep, 21, (3), 635-640. https://doi.org/10.3892/or_00000266.

Hadas, E., Derda, M. & Cholewinski, M. 2017a. Evaluation of the effectiveness of tea tree oil in treatment of *Acanthamoeba* infection. Parasitology Research, 116, (3), 997-1001. 10.1007/s00436-017-5377-2.

Hadas, E., Derda, M., Nawrot, J., Nowak, G. & Thiem, B. 2017b. Evaluation of the amoebicidal activities of *Centaurea bella, Centaurea daghestanica, Rhaponticum pulchrum* and *Tanacetum vulgare* against pathogenic *Acanthamoeba spp*. Acta Poloniae Pharmaceutica, 74, (6), 1827-1832. <Go to ISI>://WOS:000430449500022

Hahn, T.-W., O'Brien, T. P., Sah, W.-J. & Kim, J.-H. 1998. Acridine Orange Staining for Rapid Diagnosis of *Acanthamoeba* Keratitis. Japanese Journal of Ophthalmology, 42**,** (2), 108-114. https://doi.org/10.1016/S0021-5155(97)00127-5.

Hay, J., Kirkness, C. M., Seal, D. V. & Wright, P. 1994. Drug resistance and *Acanthamoeba* Keratitis: The quest for alternative antiprotozoal chemotherapy. Eye, 8**,** 555-63. http://dx.doi.org/10.1038/eye.1994.137.

Helfert, S., Estevez, A. M., Bakker, B., Michels, P. & Clayton, C. 2001. Roles of triosephosphate isomerase and aerobic metabolism in *Trypanosoma brucei*. Biochemical Journal, 357**,** (1), 117-125. 10.1042/bj3570117.

Henriquez, F. L. 2009. Khan NA: Acanthamoeba: Biology and Pathogenesis. Parasites & Vectors, 2**,** (1), 16. 10.1186/1756-3305-2-16.

Hilal, Y. & Engelhardt, U. H. 2009. A new myricetin-rhamnodiglucoside from Camellia sinensis. Natural Product Research, 23**,** (17), 1621-1629. 10.1080/14786410902975673.

Hirukawa, Y., Nakato, H., Izumi, S., Tsuruhara, T. & Tomino, S. 1998. Structure and expression of a cyst specific protein of Acanthamoeba castellanii. Biochimica et Biophysica Acta (BBA)-Gene Structure and Expression, 1398**,** (1), 47-56. https://www.sciencedirect.com/science/article/pii/S0167478198000268?via%3Dihub

Hong, Y. C., Lee, W. M., Kong, H. H., Jeong, H. J. & Chung, D. I. 2004. Molecular cloning and characterization of a cDNA encoding a laminin-binding protein (AhLBP) from *Acanthamoeba healyi*. Experimental Parasitology, 106**,** (3-4), 95-102. 10.1016/j.exppara.2004.01.011.

Hughes, C., Henderson, A., Kansiz, M., Dorling, K. M., Jimenez-Hernandez, M., Brown, M. D., Clarke, N. W. & Gardner, P. 2015. Enhanced FTIR bench-top imaging of single biological cells. Analyst, 140**,** (7), 2080-2085. 10.1039/c4an02053g.

Ikeda, Y., Miyazaki, D., Yakura, K., Kawaguchi, A., Ishikura, R., Inoue, Y., Mito, T., Shiraishi, A., Ohashi, Y., Higaki, S., Itahashi, M., Fukuda, M., Shimomura, Y. & Yagita, K. 2012. Assessment of Real-Time Polymerase Chain Reaction Detection of Acanthamoeba and Prognosis Determinants of Acanthamoeba Keratitis. Ophthalmology, 119**,** (6), 1111-1119. 10.1016/j.ophtha.2011.12.023.

Illingworth, C. D. & Cook, S. D. 1998. Acanthamoeba Keratitis. Survey of Ophthalmology, 42**,** (6), 493-508. https://doi.org/10.1016/S0039-6257(98)00004-6.

Imran, M., Muazzam, A. G., Habib, A. & Matin, A. 2016. Synthesis, characterization and amoebicidal potential of locally synthesized TiO2 nanoparticles against pathogenic Acanthamoeba trophozoites in vitro. J Photochem Photobiol B Biol, 159. 10.1016/j.jphotobiol.2016.03.014.

Inacio, J. D. F., Canto-Cavalheiro, M. M. & Almeida-Amaral, E. E. 2013. In Vitro and in Vivo Effects of (-)-Epigallocatechin 3-O-gallate on *Leishmania amazonensis*. Journal of Natural Products, 76**,** (10), 1993-1996. 10.1021/np400624d.

Inacio, J. D. F., Gervazoni, L., Canto-Cavalheiro, M. M. & Almeida-Amaral, E. E. 2014. The Effect of (-)-Epigallocatechin 3-O - Gallate In Vitro and In Vivo in *Leishmania braziliensis*: Involvement of Reactive Oxygen Species as a Mechanism of Action. PLOS Neglected Tropical Diseases, 8**,** (8), e3093. 10.1371/journal.pntd.0003093.

Ishii, T., Fujishiro, M., Masuda, M., Okudela, K., Kitamura, H., Teramoto, S. & Matsuse, T. 2004. Nutritional deficiency affects cell cycle status and viability in A549 cells: role of p27Kip1. Cancer Letters, 213**,** (1), 99-109. https://doi.org/10.1016/j.canlet.2004.03.022.

Jagtap, P. & Szabó, C. 2005. Poly(ADP-ribose) polymerase and the therapeutic effects of its inhibitors. Nature Reviews Drug Discovery, 4**,** (5), 421-440. 10.1038/nrd1718.

Jang, S. I., Jun, M. H., Lillehoj, H. S., Dalloul, R. A., Kong, I. K., Kim, S. & Min, W. G. 2007. Anticoccidial effect of green tea-based diets against *Eimeria maxima*. Veterinary Parasitology, 144**,** (1-2), 172-175. 10.1016/j.vetpar.2006.09.005.

Ji, H., Wang, J., Guo, J., Li, Y., Lian, S., Guo, W., Yang, H., Kong, F., Zhen, L., Guo, L. & Liu, Y. 2016. Progress in the biological function of alpha-enolase. Animal Nutrition, 2**,** (1), 12-17. https://doi.org/10.1016/j.aninu.2016.02.005.

Jones, C. G. 1997. Chlorhexidine: is it still the gold standard? Periodontology 2000, 15, (1), 55-62. doi:10.1111/j.1600-0757.1997.tb00105.x.

Jusman, Y., Sulaiman, S. N., Isa, N. A. M., Yusoff, I. A., Othman, N. H., Adnan, R. & Zaki, A. Capability of new features from FTIR spectral of cervical cells for cervical precancerous diagnostic system using MLP networks. TENCON 2009 - 2009 IEEE Region 10 Conference, 23-26 Jan. 2009 2009. 1-6.

Kan, Z., Wang, Y., Chen, Q., Tang, X., Thompson, H. J., Huang, J., Zhang, J., Gao, F., Shen, Y. & Wan, X. 2021. Green Tea Suppresses Amyloid β Levels and Alleviates Cognitive Impairment by Inhibiting APP Cleavage and Preventing Neurotoxicity in 5XFAD Mice. Mol Nutr Food Res, 10.1002/mnfr.202100626, e2100626. 10.1002/mnfr.202100626.

Kapuscinski, J. 1995. DAPI: a DNA-Specific Fluorescent Probe. Biotechnic & Histochemistry, 70, (5), 220-233. 10.3109/10520299509108199.

Kasten, F. H. (1967). Cytochemical Studies with Acridine Orange and the Influence of Dye Contaminants in the Staining of Nucleic Acids11This chapter is dedicated to the memory of Prof. Dr. Norbert Schümmelfeder, a devoted histochemist and experimental pathologist, who foresaw the cytochemical implications of acridine orange fluorochroming and pioneered in the evaluation of its histochemical significance. His recent death on October 11, 1965, at the age of forty-nine, has caused a great loss to the scientific community. *In:* BOURNE, G. H. & DANIELLI, J. F. (eds.) *International Review of Cytology.* Academic Press.

Katada, S., Yanagimoto, A., Matsui, Y., Hibi, M., Osaki, N., Kobayashi, S. & Katsuragi, Y. 2019. Effect of tea catechins with caffeine on energy expenditure in middle-aged men and women: a randomized, double-blind, placebo-controlled, crossover trial. European Journal of Nutrition, 10.1007/s00394-019-01976-9. 10.1007/s00394-019-01976-9.

Kaya, Y., Baldemir, A., Karaman, Ü., Ildız, N., Arıcı, Y. K., Kaçmaz, G., Kolören, Z. & Konca, Y. 2019. Amebicidal effects of fenugreek (*Trigonella foenum-graecum*) against *Acanthamoeba* cysts. Food Science & Nutrition, 7, (2), 563-571. https://onlinelibrary.wiley.com/doi/abs/10.1002/fsn3.849

Kaynak, B., Koloren, Z. & Karaman, U. 2018. Investigation of in vitro amoebicidal activities of *Ornithogalum sigmoideum* on *Acanthamoeba castellanii* cysts and trophozoites. Annals of Medical Research, 25, (4), 709-15. 10.5455/annalsmedres.2018.07.145.

Khan, N. A. 2006a. Acanthamoeba: biology and increasing importance in human health. FEMS Microbiol Rev, 30. 10.1111/j.1574-6976.2006.00023.x.

Khan, N. A. 2006b. *Acanthamoeba*: biology and increasing importance in human health. FEMS Microbiology Reviews, 30, (4), 564-595. http://dx.doi.org/10.1111/j.1574-6976.2006.00023.x.

Khan, N. A. 2007. Acanthamoeba invasion of the central nervous system. International Journal for Parasitology, 37, (2), 131-138. https://doi.org/10.1016/j.ijpara.2006.11.010.

Khan, N. A. 2010. Novel in vitro and in vivo models to study central nervous system infections due to Acanthamoeba spp. Experimental Parasitology, 126, (1), 69-72. https://doi.org/10.1016/j.exppara.2009.08.018.

Khan, N. A., Jarroll, E. L., Panjwani, N., Cao, Z. & Paget, T. A. 2000a. Proteases as markers for differentiation of pathogenic and nonpathogenic species of Acanthamoeba. Journal of Clinical Microbiology, 38, (8), 2858-2861. https://www.ncbi.nlm.nih.gov/pmc/articles/PMC87129/pdf/jm002858.pdf

Khan, N. A., Jarroll, E. L., Panjwani, N., Cao, Z. Y. & Paget, T. A. 2000b. Proteases as markers for differentiation of pathogenic and nonpathogenic species of *Acanthamoeba*. Journal of Clinical Microbiology, 38, (8), 2858-2861. <Go to ISI>://WOS:000088561700009

https://www.ncbi.nlm.nih.gov/pmc/articles/PMC87129/pdf/jm002858.pdf

Khan, N. A. & Siddiqui, R. 2009. *Acanthamoeba* affects the integrity of human brain microvascular endothelial cells and degrades the tight junction proteins. International Journal for Parasitology, 39**,** (14), 1611-1616. 10.1016/j.ijpara.2009.06.004.

Khan, Y. A., Kashiwabuchi, R. T., Martins, S. A., Castro-Combs, J. M., Kalyani, S., Stanley, P., Flikier, D. & Behrens, A. 2011. Riboflavin and Ultraviolet Light A Therapy as an Adjuvant Treatment for Medically Refractive *Acanthamoeba* Keratitis Report of 3 Cases. Ophthalmology, 118**,** (2), 324-331. https://doi.org/10.1016/j.ophtha.2010.06.041.

Khunkitti, W., Lloyd, D., Furr, J. & Russell, A. 1996. The lethal effects of biguanides on cysts and trophozoites of Acanthamoeba castellanii. Journal of applied bacteriology, 81**,** (1), 73-77.

Khunkitti, W., Lloyd, D., Furr, J. & Russell, A. 1997. Aspects of the mechanisms of action of biguanides on trophozoites and cysts of Acanthamoeba castellanii. Journal of applied microbiology, 82**,** (1), 107-114. https://sfamjournals.onlinelibrary.wiley.com/doi/abs/10.1111/j.1365-2672.1997.tb03304.x?sid=nlm%3Apubmed

Kikowska, M., Kruszka, D., Derda, M., Hadaś, E. & Thiem, B. 2020. Phytochemical Screening and Acanthamoebic Activity of Shoots from in Vitro Cultures and in Vivo Plants of Eryngium alpinum L.-The Endangered and Protected Species. Molecules, 25**,** (6). 10.3390/molecules25061416.

Kliescikova, J., Kulda, J. & Nohynkova, E. 2011a. Propylene glycol and contact-lens solutions containing this diol induce pseudocyst formation in acanthamoebae. Experimental parasitology, 127**,** (1), 326-328. https://www.sciencedirect.com/science/article/abs/pii/S0014489410002791?via%3Dihub

Kliescikova, J., Kulda, J. & Nohynkova, E. 2011b. Stress-induced pseudocyst formation-a newly identified mechanism of protection against organic solvents in Acanthamoebae of the T4 genotype. Protist, 162**,** (1), 58-69. https://www.sciencedirect.com/science/article/abs/pii/S1434461010000490?via%3Dihub

Kong, H. H., Kim, T. H. & Chung, D. I. 2000. Purification and characterization of a secretory serine proteinase of Acanthamoeba healyi isolated from GAE. Journal of Parasitology, 86**,** (1), 12-17. 10.1645/0022-3395(2000)086[0012:pacoas]2.0.co;2.

Kranenburg, O., Gebbink, M. F. & Voest, E. E. 2004. Stimulation of angiogenesis by Ras proteins. Biochimica et Biophysica Acta (BBA)-Reviews on Cancer, 1654**,** (1), 23-37. https://www.sciencedirect.com/science/article/abs/pii/S0304419X03000519?via%3Dihub

Krasny, L. & Huang, P. H. 2021. Data-independent acquisition mass spectrometry (DIA-MS) for proteomic applications in oncology. Molecular omics, 17**,** (1), 29-42. https://pubs.rsc.org/en/content/articlepdf/2021/mo/d0mo00072h

Kryczka, T., Ehlers, N., Nielsen, K. & Midelfart, A. 2012. Impact of organ culturing on metabolic profile of human corneas: preliminary results. Acta ophthalmologica, 90**,** (8), 761-767. https://onlinelibrary.wiley.com/doi/10.1111/j.1755-3768.2011.02213.x

Kulsoom, H., Baig, A. M., Siddiqui, R. & Khan, N. A. 2014. Combined drug therapy in the management of granulomatous amoebic encephalitis due to Acanthamoeba spp., and Balamuthia mandrillaris. Exp Parasitol, 145 Suppl**,** S115-20. 10.1016/j.exppara.2014.03.025.

Labbe, A., Khammari, C., Dupas, B., Gabison, E., Brasnu, E., Labetoulle, M. & Baudouin, C. 2009. Contribution of in vivo confocal microscopy to the diagnosis and management of infectious keratitis. Ocul Surf, 7**,** (1), 41-52.

Lackner, P., Beer, R., Broessner, G., Helbok, R., Pfausler, B., Brenneis, C., Auer, H., Walochnik, J. & Schmutzhard, E. 2010. Acute Granulomatous Acanthamoeba Encephalitis in an Immunocompetent Patient. Neurocritical Care, 12**,** (1), 91-94. 10.1007/s12028-009-9291-z.

Laronga, C., Yang, H.-Y., Neal, C. & Lee, M.-H. 2000. Association of the cyclin-dependent kinases and 14-3-3 sigma negatively regulates cell cycle progression. Journal of Biological Chemistry, 275, (30), 23106-23112. https://www.jbc.org/article/S0021-9258(19)66169-7/pdf

Lee, T.-J., Kim, E. J., Kim, S., Jung, E. M., Park, J.-W., Jeong, S. H., Park, S. E., Yoo, Y. H. & Kwon, T. K. 2006. Caspase-dependent and caspase-independent apoptosis induced by evodiamine in human leukemic U937 cells. Molecular Cancer Therapeutics, 5, (9), 2398-2407. 10.1158/1535-7163.Mct-06-0167.

Lee, Y.-R., Na, B.-K., Moon, E.-K., Song, S.-M., Joo, S.-Y., Kong, H.-H., Goo, Y.-K., Chung, D.-I. & Hong, Y. 2015. Essential Role for an M17 Leucine Aminopeptidase in Encystation of *Acanthamoeba castellanii*. PLoS ONE, 10, (6), e0129884. 10.1371/journal.pone.0129884.

Leitsch, D., Köhsler, M., Marchetti-Deschmann, M., Deutsch, A., Allmaier, G., Duchêne, M. & Walochnik, J. 2010. Major role for cysteine proteases during the early phase of Acanthamoeba castellanii encystment. Eukaryotic cell, 9, (4), 611-618. 10.1128/EC.00300-09.

Leitsch, D., Mbouaka, A. L., Köhsler, M., Müller, N. & Walochnik, J. 2021. An unusual thioredoxin system in the facultative parasite Acanthamoeba castellanii. Cellular and Molecular Life Sciences, 78, (7), 3673-3689. 10.1007/s00018-021-03786-x.

Lemgruber, L., Lupetti, P., De Souza, W., Vommaro, R. C. & da Rocha-Azevedo, B. 2010. The fine structure of the Acanthamoeba polyphaga cyst wall. Fems Microbiology Letters, 305, (2), 170-176. 10.1111/j.1574-6968.2010.01925.x.

Lim, N., Goh, D., Bunce, C., Xing, W., Fraenkel, G., Poole, T. R. G. & Ficker, L. 2008. Comparison of polyhexamethylene biguanide and chlorhexidine as monotherapy agents in the treatment of *Acanthamoeba* keratitis. American Journal of Ophthalmology, 145, (1), 130-135. 10.1016/j.ajo.2007.08.040.

Lin, S. D., Yang, J. H., Hsieh, Y. J., Liu, E. H. & Mau, J. L. 2014. Effect of different brewing methods on quality of green tea. Journal of Food Processing and Preservation, 38, (3), 1234-1243.

Liou, L. 2021. An Overview: Green Tea as Antioxidants. Oxidants and Antioxidants in Medical Science, 10, (7), 1.

Lloyd, D. 2014. Encystment in Acanthamoeba castellanii: A review. Experimental Parasitology, 145, S20-S27. https://doi.org/10.1016/j.exppara.2014.03.026.

Long, D. A. 1977. Raman spectroscopy. New York, 1.

Lorenzo-Morales, J., Khan, N. A. & Walochnik, J. 2015. An update on *Acanthamoeba* keratitis: diagnosis, pathogenesis and treatment. Parasite, 22. 10.1051/parasite/2015010.

Lorenzo-Morales, J., Kliescikova, J., Martinez-Carretero, E., De Pablos, L. M., Profotova, B. & Nohynkova, E. 2008. Glycogen phosphorylase in Acanthamoeba spp.: determining the role of the enzyme during the encystment process using RNA interference. Eukaryot Cell, 7. 10.1128/ec.00316-07.

Lorenzo-Morales, J., Martin-Navarro, C. M., Lopez-Arencibia, A., Arnalich-Montiel, F., Pinero, J. E. & Valladares, B. 2013a. Acanthamoeba keratitis: an emerging disease gathering importance worldwide? Trends in Parasitology, 29, (4), 181-187. 10.1016/j.pt.2013.01.006.

Lorenzo-Morales, J., Martín-Navarro, C. M., López-Arencibia, A., Arnalich-Montiel, F., Piñero, J. E. & Valladares, B. 2013b. *Acanthamoeba* keratitis: an emerging disease gathering importance worldwide? Trends in Parasitology, 29, (4), 181-187. https://doi.org/10.1016/j.pt.2013.01.006.

Lorenzo-Morales, J., Martin-Navarro, C. M., Lopez-Arencibia, A., Santana-Morales, M. A., Afonso-Lehmann, R. N., Maciver, S. K., Valladares, B. & Martinez-Carretero, E. 2010. Therapeutic Potential of a Combination of Two Gene-Specific Small Interfering RNAs against Clinical Strains of *Acanthamoeba*. Antimicrobial Agents and Chemotherapy, 54, (12), 5151-5155. https://doi.org/10.1128/AAC.00329-10.

Lu, D., Luo, L., Xu, Q. & Li, C. 1999. [A clinico-pathological study of granulomatous amoebic encephalitis]. Zhonghua bing li xue za zhi = Chinese journal of pathology, 28, (3), 169-173. http://europepmc.org/abstract/MED/11869522

Ly, T. M. C. & Muller, H. E. 1990. Ingested listeria-monocytogenes survive and multiply in protozoa. Journal of Medical Microbiology, 33, (1), 51-54. 10.1099/00222615-33-1-51.

Lyon, L. A., Keating, C. D., Fox, A. P., Baker, B. E., He, L., Nicewarner, S. R., Mulvaney, S. P. & Natan, M. J. 1998. Raman spectroscopy. Analytical Chemistry, 70, (12), 341-362.

Mafra, C. S. P., Carrijo-Carvalho, L. C., Chudzinski-Tavassi, A. M., Taguchi, F. M. d. C., Foronda, A. S., Carvalho, Fábio Ramos de Souza & de Freitas, D. 2013. Antimicrobial Action of Biguanides on the Viability of *Acanthamoeba* Cysts and Assessment of Cell Toxicity. Investigative Ophthalmology & Visual Science, 54, (9), 6363-6372. 10.1167/iovs.13-11990.

Mahboob, T., Azlan, A. M., Shipton, F. N., Boonroumkaew, P., Azman, N. S. N., Sekaran, S. D., Ithoi, I., Tan, T. C., Samudi, C., Wiart, C. & Nissapatorn, V. 2017. Acanthamoebicidal activity of periglaucine A and betulinic acid from *Pericampylus glaucus* (Lam.) Merr. in vitro. Experimental Parasitology, 183, 160-166. https://doi.org/10.1016/j.exppara.2017.09.002.

Malatyali, E., Tepe, B., Degerli, S., Berk, S. & Akpulat, H. A. 2012. In vitro amoebicidal activity of four Peucedanum species on Acanthamoeba castellanii cysts and trophozoites. Parasitol Res, 110, (1), 167-74. 10.1007/s00436-011-2466-5.

Marciano-Cabral, F. & Cabral, G. 2003. Acanthamoeba spp. as Agents of Disease in Humans. Clinical Microbiology Reviews, 16, (2), 273-307. 10.1128/cmr.16.2.273-307.2003.

Maritschnegg, P., Sovinz, P., Lackner, H., Benesch, M., Nebl, A., Schwinger, W., Walochnik, J. & Urban, C. 2011. Granulomatous Amebic Encephalitis in a Child with Acute Lymphoblastic Leukemia Successfully Treated with Multimodal Antimicrobial Therapy and Hyperbaric Oxygen. Journal of Clinical Microbiology, 49, (1), 446-448. 10.1128/jcm.01456-10.

Martín-Navarro, C. M., López-Arencibia, A., Sifaoui, I., Reyes-Batlle, M., Fouque, E., Osuna, A., Valladares, B., Piñero, J. E., Héchard, Y., Maciver, S. K. & Lorenzo-Morales, J. 2017. Amoebicidal Activity of Caffeine and Maslinic Acid by the Induction of Programmed Cell Death in Acanthamoeba. Antimicrobial Agents and Chemotherapy, 61, (6), e02660-16. doi:10.1128/AAC.02660-16.

Martinez, A. J. 1991. Infection of the central-nervous-system due to *Acanthamoeba*. Reviews of Infectious Diseases, 13, S399-S402. <Go to ISI>://WOS:A1991FD06000012

Martinez, A. J. & Janitschke, K. 1985. Acanthamoeba, an opportunistic microorganism: a review. Infection, 13, (6), 251-6.

Martinez, A. J. & Visvesvara, G. S. 1997. Free-living, amphizoic and opportunistic amebas. Brain Pathol, 7. 10.1111/j.1750-3639.1997.tb01076.x.

Mathers, W. D., Nelson, S. E., Lane, J. L., Wilson, M. E., Allen, R. C. & Folberg, R. 2000. Confirmation of confocal microscopy diagnosis of acanthamoeba keratitis using polymerase chain reaction analysis. Archives of Ophthalmology, 118, (2), 178-183. 10.1001/archopht.118.2.178.

Matsui, T., Maeda, T., Kusakabe, S., Arita, H., Yagita, K., Morii, E. & Kanakura, Y. 2018. A case report of granulomatous amoebic encephalitis by Group 1 Acanthamoeba genotype T18 diagnosed by the combination of morphological examination and genetic analysis. Diagnostic Pathology, 13, (1), 27. 10.1186/s13000-018-0706-z.

Mazur, T., Hadas, E. & Iwanicka, I. 1995. The duration of the cyst stage and the viability and virulence of acanthamoeba isolates. Tropical Medicine and Parasitology, 46, (2), 106-108. <Go to ISI>://WOS:A1995RH74300009

Mergeryan, H. 1991. The prevalence of Acanthamoeba in the human environment. Reviews of Infectious Diseases, 13, S390-S391. <Go to ISI>://WOS:A1991FD06000006

Mishell, B. B. & Shiigi, S. M. (1980). *Selected methods in cellular immunology,* Oxford, UK, WH Freeman & Co. .

Molina, J. R. & Adjei, A. A. 2006. The Ras/Raf/MAPK Pathway. Journal of Thoracic Oncology, 1, (1), 7-9. https://doi.org/10.1016/S1556-0864(15)31506-9.
Monsanto, M., Hooshyar, N., Meuldijk, J. & Zondervan, E. 2014. Modeling and optimization of green tea precipitation for the recovery of catechins. Separation and Purification Technology, 129, 129-136. https://doi.org/10.1016/j.seppur.2014.03.030.
Moon, E.-K., Lee, S., Quan, F.-S. & Kong, H.-H. 2018a. Effect of 2, 6-Dichlorobenzonitrile on Amoebicidal Activity of Multipurpose Contact Lens Disinfecting Solutions. The Korean journal of parasitology, 56, (5), 491-494. 10.3347/kjp.2018.56.5.491.
Moon, E. K., Choi, H. S., Kong, H. H. & Quan, F. S. 2018b. Polyhexamethylene biguanide and chloroquine induce programmed cell death in *Acanthamoeba castellanii*. Experimental Parasitology, 191, 31-35. 10.1016/j.exppara.2018.06.002.
Moore, M. B., McCulley, J. P., Kaufman, H. E. & Robin, J. B. 1986. Radial keratoneuritis as a presenting sign in *Acanthamoeba* keratitis. Ophthalmology, 93, (10), 1310-1315. <Go to ISI>://WOS:A1986E703700010
Mourant, J. R., Yamada, Y. R., Carpenter, S., Dominique, L. R. & Freyer, J. P. 2003. FTIR Spectroscopy Demonstrates Biochemical Differences in Mammalian Cell Cultures at Different Growth Stages. Biophysical Journal, 85, (3), 1938-1947. https://doi.org/10.1016/S0006-3495(03)74621-9.
Mukhtar, H. & Ahmad, N. 2000. Tea polyphenols: prevention of cancer and optimizing health. The American Journal of Clinical Nutrition, 71, (6), 1698S-1702S. https://doi.org/10.1093/ajcn/71.6.1698S.
Nakisah, M. A., Ida Muryany, M. Y., Fatimah, H., Nor Fadilah, R., Zalilawati, M. R., Khamsah, S. & Habsah, M. 2012. Anti-amoebic properties of a Malaysian marine sponge Aaptos sp. on *Acanthamoeba castellanii*. World Journal of Microbiology and Biotechnology, 28, (3), 1237-1244. 10.1007/s11274-011-0927-8.
Namal Senanayake, S. P. J. 2013. Green tea extract: Chemistry, antioxidant properties and food applications – A review. Journal of Functional Foods, 5, (4), 1529-1541. https://doi.org/10.1016/j.jff.2013.08.011.
Natarajan, S. B., Chandran, S. P. & Vinukonda, A. 2019. Green tea catechin loaded nanodelivery systems for the treatment of pandemic diseases. Asian J Pharm Clin Res, 12, (5), 1-7.
Navarro-Martínez, M. D., Navarro-Perán, E., Cabezas-Herrera, J., Ruiz-Gómez, J., García-Cánovas, F. & Rodríguez-López, J. N. 2005. Antifolate activity of epigallocatechin gallate against *Stenotrophomonas maltophilia*. Antimicrobial agents and chemotherapy, 49, (7), 2914-2920. https://doi.org/10.1128/AAC.49.7.2914-2920.2005.
Neff, R. J. & Neff, R. H. 1969. The biochemistry of amoebic encystment. Symp Soc Exp Biol, 23, 51-81.
Niederkorn, J. Y. 2002. The role of the innate and adaptive immune responses in Acanthamoeba keratitis. Arch Immunol Ther Exp (Warsz), 50, (1), 53-9.
Niederkorn, J. Y., Alizadeh, H., Leher, H. & McCulley, J. P. 1999. The pathogenesis of Acanthamoeba keratitis. Microbes and Infection, 1, (6), 437-443. https://doi.org/10.1016/S1286-4579(99)80047-1.
Niyyati, M., Lorenzo-Morales, J., Rezaie, S., Rahimi, F., Martin-Navarro, C. M., Mohebali, M., Maghsood, A. H., Farnia, S., Valladares, B. & Rezaeian, M. 2010. First report of a mixed infection due to *Acanthamoeba* genotype T3 and Vahlkampfia in a cosmetic soft contact lens wearer in Iran. Experimental Parasitology, 126, (1), 89-90. 10.1016/j.exppara.2009.10.009.
Niyyati, M., Sasani, R., Mohebali, M., Ghazikhansari, M., Kargar, F. & Hajialilo, E. 2018. Anti-Acanthamoeba effects of silver and gold nanoparticles and contact lenses disinfection solutions. Iran J Parasitol, 13.
Ortega-Rivas, A., Padrón, J. M., Valladares, B. & Elsheikha, H. M. 2016. *Acanthamoeba castellanii*: A new high-throughput method for drug screening in vitro. Acta Tropica, 164, 95-99. https://doi.org/10.1016/j.actatropica.2016.09.006.
Ozoe, F., Kurokawa, R., Kobayashi, Y., Jeong, H. T., Tanaka, K., Sen, K., Nakagawa, T., Matsuda, H. & Kawamukai, M. 2002. The 14-3-3 proteins Rad24 and Rad25

negatively regulate Byr2 by affecting its localization in *Schizosaccharomyces pombe*. Molecular and cellular biology, 22**,** (20), 7105-7119. 10.1128/MCB.22.20.7105-7119.2002.

Parmar, D. N., Awwad, S. T., Petroll, W. M., Bowman, R. W., McCulley, J. P. & Cavanagh, H. D. 2006. Tandem scanning confocal corneal microscopy in the diagnosis of suspected Acanthamoeba keratitis. Ophthalmology, 113**,** (4), 538-547. 10.1016/j.ophtha.2005.12.022.

Parvez, M. A. K., Saha, K., Rahman, J., Munmun, R. A., Rahman, M. A., Dey, S. K., Rahman, M. S., Islam, S. & Shariare, M. H. 2019. Antibacterial activities of green tea crude extracts and synergistic effects of epigallocatechingallate (EGCG) with gentamicin against MDR pathogens. Heliyon, 5**,** (7), e02126. https://doi.org/10.1016/j.heliyon.2019.e02126.

Patel, D. V. & McGhee, C. N. J. 2009. Acanthamoeba keratitis: a comprehensive photographic reference of common and uncommon signs. Clinical & Experimental Ophthalmology, 37**,** (2), 232-238. 10.1111/j.1442-9071.2008.01913.x.

Paveto, C., Guida, M., Esteva, M. I., Martino, V., Coussio, J., Flawia, M. M. & Torres, H. N. 2004. Anti-*Trypanosoma cruzi* activity of green tea (*Camellia sinensis*) catechins. Antimicrobial Agents and Chemotherapy, 48**,** (1), 69-74. 10.1128/aac.48.1.69-74.2004.

Perva-Uzunalic, A., Skerget, M., Knez, Z., Weinreich, B., Otto, F. & Gruner, S. 2006. Extraction of active ingredients from green tea (*Camellia sinensis*): Extraction efficiency of major catechins and caffeine. Food Chemistry, 96**,** (4), 597-605. 10.1016/j.foodchem.2005.03.015.

Pollard, T. D., Shelton, E., Weihing, R. R. & Korn, E. D. 1970. Ultrastructural characterization of f-actin isolated from *Acanthamoeba castellanii* and identification of cytoplasmic filaments as f-actin by reaction with rabbit heavy meromyosin. Journal of Molecular Biology, 50**,** (1), 91-&. 10.1016/0022-2836(70)90106-3.

Preisner, H., Habicht, J., Garg, S. G. & Gould, S. B. 2018. Intermediate filament protein evolution and protists. Cytoskeleton, 75**,** (6), 231-243. https://doi.org/10.1002/cm.21443.

Qvarnstrom, Y., Visvesvara, G. S., Sriram, R. & da Silva, A. J. 2006. Multiplex real-time PCR assay for simultaneous detection of Acanthamoeba spp., Balamuthia mandrillaris, and Naegleria fowleri. Journal of Clinical Microbiology, 44**,** (10), 3589-3595. 10.1128/jcm.00875-06.

Reichelt, J., Büssow, H., Grund, C. & Magin, T. M. 2001. Formation of a Normal Epidermis Supported by Increased Stability of Keratins 5 and 14 in Keratin 10 Null Mice. Molecular Biology of the Cell, 12**,** (6), 1557-1568. 10.1091/mbc.12.6.1557.

Rigler, R. 1969. Acridine orange in nucleic acid analysis. Annals of the New York Academy of Sciences, 157**,** (1), 211-224.

Riviere, D., Szczebara, F. M., Berjeaud, J. M., Frere, J. & Hechard, Y. 2006. Development of a real-time PCR assay for quantification of Acanthamoeba trophozoites and cysts. Journal of Microbiological Methods, 64**,** (1), 78-83. 10.1016/j.mimet.2005.04.008.

Rodriguez-Almazan, C., Arreola, R., Rodriguez-Larrea, D., Aguirre-López, B., de Gómez-Puyou, M. T., Pérez-Montfort, R., Costas, M., Gómez-Puyou, A. & Torres-Larios, A. 2008. Structural basis of human triosephosphate isomerase deficiency: mutation E104D is related to alterations of a conserved water network at the dimer interface. Journal of Biological Chemistry, 283**,** (34), 23254-23263. https://www.jbc.org/article/S0021-9258(19)49382-4/pdf

Roels, D., De Craene, S. & Kestelyn, P. 2017. Keratoneuritis is not pathognomonic of Acanthamoeba keratitis: a case report of Pseudomonas keratitis. Int Ophthalmol, 37**,** (1), 257-258. 10.1007/s10792-014-0023-9.

Ronn, R., McCaig, A. E., Griffiths, B. S. & Prosser, J. I. 2002. Impact of protozoan grazing on bacterial community structure in soil microcosms. Applied and Environmental Microbiology, 68**,** (12), 6094-6105. 10.1128/aem.68.12.6094-6105.2002.

Rosenberg, K., Bertaux, J., Krome, K., Hartmann, A., Scheu, S. & Bonkowski, M. 2009. Soil amoebae rapidly change bacterial community composition in the rhizosphere of Arabidopsis thaliana. Isme Journal, 3**,** (6), 675-684. 10.1038/ismej.2009.11.

Safdar, N., Sarfaraz, A., Kazmi, Z. & Yasmin, A. 2016. Ten different brewing methods of green tea: comparative antioxidant study. Journal of Applied Biology & Biotechnology, 4**,** (03), 033-040.

Saleh, M., Abdel-Baki, A.-A. S., Dkhil, M. A., El-Matbouli, M. & Al-Quraishy, S. 2021. Proteins of the Ciliated Protozoan Parasite *Ichthyophthirius multifiliis* Identified in Common Carp Skin Mucus. Pathogens, 10**,** (7), 790-800. https://www.mdpi.com/2076-0817/10/7/790

https://mdpi-res.com/d_attachment/pathogens/pathogens-10-00790/article_deploy/pathogens-10-00790-v3.pdf

Sanchez-Hidalgo, A., Obregón-Henao, A., Wheat, W. H., Jackson, M. & Gonzalez-Juarrero, M. 2017. Mycobacterium bovis hosted by free-living-amoebae permits their long-term persistence survival outside of host mammalian cells and remain capable of transmitting disease to mice. Environmental Microbiology, 19**,** (10), 4010-4021. https://sfamjournals.onlinelibrary.wiley.com/doi/10.1111/1462-2920.13810

Sanderson, M. J., Smith, I., Parker, I. & Bootman, M. D. 2014. Fluorescence microscopy. Cold Spring Harbor Protocols, 2014**,** (10), pdb. top071795. http://cshprotocols.cshlp.org/content/2014/10/pdb.top071795.full.pdf

Sanlier, N., Gokcen, B. B. & Altuğ, M. 2018. Tea consumption and disease correlations. Trends in Food Science & Technology, 78**,** 95-106. https://doi.org/10.1016/j.tifs.2018.05.026.

Sannella, A. R., Messori, L., Casini, A., Vincieri, F. F., Bilia, A. R., Majori, G. & Severini, C. 2007. Antimalarial properties of green tea. Biochemical and Biophysical Research Communications, 353**,** (1), 177-181. 10.1016/j.bbrc.2006.12.005.

Saoudi, S., Sifaoui, I., Chammem, N., Reyes-Batlle, M., Lopez-Arencibia, A., Pacheco-Fernandez, I., Pino, V., Hamdi, M., Jimenez, I. A., Bazzocchi, I. L., Pinero, J. E. & Lorenzo-Morales, J. 2017. Anti-*Acanthamoeba* activity of Tunisian *Thymus capitatus* essential oil and organic extracts. Experimental Parasitology, 183**,** 231-235. https://doi.org/10.1016/j.exppara.2017.09.014.

Saravanakumar, M., Manivannan, J., Sivasubramanian, J., Silambarasan, T., Balamurugan, E. & Raja, B. 2012. Molecular metabolic fingerprinting approach to investigate the effects of borneol on metabolic alterations in the liver of nitric oxide deficient hypertensive rats. Molecular and Cellular Biochemistry, 362**,** (1), 203-209. 10.1007/s11010-011-1143-4.

Seal, D. V., Kirkness, C. M., Bennett, H. G. B. & Peterson, M. 1999. Population-based cohort study of microbial keratitis in Scotland: incidence and features. Contact Lens and Anterior Eye, 22**,** (2), 49-57. https://doi.org/10.1016/S1367-0484(99)80003-4.

Segovia-Gamboa, N. C., Chávez-Munguía, B., Medina-Flores, Y., Cázares-Raga, F. E., Hernández-Ramírez, V. I., Martínez-Palomo, A. & Talamás-Rohana, P. 2010. Entamoeba invadens, encystation process and enolase. Experimental Parasitology, 125**,** (2), 63-69. https://doi.org/10.1016/j.exppara.2009.12.019.

Sekine, T., Arita, J., Yamaguchi, A., Saito, K., Okonogi, S., Morisaki, N., Iwasaki, S. & Murakoshi, I. 1991. Two flavonol glycosides from seeds of Camellia sinensis. Phytochemistry, 30**,** (3), 991-995. https://www.sciencedirect.com/science/article/abs/pii/003194229185293 9?via%3Dihub

Servin, J., Méndez, J., Portillo, N. & Villasanti, U. 2021. Antibacterial effect of green tea infusion used as a mouthwash on saliva and bacterial plaque: a randomized controlled trial. General dentistry, 69**,** (5), 72-74. http://europepmc.org/abstract/MED/34424217

Shankar, S., Suthakar, G. & Srivastava, R. K. 2007. Epigallocatechin-3-gallate inhibits cell cycle and induces apoptosis in pancreatic cancer. Front Biosci, 12**,** 5039-51. https://doi.org/10.2741/2446.

Shoff, M. E., Rogerson, A., Kessler, K., Schatz, S. & Seal, D. V. 2008. Prevalence of Acanthamoeba and other naked amoebae in South Florida domestic water. Journal of Water and Health, 6, (1), 99-104. 10.2166/wh.2007.014.

Shohaib, H. M., Nawaz, S. & Matin, A. 2016. Methanolic extract of Peganum harmala exhibit potent activity against Acanthamoeba castellanii cysts and its encystment in vitro. Pak J Pharm Sci, 29, (6), 1993-1996.

Siddiqui, R., Aqeel, Y. & Khan, N. A. 2016a. The development of drugs against *Acanthamoeba* infections. Antimicrob Agents Chemother, 60. 10.1128/aac.00686-16.

Siddiqui, R., Aqeel, Y. & Khan, N. A. 2016b. The Development of Drugs against Acanthamoeba Infections. Antimicrobial Agents and Chemotherapy, 60, (11), 6441-6450. 10.1128/aac.00686-16.

Siddiqui, R., Dudley, R. & Khan, N. A. 2012. *Acanthamoeba* differentiation: a two-faced drama of Dr Jekyll and Mr Hyde. Parasitology, 139, (7), 826-834. 10.1017/S0031182012000042.

Siddiqui, R. & Khan, N. A. 2012. Biology and pathogenesis of Acanthamoeba. Parasites & Vectors, 5, (1), 6. 10.1186/1756-3305-5-6.

Sidney, L. E., Branch, M. J., Dua, H. S. & Hopkinson, A. 2015. Effect of culture medium on propagation and phenotype of corneal stroma derived stem cells. Cytotherapy, 17, (12), 1706-1722. 10.1016/j.jcyt.2015.08.003.

Siebert, F. & Hildebrandt, P. (2008). *Vibrational spectroscopy in life science*, John Wiley & Sons.

Sifaoui, I., Lopez-Arencibia, A., Martin-Navarro, C. M., Chammem, N., Mejri, M., Lorenzo-Morales, J., Abderabba, M. & Pinero, J. E. 2013. Activity assessment of Tunisian olive leaf extracts against the trophozoite stage of *Acanthamoeba*. Parasitology Research, 112, (8), 2825-2829. 10.1007/s00436-013-3453-9.

Sifaoui, I., Lopez-Arencibia, A., Martin-Navarro, C. M., Reyes-Batlle, M., Wagner, C., Chiboub, O., Mejri, M., Valladares, B., Abderrabba, M., Pinero, J. E. & Lorenzo-Morales, J. 2017. Programmed cell death in *Acanthamoeba castellanii* Neff induced by several molecules present in olive leaf extracts. Plos One, 12, (8), 12. https://doi.org/10.1371/journal.pone.0183795.

Silva, V. A. P., Boaventura, G. T., Abboud, R. S., Ribas, J. A. S. & Chagas, M. A. 2019. Green Tea Consumption Lower Damage and Inflammatory Cytokines in Rat Cardiovascular System Under Androgenic Stimulation. American Journal of Sports Science, 7, (4), 141-148.

Singhal, T., Bajpai, A., Kalra, V., Kabra, S. K., Samantaray, J. C., Satpathy, G. & Gupta, A. K. 2001. Successful treatment of *Acanthamoeba* meningitis with combination oral antimicrobials. Pediatric Infectious Disease Journal, 20, (6), 623-627. 10.1097/00006454-200106000-00016.

Sissons, J., Kim, K. S., Stins, M., Jayasekera, S., Alsam, S. & Khan, N. A. 2005. Acanthamoeba castellanii induces host cell death via a phosphatidylinositol 3-kinase-dependent mechanism. Infection and Immunity, 73, (5), 2704-2708. 10.1128/iai.73.5.2704-2708.2005.

Soares-Silva, M., Diniz, F. F., Gomes, G. N. & Bahia, D. 2016. The Mitogen-Activated Protein Kinase (MAPK) Pathway: Role in Immune Evasion by Trypanosomatids. Frontiers in microbiology, 7, 183-183. 10.3389/fmicb.2016.00183.

Srichairatanakool, S., Ounjaijean, S., Thephinlap, C., Khansuwan, U., Phisalpong, C. & Fucharoen, S. 2006. Iron-chelating and free-radical scavenging activities of microwave-processed green tea in iron overload. Hemoglobin, 30, (2), 311-327. https://doi.org/10.1080/03630260600642666.

Stacey, D. W. 2003. Cyclin D1 serves as a cell cycle regulatory switch in actively proliferating cells. Current opinion in cell biology, 15, (2), 158-163. https://www.sciencedirect.com/science/article/abs/pii/S0955067403000085?via%3Dihub

Steenbergen, J. N., Shuman, H. A. & Casadevall, A. 2001. Cryptococcus neoformans interactions with amoebae suggest an explanation for its virulence and intracellular

pathogenic strategy in macrophages. Proceedings of the National Academy of Sciences of the United States of America, 98, (26), 15245-15250. 10.1073/pnas.261418798.
Stehrgreen, J. K., Bailey, T. M. & Visvesvara, G. S. 1989. The epidemiology of *Acanthamoeba* keratitis in the United States. American Journal of Ophthalmology, 107, (4), 331-336. 10.1016/0002-9394(89)90654-5.
Stevik, T. K., Hanssen, J. F. & Jenssen, P. D. 1998. A comparison between DAPI direct count (DDC) and most probable number (MPN) to quantify protozoa in infiltration systems. Journal of Microbiological Methods, 33, (1), 13-21. https://doi.org/10.1016/S0167-7012(98)00035-9.
Stothard, D. R., Schroeder-Diedrich, J. M., Awwad, M. H., Gast, R. J., Ledee, D. R., Rodriguez-Zaragoza, S., Dean, C. L., Fuerst, P. A. & Byers, T. J. 1998. The evolutionary history of the genus Acanthamoeba and the identification of eight new 18S rRNA gene sequence types. Journal of Eukaryotic Microbiology, 45, (1), 45-54. http://onlinelibrary.wiley.com/store/10.1111/j.1550-7408.1998.tb05068.x/asset/j.1550-7408.1998.tb05068.x.pdf?v=1&t=je8pnf2u&s=20f090ea8b455b3d74eed023ad94c86e78d936c0
Sun, X. G., Zhang, Y., Li, R., Wang, Z. Q., Luo, S. Y., Gao, M., Deng, S. J., Chen, W. & Jin, X. Y. 2006. *Acanthamoeba* keratitis - Clinical characteristics and management. Ophthalmology, 113, (3), 412-416. 10.1016/j.ophtha.2005.10.041.
Swanson, M. S. & Hammer, B. K. 2000. Legionella pneumophila pathogenesis: A fateful journey from amoebae to macrophages. Annual Review of Microbiology, 54, 567-613. 10.1146/annurev.micro.54.1.567.
Swart, A. L., Harrison, C. F., Eichinger, L., Steinert, M. & Hilbi, H. 2018. Acanthamoeba and Dictyostelium as Cellular Models for Legionella Infection. Frontiers in Cellular and Infection Microbiology, 8, (61). 10.3389/fcimb.2018.00061.
Tan, R. X. & Zou, W. X. 2001. Endophytes: a rich source of functional metabolites. Natural product reports, 18, (4), 448-459. https://pubs.rsc.org/en/content/articlelanding/2001/NP/b100918o
Tepe, B., Malatyali, E., Degerli, S. & Berk, S. 2012. In vitro amoebicidal activities of Teucrium polium and T. chamaedrys on Acanthamoeba castellanii trophozoites and cysts. Parasitol Res, 110, (5), 1773-8. 10.1007/s00436-011-2698-4.
Thamtam, V. K., Uppin, M. S., Pyal, A., Kaul, S., Rani, Y. J. & Sundaram, C. 2016. Fatal granulomatous amoebic encephalitis caused by Acanthamoeba in a newly diagnosed patient with systemic lupus erythematosus. Neurology India, 64, (1), 101-104. 10.4103/0028-3886.173662.
Thewes, S., Soldati, T. & Eichinger, L. 2019. Editorial: Amoebae as Host Models to Study the Interaction With Pathogens. Frontiers in Cellular and Infection Microbiology, 9, (47). 10.3389/fcimb.2019.00047.
Thipubon, P., Uthaipibull, C., Kamchonwongpaisan, S., Tipsuwan, W. & Srichairatanakool, S. 2015. Inhibitory effect of novel iron chelator, 1-(N-acetyl-6-aminohexyl)-3-hydroxy-2-methylpyridin-4-one (CM1) and green tea extract on growth of *Plasmodium falciparum*. Malaria Journal, 14, 9. 10.1186/s12936-015-0910-1.
Thom, S., Warhurst, D. & Drasar, B. S. 1992. ASSOCIATION OF VIBRIO-CHOLERAE WITH FRESH-WATER AMEBAS. Journal of Medical Microbiology, 36, (5), 303-306. 10.1099/00222615-36-5-303.
Thongseesuksai, T., Wongwai, P., Boonmars, T., Sanpool, O. & Laummaunwai, P. 2019. Evaluating the in vitro efficacy of gatifloxacin, levofloxacin and gentamicin against Acanthamoeba cysts. International Ophthalmology, 10.1007/s10792-019-01188-4. 10.1007/s10792-019-01188-4.
Trabelsi, H., Dendana, F., Sellami, A., Sellami, H., Cheikhrouhou, F., Neji, S., Makni, F. & Ayadi, A. 2012. Pathogenic free-living amoebae: Epidemiology and clinical review. Pathologie Biologie, 60, (6), 399-405. 10.1016/j.patbio.2012.03.002.
Trabelsi, H., Sellami, A., Dendena, F., Sellami, H., Cheikh-Rouhou, F., Makni, F., Ben Dhiaa, A. & Ayadi, A. 2010. FREE-LIVING AMOEBAE (FLA): MORPHOLOGICAL AND

MOLECULAR IDENTIFICATION OF ACANTHAMOEBA IN DENTAL UNIT WATER. Parasite-Journal De La Societe Francaise De Parasitologie, 17, (1), 67-70. 10.1051/parasite/2010171067.

Traganos, F., Darzynkiewicz, Z., Sharpless, T. & Melamed, M. 1977. Simultaneous staining of ribonucleic and deoxyribonucleic acids in unfixed cells using acridine orange in a flow cytofluorometric system. Journal of Histochemistry & Cytochemistry, 25, (1), 46-56.

Tsitsanou, K. E., Skamnaki, V. T. & Oikonomakos, N. G. 2000. Structural Basis of the Synergistic Inhibition of Glycogen Phosphorylase a by Caffeine and a Potential Antidiabetic Drug. Archives of Biochemistry and Biophysics, 384, (2), 245-254. https://doi.org/10.1006/abbi.2000.2121.

Ulsamer, A. G., Wright, P. L., Wetzel, M. G. & Korn, E. D. 1971. Plasma and phagosome membranes of *Acanthamoeba castellanii*. Journal of Cell Biology, 51, (1), 193-&. 10.1083/jcb.51.1.193.

Van Klink, F., Leher, H., Jager, M. J., Alizadeh, H., Taylor, W. & Niederkorn, J. Y. 1997. Systemic immune response to Acanthamoeba keratitis in the Chinese hamster. Ocul Immunol Inflamm, 5, (4), 235-44. 10.3109/09273949709085064.

Verani, J. R., Lorick, S. A., Yoder, J. S., Beach, M. J., Braden, C. R., Roberts, J. M., Conover, C. S., Chen, S., McConnell, K. A., Chang, D. C., Park, B. J., Jones, D. B., Visvesvara, G. S., Roy, S. L. & Team, A. K. I. 2009. National Outbreak of Acanthamoeba Keratitis Associated with Use of a Contact Lens Solution, United States. Emerging Infectious Diseases, 15, (8), 1236-1242. 10.3201/eid1508.090225.

Vichai, V. & Kirtikara, K. 2006. Sulforhodamine B colorimetric assay for cytotoxicity screening. Nature Protocols, 1, 1112. 10.1038/nprot.2006.179.

Vigueira, P. A., Ray, S. S., Martin, B. A., Ligon, M. M. & Paul, K. S. 2012. Effects of the green tea catechin (-)-epigallocatechin gallate on Trypanosoma brucei. International Journal for Parasitology-Drugs and Drug Resistance, 2, 225-229. 10.1016/j.ijpddr.2012.09.001.

Visvesvara, G. S. 2010. Amebic meningoencephalitides and keratitis: challenges in diagnosis and treatment. Current Opinion in Infectious Diseases, 23, (6), 590-594. 10.1097/QCO.0b013e32833ed78b.

Visvesvara, G. S. & Martinez, A. J. (2010). Chapter 182 - Protozoa: free-living amebae. *In:* COHEN, J., OPAL, S. M. & POWDERLY, W. G. (eds.) *Infectious Diseases (Third Edition).* London: Content Repository Only!

Visvesvara, G. S., Moura, H. & Schuster, F. L. 2007. Pathogenic and opportunistic free-living amoebae: *Acanthamoeba spp., Balamuthia mandrillaris, Naegleria fowleri,* and *Sappinia diploidea*. FEMS Immunology & Medical Microbiology, 50, (1), 1-26. http://dx.doi.org/10.1111/j.1574-695X.2007.00232.x.

Walia, R., Montoya, J. G., Visvesvera, G. S., Booton, G. C. & Doyle, R. L. 2007. A case of successful treatment of cutaneous *Acanthamoeba* infection in a lung transplant recipient. Transpl Infect Dis, 9. 10.1111/j.1399-3062.2006.00159.x.

Weisman, R. A. 1976. Differentiation in Acanthamoeba castellanii. Annual Reviews in Microbiology, 30, (1), 189-219.

Wheat, W. H., Casali, A. L., Thomas, V., Spencer, J. S., Lahiri, R., Williams, D. L., McDonnell, G. E., Gonzalez-Juarrero, M., Brennan, P. J. & Jackson, M. 2014. Long-term survival and virulence of Mycobacterium leprae in amoebal cysts. PLoS neglected tropical diseases, 8, (12), e3405-e3405. 10.1371/journal.pntd.0003405.

Woyda-Ploszczyca, A., Koziel, A., Antos-Krzeminska, N. & Jarmuszkiewicz, W. 2011. Impact of oxidative stress on Acanthamoeba castellanii mitochondrial bioenergetics depends on cell growth stage. Journal of bioenergetics and biomembranes, 43, (3), 217-225. https://link.springer.com/content/pdf/10.1007/s10863-011-9351-x.pdf

Wyganowska-Świątkowska, M., Matthews-Kozanecka, M., Matthews-Brzozowska, T., Skrzypczak-Jankun, E. & Jankun, J. 2018. Can EGCG Alleviate Symptoms of Down Syndrome by Altering Proteolytic Activity? International journal of molecular sciences, 19, (1), 248. https://doi.org/10.3390/ijms19010248.

Yang, K., Gao, Z.-Y., Li, T.-Q., Song, W., Xiao, W., Zheng, J., Chen, H., Chen, G.-H. & Zou, H.-Y. 2019. Anti-tumor activity and the mechanism of a green tea (*Camellia sinensis*) polysaccharide on prostate cancer. International Journal of Biological Macromolecules, 122, 95-103. https://doi.org/10.1016/j.ijbiomac.2018.10.101.

Yen, C.-L. E., Mar, M.-H., Craciunescu, C. N., Edwards, L. J. & Zeisel, S. H. 2002. Deficiency in methionine, tryptophan, isoleucine, or choline induces apoptosis in cultured cells. The Journal of nutrition, 132, (7), 1840-1847. https://watermark.silverchair.com/4w0702001840.pdf?token=AQECAHi208BE49Ooan9kkhW_Ercy7Dm3ZL_9Cf3qfKAc485ysgAAAskwggLFBgkqhkiG9w0BBwagggK2MIICsgIBADCCAqsGCSqGSIb3DQEHATAeBglghkgBZQMEAS4wEQQMaQ7dYInWtoUQQMc7AgEQgIICfK2VT0jVCAUZWw1OgYtoQJiEcuLujmJ9JBKUyyNhvER5TmlWq_0iYZLPY98ZAdApil6-7yO3YyeXePviW_QN0pYi-Oy3vn5zOT_kVZwcLE2AZlXD6ax-cNpfpVFFal992QHFGJc48o0WFTfiKiCtz4whTWawo0wQbTqP6Rlrn4uxGb-JdhtNKx0kzk6XX4yjhk6UHWmkvtrsRLzHafjuh7j4OEVA8GS0_uE3QIbFqXx6bLDCXZezK1X_aq5EN8IoSr5f7gP3Zu3p9nCMsX2JgTuWOrx-sE4392EJ3c3p8t3nO1BKlZqJqb3eImu0HUtDA1nikBHsLoVttI3ZDLptZXuthEBtHOUX8uoMeeLWwxYouLp2x9dsadXktAxeUBEnha2vL6AdylgWtMcf5nKPpdfFtBKs9cDUapjnJ17BIpp0lYcj9_Ty6liL1kVExc7Qh4At5GxxMzcABWmOLGfrRyoXFPgoNtEAGMh4wWyfDHumNS9qBSWpJcCKkbTUoNAFT612mnA81JTC4aACRxrQU-PyVzh_Y4p6eqGpADS6FoLYXmY0bIr5Fs5VXVGGcUB5Xok1Tr5y_o5F0xA176AmvVb2JcJY486m5cOuKBR1ujtcYu65ZOGPaySbmg22WdBvIkDq77lns6xaP5zDAL8SAJhfi75L0UljyEa-UxyJmQ4Hl0bmfM8mYc6jmiVCT4gLmH08aqUEz-mZRtGxxLaM5DfdsZBWy76EVCV55wBXErG7BNa3FVyrH5H9LH8WBYncgLfoUCe9DUNV5FT7LNZLKJyRwOPKoPWHkGD_ie_p8-RCsOpuGRNJU0IE-iE3EvnnrQuH0KP4D-FbuXAegg

https://watermark.silverchair.com/4w0702001840.pdf?token=AQECAHi208BE49Ooan9kkhW_Ercy7Dm3ZL_9Cf3qfKAc485ysgAAAskwggLFBgkqhkiG9w0BBwagggK2MIICsgIBADCCAqsGCSqGSIb3DQEHATAeBglghkgBZQMEAS4wEQQMPMBKBD0l01AlNM-dAgEQgIICfOF88PUBH2ggA6MBPHmihv0CK28iKRSxU1wJE_k4NX-bYnBQb7Rf9R4NgTsMacXA48ShHmjEhFHso62IofRFzybHj4F1qVPyiVB1CA2dHBVtpUriRySqgwGJgTSKRw-s7s_ZDHGYSSEYiBsFDk4FK_8buw7x1fEI634Nhtrf9RX4rMM44wgbQYHUZProM3aa7EMJDibpnlBVdY0Qwf5cTNVdO2ytyv8banw0Zcnsb0oLXiv9zQXe9zn3pOWjff_4nfpGK-7vlrT-bbCCyu814ndPRobhLZIxeKgHN2KwdX_jtth1J4Q5hVO0-QPBRFLii6Ef0RvFzoIxFwL70lNOsERNSqYIUlQlmH0msix51qvJiMPJghdyuAqWaJiZGDw2nYBLhAxbRleqIdf5q9RFSDsPbUYKAGFk595Y6t6rQAiZKhZDwkbDDOkzISnoFDB2Nx77kleLty26boJWjuyz6VU1l4L1fuSdBuPo7s3jHdDk82c-CRJSrj8WZXBAOv_mk3RKXvRqLb5yDHngjDFlU0KZTnj35epTf2ohoqvUKRhcH0yxHxwyIyJLGZdL7OR3ZT-QOizNhem9_W4Qp64gPifsxVQobSfB1IQ2906H_vj1o1usbQWI2M1IXz1g3y1cELsE5UzcGhah_mry5JFHCmDMcRrwkDdKhawRRrahDtCfkWCy33IjXR7JD_YoR01XXzsKTkyAtTUxroWISFbxbIY6j7hwz0QpSPFMLCjG6Z77zoMAVQRbty7_dFzIjVzpZLmPK_4Ed2yJ8KOH9BZpUHUTrJAFwtg4I2pIf206Dmk1xyJS2duonkPVL0kVElAlheoNJC2zE5hn9yns6w

Yoshikawa, G., Blanc-Mathieu, R., Song, C., Kayama, Y., Mochizuki, T., Murata, K., Ogata, H. & Takemura, M. 2019. Medusavirus, a novel large DNA virus discovered from hot spring water. Journal of Virology, 10.1128/JVI.02130-18, JVI.02130-18. 10.1128/JVI.02130-18.

Yousuf, F. A., Mehmood, M. H., Malik, A., Siddiqui, R. & Khan, N. A. 2016. Antiacanthamoebic properties of natural and marketed honey in Pakistan. Asian Pac J Trop Biomed, 6. 10.1016/j.apjtb.2016.05.010.

Yu, C. & Irudayaraj, J. 2005. Spectroscopic characterization of microorganisms by Fourier transform infrared microspectroscopy. Biopolymers, 77, (6), 368-377. https://doi.org/10.1002/bip.20247.

Zaheer, S., Hussain, A., Khalil, A., Mansha, M. & Lateef, M. 2019. In vitro anthelmintic activity of ethanolic extracts of Camellia sinensis L. and Albizia lebbeck L. against Haemonchus contortus. Punjab University Journal of Zoology, 34**,** (1), 41-45.

Zaman, V., Zaki, M. & Manzoor, M. 1999. Acanthamoeba in human faeces from Karachi. Ann Trop Med Parasitol, 93**,** (2), 189-91.

Zhivov, A., Guthoff, R. F. & Stachs, O. 2010. In vivo confocal microscopy of the ocular surface: from bench to bedside and back again. British Journal of Ophthalmology, 94**,** (12), 1557. http://bjo.bmj.com/content/94/12/1557.abstract

http://bjo.bmj.com/content/bjophthalmol/94/12/1557.full.pdf

Zhong, R. Z., Li, H. Y., Sun, H. X. & Zhou, D. W. 2014. Effects of supplementation with dietary green tea polyphenols on parasite resistance and acute phase protein response to *Haemonchus contortus* infection in lambs. Veterinary Parasitology, 205**,** (1-2), 199-207. 10.1016/j.vetpar.2014.06.022.

APPENDICES

Appendix 1

Proteins identified within *A. castellanii* culture after treatment with *C. sinensis*

N	%Cov(95)	Accession	Protein	Species	Peptides (95%)
1	54.18999791	sp|P02768|ALBU_HUMAN	Albumin OS=Homo sapiens OX=9606 GN=ALB PE=1 SV=2	HUMAN	28
2	38.0400002	sp|P04264|K2C1_HUMAN	Keratin, type II cytoskeletal 1 OS=Homo sapiens OX=9606 GN=KRT1 PE=1 SV=6	HUMAN	22
3	38.35999966	sp|P13645|K1C10_HUMAN	Keratin, type I cytoskeletal 10 OS=Homo sapiens OX=9606 GN=KRT10 PE=1 SV=6	HUMAN	20
4	46.93000019	sp|P63261|ACTG_HUMAN	Actin, cytoplasmic 2 OS=Homo sapiens OX=9606 GN=ACTG1 PE=1 SV=1	HUMAN	14
4	46.93000019	sp|P60709|ACTB_HUMAN	Actin, cytoplasmic 1 OS=Homo sapiens OX=9606 GN=ACTB PE=1 SV=1	HUMAN	14
5	26.44999921	sp|P35908|K22E_HUMAN	Keratin, type II cytoskeletal 2 epidermal OS=Homo sapiens OX=9606 GN=KRT2 PE=1 SV=2	HUMAN	15
6	13.60999942	sp|O43707|ACTN4_HUMAN	Alpha-actinin-4 OS=Homo sapiens OX=9606 GN=ACTN4 PE=1 SV=2	HUMAN	10
7	13.96999955	sp|P13797|PLST_HUMAN	Plastin-3 OS=Homo sapiens OX=9606 GN=PLS3 PE=1 SV=4	HUMAN	8
8	15.56999981	sp|P00352|AL1A1_HUMAN	Retinal dehydrogenase 1 OS=Homo sapiens OX=9606 GN=ALDH1A1 PE=1 SV=2	HUMAN	8
9	42.96000004	sp|Q01469|FABP5_HUMAN	Fatty acid-binding protein 5 OS=Homo sapiens OX=9606 GN=FABP5 PE=1 SV=3	HUMAN	9
10	7.220999897	sp|A8K2U0|A2ML1_HUMAN	Alpha-2-macroglobulin-like protein 1 OS=Homo sapiens OX=9606 GN=A2ML1 PE=1 SV=3	HUMAN	8
11	18.61999929	sp|P35527|K1C9_HUMAN	Keratin, type I cytoskeletal 9 OS=Homo sapiens OX=9606 GN=KRT9 PE=1 SV=3	HUMAN	7
12	15.17000049	sp|P11142|HSP7C_HUMAN	Heat shock cognate 71 kDa protein OS=Homo sapiens OX=9606 GN=HSPA8 PE=1 SV=1	HUMAN	6
13	23.79000038	sp|P31947|1433S_HUMAN	14-3-3 protein sigma OS=Homo sapiens OX=9606 GN=SFN PE=1 SV=1	HUMAN	6
14	1.554000005	sp|Q9Y6R7|FCGBP_HUMAN	IgGFc-binding protein OS=Homo sapiens OX=9606 GN=FCGBP PE=1 SV=3	HUMAN	5
15	7.163000107	sp|P22079|PERL_HUMAN	Lactoperoxidase OS=Homo sapiens OX=9606 GN=LPO PE=1 SV=2	HUMAN	5
16	15.67000002	sp|P06733|ENOA_HUMAN	Alpha-enolase OS=Homo sapiens OX=9606 GN=ENO1 PE=1 SV=2	HUMAN	5
17	6.741999835	sp|P29401|TKT_HUMAN	Transketolase OS=Homo sapiens OX=9606 GN=TKT PE=1 SV=3	HUMAN	4
18	40.0000006	sp|P62937|PPIA_HUMAN	Peptidyl-prolyl cis-trans isomerase A OS=Homo sapiens OX=9606 GN=PPIA PE=1 SV=2	HUMAN	4
19	26.91000104	sp|P60174|TPIS_HUMAN	Triosephosphate isomerase OS=Homo sapiens OX=9606 GN=TPI1 PE=1 SV=4	HUMAN	5
20	22.75999933	sp|P31946|1433B_HUMAN	14-3-3 protein beta/alpha OS=Homo sapiens OX=9606 GN=YWHAB PE=1 SV=3	HUMAN	5
21	0.536700012	sp|Q7Z5P9|MUC19_HUMAN	Mucin-19 OS=Homo sapiens OX=9606 GN=MUC19 PE=1 SV=3	HUMAN	4

22	19.58999932	sp|P63104|1433Z_HUMAN	14-3-3 protein zeta/delta OS=Homo sapiens OX=9606 GN=YWHAZ PE=1 SV=1	HUMAN	4
23	25.33999979	sp|P12273|PIP_HUMAN	Prolactin-inducible protein OS=Homo sapiens OX=9606 GN=PIP PE=1 SV=1	HUMAN	3
24	14.49999958	sp|P40926|MDHM_HUMAN	Malate dehydrogenase, mitochondrial OS=Homo sapiens OX=9606 GN=MDH2 PE=1 SV=3	HUMAN	4
25	16.58000052	sp|P37802|TAGL2_HUMAN	Transgelin-2 OS=Homo sapiens OX=9606 GN=TAGLN2 PE=1 SV=3	HUMAN	4
26	3.621999919	sp|Q02413|DSG1_HUMAN	Desmoglein-1 OS=Homo sapiens OX=9606 GN=DSG1 PE=1 SV=2	HUMAN	3
27	6.889999658	sp|P07237|PDIA1_HUMAN	Protein disulfide-isomerase OS=Homo sapiens OX=9606 GN=P4HB PE=1 SV=3	HUMAN	3
28	6.535000354	sp|P30101|PDIA3_HUMAN	Protein disulfide-isomerase A3 OS=Homo sapiens OX=9606 GN=PDIA3 PE=1 SV=4	HUMAN	3
29	2.239000052	sp|P01023|A2MG_HUMAN	Alpha-2-macroglobulin OS=Homo sapiens OX=9606 GN=A2M PE=1 SV=3	HUMAN	3
30	14.01000023	sp|P04075|ALDOA_HUMAN	Fructose-bisphosphate aldolase A OS=Homo sapiens OX=9606 GN=ALDOA PE=1 SV=2	HUMAN	3
31	10.98000035	sp|O95274|LYPD3_HUMAN	Ly6/PLAUR domain-containing protein 3 OS=Homo sapiens OX=9606 GN=LYPD3 PE=1 SV=2	HUMAN	3
32	15.79000056	sp|P15531|NDKA_HUMAN	Nucleoside diphosphate kinase A OS=Homo sapiens OX=9606 GN=NME1 PE=1 SV=1	HUMAN	2
32	11.18000001	sp|P22392|NDKB_HUMAN	Nucleoside diphosphate kinase B OS=Homo sapiens OX=9606 GN=NME2 PE=1 SV=1	HUMAN	1
33	10.8099997	sp|P09210|GSTA2_HUMAN	Glutathione S-transferase A2 OS=Homo sapiens OX=9606 GN=GSTA2 PE=1 SV=4	HUMAN	2
33	10.8099997	sp|Q16772|GSTA3_HUMAN	Glutathione S-transferase A3 OS=Homo sapiens OX=9606 GN=GSTA3 PE=1 SV=3	HUMAN	2
33	10.8099997	sp|P08263|GSTA1_HUMAN	Glutathione S-transferase A1 OS=Homo sapiens OX=9606 GN=GSTA1 PE=1 SV=3	HUMAN	2
34	44.67000067	sp|P0CG48|UBC_HUMAN	Polyubiquitin-C OS=Homo sapiens OX=9606 GN=UBC PE=1 SV=3	HUMAN	3
34	44.53999996	sp|P0CG47|UBB_HUMAN	Polyubiquitin-B OS=Homo sapiens OX=9606 GN=UBB PE=1 SV=1	HUMAN	3
34	26.55999959	sp|P62987|RL40_HUMAN	Ubiquitin-60S ribosomal protein L40 OS=Homo sapiens OX=9606 GN=UBA52 PE=1 SV=2	HUMAN	3
34	21.78999931	sp|P62979|RS27A_HUMAN	Ubiquitin-40S ribosomal protein S27a OS=Homo sapiens OX=9606 GN=RPS27A PE=1 SV=2	HUMAN	3
35	17.85999984	sp|P07737|PROF1_HUMAN	Profilin-1 OS=Homo sapiens OX=9606 GN=PFN1 PE=1 SV=2	HUMAN	2
36	9.00600031	sp|P05089|ARGI1_HUMAN	Arginase-1 OS=Homo sapiens OX=9606 GN=ARG1 PE=1 SV=2	HUMAN	2
37	7.435999811	sp|P48594|SPB4_HUMAN	Serpin B4 OS=Homo sapiens OX=9606 GN=SERPINB4 PE=1 SV=2	HUMAN	3
37	7.435999811	sp|P29508|SPB3_HUMAN	Serpin B3 OS=Homo sapiens OX=9606 GN=SERPINB3 PE=1 SV=2	HUMAN	3
38	4.039999843	sp|Q08188|TGM3_HUMAN	Protein-glutamine gamma-glutamyltransferase E OS=Homo sapiens OX=9606 GN=TGM3 PE=1 SV=4	HUMAN	2
39	15.64999968	sp|P68871|HBB_HUMAN	Hemoglobin subunit beta OS=Homo sapiens OX=9606 GN=HBB PE=1 SV=2	HUMAN	2
40	5.987999961	sp|P07195|LDHB_HUMAN	L-lactate dehydrogenase B chain OS=Homo sapiens OX=9606 GN=LDHB PE=1 SV=2	HUMAN	2
41	6.287000328	sp|P40925|MDHC_HUMAN	Malate dehydrogenase, cytoplasmic OS=Homo sapiens OX=9606 GN=MDH1 PE=1 SV=4	HUMAN	2
42	3.068999946	sp|P06396|GELS_HUMAN	Gelsolin OS=Homo sapiens OX=9606 GN=GSN PE=1 SV=1	HUMAN	4
43	6.396000087	sp|P0DMV9|HS71B_HUMAN	Heat shock 70 kDa protein 1B OS=Homo sapiens OX=9606 GN=HSPA1B PE=1 SV=1	HUMAN	3
43	6.396000087	sp|P0DMV8|HS71A_HUMAN	Heat shock 70 kDa protein 1A OS=Homo sapiens OX=9606 GN=HSPA1A PE=1 SV=1	HUMAN	3

43	6.396000087	sp|P34931|HS71L_HUMAN	Heat shock 70 kDa protein 1-like OS=Homo sapiens OX=9606 GN=HSPA1L PE=1 SV=2	HUMAN	3
44	7.75000006	sp|Q9UDX4|S14L3_HUMAN	SEC14-like protein 3 OS=Homo sapiens OX=9606 GN=SEC14L3 PE=1 SV=1	HUMAN	2
45	12.94	sp|P62258|1433E_HUMAN	14-3-3 protein epsilon OS=Homo sapiens OX=9606 GN=YWHAE PE=1 SV=1	HUMAN	3
46	14.14999962	sp|P0DOY3|IGLC3_HUMAN	Immunoglobulin lambda constant 3 OS=Homo sapiens OX=9606 GN=IGLC3 PE=1 SV=1	HUMAN	1
46	14.14999962	sp|P0DOY2|IGLC2_HUMAN	Immunoglobulin lambda constant 2 OS=Homo sapiens OX=9606 GN=IGLC2 PE=1 SV=1	HUMAN	1
46	14.14999962	sp|P0CG04|IGLC1_HUMAN	Immunoglobulin lambda constant 1 OS=Homo sapiens OX=9606 GN=IGLC1 PE=1 SV=1	HUMAN	1
46	14.14999962	sp|P0CF74|IGLC6_HUMAN	Immunoglobulin lambda constant 6 OS=Homo sapiens OX=9606 GN=IGLC6 PE=1 SV=1	HUMAN	1
46	14.14999962	sp|A0M8Q6|IGLC7_HUMAN	Immunoglobulin lambda constant 7 OS=Homo sapiens OX=9606 GN=IGLC7 PE=1 SV=3	HUMAN	1
46	10.64999998	sp|P0DOX8|IGL1_HUMAN	Immunoglobulin lambda-1 light chain OS=Homo sapiens OX=9606 PE=1 SV=1	HUMAN	2
46	7.009000331	sp|B9A064|IGLL5_HUMAN	Immunoglobulin lambda-like polypeptide 5 OS=Homo sapiens OX=9606 GN=IGLL5 PE=2 SV=2	HUMAN	1
46	6.837999821	sp|P01721|LV657_HUMAN	Immunoglobulin lambda variable 6-57 OS=Homo sapiens OX=9606 GN=IGLV6-57 PE=1 SV=2	HUMAN	1
46	6.837999821	sp|P01700|LV147_HUMAN	Immunoglobulin lambda variable 1-47 OS=Homo sapiens OX=9606 GN=IGLV1-47 PE=1 SV=2	HUMAN	1
46	6.837999821	sp|P01699|LV144_HUMAN	Immunoglobulin lambda variable 1-44 OS=Homo sapiens OX=9606 GN=IGLV1-44 PE=1 SV=2	HUMAN	1
46	6.780000031	sp|P01709|LV208_HUMAN	Immunoglobulin lambda variable 2-8 OS=Homo sapiens OX=9606 GN=IGLV2-8 PE=1 SV=2	HUMAN	1
46	6.780000031	sp|P01703|LV140_HUMAN	Immunoglobulin lambda variable 1-40 OS=Homo sapiens OX=9606 GN=IGLV1-40 PE=1 SV=2	HUMAN	1
46	6.780000031	sp|A0A075B6J9|LV218_HUMAN	Immunoglobulin lambda variable 2-18 OS=Homo sapiens OX=9606 GN=IGLV2-18 PE=3 SV=2	HUMAN	1
46	6.723000109	sp|P01706|LV211_HUMAN	Immunoglobulin lambda variable 2-11 OS=Homo sapiens OX=9606 GN=IGLV2-11 PE=1 SV=2	HUMAN	1
47	30.84000051	sp|P01834|IGKC_HUMAN	Immunoglobulin kappa constant OS=Homo sapiens OX=9606 GN=IGKC PE=1 SV=2	HUMAN	2
47	15.42000026	sp|P0DOX7|IGK_HUMAN	Immunoglobulin kappa light chain OS=Homo sapiens OX=9606 PE=1 SV=1	HUMAN	2
48	10.00000015	sp|P09211|GSTP1_HUMAN	Glutathione S-transferase P OS=Homo sapiens OX=9606 GN=GSTP1 PE=1 SV=2	HUMAN	2
49	6.143999845	sp|P02533|K1C14_HUMAN	Keratin, type I cytoskeletal 14 OS=Homo sapiens OX=9606 GN=KRT14 PE=1 SV=4	HUMAN	4
49	6.131000072	sp|P08779|K1C16_HUMAN	Keratin, type I cytoskeletal 16 OS=Homo sapiens OX=9606 GN=KRT16 PE=1 SV=4	HUMAN	4
49	3.051000088	sp|Q8N1A0|KT222_HUMAN	Keratin-like protein KRT222 OS=Homo sapiens OX=9606 GN=KRT222 PE=1 SV=1	HUMAN	1
49	2.250000089	sp|P08727|K1C19_HUMAN	Keratin, type I cytoskeletal 19 OS=Homo sapiens OX=9606 GN=KRT19 PE=1 SV=4	HUMAN	1
49	2.122999914	sp|P35900|K1C20_HUMAN	Keratin, type I cytoskeletal 20 OS=Homo sapiens OX=9606 GN=KRT20 PE=1 SV=1	HUMAN	1
49	2.082999982	sp|Q04695|K1C17_HUMAN	Keratin, type I cytoskeletal 17 OS=Homo sapiens OX=9606 GN=KRT17 PE=1 SV=2	HUMAN	1
49	1.974000037	sp|P19012|K1C15_HUMAN	Keratin, type I cytoskeletal 15 OS=Homo sapiens OX=9606 GN=KRT15 PE=1 SV=3	HUMAN	1
50	10.67999974	sp|P13647|K2C5_HUMAN	Keratin, type II cytoskeletal 5 OS=Homo sapiens OX=9606 GN=KRT5 PE=1 SV=3	HUMAN	6
51	8.054000139	sp|P25311|ZA2G_HUMAN	Zinc-alpha-2-glycoprotein OS=Homo sapiens OX=9606 GN=AZGP1 PE=1 SV=2	HUMAN	2
52	6.917999685	sp|P01591|IGJ_HUMAN	Immunoglobulin J chain OS=Homo sapiens OX=9606 GN=JCHAIN PE=1 SV=4	HUMAN	2

53	20.40999979	sp|P01040|CYTA_HUMAN	Cystatin-A OS=Homo sapiens OX=9606 GN=CSTA PE=1 SV=1	HUMAN	2
54	2.734999917	sp|A8K7I4|CLCA1_HUMAN	Calcium-activated chloride channel regulator 1 OS=Homo sapiens OX=9606 GN=CLCA1 PE=1 SV=3	HUMAN	2
54	0.870500039	sp|Q14CN2|CLCA4_HUMAN	Calcium-activated chloride channel regulator 4 OS=Homo sapiens OX=9606 GN=CLCA4 PE=1 SV=2	HUMAN	1
55	7.648999989	sp|P01876|IGHA1_HUMAN	Immunoglobulin heavy constant alpha 1 OS=Homo sapiens OX=9606 GN=IGHA1 PE=1 SV=2	HUMAN	2
56	19.34999973	sp|Q9H299|SH3L3_HUMAN	SH3 domain-binding glutamic acid-rich-like protein 3 OS=Homo sapiens OX=9606 GN=SH3BGRL3 PE=1 SV=1	HUMAN	2
57	3.581999987	sp|P02787|TRFE_HUMAN	Serotransferrin OS=Homo sapiens OX=9606 GN=TF PE=1 SV=3	HUMAN	3
58	2.687999979	sp|P06744|G6PI_HUMAN	Glucose-6-phosphate isomerase OS=Homo sapiens OX=9606 GN=GPI PE=1 SV=4	HUMAN	1
59	5.296999961	sp|Q13228|SBP1_HUMAN	Methanethiol oxidase OS=Homo sapiens OX=9606 GN=SELENBP1 PE=1 SV=2	HUMAN	2
60	0.156200002	sp|Q9HC84|MUC5B_HUMAN	Mucin-5B OS=Homo sapiens OX=9606 GN=MUC5B PE=1 SV=3	HUMAN	1
61	4.148000106	sp|Q8N4F0|BPIB2_HUMAN	BPI fold-containing family B member 2 OS=Homo sapiens OX=9606 GN=BPIFB2 PE=1 SV=2	HUMAN	3
62	14.2900005	sp|P10599|THIO_HUMAN	Thioredoxin OS=Homo sapiens OX=9606 GN=TXN PE=1 SV=3	HUMAN	1
63	2.598999999	sp|P11021|BIP_HUMAN	Endoplasmic reticulum chaperone BiP OS=Homo sapiens OX=9606 GN=HSPA5 PE=1 SV=2	HUMAN	2
64	10.54999977	sp|Q06830|PRDX1_HUMAN	Peroxiredoxin-1 OS=Homo sapiens OX=9606 GN=PRDX1 PE=1 SV=1	HUMAN	2
65	10.81999987	sp|P48668|K2C6C_HUMAN	Keratin, type II cytoskeletal 6C OS=Homo sapiens OX=9606 GN=KRT6C PE=1 SV=3	HUMAN	6
65	10.81999987	sp|P02538|K2C6A_HUMAN	Keratin, type II cytoskeletal 6A OS=Homo sapiens OX=9606 GN=KRT6A PE=1 SV=3	HUMAN	6
65	7.622999698	sp|O95678|K2C75_HUMAN	Keratin, type II cytoskeletal 75 OS=Homo sapiens OX=9606 GN=KRT75 PE=1 SV=2	HUMAN	4
66	8.980000019	sp|P27348|1433T_HUMAN	14-3-3 protein theta OS=Homo sapiens OX=9606 GN=YWHAQ PE=1 SV=1	HUMAN	2
67	2.639999986	sp|O75083|WDR1_HUMAN	WD repeat-containing protein 1 OS=Homo sapiens OX=9606 GN=WDR1 PE=1 SV=4	HUMAN	1
68	5.139999837	sp|P30044|PRDX5_HUMAN	Peroxiredoxin-5, mitochondrial OS=Homo sapiens OX=9606 GN=PRDX5 PE=1 SV=4	HUMAN	1
69	7.81499967	sp|P13796|PLSL_HUMAN	Plastin-2 OS=Homo sapiens OX=9606 GN=LCP1 PE=1 SV=6	HUMAN	6
70	3.200000152	sp|P36952|SPB5_HUMAN	Serpin B5 OS=Homo sapiens OX=9606 GN=SERPINB5 PE=1 SV=2	HUMAN	1
71	4.331000149	sp|P18669|PGAM1_HUMAN	Phosphoglycerate mutase 1 OS=Homo sapiens OX=9606 GN=PGAM1 PE=1 SV=2	HUMAN	1
72	0.742299994	sp|Q9UQC9|CLCA2_HUMAN	Calcium-activated chloride channel regulator 2 OS=Homo sapiens OX=9606 GN=CLCA2 PE=1 SV=2	HUMAN	1
73	2.216999978	sp|P00738|HPT_HUMAN	Haptoglobin OS=Homo sapiens OX=9606 GN=HP PE=1 SV=1	HUMAN	1
74	1.975999959	sp|P49590|SYHM_HUMAN	Histidine--tRNA ligase, mitochondrial OS=Homo sapiens OX=9606 GN=HARS2 PE=1 SV=1	HUMAN	1
75	13.35999966	sp|P61981|1433G_HUMAN	14-3-3 protein gamma OS=Homo sapiens OX=9606 GN=YWHAG PE=1 SV=2	HUMAN	3
76	4.904000089	sp|P08729|K2C7_HUMAN	Keratin, type II cytoskeletal 7 OS=Homo sapiens OX=9606 GN=KRT7 PE=1 SV=5	HUMAN	2
77	6.328999996	sp|Q9UHA7|IL36A_HUMAN	Interleukin-36 alpha OS=Homo sapiens OX=9606 GN=IL36A PE=1 SV=1	HUMAN	1
78	2.751999907	sp|Q96IG2|FXL20_HUMAN	F-box/LRR-repeat protein 20 OS=Homo sapiens OX=9606 GN=FBXL20 PE=1 SV=2	HUMAN	1

79	1.138000004	sp|Q6ZSS7|MFSD6_HUMAN	Major facilitator superfamily domain-containing protein 6 OS=Homo sapiens OX=9606 GN=MFSD6 PE=1 SV=2	HUMAN	1
80	6.338000298	sp|P69905|HBA_HUMAN	Hemoglobin subunit alpha OS=Homo sapiens OX=9606 GN=HBA1 PE=1 SV=2	HUMAN	1
81	1.374999993	sp|P12081|HARS1_HUMAN	Histidine--tRNA ligase, cytoplasmic OS=Homo sapiens OX=9606 GN=HARS1 PE=1 SV=2	HUMAN	1
82	0.89069996	RRRRRsp|P46019|KPB2_HUMAN	REVERSED Phosphorylase b kinase regulatory subunit alpha, liver isoform OS=Homo sapiens OX=9606 GN=PHKA2 PE=1 SV=1	HUMAN	1
83	6.682000309	sp|P13929|ENOB_HUMAN	Beta-enolase OS=Homo sapiens OX=9606 GN=ENO3 PE=1 SV=5	HUMAN	2
84	4.077000171	sp|P00558|PGK1_HUMAN	Phosphoglycerate kinase 1 OS=Homo sapiens OX=9606 GN=PGK1 PE=1 SV=3	HUMAN	1
85	4.368999973	sp|P07339|CATD_HUMAN	Cathepsin D OS=Homo sapiens OX=9606 GN=CTSD PE=1 SV=1	HUMAN	1
86	2.267999947	sp|P06576|ATPB_HUMAN	ATP synthase subunit beta, mitochondrial OS=Homo sapiens OX=9606 GN=ATP5F1B PE=1 SV=3	HUMAN	1
87	10.70000008	sp|P30086|PEBP1_HUMAN	Phosphatidylethanolamine-binding protein 1 OS=Homo sapiens OX=9606 GN=PEBP1 PE=1 SV=3	HUMAN	1
88	1.417000033	sp|P20742|PZP_HUMAN	Pregnancy zone protein OS=Homo sapiens OX=9606 GN=PZP PE=1 SV=4	HUMAN	2
89	6.332000345	sp|P13646|K1C13_HUMAN	Keratin, type I cytoskeletal 13 OS=Homo sapiens OX=9606 GN=KRT13 PE=1 SV=4	HUMAN	3
90	10.74000001	sp|P0DP25|CALM3_HUMAN	Calmodulin-3 OS=Homo sapiens OX=9606 GN=CALM3 PE=1 SV=1	HUMAN	1
90	10.74000001	sp|P0DP24|CALM2_HUMAN	Calmodulin-2 OS=Homo sapiens OX=9606 GN=CALM2 PE=1 SV=1	HUMAN	1
90	10.74000001	sp|P0DP23|CALM1_HUMAN	Calmodulin-1 OS=Homo sapiens OX=9606 GN=CALM1 PE=1 SV=1	HUMAN	1
91	3.190999851	sp|P24855|DNAS1_HUMAN	Deoxyribonuclease-1 OS=Homo sapiens OX=9606 GN=DNASE1 PE=1 SV=1	HUMAN	1

Appendix 2

Proteins identified within *A. castellanii* culture before treatment with *C. sinensis*

N	%Cov(95)	Accession	Proteins	Species	Peptides (95%)
1	59.76999998	sp|P02768|ALBU_HUMAN	Albumin OS=Homo sapiens OX=9606 GN=ALB PE=1 SV=2	HUMAN	32
2	37.88999915	sp|P04264|K2C1_HUMAN	Keratin, type II cytoskeletal 1 OS=Homo sapiens OX=9606 GN=KRT1 PE=1 SV=6	HUMAN	22
3	26.78000033	sp|P11142|HSP7C_HUMAN	Heat shock cognate 71 kDa protein OS=Homo sapiens OX=9606 GN=HSPA8 PE=1 SV=1	HUMAN	15
4	51.99999809	sp|P63261|ACTG_HUMAN	Actin, cytoplasmic 2 OS=Homo sapiens OX=9606 GN=ACTG1 PE=1 SV=1	HUMAN	17
4	51.99999809	sp|P60709|ACTB_HUMAN	Actin, cytoplasmic 1 OS=Homo sapiens OX=9606 GN=ACTB PE=1 SV=1	HUMAN	17
5	31.45999908	sp|P35527|K1C9_HUMAN	Keratin, type I cytoskeletal 9 OS=Homo sapiens OX=9606 GN=KRT9 PE=1 SV=3	HUMAN	13
6	40.0000006	sp|P63104|1433Z_HUMAN	14-3-3 protein zeta/delta OS=Homo sapiens OX=9606 GN=YWHAZ PE=1 SV=1	HUMAN	10
7	25.85999966	sp|P13645|K1C10_HUMAN	Keratin, type I cytoskeletal 10 OS=Homo sapiens OX=9606 GN=KRT10 PE=1 SV=6	HUMAN	10
8	39.6299988	sp|P06733|ENOA_HUMAN	Alpha-enolase OS=Homo sapiens OX=9606 GN=ENO1 PE=1 SV=2	HUMAN	11
9	24.09999967	sp|P08779|K1C16_HUMAN	Keratin, type I cytoskeletal 16 OS=Homo sapiens OX=9606 GN=KRT16 PE=1 SV=4	HUMAN	9
10	13.39000016	sp|O43707|ACTN4_HUMAN	Alpha-actinin-4 OS=Homo sapiens OX=9606 GN=ACTN4 PE=1 SV=2	HUMAN	9
11	7.703000307	sp|A8K2U0|A2ML1_HUMAN	Alpha-2-macroglobulin-like protein 1 OS=Homo sapiens OX=9606 GN=A2ML1 PE=1 SV=3	HUMAN	9
12	22.4999994	sp|P06576|ATPB_HUMAN	ATP synthase subunit beta, mitochondrial OS=Homo sapiens OX=9606 GN=ATP5F1B PE=1 SV=3	HUMAN	9
13	23.7499997	sp|P00352|AL1A1_HUMAN	Retinal dehydrogenase 1 OS=Homo sapiens OX=9606 GN=ALDH1A1 PE=1 SV=2	HUMAN	10

14	45.78000009	sp|P60174|TPIS_HUMAN	Triosephosphate isomerase OS=Homo sapiens OX=9606 GN=TPI1 PE=1 SV=4	HUMAN	7
15	42.96000004	sp|Q01469|FABP5_HUMAN	Fatty acid-binding protein 5 OS=Homo sapiens OX=9606 GN=FABP5 PE=1 SV=3	HUMAN	8
16	16.89999998	sp|P35908|K22E_HUMAN	Keratin, type II cytoskeletal 2 epidermal OS=Homo sapiens OX=9606 GN=KRT2 PE=1 SV=2	HUMAN	9
17	12.86000013	sp|P13797|PLST_HUMAN	Plastin-3 OS=Homo sapiens OX=9606 GN=PLS3 PE=1 SV=4	HUMAN	7
18	1.998000033	sp|Q9Y6R7|FCGBP_HUMAN	IgGFc-binding protein OS=Homo sapiens OX=9606 GN=FCGBP PE=1 SV=3	HUMAN	7
19	36.6899997	sp|P31947|1433S_HUMAN	14-3-3 protein sigma OS=Homo sapiens OX=9606 GN=SFN PE=1 SV=1	HUMAN	8
20	22.49000072	sp|P40926|MDHM_HUMAN	Malate dehydrogenase, mitochondrial OS=Homo sapiens OX=9606 GN=MDH2 PE=1 SV=3	HUMAN	6
21	9.741999954	sp|P02787|TRFE_HUMAN	Serotransferrin OS=Homo sapiens OX=9606 GN=TF PE=1 SV=3	HUMAN	6
22	24.44999963	sp|P04075|ALDOA_HUMAN	Fructose-bisphosphate aldolase A OS=Homo sapiens OX=9606 GN=ALDOA PE=1 SV=2	HUMAN	6
23	27.16999948	sp|P18669|PGAM1_HUMAN	Phosphoglycerate mutase 1 OS=Homo sapiens OX=9606 GN=PGAM1 PE=1 SV=2	HUMAN	5
24	8.848000318	sp|P22079|PERL_HUMAN	Lactoperoxidase OS=Homo sapiens OX=9606 GN=LPO PE=1 SV=2	HUMAN	5
25	19.24999952	sp|Q9UDX4|S14L3_HUMAN	SEC14-like protein 3 OS=Homo sapiens OX=9606 GN=SEC14L3 PE=1 SV=1	HUMAN	5
26	43.63999963	sp|P62937|PPIA_HUMAN	Peptidyl-prolyl cis-trans isomerase A OS=Homo sapiens OX=9606 GN=PPIA PE=1 SV=2	HUMAN	5
27	5.909999833	sp|Q02413|DSG1_HUMAN	Desmoglein-1 OS=Homo sapiens OX=9606 GN=DSG1 PE=1 SV=2	HUMAN	6
28	11.87999994	sp|P30101|PDIA3_HUMAN	Protein disulfide-isomerase A3 OS=Homo sapiens OX=9606 GN=PDIA3 PE=1 SV=4	HUMAN	5
29	30.14999926	sp|P37802|TAGL2_HUMAN	Transgelin-2 OS=Homo sapiens OX=9606 GN=TAGLN2 PE=1 SV=3	HUMAN	5
30	0.656000013	sp|Q7Z5P9|MUC19_HUMAN	Mucin-19 OS=Homo sapiens OX=9606 GN=MUC19 PE=1 SV=3	HUMAN	4
31	16.76000059	sp|O95274|LYPD3_HUMAN	Ly6/PLAUR domain-containing protein 3 OS=Homo sapiens OX=9606 GN=LYPD3 PE=1 SV=2	HUMAN	4
32	9.149000049	sp|P29401|TKT_HUMAN	Transketolase OS=Homo sapiens OX=9606 GN=TKT PE=1 SV=3	HUMAN	4
33	3.12099997	sp|P01023|A2MG_HUMAN	Alpha-2-macroglobulin OS=Homo sapiens OX=9606 GN=A2M PE=1 SV=3	HUMAN	4
34	15.60000032	sp|P48668|K2C6C_HUMAN	Keratin, type II cytoskeletal 6C OS=Homo sapiens OX=9606 GN=KRT6C PE=1 SV=3	HUMAN	8
34	15.60000032	sp|P02538|K2C6A_HUMAN	Keratin, type II cytoskeletal 6A OS=Homo sapiens OX=9606 GN=KRT6A PE=1 SV=3	HUMAN	8
35	34.86999869	sp|P22392|NDKB_HUMAN	Nucleoside diphosphate kinase B OS=Homo sapiens OX=9606 GN=NME2 PE=1 SV=1	HUMAN	4
35	25	sp|P15531|NDKA_HUMAN	Nucleoside diphosphate kinase A OS=Homo sapiens OX=9606 GN=NME1 PE=1 SV=1	HUMAN	3
36	29.53000069	sp|P0DP25|CALM3_HUMAN	Calmodulin-3 OS=Homo sapiens OX=9606 GN=CALM3 PE=1 SV=1	HUMAN	4

36	29.53000069	sp|P0DP24|CALM2_HUMAN	Calmodulin-2 OS=Homo sapiens OX=9606 GN=CALM2 PE=1 SV=1	HUMAN	4
36	29.53000069	sp|P0DP23|CALM1_HUMAN	Calmodulin-1 OS=Homo sapiens OX=9606 GN=CALM1 PE=1 SV=1	HUMAN	4
37	13.24999928	sp|P00338|LDHA_HUMAN	L-lactate dehydrogenase A chain OS=Homo sapiens OX=9606 GN=LDHA PE=1 SV=2	HUMAN	4
38	10.10000035	sp|P00738|HPT_HUMAN	Haptoglobin OS=Homo sapiens OX=9606 GN=HP PE=1 SV=1	HUMAN	4
39	14.91000056	sp|P05089|ARGI1_HUMAN	Arginase-1 OS=Homo sapiens OX=9606 GN=ARG1 PE=1 SV=2	HUMAN	4
40	8.268000185	sp|P07237|PDIA1_HUMAN	Protein disulfide-isomerase OS=Homo sapiens OX=9606 GN=P4HB PE=1 SV=3	HUMAN	3
41	17.5699994	sp|P08263|GSTA1_HUMAN	Glutathione S-transferase A1 OS=Homo sapiens OX=9606 GN=GSTA1 PE=1 SV=3	HUMAN	4
41	14.40999955	sp|P09210|GSTA2_HUMAN	Glutathione S-transferase A2 OS=Homo sapiens OX=9606 GN=GSTA2 PE=1 SV=4	HUMAN	3
42	17.85999984	sp|P30041|PRDX6_HUMAN	Peroxiredoxin-6 OS=Homo sapiens OX=9606 GN=PRDX6 PE=1 SV=3	HUMAN	3
43	17.64999926	sp|P62258|1433E_HUMAN	14-3-3 protein epsilon OS=Homo sapiens OX=9606 GN=YWHAE PE=1 SV=1	HUMAN	4
44	21.14000022	sp|P31946|1433B_HUMAN	14-3-3 protein beta/alpha OS=Homo sapiens OX=9606 GN=YWHAB PE=1 SV=3	HUMAN	5
45	15.09999931	sp|P25311|ZA2G_HUMAN	Zinc-alpha-2-glycoprotein OS=Homo sapiens OX=9606 GN=AZGP1 PE=1 SV=2	HUMAN	3
46	11.6899997	sp|P14550|AK1A1_HUMAN	Aldo-keto reductase family 1 member A1 OS=Homo sapiens OX=9606 GN=AKR1A1 PE=1 SV=3	HUMAN	3
47	10.17000005	sp|Q13228|SBP1_HUMAN	Methanethiol oxidase OS=Homo sapiens OX=9606 GN=SELENBP1 PE=1 SV=2	HUMAN	3
48	4.617999867	sp|Q08188|TGM3_HUMAN	Protein-glutamine gamma-glutamyltransferase E OS=Homo sapiens OX=9606 GN=TGM3 PE=1 SV=4	HUMAN	2
49	8.73600021	sp|P0DMV9|HS71B_HUMAN	Heat shock 70 kDa protein 1B OS=Homo sapiens OX=9606 GN=HSPA1B PE=1 SV=1	HUMAN	5
49	8.73600021	sp|P34931|HS71L_HUMAN	Heat shock 70 kDa protein 1-like OS=Homo sapiens OX=9606 GN=HSPA1L PE=1 SV=2	HUMAN	5
49	8.73600021	sp|P0DMV8|HS71A_HUMAN	Heat shock 70 kDa protein 1A OS=Homo sapiens OX=9606 GN=HSPA1A PE=1 SV=1	HUMAN	5
50	2.734999917	sp|A8K7I4|CLCA1_HUMAN	Calcium-activated chloride channel regulator 1 OS=Homo sapiens OX=9606 GN=CLCA1 PE=1 SV=3	HUMAN	2
51	16.18999988	sp|P09211|GSTP1_HUMAN	Glutathione S-transferase P OS=Homo sapiens OX=9606 GN=GSTP1 PE=1 SV=2	HUMAN	3
52	38.78000081	sp|P01040|CYTA_HUMAN	Cystatin-A OS=Homo sapiens OX=9606 GN=CSTA PE=1 SV=1	HUMAN	3
53	3.068999946	sp|P06396|GELS_HUMAN	Gelsolin OS=Homo sapiens OX=9606 GN=GSN PE=1 SV=1	HUMAN	2
54	6.741999835	sp|P50395|GDIB_HUMAN	Rab GDP dissociation inhibitor beta OS=Homo sapiens OX=9606 GN=GDI2 PE=1 SV=2	HUMAN	2

55	7.784000039	sp|P40925|MDHC_HUMAN	Malate dehydrogenase, cytoplasmic OS=Homo sapiens OX=9606 GN=MDH1 PE=1 SV=4	HUMAN	2
56	33.64000022	sp|P01834|IGKC_HUMAN	Immunoglobulin kappa constant OS=Homo sapiens OX=9606 GN=IGKC PE=1 SV=2	HUMAN	2
56	16.82000011	sp|P0DOX7|IGK_HUMAN	Immunoglobulin kappa light chain OS=Homo sapiens OX=9606 PE=1 SV=1	HUMAN	2
57	16.89999998	sp|P69905|HBA_HUMAN	Hemoglobin subunit alpha OS=Homo sapiens OX=9606 GN=HBA1 PE=1 SV=2	HUMAN	2
58	15.64999968	sp|P68871|HBB_HUMAN	Hemoglobin subunit beta OS=Homo sapiens OX=9606 GN=HBB PE=1 SV=2	HUMAN	2
58	6.802999973	sp|P69892|HBG2_HUMAN	Hemoglobin subunit gamma-2 OS=Homo sapiens OX=9606 GN=HBG2 PE=1 SV=2	HUMAN	1
58	6.802999973	sp|P69891|HBG1_HUMAN	Hemoglobin subunit gamma-1 OS=Homo sapiens OX=9606 GN=HBG1 PE=1 SV=2	HUMAN	1
58	6.802999973	sp|P02100|HBE_HUMAN	Hemoglobin subunit epsilon OS=Homo sapiens OX=9606 GN=HBE1 PE=1 SV=2	HUMAN	1
58	6.802999973	sp|P02042|HBD_HUMAN	Hemoglobin subunit delta OS=Homo sapiens OX=9606 GN=HBD PE=1 SV=2	HUMAN	1
59	2.720000036	sp|P55786|PSA_HUMAN	Puromycin-sensitive aminopeptidase OS=Homo sapiens OX=9606 GN=NPEPPS PE=1 SV=2	HUMAN	2
59	2.720000036	sp|A6NEC2|PSAL_HUMAN	Puromycin-sensitive aminopeptidase-like protein OS=Homo sapiens OX=9606 GN=NPEPPSL1 PE=2 SV=3	HUMAN	1
60	12.07000017	sp|P40121|CAPG_HUMAN	Macrophage-capping protein OS=Homo sapiens OX=9606 GN=CAPG PE=1 SV=2	HUMAN	2
61	18.17999929	sp|P30086|PEBP1_HUMAN	Phosphatidylethanolamine-binding protein 1 OS=Homo sapiens OX=9606 GN=PEBP1 PE=1 SV=3	HUMAN	2
62	15.06000012	sp|P23528|COF1_HUMAN	Cofilin-1 OS=Homo sapiens OX=9606 GN=CFL1 PE=1 SV=3	HUMAN	2
62	6.627000123	sp|Q9Y281|COF2_HUMAN	Cofilin-2 OS=Homo sapiens OX=9606 GN=CFL2 PE=1 SV=1	HUMAN	1
63	5.643000081	sp|P14384|CBPM_HUMAN	Carboxypeptidase M OS=Homo sapiens OX=9606 GN=CPM PE=1 SV=2	HUMAN	2
64	6.917999685	sp|P01591|IGJ_HUMAN	Immunoglobulin J chain OS=Homo sapiens OX=9606 GN=JCHAIN PE=1 SV=4	HUMAN	2
65	5.600000173	sp|P36952|SPB5_HUMAN	Serpin B5 OS=Homo sapiens OX=9606 GN=SERPINB5 PE=1 SV=2	HUMAN	2
66	19.34999973	sp|Q9H299|SH3L3_HUMAN	SH3 domain-binding glutamic acid-rich-like protein 3 OS=Homo sapiens OX=9606 GN=SH3BGRL3 PE=1 SV=1	HUMAN	2
67	12.25999966	sp|Q9UBH0|I36RA_HUMAN	Interleukin-36 receptor antagonist protein OS=Homo sapiens OX=9606 GN=IL36RN PE=1 SV=1	HUMAN	2
68	0.347099989	sp|Q9HC84|MUC5B_HUMAN	Mucin-5B OS=Homo sapiens OX=9606 GN=MUC5B PE=1 SV=3	HUMAN	2
69	1.803000085	sp|Q9UQC9|CLCA2_HUMAN	Calcium-activated chloride channel regulator 2 OS=Homo sapiens OX=9606 GN=CLCA2 PE=1 SV=2	HUMAN	2

70	12.38999963	sp|P46439|GSTM5_HUMAN	Glutathione S-transferase Mu 5 OS=Homo sapiens OX=9606 GN=GSTM5 PE=1 SV=3	HUMAN	2
71	3.293000162	sp|P26038|MOES_HUMAN	Moesin OS=Homo sapiens OX=9606 GN=MSN PE=1 SV=3	HUMAN	2
71	3.259000182	sp|P35241|RADI_HUMAN	Radixin OS=Homo sapiens OX=9606 GN=RDX PE=1 SV=1	HUMAN	2
71	3.24199982	sp|P15311|EZRI_HUMAN	Ezrin OS=Homo sapiens OX=9606 GN=EZR PE=1 SV=4	HUMAN	2
72	17.35000014	sp|P29034|S10A2_HUMAN	Protein S100-A2 OS=Homo sapiens OX=9606 GN=S100A2 PE=1 SV=3	HUMAN	2
73	12.91999966	sp|P02533|K1C14_HUMAN	Keratin, type I cytoskeletal 14 OS=Homo sapiens OX=9606 GN=KRT14 PE=1 SV=4	HUMAN	5
74	2.401999943	sp|Q8N4F0|BPIB2_HUMAN	BPI fold-containing family B member 2 OS=Homo sapiens OX=9606 GN=BPIFB2 PE=1 SV=2	HUMAN	2
75	4.281000048	sp|P11021|BIP_HUMAN	Endoplasmic reticulum chaperone BiP OS=Homo sapiens OX=9606 GN=HSPA5 PE=1 SV=2	HUMAN	3
76	14.2900005	sp|P10599|THIO_HUMAN	Thioredoxin OS=Homo sapiens OX=9606 GN=TXN PE=1 SV=3	HUMAN	1
77	1.049000025	sp|P13639|EF2_HUMAN	Elongation factor 2 OS=Homo sapiens OX=9606 GN=EEF2 PE=1 SV=4	HUMAN	1
78	3.85800004	sp|P37837|TALDO_HUMAN	Transaldolase OS=Homo sapiens OX=9606 GN=TALDO1 PE=1 SV=2	HUMAN	1
79	21.01999968	sp|P0CG48|UBC_HUMAN	Polyubiquitin-C OS=Homo sapiens OX=9606 GN=UBC PE=1 SV=3	HUMAN	1
79	20.96000016	sp|P0CG47|UBB_HUMAN	Polyubiquitin-B OS=Homo sapiens OX=9606 GN=UBB PE=1 SV=1	HUMAN	1
79	12.5	sp|P62987|RL40_HUMAN	Ubiquitin-60S ribosomal protein L40 OS=Homo sapiens OX=9606 GN=UBA52 PE=1 SV=2	HUMAN	1
79	10.26000008	sp|P62979|RS27A_HUMAN	Ubiquitin-40S ribosomal protein S27a OS=Homo sapiens OX=9606 GN=RPS27A PE=1 SV=2	HUMAN	1
80	2.479000017	sp|P00813|ADA_HUMAN	Adenosine deaminase OS=Homo sapiens OX=9606 GN=ADA PE=1 SV=3	HUMAN	1
81	11.87999994	sp|P31151|S10A7_HUMAN	Protein S100-A7 OS=Homo sapiens OX=9606 GN=S100A7 PE=1 SV=4	HUMAN	2
82	4.368999973	sp|P07339|CATD_HUMAN	Cathepsin D OS=Homo sapiens OX=9606 GN=CTSD PE=1 SV=1	HUMAN	1
83	1.97100006	sp|P06744|G6PI_HUMAN	Glucose-6-phosphate isomerase OS=Homo sapiens OX=9606 GN=GPI PE=1 SV=4	HUMAN	1
84	0.452800002	sp|P15924|DESP_HUMAN	Desmoplakin OS=Homo sapiens OX=9606 GN=DSP PE=1 SV=3	HUMAN	1
85	1.87400002	sp|O00391|QSOX1_HUMAN	Sulfhydryl oxidase 1 OS=Homo sapiens OX=9606 GN=QSOX1 PE=1 SV=3	HUMAN	1
86	4.390000179	sp|P04792|HSPB1_HUMAN	Heat shock protein beta-1 OS=Homo sapiens OX=9606 GN=HSPB1 PE=1 SV=2	HUMAN	1
87	1.975999959	sp|P49590|SYHM_HUMAN	Histidine--tRNA ligase, mitochondrial OS=Homo sapiens OX=9606 GN=HARS2 PE=1 SV=1	HUMAN	1
88	10.00000015	sp|P13647|K2C5_HUMAN	Keratin, type II cytoskeletal 5 OS=Homo sapiens OX=9606 GN=KRT5 PE=1 SV=3	HUMAN	6
89	2.648000047	sp|P02675|FIBB_HUMAN	Fibrinogen beta chain OS=Homo sapiens OX=9606 GN=FGB PE=1 SV=2	HUMAN	1

90	1.947999932	sp|P02790|HEMO_HUMAN	Hemopexin OS=Homo sapiens OX=9606 GN=HPX PE=1 SV=2	HUMAN	1
91	1.057999954	sp|P18206|VINC_HUMAN	Vinculin OS=Homo sapiens OX=9606 GN=VCL PE=1 SV=4	HUMAN	1
92	2.673999965	sp|P50452|SPB8_HUMAN	Serpin B8 OS=Homo sapiens OX=9606 GN=SERPINB8 PE=1 SV=2	HUMAN	1
92	2.659999952	sp|P50453|SPB9_HUMAN	Serpin B9 OS=Homo sapiens OX=9606 GN=SERPINB9 PE=1 SV=1	HUMAN	1
92	2.638999932	sp|P30740|ILEU_HUMAN	Leukocyte elastase inhibitor OS=Homo sapiens OX=9606 GN=SERPINB1 PE=1 SV=1	HUMAN	1
92	2.563999966	sp|P48594|SPB4_HUMAN	Serpin B4 OS=Homo sapiens OX=9606 GN=SERPINB4 PE=1 SV=2	HUMAN	1
92	2.563999966	sp|P29508|SPB3_HUMAN	Serpin B3 OS=Homo sapiens OX=9606 GN=SERPINB3 PE=1 SV=2	HUMAN	1
92	2.469000034	sp|O75830|SPI2_HUMAN	Serpin I2 OS=Homo sapiens OX=9606 GN=SERPINI2 PE=1 SV=1	HUMAN	1
93	3.585999832	sp|P02774|VTDB_HUMAN	Vitamin D-binding protein OS=Homo sapiens OX=9606 GN=GC PE=1 SV=2	HUMAN	1
94	2.549999952	sp|P01876|IGHA1_HUMAN	Immunoglobulin heavy constant alpha 1 OS=Homo sapiens OX=9606 GN=IGHA1 PE=1 SV=2	HUMAN	1
95	25.2700001	sp|P63267|ACTH_HUMAN	Actin, gamma-enteric smooth muscle OS=Homo sapiens OX=9606 GN=ACTG2 PE=1 SV=1	HUMAN	10
95	25.20000041	sp|P68133|ACTS_HUMAN	Actin, alpha skeletal muscle OS=Homo sapiens OX=9606 GN=ACTA1 PE=1 SV=1	HUMAN	10
95	25.20000041	sp|P68032|ACTC_HUMAN	Actin, alpha cardiac muscle 1 OS=Homo sapiens OX=9606 GN=ACTC1 PE=1 SV=1	HUMAN	10
95	25.20000041	sp|P62736|ACTA_HUMAN	Actin, aortic smooth muscle OS=Homo sapiens OX=9606 GN=ACTA2 PE=1 SV=1	HUMAN	10
96	15.60000032	sp|P04259|K2C6B_HUMAN	Keratin, type II cytoskeletal 6B OS=Homo sapiens OX=9606 GN=KRT6B PE=1 SV=5	HUMAN	8
97	16.59999937	sp|P61981|1433G_HUMAN	14-3-3 protein gamma OS=Homo sapiens OX=9606 GN=YWHAG PE=1 SV=2	HUMAN	4
98	22.96999991	sp|Q16772|GSTA3_HUMAN	Glutathione S-transferase A3 OS=Homo sapiens OX=9606 GN=GSTA3 PE=1 SV=3	HUMAN	4
99	6.396999955	sp|P08729|K2C7_HUMAN	Keratin, type II cytoskeletal 7 OS=Homo sapiens OX=9606 GN=KRT7 PE=1 SV=5	HUMAN	3
100	1.417000033	sp|P20742|PZP_HUMAN	Pregnancy zone protein OS=Homo sapiens OX=9606 GN=PZP PE=1 SV=4	HUMAN	2
101	6.018999964	sp|P23284|PPIB_HUMAN	Peptidyl-prolyl cis-trans isomerase B OS=Homo sapiens OX=9606 GN=PPIB PE=1 SV=2	HUMAN	1
102	3.779000044	sp|Q9UJ70|NAGK_HUMAN	N-acetyl-D-glucosamine kinase OS=Homo sapiens OX=9606 GN=NAGK PE=1 SV=4	HUMAN	1
103	6.328999996	sp|Q9UHA7|IL36A_HUMAN	Interleukin-36 alpha OS=Homo sapiens OX=9606 GN=IL36A PE=1 SV=1	HUMAN	1
104	0.606400007	sp|Q9P2K8|E2AK4_HUMAN	eIF-2-alpha kinase GCN2 OS=Homo sapiens OX=9606 GN=EIF2AK4 PE=1 SV=3	HUMAN	1
105	3.816999868	sp|Q99536|VAT1_HUMAN	Synaptic vesicle membrane protein VAT-1 homolog OS=Homo sapiens OX=9606 GN=VAT1 PE=1 SV=2	HUMAN	1

106	2.991000004	sp|Q96HE7|ERO1A_HUMAN	ERO1-like protein alpha OS=Homo sapiens OX=9606 GN=ERO1A PE=1 SV=2	HUMAN	1
107	2.315000072	sp|Q8NBS9|TXND5_HUMAN	Thioredoxin domain-containing protein 5 OS=Homo sapiens OX=9606 GN=TXNDC5 PE=1 SV=2	HUMAN	1
108	1.741000079	sp|Q8IUH5|ZDH17_HUMAN	Palmitoyltransferase ZDHHC17 OS=Homo sapiens OX=9606 GN=ZDHHC17 PE=1 SV=2	HUMAN	1
109	2.931999974	sp|Q5H9E4|S2553_HUMAN	Solute carrier family 25 member 53 OS=Homo sapiens OX=9606 GN=SLC25A53 PE=2 SV=1	HUMAN	1
110	8.696000278	sp|P80511|S10AC_HUMAN	Protein S100-A12 OS=Homo sapiens OX=9606 GN=S100A12 PE=1 SV=2	HUMAN	1
111	4.183999822	sp|P54819|KAD2_HUMAN	Adenylate kinase 2, mitochondrial OS=Homo sapiens OX=9606 GN=AK2 PE=1 SV=2	HUMAN	1
112	5.392000079	sp|P52565|GDIR1_HUMAN	Rho GDP-dissociation inhibitor 1 OS=Homo sapiens OX=9606 GN=ARHGDIA PE=1 SV=3	HUMAN	1
113	6.122000143	sp|P30085|KCY_HUMAN	UMP-CMP kinase OS=Homo sapiens OX=9606 GN=CMPK1 PE=1 SV=3	HUMAN	1
114	4.853999987	sp|P30043|BLVRB_HUMAN	Flavin reductase (NADPH) OS=Homo sapiens OX=9606 GN=BLVRB PE=1 SV=3	HUMAN	1
115	3.190999851	sp|P24855|DNAS1_HUMAN	Deoxyribonuclease-1 OS=Homo sapiens OX=9606 GN=DNASE1 PE=1 SV=1	HUMAN	1
116	3.527000174	sp|P23141|EST1_HUMAN	Liver carboxylesterase 1 OS=Homo sapiens OX=9606 GN=CES1 PE=1 SV=2	HUMAN	1
117	1.957999915	sp|P22735|TGM1_HUMAN	Protein-glutamine gamma-glutamyltransferase K OS=Homo sapiens OX=9606 GN=TGM1 PE=1 SV=4	HUMAN	1
118	2.864000015	sp|P16930|FAAA_HUMAN	Fumarylacetoacetase OS=Homo sapiens OX=9606 GN=FAH PE=1 SV=2	HUMAN	1
119	1.950999908	sp|P13473|LAMP2_HUMAN	Lysosome-associated membrane glycoprotein 2 OS=Homo sapiens OX=9606 GN=LAMP2 PE=1 SV=2	HUMAN	1
120	1.374999993	sp|P12081|HARS1_HUMAN	Histidine--tRNA ligase, cytoplasmic OS=Homo sapiens OX=9606 GN=HARS1 PE=1 SV=2	HUMAN	1
121	11.42999977	sp|P07737|PROF1_HUMAN	Profilin-1 OS=Homo sapiens OX=9606 GN=PFN1 PE=1 SV=2	HUMAN	1
122	10.71000025	sp|P04155|TFF1_HUMAN	Trefoil factor 1 OS=Homo sapiens OX=9606 GN=TFF1 PE=1 SV=1	HUMAN	1
123	2.428000048	sp|P02679|FIBG_HUMAN	Fibrinogen gamma chain OS=Homo sapiens OX=9606 GN=FGG PE=1 SV=3	HUMAN	1
124	4.077000171	sp|P00558|PGK1_HUMAN	Phosphoglycerate kinase 1 OS=Homo sapiens OX=9606 GN=PGK1 PE=1 SV=3	HUMAN	1
125	15.79000056	sp|O75368|SH3L1_HUMAN	SH3 domain-binding glutamic acid-rich-like protein OS=Homo sapiens OX=9606 GN=SH3BGRL PE=1 SV=1	HUMAN	1
126	2.531999908	sp|O60218|AK1BA_HUMAN	Aldo-keto reductase family 1 member B10 OS=Homo sapiens OX=9606 GN=AKR1B10 PE=1 SV=2	HUMAN	1
127	5.982999876	sp|A0A0J9YXX1|HV5X1_HUMAN	Immunoglobulin heavy variable 5-10-1 OS=Homo sapiens OX=9606 GN=IGHV5-10-1 PE=3 SV=1	HUMAN	1

128	4.058000073	sp|P02749|APOH_HUMAN	Beta-2-glycoprotein 1 OS=Homo sapiens OX=9606 GN=APOH PE=1 SV=3	HUMAN	1
129	4.049000144	sp|P07477|TRY1_HUMAN	Trypsin-1 OS=Homo sapiens OX=9606 GN=PRSS1 PE=1 SV=1	HUMAN	1
130	5.285999924	sp|Q92520|FAM3C_HUMAN	Protein FAM3C OS=Homo sapiens OX=9606 GN=FAM3C PE=1 SV=1	HUMAN	1
131	0.887900032	sp|Q02487|DSC2_HUMAN	Desmocollin-2 OS=Homo sapiens OX=9606 GN=DSC2 PE=1 SV=1	HUMAN	1
132	6.837999821	sp|P01721|LV657_HUMAN	Immunoglobulin lambda variable 6-57 OS=Homo sapiens OX=9606 GN=IGLV6-57 PE=1 SV=2	HUMAN	1
132	6.837999821	sp|P01700|LV147_HUMAN	Immunoglobulin lambda variable 1-47 OS=Homo sapiens OX=9606 GN=IGLV1-47 PE=1 SV=2	HUMAN	1
132	6.837999821	sp|P01699|LV144_HUMAN	Immunoglobulin lambda variable 1-44 OS=Homo sapiens OX=9606 GN=IGLV1-44 PE=1 SV=2	HUMAN	1
132	6.780000031	sp|P01709|LV208_HUMAN	Immunoglobulin lambda variable 2-8 OS=Homo sapiens OX=9606 GN=IGLV2-8 PE=1 SV=2	HUMAN	1
132	6.780000031	sp|P01703|LV140_HUMAN	Immunoglobulin lambda variable 1-40 OS=Homo sapiens OX=9606 GN=IGLV1-40 PE=1 SV=2	HUMAN	1
132	6.780000031	sp|A0A075B6J9|LV218_HUMAN	Immunoglobulin lambda variable 2-18 OS=Homo sapiens OX=9606 GN=IGLV2-18 PE=3 SV=2	HUMAN	1
132	6.723000109	sp|P01706|LV211_HUMAN	Immunoglobulin lambda variable 2-11 OS=Homo sapiens OX=9606 GN=IGLV2-11 PE=1 SV=2	HUMAN	1
132	3.703999892	sp|P0DOX8|IGL1_HUMAN	Immunoglobulin lambda-1 light chain OS=Homo sapiens OX=9606 PE=1 SV=1	HUMAN	1
133	1.138000004	sp|Q6ZSS7|MFSD6_HUMAN	Major facilitator superfamily domain-containing protein 6 OS=Homo sapiens OX=9606 GN=MFSD6 PE=1 SV=2	HUMAN	1
134	3.802999854	sp|P02788|TRFL_HUMAN	Lactotransferrin OS=Homo sapiens OX=9606 GN=LTF PE=1 SV=6	HUMAN	2
135	6.7900002	sp|Q5VSP4|LC1L1_HUMAN	Putative lipocalin 1-like protein 1 OS=Homo sapiens OX=9606 GN=LCN1P1 PE=5 SV=1	HUMAN	1
135	6.25	sp|P31025|LCN1_HUMAN	Lipocalin-1 OS=Homo sapiens OX=9606 GN=LCN1 PE=1 SV=1	HUMAN	1
136	3.737999871	sp|P30044|PRDX5_HUMAN	Peroxiredoxin-5, mitochondrial OS=Homo sapiens OX=9606 GN=PRDX5 PE=1 SV=4	HUMAN	1
137	2.98999995	sp|Q9UNP9|PPIE_HUMAN	Peptidyl-prolyl cis-trans isomerase E OS=Homo sapiens OX=9606 GN=PPIE PE=1 SV=1	HUMAN	1
138	4.306000099	sp|P01009|A1AT_HUMAN	Alpha-1-antitrypsin OS=Homo sapiens OX=9606 GN=SERPINA1 PE=1 SV=3	HUMAN	1
139	9.183999896	sp|P04080|CYTB_HUMAN	Cystatin-B OS=Homo sapiens OX=9606 GN=CSTB PE=1 SV=2	HUMAN	1
140	7.558000088	sp|P13693|TCTP_HUMAN	Translationally-controlled tumor protein OS=Homo sapiens OX=9606 GN=TPT1 PE=1 SV=1	HUMAN	1
141	6.306000054	sp|P04179|SODM_HUMAN	Superoxide dismutase [Mn], mitochondrial OS=Homo sapiens OX=9606 GN=SOD2 PE=1 SV=3	HUMAN	1
142	3.635999933	sp|P01857|IGHG1_HUMAN	Immunoglobulin heavy constant gamma 1 OS=Homo sapiens OX=9606 GN=IGHG1 PE=1 SV=1	HUMAN	1
142	2.672999911	sp|P0DOX5|IGG1_HUMAN	Immunoglobulin gamma-1 heavy chain OS=Homo sapiens OX=9606 PE=1 SV=2	HUMAN	1

143	1.501000021	sp|P02671|FIBA_HUMAN	Fibrinogen alpha chain OS=Homo sapiens OX=9606 GN=FGA PE=1 SV=2	HUMAN	1
144	12.15000004	sp|Q9UJC5|SH3L2_HUMAN	SH3 domain-binding glutamic acid-rich-like protein 2 OS=Homo sapiens OX=9606 GN=SH3BGRL2 PE=1 SV=2	HUMAN	1
145	3.448000178	sp|Q9BQR3|PRS27_HUMAN	Serine protease 27 OS=Homo sapiens OX=9606 GN=PRSS27 PE=1 SV=1	HUMAN	1
146	2.637000009	sp|Q92485|ASM3B_HUMAN	Acid sphingomyelinase-like phosphodiesterase 3b OS=Homo sapiens OX=9606 GN=SMPDL3B PE=1 SV=2	HUMAN	1
147	3.117999993	sp|P27797|CALR_HUMAN	Calreticulin OS=Homo sapiens OX=9606 GN=CALR PE=1 SV=1	HUMAN	1
148	0	RRRRRsp|Q5T124|UBX11_HUMAN	REVERSED UBX domain-containing protein 11 OS=Homo sapiens OX=9606 GN=UBXN11 PE=1 SV=2	HUMAN	0
149	0.757199991	sp|Q86WG5|MTMRD_HUMAN	Myotubularin-related protein 13 OS=Homo sapiens OX=9606 GN=SBF2 PE=1 SV=1	HUMAN	1
150	0	sp|Q9HC38|GLOD4_HUMAN	Glyoxalase domain-containing protein 4 OS=Homo sapiens OX=9606 GN=GLOD4 PE=1 SV=1	HUMAN	0